Al-Fotawi, Randa (2014) *The use of an induced muscle flap to reconstruct mandibular defects.* PhD thesis.

The Use of an Induced Muscle Flap to Reconstruct Mandibular Defects

Randa Al-Fotawi

For the degree of Doctor of Philosophy

University of Glasgow

MVLS College, Medical School, Glasgow Dental School, the University of Glasgow

An Experiment is a question which science poses to nature and a, measurement is the recording of nature's answer ……

Max Planck, Scientific Autobiography and other 1949

Dedication

I would like to dedicate this thesis to everyone who believed in me, empowered me to strive for success and resume my life again.

Contents

LIST OF CONTENTS

List of Tables

List of Figures

Acknowledgement

Preface

The study was carried out at the Centre of Cell Engineering, Small Animal Research Facility at Biological Services, Radiology Department at Glasgow Dental Hospital and School, University Of Glasgow; the Academic Unit of Bone Biology, Department of Human Metabolism, University of Sheffield Medical School; Oral Pathology Department, Guy`s Hospital, King`s College London.

The study represents original work carried out by the author and has not been submitted in any form to any other university.

Author`s Declaration

I hereby declare that the research reported within this thesis is my own work, unless otherwise stated, and that at the time of submission is not being considered elsewhere for any other academic qualification.

Randa AL-Fotawi

Abstract

The treatment of challenging large osseous defects presents a formidable problem for orthopaedic and maxillofacial surgeons. Autogenous bone grafting is the present method of choice to replace the lost tissue, but supplies of autologous bone are limited and harvesting of the graft is associated with donor site morbidity. Artificial biomaterials hold much promise, but do not, by themselves, supply the osteoprogenitor cells needed for bone formation. Moreover, there are often issues with resorption of the scaffold used in the biomaterial, as well as limited vascularity. This study investigates the novel application of a composite bone mineral (Cerament ^{TM} Spine Support) as an injectable bone cement loaded with cytokines and seeded with induced mesenchymal stromal cells, for maxillofacial reconstruction in rabbits. This study aims to test the feasibility of converting a pedicled muscle flap into bone to reconstruct a critical-size defect in the mandible as the above three components would theoretically have the combined effect of osteoconduction, osteoinduction and osteogenesis. The study included a comprehensive assessment of bone regeneration using plain radiography, Cone Beam computerized Tomography (CBCT), Micro-Computerized Tomography (micro-CT) and histology.

Results at 3 months following surgery showed areas of bone formation and remnants of residual cement throughout the muscle and connective tissue in the surgical defect. Data analysis showed that complete bone integration or incorporation for the reconstruction of the surgical defect was not achieved. However, the regenerated bone displayed a high degree of remodeling with an intricate network of woven bone trabeculae within the cement. The bone was thicker in the bucco-lingual direction and exhibited more red and fatty marrow spaces compared to the contralateral (non-operated) side.

The study confirmed that bone formation within a muscle flap in the maxillofacial region is possible. However, a wide range of variation in the patterns of bone formation was seen among the samples. The findings demonstrated the remarkable potential for the use of autologous muscle flaps as bioreactors for injectable scaffoldings, BMP, rMSCs to facilitate the reconstruction of maxillofacial bony defects.

Abbreviations and definitions

Abbreviation	Definition
	XX
A	
A-MEM	Alpha-Modified Eagle`s Medium
ACB	Absorbable Collagen block
ADSCs	Adipose stem Cells
Ad-BMP-2	Adenovirous vector encode for BMP-2
ALK2	Transmembrane receptors to BMP receptor
ALP	Alkaline Phosphatase
AO	Arbeitsgemeinschaft für Osteosynthesefragen
ASCs	Adipose Stem Cells
ATPase	Adenosine Triphosphatase
AHBMSCs	Autologous human bone marrow stromal cells
B	
BTCP	Beta-TriCalcium Phosphate
BD	Bone Density
BCB	Bovine Cancellous Bone
BC	Bone construct
BCP	Biphasic Calcium Phosphate
b-FGF	basic Fibroblast-Growth Factors
Bio-Oss	A commercially available bovine bone substitute
BM	Bone Marrow
BMA	Bone Marrow Aspirate
BMC	Bone Marrow Cells
BMD	Bone Mineral Density
BMG	Bone Matrix Gelatin
BMP	Bone Morphogenic Protein
BMP-7	Bone Morphogenic Protein-7
BMP RIA	Bone Morphogenic Protein Receptor type II
BMSCs	Bone Mesenchymal Stromal Cells
BrdU	Analogue 5-bromo-2-deoxyuridine
BRONJ	Bisphosphanate-Related Osteonecrosis of the Jaw
BS	Bone Scaffold
BS	Bone Surface area
BSA	Bovin Serum Albumin
BV	Bone Volume
BV/BS	Bone Volume/Bone surface

Abbreviation	Definition
BV/TV	Bone Volume/Total Volume
BVF	Bone volume fraction
C	
C2CI2 Cells	Murine myoblast cells line.
Ca Cl$_2$	Calcium Chloride
CAM	Computer aid manufacturing
CBB	Calcined Bovine Bone
CBCT	Cone Beam Computerized Tomography
cbfa1	Core Binding Factor alpha-1
CC FDAB	Crushed cancellous Freeze Derived Allograft Bone
CD8	Glycoprotein co receptor for major histocompatibility complex
CD10	Protein receptors found on Hematopoietic Cells
CD11b	Intergren receptor in bone marrow cells mainly leukocyte
CD13	Protein surface marker found on granulocyte, monocyte, endothelial and osteoclast cells
CD14	Protein co- receptor on Macrophage
CD19	Protein surface marker B- Lymphocyte
CD27 or LNGFR	Low affinity Nerve Growth Factor Receptor
CD34	Glycoprotein suface marker for Hematopoietic and Endothelial Cells
CD44	Glycoprotein surface marker of MSCs, and cancer stem cells
CD45	Glycoprotein surface marker for hematopoietic cells
CD49	Protein surface marker for MSCs
CD73	Glycoprotein on membrane of differentiated lymphocyte
CD79a	Glycoprotein on membrane of B cells and plasma cells.
CD90	Protein cell surface marker for Stem cells, and on hematopoietic cells
CD105	Glycoprotein marker for Enothelial cells(angiogenesis)
CD117	Protein Cytokine receptor expressed on surface of HSCs
CD133	Glycoprotein surface marker in HSCs
CD166	Glycoprotein surface marker mainly for MSCs, osteoblasts, osteoclasts and leukocytes
CDHA	Calcium Deficient Hydroxyapatite
CFE	Colony Forming Efficiency
CFU-F	Colony Forming Unite-Fibroblasts

Abbreviation	Definition
CH3	Hydrocarbon
CHA	Coral Hydroxyapatite
CIP	Calcification Initiator Protein
CM-Dill	Chloro methylated Dilanaloge
CMV	Cytomegalo-Virus
Col	Collagen
COOH	Carboxyl group
CaP	Calcium phosphate
CPB	Calcium Phosphate block
CPC	Calcium Phosphate Cement
CPP	Calcium phosphate particles
CRM	Compression Resistant Matrix
CRU	Condylar Ramus Unite
CSD	Calcium Sulphate Dihydrate
CSD	Critical size Defect
CS	Calcium sulphate
CSS	Cerament Spine Support
α CSH	Alpha-Calcium sulphate Hemihydrate
β CSH	Beta- Cacium sulphate Hemihydrate
CTX	Carboxy-terminal collagen crosslinks
D	
2D	Two Dimensional
3D	Three Dimensional
D7-FIB	D7-Fibrobalst Anti-Body
DAPI	4',6-diamidino-2-phenylindole
DASH	Disability of the Arm, Shoulder & Hand
DBM	Demineralized Bone Matrix
DBPs	Demineralized Bone Powder
DDS	Drug Delivery System
DEXA	Dual Energy X-ray Absorptiometry
DMD	Duchenne Muscular Dystrophy
DMEM	Dulbecco` Modified Eagle`s Medium
DMSO	Dimethylsulfaoxide
DNA	Deoxyribonucleic acid
DPC	Dystrophin Protein Complex
DPBS	Dulbecco`s phosphate buffered saline
E	
EBSD	Electron back scatter diffraction

Abbreviation	Definition
ECGM	Endothelial Cell Growth Medium
ECM	Extra Cellular Matrix
EDTA	Ethylenediami-netetraacetic Acid
EDX	Energy Dispersive Xray analysis
EGF	Epidermal Growth Factor
eHAC	Equine Hydroxyapatite Collagen
EIP	Extensor Indices Propirus
EPL	Extensor Pollicis Longus tendon
F	
FACS	Fluorsence Activated Cell Sorting
FCS	Fetal calf serum
FCU	Freeze dried Cow Urine
FDA	Food and Drug Adminsteration
FGF-2	Fibroblast Growth Factor-2
FGFR3	Fibroblast Growth Factor-R3
FGFR2	Fibroblast Growth Factor-R2
FGFR1	Fibroblast Growth Factor-R1
FITC	Fluorescence ThioCyanate
FOP	Fibrodysplasia Oddificans Progressiva receptors
FOV	Field of view
FTIR	Fourier Transform InfraRed spectroscopy
G	
GA	Gultra-Aldehyde
GA	General Anaesthesia
GAPDH	Glyceraldhyde-3-Phosphate Dehydrogenase
GF	Growth Factors
Gfp$^+$	Green fluorescent protein
GMP	Good Manufacturing Practice
H	
HA	Hydroxyapatite
hBMSCs	Human Bone Marrow Stromal Cells
H&E	Hematoxylin and Eosin
HIF-1alpha	Hypoxia Induced Factor one alpha
HLA-DR	Cell surface receptor by leukocyte, this part of major histo-compatibility complex class -II.
HMDS	Hexamethyldisilazane
HME	Hematopoietic Micro Environment

Abbreviation	Definition
HPMC	Hydroxy Propyl Methyl Cellulose
HSCs	Hematopoietic Stem Cells
HU	Hounsfield Unit
I	
IBS	Injectable Bone Substitute
i-CAT	Imaging sciences international-computed axial tomography
ID	Identification Number
IFA	Immuno Fluorescent Assay
IHC	Immunohistochemistry
IM	Intra-Muscular
IPMF	Induced pedicled muscle flap
ISCT	International Society of Cell Therapy
ISO	In Situ Osteogensis
L	
Lac Z	Structural gene encode for ß-glactosidase
LIPUS	Low Intensity Pulsed Ultra Sound
LLLT	Low-Level-Laser- Therapy
M	
µm	Micrometre
µM	Micromole
MAPK	Mitogen-Activated Kinases
MAPCs	Multi-Adult Progenitor Cells
MAR	Mineral Apposition Rate
MCPM	Mono Calcium Phosphate Monohydrate
MCi	Millicurie
MD	Mineral Density
MDSCs	Muscle Derived Stem Cells
Mg2	Magnesium ion
MHC-II	Major Histocompatibility Complex II
Micro-CT	Micro-Computerized Tomography
MMP	Matrix Metallo-Proteinase
MPa	Mega Pascal
MPC	Mesenchymal Progenitor Cells
MRI	Magnetic Resonant Tomography
MRSA	Methicillin Resistant Staphylococcus Aureus
MSCs	Mesenchymal Stromal Cells
m SS	peri-Mineralized Silk fibrin protein Scaffold
MTT	Methyle ThiazolyTetrazlium

Abbreviation	Definition
MUC-18	Glycoprotein surface marker for endothelial cells
MVLS	Medical Veterinary, and Life Sciences
N	
nHA	nano-Hydroxyapatite
nHAC	nano-Hydroxyapatite Collagen
NH2	Amine group
Nm	Newton-millimetre
NSAID	Non-Steroidal Anti-Inflammatory Drug
O	
OC/Luc	Osteocalcin/Luciferen transgenic mice
OCN	OsteoCalcin
OCP	Octa-Calcium-Phosphate
OD	Optical Density
ODI	Oswestry Disability Questionnaire
OPC	Osteoblastic Precursor Cells
OPN	Osteopontin
OH	Hydroxide
OVX	Ovariectomy
OY	Osteogenic yield
P	
PA	Polyamide
PBCM	Particulate Bone Cancellous Marrow
PBS	Phosphate Buffer Saline
PCL	Poly caprolactone
PCNA	Proliferating Cells Nuclear Antigen
PCR	Polymerase Chain Reaction
pDA	Polydopamine
P-DED	Polymer-DimethylEthyleneDiamine
PDGF	Platelet Derived Growth Factors
pDNA	plasmid Deoxyribonucleic acid
PE	Polyethylene
PEGDA	Photo polymerized polyethylene glycol diacrylate based
PEGFP	Plasmid mammalian vector Expressed Green Fluorescent Protein
Pi	In organic Phosphate
Pit 1	Co-transport pituitary specific positive transcription factors
PLA	Poly-L-Lactide

Abbreviation	Definition
PLC	Poly-D-Lactide with Collagen type1
PLGA	Poly lactic-co-glycolic acid
PLL	70-L-Lactide-co-30 DL-Lactide
PLLA	Poly Lactic-L-Acide
PM	Pura Matrix
PMCB	Particulate Marrow Cancellous Bone
PMMA	Poly Methyl Methacrylate
PPARG	Peroxisome Proliferator Activated Receptor Gamma
PPF	Polypropylene Fumarate
Proto-oncogene c-SRC	Protein receptor encode for SRC gene
PRP	Plasma Rich Protein
PUR	Poly Urethane
Q	
QoL	Quality of Life
QS	Quantitative Scoring
ΣQS	Sum Quantitative Scoring
R	
Rb	Rabbit
RT-PCR	Reverse transcription polymerase chain reaction
rh-BMP-7	recombinant human-Bone Morphogenic Protein
rhOP-1	Recombinant human Osteogenic Protein 1
rMSCs	rabbit Mesenchymal Stromal Cells
ROD	Region of Defect
Run x2	Runt-related transcription factor for osteoblastic differentiation
S	
S1P	Sphingosine-1-phosphate
SBF	Simulated Body fluid
S/C	Sub-cutaneous
SCID	Immunodeficiency mice
SEM	Scanning electronic Microscopy
SD	Sprague-Dawley rat
SLS	Selective Laser Sintering

Abbreviation	Definition
SRC	Schmidt-Ruppin-A2 IS A pro-oncogene for tyrosine protein kinase.
SRS	Skeletal Repair System
SS	Silk fibre Scaffold
Stro -1	Cell surface marker in MSCs and expressed in endothelium
T	
Taq	Thermus a quaticus
Tb.Th	Trabecular Thickness
Tb.Sp	Trabecular Separation
Tb.N	Trabecular Number
TC	Tooth Construct
TCP	Tri-Calcium Phosphate
TEM	Transmission Electron Microscopy
TGF	Transforming Growth Factor
TGF-b I	Transforming Growth Factor beta
Ti	Titanium
TRAP	Tartrate Resistant Acid Phosphate
TRITC	Tetramethylrhodamine isothiocyanate
TS	Tooth Scaffold
TWIST	Transaction Workflow Innovation Standards Team
U	
UV	Ultra-violet light
V	
VAS	Visual Analogue Scale
VEGF	Vascular Endothelial Growth Factor
VOI	Volume Of Interest
VSM	Vinyl Styrene Microbeads
W	
WDX	Wave length dispersive X-ray
WSAT	White Subcutaneous Adipose Tissue
WSTs	Water soluble Tetrazolium salts
MTS	(3-(4,5-dimethylthiazol-2-yl)-5-(3-carboxymethoxyphenyl)-2-(4-sulfophenyl)-2H-tetrazolium
X	
XTT	2,3-bis-(2-methoxy-4-nitro-5-sulfophenyl)-2H-tetrazolium-5-carboxanilide

Chapter 1
Introduction

Table of Contents

1 Introduction

Overview

The reconstruction of critical size defect bony defects in the maxillofacial region remains a major surgical challenge. The size of the defect and the effect of radiation therapy on the blood supply of the surrounding tissues are the main limiting factors of successful reconstruction. Most of the published data are based on expert opinion, and the available comprehensive studies provide limited objective guidelines for successful treatment (Assael, 2009). The surgical techniques for facial reconstruction are based on regional, historical, and individual opinion rather than high quality evidence. In addition, researchers do not agree on clear outcome measures for comparative studies (Assael, 2009). The gold standard method for reconstruction of long bones remains the microvascular bone graft; however this method is associated with morbidities and the method requires healthy donor tissues and surgical expertise. Therefore, there is a need for alternative treatment strategies (Gimbel et al, 2007). Bone bio-engineering provides a potential alternative to autogenous grafts. The present study evaluates the possibility of inducing bone formation within a pedicled muscle flap using Calcium Sulphate/Hydroxyapatite cement (Cerament ^{TM} |Spinal Support), Bone Morphogenic Protein-7 (BMP-7) and rabbit Mesenchymal Stromal Cells (rMSCs) for reconstruction of mandibular defects in rabbits.

1.1 Techniques for reconstruction of large bony defects in the maxillofacial region

1.1.1 Non-vascularised bone grafts

Autogenous bone is an effective graft as it provides osteoconduction, osteoinduction and osteogenesis. Osteoconduction occurs when the bone graft material serves as a scaffold for new bone growth that is extend to the native bone (Perciaccante and Jeffery, 2007). *Osteoinduction* involves stimulating osteoprogenitor cells to differentiate into osteoblasts which then begin new bone formation (Perciaccante and Jeffery, 2007). The most widely studied type of osteoinductive cell mediators are BMPs which can be found in large concentrations in cortical bone (Perciaccante and Jeffery, 2007). Osteogenesis occurs when osteoblasts originating from the bone graft material contribute to new bone growth. At present, many surgeons choose a cortico-cancellous block graft taken from the anterior or posterior iliac crest for jaw reconstruction (Goh et al, 2008). The success of these grafts may be dependent on the way the bone is fixed because the survival depends on the graft revascularization from the recipient site (Goh et al, 2008). This revascularization is leading the process of resorption and deposition of new bone that is known as creeping substitution (Goh et al, 2008). However, there are three major limitations with using an autogenous free bone graft; poor osseointegration and excessive resorption when the defect is larger than 6 to 9 cm^3, insufficient blood supply to the graft and surrounding tissues due to irradiation scarring and infection, and donor site morbidity (Kessler et al, 2005).

1.1.2 Particulate cancellous bone marrow graft (PCBM)

This method of grafting has been proven to attain superior osteogenic potential and lower rates of surgical complication compared to cortical graft (Rappaport, 1971). PCBM graft is placed in a frame or crib to maintain its physical dimensions and to provide mechanical stability. Titanium, Vitallium, tantalum, chrome cobalt and stainless steel metal cribs are frequently used to deliver the PCBM (Samman et al, 1999; Tideman and Lee 2006; Tideman et al, 1998; Cheung et al, 1997). These metal trays have clear disadvantages, especially for the patients who will be subjected to radiotherapy. Further limitations of the trays are wound dehiscence, tray exposure and post-operative infection (Kinoshita et al, 1997; Louis et al, 2004). Thus introduction of resorbable alloplastic trays to the world of maxillofacial reconstruction has attracted the attention of many researchers to test its feasibility before clinical application (Kinoshita et al, 1997; Louis et al, 2004). The use of the patient`s own mandible after scrubbing the pathological tissues from the bone has also been used for reconstruction. The bone is then autoclaved or freeze dried before being filled with PBCM. Variable rates of success have been reported in animal and human trials (Simon et al, 2006; Lee et al, 2010a). The main reported disadvantages included graft resorption and wound dehiscence which may lead to loss of the graft (Lee et al, 2010a). PBCM grafts are not recommended in patients with malignant tumors where scar, fibrosis and lack of vascularity are significant problems with the covering soft tissues (Goh et al, 2008).

1.1.3 Pedicled composite flaps

This flap is composed of bone, muscle or skin, attached to their feeding blood vessels (vein and artery), it become more popular in the field of maxillofacial reconstruction as it overcomes the problems associated with the reduced vascularity at the recipient site. Many techniques have been advocated and their feasibility has been investigated. Pedicled composite flap based on sternocleidomastoid muscle is used for mandibular reconstruction. However, their aesthetic results were not always acceptable (Goh et al, 2008) and are also associated with donor site morbidity (Torroni, 2009).

1.1.4 Microvascular free flap

Mandibular reconstruction using microvascular free flap is the gold standard teachnique as it provides a satisfactory functional reconstruction (He et al, 2007). In a prospective study, 82 irradiated mandibles were reconstructed using free vascular bone flap, 20 cases were followed up for 10 years and a 90% success rate was reported (Hidalgo and Pusic, 2002). However, shaping of microvascular bone graft to restore complex 3-dimensional orbito-maxillary defects is difficult to achieve (He et al, 2007). Furthermore, the iliac crest free vascular flap has a short vascular pedicle and the lack of segmental perforating vessels limits its use (Hartman et al, 2002). On the contrary to this, the fibula flap has a broad clinical application; it can provide up to 30 cm bone length (Hidalgo and Pusci, 2002; Taylor et al, 1976). However, presence of vascular disease hinders use of this flap. Another limitation for the fibula flap which is debated in the literature and relates to its inadequate height in relation to the dentate jaw (Horiuchi et al, 1995).

1.1.5 Tissue engineering & regenerative medicine

Tissue engineering was initially introduced to describe the technology producing biological tissue in vitro (Whitman et al, 1997). Recently, the term regenerative medicine has been used to describe the development of technology and surgical procedures for the regeneration of tissue in vivo (Lynch et al, 2008). The working goal of tissue engineering is the implementation of existing knowledge for the creation of a product (tissue) that can resemble autogenous tissue and is able to act as a substitute for any lost tissue at any point in time. The objectives of tissue engineering and regenerative medicine are to promote regeneration and, ideally, true regeneration of tissue structure and function more predictably, and less invasively than autogenous grafting techniques (Lynch et al, 2008)

Tissue bioengineering originated with the introduction of three-dimensional biomaterial scaffolds to support regeneration and to substitute autografts. Numerous matrices, including allogenic, xenogenic and synthetic graft materials are available on the market for use in oral surgical procedures and orthopedic surgery. The exact mechanism of the action of these matrices is to provide a foundation for cells to migrate from the wound edges (osteoconduction), eventually leading to the repair of the defect. The main disadvantage of using scaffolds alone is the lack of osteoinductive properties (Lynch et al, 2008). The major turning point in the arena of bone reconstruction was the introduction of BMPs. BMP promotes osteoinduction, thus inducing osteoprogenitor cells to produce bone, and resulting in chemo-attraction for the mesenchymal stem cells to the defect area (Herford et al, 2007). At the level of preclinical animal studies, the use of BMP reported promising results (Abu-Serriah et al, 2005; Ayoub et al, 2007; Miguez et al, 2011). A few cases were also published on successful reconstruction of the

maxillofacial region in clinical trials using BMP (Chao et al, 2006; Moghadam et al, 2004; Herford et al, 2007). Two prospective longitudinal controlled clinical trials were carried out using BMP and scaffolds (Herford and Cicci`u M, 2010; Herford et al, 2007). From both studies, authors concluded that BMP-2 is an effective alternative for bone regeneration.   On the contrary, Herford et al (2011) concluded that BMP cannot replace autogenous bone graft in large bone defect due to the reported failure rate which was 13.9%.

In the same vein, Ferretti and Ripamonti (2002) tested bone regeneration in mandibular critical continuity defects of humans with naturally derived BMPs. This was compared with bone regeneration with autologous bone grafts. The BMP was delivered from human cortical bone chips. The latter was mixed with demineralized bovine bone matrix to form the construct for the experimental group. Data from the morphometric analysis of the BMP graft showed highly active osteogenesis compared with the autogenous bone graft control group. Although there is definitely a future for engineered grafts using BMP, the long term side effect of cytokines are not yet reported (Goh et al, 2008). Another limiting factor is related to the costs involved in using the currently available BMPs – as they are high and limited their use on a large scale (Goh et al, 2008).

Another dimension of bone tissue engineering is the use of prefabricated bioengineered bone grafts. Detailed description and variety of techniques reported in literature are covered in section (2.5).

1.2 Mesenchymal stromal cells (MSCs)

In this research the term MSCs and BMSCs will be used to describe the multi potential mesenchymal stromal cells derived from bone marrow. However the term rabbit Mesenchymal Stromal Cell (rMSCs) will be used to refer to rabbit adherent cells that are clonogenic and capable of extended proliferation, as defined by Bianco et al (2001).

It has been suggested that these cells exhibit a high capacity for self-replication and it was found that 1ml of MSCs, under optimal conditions, could generate billions of cells. In addition, multi colony derived strains of MSCs can be passaged more than 25 times (50 cell doubling time) in vitro (Bianco et al, 2001). Furthermore, Jiang et al (2002) found that MSCs can be expanded for more than 80 cell doublings.

1.2.1 Heterogeneity of the MSC population

The MSCs population always has a tendency to exhibit a heterogeneous nature. Upon examination of these colonies, different cell morphologies (spindle shaped to large flat cell), range of colony sizes and representing varying growth rates (Gronthos et al, 2001). Satomura et al (2000) stated that the behavior of these MSC colonies in culture medium does not reflect the degree of multipotency of a selected clone in vivo. The ability to isolate the subset of marrow stromal cells that hold the ability to replicate and differentiate would be of utmost importance for clinical applications. Several laboratories have developed monoclonal antibodies using MSCs as an immunogen in order to identify one or more markers suitable for identification and sorting of stromal cell preparations (Bruder and Caplan, 1989; Joyner et al, 1997; Gindraux et al, 2007; Kaiser et al 2007). Researchers performed direct enrichment (isolation) to study native phenotyping of these cells by using immuno-detection and immuno-magnetic methods and comparison of the MSCs from mouse, rat and human BM. They demonstrated that

all rodent multipotential CFU-Fs are contained within the CD49 positive cell population (Gindraux et al, 2007). Therefore, CD49 is protein surface marker that allows direct enrichment of bone marrow MSCs (Gindraux et al, 2007).

In 2005, the International Society of Cell Therapy (ISCT) confirmed MSCs under standard culture conditions must first have adherent growth characteristics; second, MSCs express CD90, CD73 and CD105 and express CD19, CD14, CD34, or CD11b or CD45 and HLA-DR surface molecule. Third, MSCs can differentiate into bone cells, fat cell and cartilage cells (Horwitz et al, 2005). However, it is not clear whether highly purified or cloned MSCs population is needed for bone engineering (Mao et al, 2006). Stem cell populations are heterogeneous and include both the mesenchymal and hematopoietic stem cells.

1.2.2 Postnatal marrow stromal cells (tissue-specific adult) of the vascular wall

Pericytes are the cells found on the walls of blood vessels and line the bone marrow. These cells showed similar properties to MSCs with regards to cell surface markers and their response to different cytokines. Moreover, pericytes are potential progenitor cells (Diaz-Flores et al, 1991; Doherty and Canfield, 1999). There was clear evidence that pericytes may be recruited during angiogenesis from neighboring residential mesenchymal cells, endothelial cells or their progenitors. Moreover, bone marrow pericytes might also be heterogeneous in their mode of development and origin (Bianco et al 2010).

1.2.3 Orthodox plasticity of marrow stromal cells

One of the important characteristics of the bone marrow stromal cells is cell plasticity both in vivo and in vitro. It has been called orthodox because this plasticity remains within the context of the organ from which the cells were derived. The primary implication of these findings is the physiologic need for plasticity of connective tissue cells, basically to adapt different tissues that live next to one another during organ growth. Furthermore, cell plasticity would help maintain the organ from which they were derived. Researchers have indicated that there were key factors controlling cell differentiation. An example of a gene controlling the osteogenic commitment of the cells is core binding factor α1 (cbfa1), also known as RUNX2 which is commonly recognised in MSCs from bone marrow (Satomura et al, 2000). In conclusion, the fact that a single skeletal segment contains all cells type (chondrocytes, osteoblasts, reticular cells, and adipocytes) means that these cells should carry a marker of osteogenic commitment. Moreover, these cells are simultaneously present at different stages of organogenesis; therefore these cells have the capability to shift to one another within the same group of cells under specific circumstances (Bianco et al, 2001).

1.2.4 Unorthodox Plasticity of Marrow Stromal Cells

Progenitor cells can be found in different tissues and have the ability to differentiate into cells that are unrelated to the native tissue (Ferrari et al, 1998; Woodbury et al, 2000). Ferrari et al (1998) found that marrow contained systemically transplantable myogenic progenitors that have the same potential, while Bjornson (1999) tested the feasibility of turning neural stem cells into hematopoietic cells in irradiated mice. Lagasse et al (2000) studied at the possibility for the bone marrow to generate hepatocytes. Whereas Mezey et al (2000) investigated the feasibility of bone marrow to generate neural cells. Reyes et al (2002; 2001), Schwartz et al (2002) and Oswald et al (2004) identified that MSCs can differentiate not only into a mesenchymal lineage but also into an endothelium and endoderm lineage. If the marrow stromal cells can form liver, brain, and muscle then there must be mechanisms ensuring that there is no unwanted tissue or organ formation inside the marrow itself. Thus, a signal system for tissue renewal must exist for cell differentiation (Bianco et al, 2001).

One important fact about stem cells is that plasticity, self-maintenance is limited to specific times and events in vivo, but is limited at ex-vivo. As mentioned earlier MSCs can be cultured for long time (50 passage), but this property will lost once skeletal growth has ceased. This quiescence is a mechanism to preserve stem cell numbers while preventing DNA damage.

1.2.5 Transplantation and Transplantability of Marrow Stromal Cells

Extensive research explored the transplantability of MSCs, the outcome of this research has revealed that neither the ideal ex-vivo expansion conditions nor the ideal carrier, and the number of cells that are required for the regeneration of a volume of bone have not been optimised (Goshima et al, 1991; Kon et al, 2000). MSC are immune modulating cells;

they lack the expression of major histocompatibility complex class II (MHC-II). These properties are retained even after an osteogenic induction in vitro and seem to be similar in bone MSCs and adipogenic MSCs. This suggests that allogenic transplantation of MSCs would be possible, for example in the context of tissue engineering (Niemeyer et al, 2007). Moreover, Groh et al (2005) described a novel interaction between blood monocytes and bone marrow-derived MSCs, which results in inhibition of T-lymphocyte activation. This inhibition is mediated by cytokines released from MSCs Transforming Growth Factor (TGF).

1.2.6 Microenvironment and stem cell properties in-vitro and in- vivo

The microenvironment is a compartment, where the cell component is long-living and constantly exposed to the extracellular matrix. The microenvironment is implicated in both the support and maintenance of either a differentiated or an undifferentiated status of the MSCs. There are different elements that could affect the cells; these are oxygen tension, glucose concentration, growth factors, physiochemical nature of the environment including the pH, ionic strength (e.g. Ca^{2+} concentration) and load. Their roles are crucial for the maintenance of stem cell properties and the possibility of reprogramming their commitment (Figure 1.1).
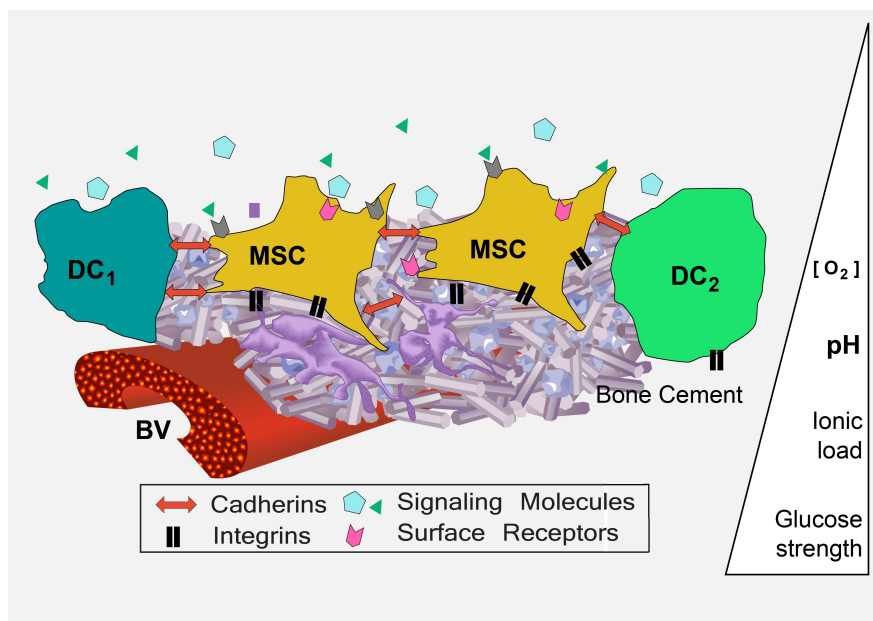
Figure 1.1: Mesenchymal stromal cell niche. MSCs are shown in their putative perivascular niche (BV, blood vessel), interacting with (1) various other differentiated cells (DC1, DC2, etc.) by means of cell-adhesion molecules, such as cadherins, (2) extracellular matrix and cement (ECM, Bone cement) deposited by the niche cells mediated by integrin receptors, and (3) signaling molecules, which may include autocrine, paracrine, and endocrine factors. Another variable is O_2 tension, with hypoxia, ionic load and glucose strength associated with MSCs in the bone marrow niche (Modified from Kolf et al, 2007).

For cell culture of MSCs the culture medium and conditions play a critical role in selecting MSC subpopulations and influencing their fate. An example of this is that careful in vitro manipulation of cells during culture can prevent cells reaching a terminal differentiation stage that can jeopardize their ability to proliferate and differentiate after delivery in vivo. The effects of growth factors on MSCs have been investigated extensively (Gronthos & Simmons, 1995; Rodan et al, 1989). It has been found that fibroblast growth factor-2 (FGF-2) showed higher ability to promote the proliferation of these cells compared to other growth factors that were analysed in the same study (Bianchi et al, 2001; Martin et al, 1997). Dexamethasone can effectively induce the osteogenic potential of these cells. Interestingly, the addition of FGF-2 to dexamethasone treated cultures could enhance the expression of the osteogenic phenotype (Bianchi et al, 2001). Furthermore, Gronthos and Simmon (1996) have

demonstrated that the presence of growth factors is required for the proliferation of these cells in the absence of serum in the culture medium. It has been observed that drops in cell proliferation rate occur when other components of marrow microenvironment are removed which may be responsible for a complex network of soluble and cell-contact signals to bone MSCs (Bianchi et al, 2001).

On the same line, Castano-Izquierdo et al (2007) revealed that the in-vitro culture time of MSCs is a critical factor for their ability to regenerate bone when implanted into an orthotopic site. Their finding was in agreement with previous studies where scaffolds seeded with MSCs and pre-cultured in osteogenic media for very short time (6-7 days) showed the highest osteoinductivity (van den Dolder et al, 2002; Sikavitsas et al, 2003).

In-vivo cell survival depends entirely on finding an adequate environment. Cell expanded ex vivo were selected for their adherence to plastic. Therefore the use of a scaffold is essential for the cell to provide self-sustained microenvironment for more than 4 months (Bianchi et al, 2001). A scaffold provides the cells with a niche in which they can stick together and manipulate the substrate to create a local environment where they can thrive for long periods of time. Apparently, the chemical composition of the matrix did not affect cell survival or expression of the transgene.

1.2.7 The osteogenic potency of MSCs from different sources or regions

Interestingly, researchers have found a difference between MSCs from long bones and MSCs from the mandible. It has been found that human mandibular, or maxillary marrow stromal cells showed stronger expression of osteoblastic markers, delayed senescence and increased cell proliferation with respect to iliac-crest-derived marrow cells from the same patients (Akintoye et al, 2006). This suggests distinct functions, differentiation potential and osteogenic potential of mandibular vs long-bone marrow

stromal cells. Mandible MSCs cultures form more colonies, referring to an increased CFU population (Aghaloo et al, 2010).

Research for MSC-like cells in specific tissues had led to the discovery of a variety of stem cells in every organ and tissue in the body in the past decade (Kolf et al, 2007; Baksh et al, 2004; Porada et al, 2006). To date, five different human dental stem/progenitor cells have been isolated and characterized. These cells have self-renewal potential and exhibited potent capacities to differentiate into odontogenic cells. However, they are also able to form other cells lineages similar to BMSCs, but differ in potency (Huang et al, 2009). It has been found that dental pulp stem cells appear to be more committed to odontogenic rather than osteogenic development. Conversely, promising results were reported when using dental stem cells for bone regeneration, where no significant difference in newly formed bone was found between MSCs from bone marrow and dental pulp stem cells (Yamada et al, 2011). However, a study by Ryu et al (2011) on the osteogenic differentiation of human MSCs periosteal-derived cells showed that the periosteal-derived cells have good osteogenic capacity. What is more important was the ability of deciduous stem cells to transplanted between child and parent in vivo, i.e. without causing an allogenic graft rejection (Yamada et al, 2011).

On the other hand, MSCs derived from adipose tissue and umbilical cord blood are morphologically and immunophenotypically similar to bone marrow derived MSCs (Kern et al, 2006). The umbilical cord derived MSCs form the fewest colonies and show the highest proliferation capacity, whereas adipose tissue derived MSCs form the greatest number of colonies, and bone marrow MSCs have the lowest proliferation capacity compared to other sources (Mareschi et al, 2001; Ballen et al, 2008). Studies which investigate upon the use of human adipose-derived stromal cells (ASCs) have found cells were utilised to replace bone loss in critical size calvaria defects in a rat model

(Rhee et al, 2011; Halvorsen et al, 2000). Studies reported the success of ASCs in the reconstruction of the cranium, maxilla, and mandible (Lendeckel et al, 2004; Mesimaki et al, 2009; Kulakov et al, 2008). Muscle derived stem cell (MDSCs) have been investigated to test their osteogenic potential. It has been found that, it was involved in endochondral bone regeneration during cranial defect healing (Gao et al, 2011). Furthermore, these cells were facilitated bone regeneration by excreting an anti-inflammatory role (Gao et al, 2011). MDSCs also chemo attracted vascular cells from the host and promoted angiogenesis.

1.3 Biomaterials

The demand for biomaterials to be used for the reconstruction of bone defects and for application in compromised clinical situations like critical-size defect scenarios or immunocompromised patients resulted in the development of the concept of the 3rd generation of biomaterials. The main desired properties of bone substitute materials are biocompatibility, bioactivity, osteointegration, osteoconduction, biodegradability, osteoinduction and the ability to attain adequate mechanical properties. The ideal scaffold materials have not yet been produced (Tanner, 2010) so none are commercially available. There are several materials currently being tested and many refinments are still necessary before its clinical use.

Several inorganic and organic biomaterials are available for orthopedic and dental applications, including ceramics, demineralized allograft, polymers and composites. These bone substitute materials are prepared as various physical forms, such as powders, granules, dense blocks, putties, pastes, gels and porous scaffolds. Generally, ceramics hold a prominent position in orthopedic and craniofacial applications, due to their properties. The ceramic materials can be bio-compatible and osteoconductive

(Best et al, 2007). The main bone substitutes that are currently available are of both natural and artificial origin.

1.3.1 Allograft

Demineralized Bone Matrix (DBM) is allograft bone that has been demineralized and processed, leaving a denatured form of the protein matrix remaining(Ilan and Ladd, 2002). The processing, which includes chemical and radiation treatment, mechanically weakens the bone and its bone formation potential. DBM induce osteoinduction in animal models and therefore suggests the presence of growth factors (Urist, 2002). A human model for osteoinduction does not exist. DBM is usually presented in the form of a dry, moldable, or injectable paste; in 2005, the fastest growing bone graft material was demineralized bone matrix (DBM) allograft possessing acknowledged osteoconductive and osteoinductive properties (Lee et al, 2005). DBM is produced alone or in combination with carriers, such as glycerol, gelatin, collagen and hyaluronic acid. The main disadvantages of the DBM are that it is a human derived material with the potential for transmission of disease and potential immunogenicity, this together with the poor mechanical properties results in limited applicability (Ilan and Ladd, 2003).

1.3.2 Mineral Substitute

Mineral substitutes are osteoconductive. The most popular mineral substitute is ceramic, when applied at boney sites it decreases the remodeling and resorption capability of bone (Ilan and Ladd, 2003).

1.3.2.1 Ceramic

Most orthopedic ceramics are composed of Hydroxyapatite (HA), tricalcium phosphate (TCP) or a mixture commonly called biphasic calcium phosphate (BCP). These brittle materials have limited tensile strength. They are available in the form of blocks with more extensive interconnected porosity permitting more bony ingrowth but weakening the material; the ideal pore size is thought to be between 150 and 500 microns (Truumees and Herkowitz, 1999; Tanner, 2010). Both sintered and non-sintered porous substances are available, the latter is associated with a faster resorption rate.

Coralline HA (Pro Osteon (Interpore Cross International, Irvine, CA)) is coral material that is thermo-chemically treated with ammonium phosphate, that has a porosity similar to bone. The heat treatment converts 95% of the coral's calcium carbonate into more slowly resorbed HA. When used clinically, bone in-growth has been demonstrated extensively in pores and osteoblasts evident on the surface of the material (Shors, 1999). Alpha and beta forms of TCP salt were released in the US in 2001 (Vitoss, Orthovita, Malvern, PA, USA). β-TCP has an ultrastructure that demonstrates "polyporosity," with its pores of varying diameter ranging from 1 to 1000 μm (Resnick , 2002). ß-TCP shows favorable characteristics in terms of fracture toughness, hardness and resistance to resorption as well as a controlled resorption rate (Viswanath et al, 2008).

Calcium sulphate (CS) or (plaster of Paris), results from the calcination of gypsum ($CaSO_4 \cdot 2\,H_2O$), which partially dehydrates to produce a hemi-hydrate ($CaSO_4 \cdot 1/2\,H_2O$). It is a non-physiological salt, but has been used for bone implant for a decyed (Dreesman, 1892). Osteoset (Wright Medical Technology, Inc, Arlington, TN), Calceon (Synthes, USA) and BonePlast (InterporeCross, USA) are available in the market in different forms pellet, block and as an injectable. Resorption of calcium sulfate is rapid, with total resorption observed as early as a few weeks, but longer resorption times have been reported depending on the formulation and configuration of the material, the size and local environment of the defect, and the presence of additives.

The fast resorption occurs by dissolution and replacement with trabecular bone has been shown (Kelly et al, 2001). It is approved for as bone filling material by orthopedics. CS potentially provides immediate stability, but requires augmented fixation, given its rapid resorption. The addition of HA has been shown to provide osteoconductivity, to allow integration with newly formed bone and to provide sufficient strength after the early healing phase, as for example in the injectable Cerament™ (Bone Support AB, Sweden) (Nilsson, 2003) (Figure 1.2). The latter material was utilized in this research and detailed descriptions of the injectable CS/HA material and its pre-clinical and clinical applications are described in chapter 2, (sections 2.4.2, 2.5.3) and chapter 5, (section 2.5.1).

Figure 1.2: Photograph of the commercially available Cerament ^{TM} Spinal Support, which consists of a set of two syringes, the top one contains the powder phase of the product which is composed of CS hemihydrate 60% and HA 40%, the bottom syringe contains the liquid phase Cerament|CTRU which is composed of water and iodine the opecifier.

1.3.3 Bioactive Glass

Biactive glass are a group of surface reactive glass-ceramic biomaterials and include the original bioactive glass, The biocompatibility of these glasses has led them to be investigated extensively for use as implant materials in the human body to repair and replace diseased or damaged bone.

An example of bioactive glass is silica based material with a biocompatible material such as calcium phosphate, forming a bond between the implant and the host tissue. It forms carbonated apatite, as with the calcium phosphate cements. A particulate Bioglass, Novabone (US Biomaterials Corporation, Alachua, Florida) has shown rapid replacement with native bone in rabbit tibial defects after 2 weeks, compared with 12 weeks for the replacement of HA. Cortoss (Orthovita, Malvern, PA) is composite polymeric cement with bioactive glass which forms a bond with bone, but the material itself does not resorb (Ilan and Ladd, 2003). The bioactive glasses are useful tool for osteoporotic fractures (such as vertebral compression fractures) and hardware augmentation in osteoporotic bone.

1.3.4 Polymers

Poly Methyl Methacrylate (PMMA) bone cement was first reported as useful in unstable long bone fractures and was popular for use in vertebral surgery (Jensen et al, 1997). The main disadvantage of PMMA is systemic and local toxicity that makes it an unpopular choice fororthopedic surgeon when other materials are available. Another popular resorbable polymer is poly(lactic-co-glycolic acid (PLGA) and poly lactic-L-acid(PLLA).

1.3.5 Mineral composites

Cancellous bone and mineral substitutes combined with DBM provide potential osteoinduction and osteoconduction. Opteform includes both DBM (using Osteofil, RTI) and cancellous bone, (Exatech, Alachua, Florida, USA). Allomatrix (Allosource + Wright Medical) is DBM combined with calcium sulfate. The formulations include putty, a block and injectable varieties. The combination of DBM with calcium sulfate has been shown to be relatively safe and effective in treating bone defects (Kelly et al, 2001). Another mineral composite is a combination of bovine collagen matrix, HA, and tricalcium phosphate (Collagraft, Zimmer, Inc., Warsaw, IN and NeuColl, Campbell, CA). It was one of the first bone substitutes and was approved by the FDA in 1993 (Ilan and Ladd, 2002) for treatment of orthopedic surgery to provide osteoconduction, and when used with autologous bone marrow aspirate demonstrates both osteoconductive and osteoinductive capabilities, perhaps even osteogensis. The later material, however, has lack of structural support (Scaglione and Buchman, 1997).

1.3.6 Injectable Cement

Injectable mineral cements have an advantage over blocks, granules and pellets, in that a custom fill of the defect is possible and a less invasive procedure is required. BoneSource is an injectable calcium phosphate cement approved for craniofacial defects (Howmedica Leibinger Inc., Dallas, TX). A multicenter FDA-monitored study demonstrated the effectiveness of BoneSource for metaphyseal fractures in various open and closed injuries in 38 patients, showing effectiveness and healing at least comparable to autograft bone (Dickson et al, 2002). Norian (Synthes USA, Paoli, PA) is a powdered calcium phosphate and calcium carbonate, mixed with soluble sodium phosphate (Ilan and Ladd, 2003). It is approved for general orthopedic use in metaphyseal defects. The advantage of the later is that it does not require a dry setting medium, which can be troublesome in a fracture setting. An additional calcium phosphate cement named alpha ABS (ETEX Inc, Cambridge, MA and Depuy) is supported by positive results in animal studies, and is approved for dental applications (Knaack et al, 1998). A summary of the commercially available composite ceramics is found in (Table 1, appendix1.2).

1.3.7 Proteins and growth factors

Bone marrow aspirate (BMA) is readily obtainable from the bone marrow of the anterior iliac crest. BMA is highly cellular including osteoprogenitor cells and a concentration of protein factors that stimulate bone growth in favorable conditions (Muschler et al, 2001; Muschler and Midura, 2002). The aspirate has become more popular in clinical practice among other osteoinductive material (Ilan and Ladd, 2003).

1.3.7.1 Plasma-Rich-Protein (PRP)

PRP is ultra-concentrated, centrifuged blood. It contains a mixture of growth factors and an autologous modification of fibrin glue. It has been suggested that PRP may enhance a 15-30% increase in trabecular bone density (Marx et al, 1998). The large number of platelets found in PRP and growth factors as platelet derived growth factors (PDGF) and transforming growth factor-β (TGF-β), as well as insulin-like growth factor-I (IGF-I). The potential effects of PDGF include the stimulation of mitogenesis of marrow stem cells and the stimulation of angiogenesis (Lieberman et al, 2002). Similary,TGF-β has been shown to stimulate mitogenesis of precursors, to stimulate the deposition of a collagen matrix for connective tissue healing and bone formation, and inhibit bone resorption (Mohan and Baylink, 1991).

1.3.7.2 BMPs

BMP-7 and BMP-2 are the available bone inducer for clinical use. BMP-7 is also known as OP-1, (Osteogenic Protein-1, Stryker Biotech, Hopkinton, MA) and is a human-recombinant protein that has received humanitarian device exemption (HDE) by the FDA. OP-1 has shown huge effect in animal studies and has shown advantageous healing over autograft in clinical trial (Friedlaender et al, 2001). It is used in spinal fusions using a bovine-derived collagen sponge as the carrier. But antibodies to both the bovine collagen and OP-1 have been identified (Friedlaender et al, 2001). No sides effect have been reported with the antibodies however, to date and the significance of antibody formation is unknown (Friedlaender et al, 2001). In animal studies, the bone regeneration has been successful using rhBMP-2. Prospective, randomized trials evaluating spinal fusion demonstrated healing and improved outcomes in the patients treated with rhBMP-2 and a HA/β-TCP substitute, compared with fusion with autografts (Lieberman et al, 2002; Boden et al, 2000).

1.4 Scaffold-cell interaction

1.4.1 Scaffolds

Scaffold materials suitable for tissue engineering vary in porosity, composition, and biodegradability to best mimic the requirements of the tissue to be replaced. Bone is a complex tissue with highly porous morphology in the spongy bone and with solid compact structure in the cortical bone. The tissue engineering of bone requires strategies to design three dimensional (3D) scaffolds that closely mimic the anatomical organization of bone and its tissue matrix. Changes in scaffold geometry may impact on the flow of medium across the scaffold and thus affect the supply of gases and nutrients and the removal of metabolites (Detamore and Athanasiou, 2005). The number of pores of various scaffolds was related to increased vascularisation and osteointegration in vivo, but the increased pore volume reduced the mechanical stability of the scaffold (Karageorgiou and Kaplan, 2005; Tanner, 2010).

Surface modifications of biomaterials can enhance cell adhesion. The use of the tri-peptide sequence of the amino acids (arginine, glycine, aspartic acid) promoted cell adhesion (Hubbell, 2003; Langer and Tirrell, 2004). Using alkane thiol self-assembled monolayers with well-defined chemistries (OH, CH_3, NH_2 and COOH) and fibronectin-coating, sustained the growth of myoblasts and osteoblasts (Ulman, 1996). Wiedmann et al, (2007) studied the rate of osteoblast proliferation and bone formation in 16 different types of commercially available biomaterial scaffolds. The results showed that 4 of the tested scaffolds had a better proliferation rate and cell density and those were collagen based, hyaluronic acid-based membranes and an organic silicone- based membranes. Paradoxically, Bio-oss (deproteinized sterilized bovine bone) showed the lowest proliferation rates. Further studies have investigated the type of matrix material

that would support the MSCs and affect their differentiation (Krebsbach et al, 1997). Jager et al (2005) confirmed that collagens I and III and poly lactic –L- acid (PLLA) porous scaffolds induced MSC differentiation even without using osteogenic media.

Finally, the effect of nano-topography technology on matrix fabrication has been investigated. Dalby et al (2007) found that introduction of nano-scale patterns into surfaces could stimulate the osteogenic potential of MSCs. It also controls MSC growth and maintenance (McMurray et al, 2011). The rationale behind the biomimetic scaffold is that it mimics the extra cellular matrix's natural support for the cells, therefore a nano-scaled structure could enhance cell attachment, proliferation, and differentiation (Liao, et al, 2008).   Moreover, there have been some indications that scaffold geometry which restricted vascular invasion, preferentially produced cartilage instead of bone (Kuboki et al, 1995).

1.4.2 Tissue engineering and vascularisation

Sufficient blood supply is required to achieve successful tissue regeneration. Reconstruction of large bony defects is another area where lack of vascularity is a main obstacle for complete regeneration. Enhancement of angiogenesis improves the healing of diseased tissues (Hughes et al, 2004). The process of vascularisation requires angiogenesis, the formation of new vessels from endothelial precursors. One strong stimulus for vascularisation is hypoxia (Bicknell and Harris, 2004). Vascular endothelial growth factor (VEGF) is the best known, which stimulates cells to produce matrix metalloproteinases (MMPs), degrading the surrounding extracellular matrix. This in turn creates a highly pro-angiogenic environment prompting endothelial cell migration and proliferation. Subsequently, pericytes proliferate and migrate towards newly formed vessel sprouts and induce maturation by forming a single cell layer around the vessel sprout (Bruick and McKnight, 2001; Hoeben et al, 2004). A basic fibroblast growth factor (bFGF/FGF2) has high angiogenic potential. This factors induce endothelial cells to produce both MMPs and VEGF and increases VEGF receptor expression thus enforcing the VEGF signal and locking endothelial precursor cells into a mature phenotype. Like VEGF, FGF2 stimulates endothelial cell migration, pericyte attraction, and matrix deposition (Presta et al, 2005). Both growth factors act synergistically and may be applied together to scaffolds achieving fully developed mature blood vessels (Asahara et al, 1995; Giavazzi et al, 2003; Laschke et al, 2006).

1.5 Promotion of osteogenesis within muscle flap

Muscle is a rich source of osteoprogenitor cells and has the advantage of being intrinsically osteogenic. Skeletal muscle cells by nature maintain multilineage potential and satellite cells are capable of adiopogenic and osteogenic differentiation (Asakura et al, 2001; Wada et al, 2002).

This is seen most dramatically in genetic diseases such fibrous dysplasia ossificans progressiva (FOP) where patients develop a second skeleton as muscle spontaneously ossifies (Shore and Laplan, 2008). Heterotopic ossification of muscle is also common after joint replacement surgery and following blast injuries (Stoltny et al, 2007; Covey, 2006). Although these are worrying medical conditions, they might suggest novel opportunities for regenerative medicine to address circumstances where it is necessary to grow large amounts of new bone in areas that require a rich blood supply. The relative value of the various different approaches to bone regeneration will only become obvious with more research. Understanding the patho-physiology of these medical conditions may add some light and enlighten the researcher looking at novel options in regenerative medicine.

Chapter 2

Literature Review

Table of contents

2 Literature Review

2.1 Mandibular reconstruction with Mesenchymal stromal cells (MSCs) & Osteoprogenitor cells

2.1.1 The application of osteoprogenitor cells and bio-scaffold

Schliephake et al (2001) studied the implantation of autogenous osteoprogenitor cells in pyrolised bovine bone (porous calcium phosphate) scaffolds in segmental bone defects (35 mm) in the mandible of 8 sheep. These were divided into the experimental group (scaffold + osteoprogenitor cells) and the control group (scaffold only). After 5 months significantly more bone formation was found in the experimental group (p < 0.0280. The amount of bone regenerated was moderate (34%). The authors claimed that this might have been due to insufficient numbers of osteoprogenitor cells. The authors harvested the cancellous bone from the iliac crest of the animal model, which may raise the question as to how clinically applicable this method is since the main aim of bone bioengineering is to avoid donor side morbidity.

Groger et al (2003) investigated bone regeneration with periosteum stem cells in a in a bioabsorbable three-dimensional polymer fleece as a scaffold, in critical-size mandibular defects (20 mm x 10 mm) in 6 minipigs. In 4 cases the defect was treated with cells and scaffold (experimental group), and in the control group (n=2) the scaffold was applied alone. Radiographic assessment at 90 days (n=3), and 180 days (n=3) following surgery showed more bone formation in experimental group. The small sample size made it difficult to draw any valid conclusions.

Alhadlaq and Mao (2003) tissue engineered a human-shaped mandibular condyle from a single population of rat MSCs that had been induced to differentiate into the chondrogenic and osteogenic lineages and were seeded into a photopolymerized poly ethylene glycol diacrylate-based (PEGDA) hydrogel. Microscopically, mineral

deposition at the osteogenic layer and extracellular matrix in the chondrogenic layer was detected.

Abukawa el al (2004) used MSCs seeded onto a poly-DL-lactic-co-glycolic acid (PLGA) scaffold to fill full thickness mandibular defects (20 mm x 20mm) in one minipig. The constructs (n=2) were placed in 2 of the four created defects. One unseeded scaffold and one empty defect served as controls. After 6 weeks the experimental sites showed uniformly radiodense tissues distributed throughout with complete bony bridging between native bone and the constructs. Histological examination showed highly cellular bone with bony trabeculae identified in the centre. As only one animal model with 4 defects was used it is difficult to draw any significant conclusions. There was no quantitative assessment for the amount of new bone formation and no in vitro assessment of the osteogenic potential for the seeded cells.

Ren et al (2005) investigated the regeneration of critical-size (12 mm x 5 mm) mandibular defects in 12 New Zealand white rabbits using MSCs in PLGA. The rabbits were divided into three groups; (1) MSCs and PLGA, (2) PLGA alone and (3) empty defect. Histological assessment at 12 weeks showed bone formation from the rim towards the centre with complete bony union in the experimental group. No histomorphometric analysis was performed.

Henkel et al (2005) applied biomatrices, made from 60% HA and 40% beta-tricalciumphosphate, with osteoblasts to critical-size defects (>50 mm^3) in the anterior part of the mandible of 16 minipigs which were divided into 4 groups; (group 1) the defect was kept empty, (group 2) suspension of cultured autologous osteoblasts was applied in the defect, (group 3) porous biomatrices were used alone, and (group 4) cells and scaffold. Five weeks postoperatively there was a reduction in the size of

the defects in all groups, with the greatest apposition of bone in group 2 (54%) and the least in the control group (44%). Morphometric analysis revealed that the greatest defect reduction was observed in group 3, with a mean of 72% of the defect filled by new bone. The authors suggested that the poor result with the osteoblasts might be due to inadequate nutrition of the cells residing in the carrier material leading to a limited stimulation of ossification. The age of the animals may also have contributed to these finding. The animals were sacrificed at 5 weeks which was insufficient for complete bone regeneration and ossification. The defect was a three-walled defect and the periosteum was left intact which might have contributed to the bone regeneration.

Wu et al (2006) used BMSCs seeded in porous β-TCP in segmental defects created in the mandible of dogs. These were divided into; group 1, BMSCs and β-TCP, group 2, β-TCP alone, group 3, autologous bone grafts. After 12 weeks complete bone regeneration in the mandibular defects in both groups 1 and 3 was obvserved. Volume density, histomorphometric and mechanical testing were not evaluated for the newly formed bone.   Furthermore, the authors did not mention the sample size of the experimental group or that of the created defect.

Mankani et al (2006) studied human bone marrow stem cells (BMSC) on hydroxyl apatite and tricalcium phosphate scaffolds (HA /TCP) in bone defects in the calvarial bone of 34 mice, in 22 of which they also created 7 mm mandibular defects. In the mandibular cases, the experimental group (n=15), received BMSCs and HA/TCP and the control group (n=7) received scaffold alone.   Histological examination was carried out on a semi-quantitative logarithmic scale with a score of 0 corresponding to no bone formation and 4 corresponding to bone formation occupying greater than one half of the section. The bone formation in the mandibular cases scored 1.9. The

bone had a lamellar structure oriented around individual particles of the scaffold. The finding of poor bone formation in the mandible was blamed on the mobility of the mandible after surgery. A subjective tool was used for the assessment of the quantity of bone. Mechanical testing was not applied to the mandibular bone.

Qing et al (2006) reported on the reconstruction of 25 mm x 10 mm segmental mandibular defects in 10 Guanzhong goats with mesenchymal stem cells seeded into natural poritos (coral granules) that were implanted into a titanium framework stent (experimental group n=5). The other 5 received the poritos alone (control). At 16 weeks new bone was observed on the surface and in the pores of natural coral in all specimens from the experimental group. But no quantitative assessment was carried out and the titanium framework obscured the X-ray assessment of new bone formation.

Wang et al (2007) evaluated neonatal rabbit MSCS in biomimetic nano-hydroxyl apatite/polyamide (n-HA/PA) composite scaffolds for the repair if critical-size mandibular defects (12 mm x 8 mm) in 76 rabbits. One group received pure n-HA/PA and the other group received n-HA/PA scaffolds loaded with MSCs. At 12 weeks, histological and microradiographic assessments showed that the density and the quantity of bone maturation were almost the same in both groups but the group that received the MSCs had enhanced bone formation in the early stages. The authors did not assess the regenerated bone mechanically in vivo. The use of MSCs from neonatal rabbits was not clearly justified.

He et al (2007) studied the reconstruction of segmental (30 mm) mandibular defects using BMSCs with β-TCP scaffolds in six beagle dogs. Data on the shape of the dogs` mandibles were obtained from computed tomographic scanning. 3D mandibular models were constructed using stereolithography and the defects were

created on the model to allow fabrication of the β-TCP scaffold using CAD-CAM. The dogs were divided in two groups; the experimental group (n=3) that received BMSCs and scaffold, and the empty scaffold (control) group (n=3). Three months postoperatively radiographic assessment showed a higher radiodensity mean (0.60) in the experimental group and the mean compressive strength for the generated bone in the experimental group was 102.77 N/mm^2 (control group, 42.9 N/mm^2). The authors introduced a novel method for fabricating scaffolds. The study was conducted on a growing animal model (1-2 year old), this will have augmented the potential for bone regeneration. Despite the small sample size the study demonstrated the importance of the BMSCs in bone regeneration.

On a larger sample size Yuan et al (2007) investigated BMS cells for regenerating mandibular bone defects (30 mm) using β-TCP in 16 adult mongrel dogs. The animals were divided into 3 groups; experimental group (n=6) that received the seeded scaffold, an autograft group (n=4) that received autologous mandibular bone, and a β-TCP only group (n=6). At 32 weeks minimal bone formation with only fibrous connection was observed in the β- TCP alone group while bony union was seen in the experimental group. Three point biomechanical bending testing showed that the regenerated bone in the experimental group had properties that were comparable to those of the contralateral non-operated bone as well as the bone in the autograft group. The study emphasised the importance of the osteoproginator cells in bone regeneration. Unfortunately, the authors did not provide the details of the radiolographic assessment.

Palarie (2008) investigated the use of a collagen/calcium phosphate scaffold and bone marrow aspirate for new bone formation in critical-size jaw defects in 30 New Zealand white rabbits. Defects of different sizes were created; <5 mm (n=10), <10

mm (n=10), and >10 mm (n=10). After 4 weeks all 3 groups demonstrated new bone formation that had a microscopic structure similar to that of mature bone. No statistical analysis was performed and assessment only at 4 weeks seems a little too early to draw any conclusions.

Schliephake et al (2009) tested in vitro cultivation techniques on bone regeneration. Bilateral critical-size defects (5 mm) were created in 30 thymic nude rat mandibles and were constrcted with scaffolds seeded with osteoprginatior cells. The cells were seeded in three different scaffolds; (a) porous calcium carbonate, (b) custom-made porous scaffolds of mineralized collagen, and (c) TCP. The cases were divided into four groups; group 1, empty scaffolds (control), group 2, scaffold seeded with cells and kept under static conditions for 24 hours before implantation, group 3, scaffold seeded with cells cultivated for 14 days under static conditions, and group 4, scaffold seeded with cells cultivated for 14 days in a bioreactor (perfusion chamber connected to a pump system which allows peristaltic pumping of fresh medium, and is kept at a controlled oxygen level). After 6 weeks most of the grafted cells could no longer be detected and group 2 had the highest bone volume density (21.3%) but there was no statistically significant difference between the groups. The disappearance of the seeded cells was attributed to the cells being more prone to apoptosis due to their differentiated nature. The appliactuion of the cells was associated with more bone formation. The failure of the dynamic culturing (bioreactor) to contribute to better results may be attributed to the volume of the scaffolds which was small.

Zhao et al (2009) assessed the effects of apatite-coated silk fibroin (mSS) seeded with osteogenically induced autologous BMSCsin the reconstruction of bilateral inferior mandibular border defects (20 mm x 10 mm) in 14 mongrel dogs The defects were randomly allocated into the following groups; (1) silk fibroin scaffolds (SS) alone

(n = 4); (2) mSS alone (n = 4); (3) SS with BMSCs (n = 4); (4) mSS with BMSCs (n = 4) and (5) autogenous bone (n = 4),(6) untreated negative controls (n = 4). New bone formation was observed from 4 weeks post-surgery, and the defect site was completely regenerated after 12 months in group 4. In group 3 more residual silk scaffolds remained at the centre of the defect compared. The bone mineral density (BMD) of group 4 at 12 months was close to that of untreated bone (p > 0.05). There was no significant difference in bone formation between groups 4 and 5 (p > 0.05). The study did not demonstrate the biocompatibility, or cytotoxicity characteristics of the material. The long follow-up period is unusual but makes comparison with other research difficult.

Wang et al (2009) performed bilateral vertical alveolar ridge augmentation with β-tricalcium phosphate (TCP) and autologous osteoblasts in the mandible of 6 beagle dogs, these were divided into 3 groups; group A, β-TCP/osteoblasts (n=4), group B, β-TCP alone (n=4), and group C, autogenous iliac bone (n=4). A sequential fluorescent labelling method using tetracycline hydrochloride, calcein, and alizarin red was carried out. The main objective of the later method was to assess new bone formation and mineralization over time. The radio-opacity of the augmented ridges increased and the bony interface between the graft and host bone was obscured. The fluorochrome labelling showed intense fluorescent areas in the centre of the grafts in group A at 4, and 12 weeks however, this remained inferior to group C. Although this paper did not fit the inclusion criteria for the regeneration of critical-size defects in the mandibular bone the authors represented a clear and useful methodology, using bone labelling, for the assessment of bone regeneration in a tissue engineered construct in vivo.

Von Wilmowsky et al (2010) used autologous autoclaved bone grafts seeded with BMSCs in a collagen matrix to repair 3 cm x 2.5 cm lower border defects in the mandibles in 8 adult pigs. The animals were divided into two groups; experimental group, autoclaved bone segment filled with BMSCs in collagen matrix, control group, autoclaved bone with collagen matrix alone. After 120 days the autoclaved grafts served as a matrix (osteoconductive scaffold), which allowed the ingrowth of newly formed vessels from the adjacent bone. Histology and microradiographic assessment for the experimental group revealed that there was bone bridging. Whereas, in the control group there were sporadic signs of bone formation and remodelling within the graft. Using the autoclaved graft without BMSCs appeared to result in a foreign body reaction which gradually resorbed the graft and replaced it by fibrous tissue. The method presented here has a limited clinical application especially in invasive malignant lesions. However, the study highlights the importance of persevering the structural charcaertistics of the bone to stimulate regeneration and osseoinduction.

Porous nanohydroxyapatite-polyamide scaffolds (n-HA/PA) were tested by Guo et al (2012). The biological activity of n- HA/PA biomaterials was initially characterized in vitro. For the in vivo study, bilateral critical-size bone defects in the angle (15 mm× 8 mm) and body (15 mm× 8 mm × 2.5 mm) of the mandible of thirty-six New Zealand white rabbits were created. The animals were divided as follows; for the mandibular angle, pure n-HA/PA implants (n=12 defect), Polyethylene (PE) (n=6), and blank controls (n=6) and the implantation of BMSC-n-HA/PA constructs (n=12). For the mandibular body group,   (group 1) n-HA/PA (n=18 defects), and (group 2) BMSC-n-HA/PA (N=18). Radiographic and histological analysis at 12 weeks showed quick new bone formation restoring the critical-size defect in the marrow-sparse region of the mandibular angle in groups that were grafted with BMSC-n-HA/PA. New bone formation was evident much earlier and in more significant quantities in the

mandibular body groups. Histologically, at 12 weeks the new bone formation of both the n-HA/PA and the BMSCn-HA/PA groups was significant and little difference could be detected. The source of BMSCs bone marrow used in vivo was not clearly demonstrated. The radiographic assessment for the experimental groups was not consistent i.e. plain radiograph was undertaken for mandibular angle group, whereas, micro-CT was performed for the mandibular body group. The resorption rate of the implanted construct was not discussed in relation to bone formation.

Bhumiratana et al (2013) used autogenous adipose-derived stem cells (ASCs) seeded in fabricated trabecular bone of adult bovine knees that were cultured in osteogenic medium in perfusion bioreactors for 3 weeks. These constructs were then used to replace the condyles and a portion of the ramus in 6 minipigs (intervention group) with another 6 receiving only decellularized bone block (control group). All grafts were rigidly fixed using 2.0 mm titanium miniplates. The engineered bone grafts significantly restored the condyle height compared to the control at 3 and 6 months. Micro-CT and histological analysis showed infiltration of the native bone into the proximal part of the intervention group only. The majority of the implanted engineered bone graft was intact while a significant portion of the bone block in the control group was resorbed in the first three months. The process of culturing ASCs and the scaffold in a bioreactor for 3 weeks adds novelty to this study. However, the author did not study the interaction between the scaffold and ASCs. Only descriptive data were presented with the quantity of the new bone not assessed.

2.1.2 The application of osteoprogenitor cells, BMPs, and growth factors

Arosarena et al (2003) studied the regeneration of critical-size (4 mm) mandibular body defects with bone morphogenic protein (BMP) and bone marrow cells in bovine

collagen and calcium hydroxyapatite, in 37 male Fischer rats. The rats were divided into five treatment groups; bone marrow cell suspension (group 1), synthetic bone matrix consisting of bovine collagen and calcium hydroxyapatite cement (group 2), synthetic bone matrix and marrow cells (group 3); matrix with 100 µg BMP (group 4), and matrix with BMP and marrow cells (group 5). After 8 weeks there were more osteoid and larger marrow spaces in the bone samples of groups 4 and 5 than in groups 2 and 3 (p < 0.001). There was more significant fibrous tissue ingrowth in groups 2 and 3 (p < 0.001). The volumes of mature bone, new bone, and the remaining cement did not differ significantly among all groups. There was an almost equal amount of osteoid and marrow spaces in both groups 4 and 5, which questions the role of the marrow cells and their effect on bone regeneration.

Chen et al (2004) combined rabbit MSCs and rhBMP-2 in natural coral scaffolds that had been carefully moulded into the shape of a 4-year-old child`s mandibular condyle that was then implanted into pockets created in the back of 10 nude mice. 6 scaffolds (experimental group) received the cells and 4 scaffolds were left empty. After 2 months new bone grafts in the shape of a human condyle had been successfully developed. Histologically, new bone was observed on the surface and in the pores of the natural coral in the cell seeding group, whereas in the control groups there was no evidence of osteogenesis. The authors did not use any tools for qualitative or quantitative assessment.

A study by Kim et al (2013a) treated 5 rabbit mandibular lower border defects (1.5 cm × 0.7 cm) with electrical stimulation and rhBMP-2 application. A custom scaffold was developed consisting of an inner component prepared by seeding a collagen sponge with hBMSCs and hydrogel and an outer component made of polycaprolactone (PCL). An electrical stimulation device was installed between the inner and the outer

layers. The animals were divided into three groups; group 1, collagen sponge with

hBMSCs and rhBMP-2 but no electrical stimulation, group 2, collagen sponge with

hBMSCs and rhBMP-2 with electrical stimulation 1 week after surgery, group 3,

collagen sponge with hBMSCs and electrical stimulation and rhBMP-2 injection into

the defect site directly (5 µg/defect) 1 week after the end of the electrical stimulation.

Four weeks after surgery group 3 showed more new bone formation, compared with

Groups 1 and 2. Group 2 showed a higher bone volume (BV) by 260 % ($p < 0.01$)

compared with group 1, and group 3 showed a higher BV by 442 % ($p < 0.01$)

compared with group 1. The resorption rate of the scaffold used and how this related

to the pattern and amount of bone formation was not discussed, but PCL took a

longer time to resorb. The early sacrifice of the animals (4 weeks) did not allow

assessment of bone formation to fill larger bone defects.

Su et al (2013) investigated the dual delivery of bone morphogenetic protein-2 (BMP-

2) and basic fibroblast growth factor (bFGF) on polylactic-poly Glycolic

acid/Polycaprolactan/nano-hydroxy apatite (PLGA/PCL/nHA) loaded with vascular

stents composed of poly(L-lactide-co-caprolactone)/collagen/nHA (PLCL/Col/nHA)

for bilateral bone defects (26 mm× 5 mm × 3 mm) in 36 rabbits. The cases were

divided into six groups; (group A) scaffold alone (n = 6); (group B) BMSCs/scaffold (n

= 6); (group C) BMSCs/bFGF/scaffold (n = 6); (group D) BMSCs/BMP-2/scaffold (n =

6); (group E) BMSCs/bFGF/BMP-2/scaffold (n = 6); and (group F) empty (n = 6). New

bone formation was found in the implanted area in all groups, except group F. The

amount of new bone formation in group E & D was significantly more than the other

groups both at weeks 4 and 12. At 12 weeks groups D and E showed complete bone

regeneration with group E showing more mature new bone and blood vessel

formation. The paper presents a comprehensive in vitro experiment and was

complemented with an in vivo application of different treatments. The author

demonstrated the result of in vitro experimentation about the release kinetics of different growth factors in relation to the use of a scaffold/hydrogel, but did not comment clearly if the same constructs were used in animal studies as well.

2.2 The application of injectable scaffold in vivo

2.2.1 The use of injectable bone substitutes in heterotopic sites

A trial by Yamada et al (2003) was conducted to determine the efficacy of the combination of fibrin glue, β-TCP and MSCs, in providing a three- dimensional template for bone regeneration in heterotopic sites in 18 rats. The animals were assigned into one experimental group which received (MSC/TCP and fibrin glue admixtures) and one control group which received (fibrin glue and TCP admixtures). At 8 weeks only the experimental group had subcutaneous nodules that were hard and resisted compression. Histologically, the nodules contained bone. Osteopontin and osteocalcin were identified in the experimental. Quantification of the amount of bone formation using for instance micro-CT or histomorphometry was not performed. The bone quality was also not assessed.

Trojani et al (2006) used injectable hydroxyapatite/ tri-calcium phosphate (HA/TCP) particles in suspension in self-hardening Si-hydroxypropylmethylcellulose (HPMC) with BMSCs. 30 C57BL/6 mice received the HPMC/HA-TCP with stem cells in two sites; subcutaneous (SC) tissue at dorsal skin between the scapulae and intramuscular (IM) in the hind leg. The animals were divided into three study groups; group1, HPMC mixed with BMSCs, group 2, HMPC/HA-TCP without BMSCs, and group 3, HMPC/HA-TCP mixed with BMSCs. At 8 weeks there was no difference between the injection sites. 7 implants out of 10 were full of new bone. The woven bone was in contact with the ceramic, and numerous multinucleated giant cells were

attached to HA/TCP particles. Histological analysis was the only tool used for the assessment of the bone formation.

Kang et al (2008) investigated the use of an apatite-coated poly (lactic-co-glycolic acid) PLGA microsphere injectable scaffold for bone tissue engineering. The constructs were injected into the subcutaneous dorsum of 12 athymic female mice. These were divided into 2 groups; group 1 (n=6) implanted with apatite coated PLGA and osteoblasts and group 2 (n=6) implanted with plain PLGA and osteoblasts. After 6 weeks osteoblasts implanted in group 1 induced bone formation in the space between the microspheres and this was statistically significantly more than in group 2. Immunohistochemical and biomechanical analysis of the tissue-engineered bone would have been useful to determine its quality. The authors did not comment on the flow rate of the scaffold, injectability and the setting time.

Kim et al (2009) developed an injectable pH/thermo-sensitive hydrogel containing human MSCs and recombinant human bone morphogenetic protein-2 (rhBMP-2). The hydrogel co-polymer was injected subcutaneously on the dorsum of 20 nude mice. The animals were divided into 4 groups; group 1, hydrogel only, group 2, hydrogel with rhBMP-2, group 3, hygrogel and hMSCs, and group 4, hydrogel/rhBMP-2/hMSCs. Fluorescence microscopy at 7 weeks showed significant fluoresence that was uniformly distributed throughout the implanted hydrogels. This meant that the MSCs were viable and proliferating. Group 4 had more significant calcium/mineralization staining and ALP activity. However, there was no actual fomation of bone possibly due to the lack of osteoinductive potential of the hydrogel.

2.2.2 The use of injectable bone substitutes in orthotropic sites

Gauthier et al (2003) tested the feasibility of using two injectable scaffolds namely a biphasic calcium phosphate with cellulose polymer (IBS) and calcium phosphate cement (CPC). A critical-size defect was prepared in the femoral bone of 10 rabbits. The defects were filled with; group 1, IBS (40-80 µm particle size), group 2, IBS (80-200 µm particle size), and group 3, CPC. After three weeks both materials were found to be biocompatible and bioactive. Newly formed bone was found in close contact with the IBS granules on the periphery and within the bone defect which using microtomography was shown to create an interconnected new bone network. I group 3, the newly formed bone only developed on the surface of the cement. This paper introduces a new idea of using microtomography techniques to describe bone colonisation as a result of using an injectable Calcium phosphate scaffold. No mechanical testing or quantitative analyses were performed. Data relating to the setting time of the material in vivo was omitted.

Mankani et al (2008) used human BMSCs along with HA/TCP particles mixed within fibrin glue. The constructs were implanted either into the dorsal subcutaneous space or onto the calvarium of 23 immunodeficient mice. Two techniques were tested, injection which was considered as the experimental group and wide surgical exposure which was considered as the control group. The grafts were harvested at different time scales ranging from 7 to 110 weeks. Comparable results were recorded between the subcutaneous and calvarial sites and there was no difference between the two techniques concerning the amount of bone formation, bone morphology and mechanically properties. The long term follow-up was useful but it would have been ideal if the grafts were radiographed using computerized tomography for assessment of bone regeneration and union to the underlying native bone.

Yoshimi et al (2009) used self-assembling peptide nanofibers (pura-matrix {PM}), dog platelet-rich plasma (PRP), and dog MSCs as injectable scaffolds for the treatment of bilateral mandibular defects (10 mm x 10 mm). The cases were randomly divided into the following groups; (1) empty defect, (2) PM alone, (3) PM/PRP, (4) PM/MSCs, and (5) PM/MSCs/PRP. At 8 weeks the bone regeneration by group 5 showed lamellar bone, whereas less mature bone was observed in group 4. Histomorphometrically, the percentage of newly formed bone areas comprised 12.39% (group 1), 25.28% (group 2), 27.72% (group 3), 50.07% (group 4), and 58.43% (group 5). The paper presented another dimension for the fabrication of an injectable scaffold using nano-fibers. The results are promising, but it would have been more clinically useful if it has been tested on a continuity defect. The authors did not give the actual sample size and the injectability, setting time, and consistency of the material were not provided.

Stephan et al (2010) tested the injectable biopolymer chitosan together with an inorganic phosphate seeded with MSCs and BMP-2 to regenerate calvarial critical-size (8 mm) defects in 30 male rats. The animals were divided into five groups of 6 animals each; (1) chitosan gel, (2) gel loaded with MSCs, (3) gel loaded with BMP-2, (4) gel loaded with both MSC and BMP-2, (5) empty defect. At 8 weeks new areas of bone growth were seen in the defects of all the treated animals. Group 4 had significantly more bone regeneration. Immunohistochemistry detected viable MSC cells and confirmed their contribution to the new bone formation. The idea of using green fluorescent protein labelled MSCs was a novel way to test cell viability and proliferation. However the flowability of the injected material, its consistency, and setting time were not discussed. Further, qualitative analysis for the regenerated calvarial bone was not assessed either by mechanical testing or histomorphometric analysis.

Lee et al (2010b) compared apatite-coated porous poly lactic-co-glycolic acid (PLGA) microspheres versus coated PLAG non-porous microspheres as injectable bone substitutes in the regeneration of critical-size defects in the calvaria of 20 mice. In 10 cases the defect was left empty (control), 5 received the apatite-coated porous PLGA and 5 received the coated non-porous PLGA. After 8 weeks new bone was formed in the space between the microspheres in the non-porous PLGA while the porous microspheres showed new bone formation at the interconnected pores as well as in the void space between microspheres. There was significantly more bone formation at the mid-portion of the regenerated bone in the porous PLGA group. The in-vivo grafting of the scaffold was performed leaving the periosteum intact. This could have masked the effect of the test scaffolds. There was no radiographic assessment or qualitative analysis applied.

Lippens et al (2010) investigated the use of chemically modified pluroic F127 hydrogel (Plu-ALA-L) and pre-differentiated BMSCs in non-critical-size unicortical tibial defects in 8 goats. The cases were divided into 4 groups; (1) gelatin CultiSpher-S microcarriers/Plu-ALA-L/BMSCs, (2) hydroxyapatite tubular/Plu-ALA-L/BMSCs, (3) empty defects, (4) Plu ALA-L alone. At 2 and 4 weeks bone regeneration in groups 1 and 2 was comparable to groups 3 and 4. However, at 6 and 8 weeks more bone was seen in groups 1 and 2. The assessment at 8 weeks was too early for complete bone regeneration. The use of polymers alone is inadequate for the reconstruction of continuity critical-size defects due to their low mechanical properties.

Truedsson et al (2010) investigated the capacity of Calcium sulphate 60%/ Hydroxyapatite 40% (Cerament^{TM}), an injectable bone substitute, to guide bone generation from a cortical surface. Twenty-seven male Sprague–Dawley rats (9 weeks; 300–320 g) had 1.5 x 5 mm deep holes drilled 5 mm below the tibial growth

plate. A titanium screw (2 mm x 7 mm) was screwed 4 mm into the bone. After screw implantation, Cerament putty was placed around the screw on the tibial bone surface. On the contralateral tibia, the same amount of Cerament[TM] was applied onto the bone surface in a 3-mm-thick layer. Another Eighteen male rats (9 weeks; 300–320 g) were sham-operated, in one tibia. In addition, three untreated rats were sacrificed at the start of the study. In the 3-week follow up of the experimental group, three out of nine rats were swollen around the material. When the tissue was aspirated, a clear liquid was obtained. The soft tissues had normal colour. Histologically, in both groups, the mean thickness of the bone cortex increased significantly from 473± 58 mm at day 0 to 1193 ± 255 mm (Cerament[TM] cases) and 942 ± 323 mm (sham) after 3 weeks. In the Cerament [TM] group, the mean new bone thickness remained constant (1258 ± 288 mm) until the end of the experiment at 12 weeks, while the sham group demonstrated a return to initial cortical thickness (591 ± 73 mm) at 12 weeks. The newly formed bone in the Cerament[TM] group was highly trabecular after 3 weeks but attained a normal trabecular structure of the cortex after 12 weeks. The authors concluded in this study, that the Cerament[TM] may guide bone generation from an intact cortical bone surface and may become a useful alternative to autologous bone, both to fill defects and to increase bone volume by cortical augmentation. The authors injected the cement directly on cortical bone, without creating a defect in bone to simulate clinical application of the cement.

Dumas et al (2012) evaluated the ability of injectable lysine-derived polyurethane (PUR)/allograft biocomposites to promote bone healing in critical-sized (15 mm) calvarial defects in 70 rabbits. The biocomposites exhibited favorable injectability, characterized by a low yield stress to initiate flow of the material and a high initial viscosity to minimize the adverse phenomenon of extravasation. The animals were divided into four study groups; (A) (n=20) empty defect, (B) (n=20) injectable calcium

phosphate cement (CPC), (C) (n=20) PUR/allograft, and (D) (n=10) BMP-2 with PUR/ allograft. At 12 weeks group A showed minimal bone formation near the edges of the defect. Bone ingrowth was observed around the perimeter of group C with traces of bone in the centre and extensive polymer. Group D revealed extensive bone growth around the composite as well as throughout the pores of the material. In 5 of the animals bone had completely bridged the defect and this was significantly greater than the other treatment groups (p < 0.0009). The paper introduced a new strategy for the reconstruction of bone defects by combining allograft and alloplast in an injectable form. The quality of the new bone was assessed via mineral density but it would have been useful if 3D evaluation of the bone volume and architecture was obtained with micro-CT analysis.

Xia et al (2012) investigated bone engineering using BMSCs and an injectable sodium alginate/gelatin scaffold in rabbit models. The phenotype of the BMSCs was examined by mineralized nodule formation and type I collagen expression. The biocompatibility of the scaffold and osteogenic cells were examined by decalcified histological sections. 15 New Zealand rabbits were randomly divided into three groups; (A) scaffold-cell group (n= 6), (B) scaffold group (n= 6), and (C) control group (n =3). Critical-size calvarial defects (15 mm) were created and the scaffolds were injected one week after surgery. Twelve weeks after implantation, the defect region in group A was completely filled with bone tissue, and the edge was nearly undetectable. Histological assessment showed mature bone tissue with osteons. The mechanical properties, setting time, and consistency of the material were not discussed and no quantitative assessment of bone formation was performed.

So any further investigations on this system, would have been essential.

2.3 Human Clinical trials

2.3.1 Reconstruction of the jaw using scaffold and BMP

Moghadam et al (2001) presented a case of mandibular reconstruction using a BMP bio implant in a 40 year old patient following resection of an ameloblastoma in the mandible. The BMP with a poloxamer-based gel was packed in a pocket created by the buccal muscle and the reconstruction plate. Three pieces of allogenic bone impregnated with human BMP were placed below the reconstruction plate. Radiographic and histological assessment (9 months) of the newly formed tissues revealed viable bone with numerous osteocytes and vascular channels beneath a layer of connective tissue. The role of this biomaterial in the reconstruction of the mandible was not discussed and the authors did not mention from which area the biopsy was taken.

A prospective study conducted by Ferretti and Ripamonti (2002) compared bone regeneration in mandibular continuity defects using either BMP or autologous bone grafts. The BMP was mixed with demineralized bovine bone matrix to form the construct (OD). Thirteen patients with segmental mandibular defects were divided into; (A) 6 who received the OD and (B) 7 who received the autologous bone graft. Both grafts were loaded into a preformed titanium mesh. Patients were followed up clinically and radiographically at 1 and 6 weeks, 3, 6, and 12–month till 4 years post implantation. Biopsy was taken for histological and morphometric analysis at 3 months. Radiographic analysis showed good bone consolidation for the patients from group B. One case from group A showed almost complete ossification of the defect 4 years post-surgery, but four cases showed no histological evidence of osteogenic activity. Similarly, two patients from group B had no histological evidence of osteogenesis. Different sizes of the defects were included in this study, which ranged

from hemimandibulectomy to a less than 5 cm defect , these variations will have had effects on the different success rates obtained. The author did not mention the criteria of allocation of the cases into different study groups.

Chao et al (2006) presented a case of a 9 year old boy with a juvenile active ossifying fibroma that was resected leaving the periosteum intact to create a pocket suitable for the placement of BMP-2. A pre-shaped titanium reconstruction plate was made on a stereolithographic model. 12 cm of mandibular bone was removed and the created soft tissue pocket was packed with a composite consisting of BMP, collagen sponge and granules of 85% tricalcium phosphate and 15% hydroxyapatite. Follow up was performed at 6, 8, 12, 24 and 36 weeks with clinical and CT examination. At 6 weeks the graft showed bone filling the defect from edge to edge with mesial radiolucencies, so more rh-BMP-2 was applied to that area. Twelve weeks assessment recorded an increase in the bone density, and a decrease in the size of the mesial gap, with evidence of continued bone formation and remodelling. The author did not justify the use of BMP-2 subtype over the other commercially available BMPs.

Heliotis et al (2006) used the preparation of a vascularised bone flap extra-skeletally. A 60 year old patient had a hemimandibulectomy together with radiotherapy for a malignant tumour 7 years previously with no reconstruction. As a result the soft tissues in the area had contracted and so could be treated with the conventional microvascular flap. Three blocks of HA were adjusted to the shape of the mandibular body and ramus, Osteogenic Protein 1 (OP-1) was smeared over the blocks, and then implanted in the pectoralis major muscle for 15 weeks. The implanted composite was raised with the attached muscle pedicled on the thoracoacromial artery. The pedicle was covered by a free skin graft and an external fixation device was used to

secure the graft. Biopsy specimens were taken from the graft before fixation at the recipient site. After 6 months, clinical examination showed bony union between the graft and the adjacent mandible, with normal mandibular movement. Histologically, the graft was composed of 17% bone, 37% HA, and 46% fibrovascular tissue. After 5 months the patient developed MRSA infection at the graft site and, the bone graft was removed. Surprisingly the amount of bone formation was 17% after 3 months, despite the fact the HA was implanted in vascular tissue and OP-1 was applied. The MRSA infection might have occurred due to the external fixation. Since the author managed to use a pedicle flap based on the thoracoacromial artery it would be more logical to use autogenous bone from scapula instead, which could have saved the patient having to undergo two surgeries.

Herford et al (2007) used BMP-2 in a bovine collagen type 1 sponge carrier for the regeneration of the premaxillary cleft in 12 patients with unilateral cleft premaxilla and oro-nasal communication. Two of the patients were grafted using particulate marrow cancellous bone (PMCB). At 4 months CT analysis showed the mean bone volume ratio between the preoperative and postoperative scans to be 71.7% in the BMP-2 cases and 78.1% in PMCB group. The author concluded that BMP-2 is an effective alternative to conventional grafting technique. Bone density was not measured in the study. Only two cases were allocated to the control group which makes comparison between the two groups difficult and a 4 month assessment may be too early to draw a final conclusion on the effectiveness of the method used.

Clokie and Sandor (2008) reported on 10 cases with major mandibular defects following resection as a result of either ameloblastoma or osteomyelitis. Immediately after resection of the lesions the defects were spanned with reconstruction plates and the defects were filled with a bioimplant containing bone morphogenic protein-7

(BMP-7) in demineralized bone matrix (DBM) suspended in a reverse-phase medium. Radiographic evidence of mandibular bone formation was found in all cases. After 1 year, functional and aesthetic reconstruction of the mandible was complete. The authors presented a successful reconstruction of large mandibular defects using the synthetic bone and BMP without the problems associated with autogenous bone grafting. However, only plain radiographs were taken for the post-operative follow up and no bone biopsy was performed.

Herford and Cicciu (2010) used 4.2 mg rhBMP-2 with absorbable collagen sponge (ACS) to regenerate a mandibular defect in a 25 year old woman 7 months following resection of a giant cell tumour. Bone was harvested from the hip and was placed in the defect together with the ACS and rhBMP-2. Radiography showed evidence of bone formation as early as 3, 4 and 6 months postoperatively. This paper provides a promising new method for the reconstruction mandibular continuity but the post-operative assessments time was too short to draw any firm conclusions.

Following preclinical evaluations, Kokemueller et al (2010) used cylindrical β-TCP scaffolds (25 mm long) filled intraoperatively with bone marrow harvest, implanted in the latissmus dorsi muscle and left for 6 months in a 57 year old male patient with a chronic history of osteomyelitis of the jaw who had a continuity resection. A highly vascularised soft tissue flap was then transferred to close the wound and to create a soft tissue bed.   The cylinders were harvested and reinserted into a titanium mesh to then reconstruct the mandible. The patient was followed up for a year and there were no signs of infection or rejection at the site of transplantation. A one year follow up might not be long enough to draw a final conclusion. The author in this study adapted the titanium mesh on a commercially available skull; however using stereolithography

to retrieve a 3D model of the patient would have been a more accurate alternative.

This is a single case report and larger studies are required before wider application.

So, a summarizing statement is required.

2.3.2 Reconstruction of mandibular critical-size defects using MSCs

Following preclinical animal evaluation, Kinoshita et al (1997) used a poly (L-Lactide) (PLLA) mesh tray and autogenous particulate cancellous bone and marrow (PCBM) to reconstruct the mandible following partial (alveolar process) resection due to carcinoma. A PLLA mesh was formed in the shape of the alveolar ridge. The mesh tray was fixed in the mandible and filled with PCBM and hydroxyapatite. Six months postoperatively, the height of the mandible increased and the alveolar ridge was reconstructed to a favourable shape. The patient was able to use their denture for 2 years after the operation. In a second case a 62 year old patient with an anterior mandibular segmental resection was reconstructed with a PLLA mesh tray filled with PCBM fixed to the mandibular stumps on each end. Three months after the operation, solid bone was found in the shape of the tray and the continuity of the mandible was completely regenerated. The follow-up time for the second case was 3 months which is too short to reach any useful conclusions but it was 2 years for the 1st case. There was no histological analysis presented for any of the cases. The nature of the tumour of the second case was neither mentioned nor discussed.

Warnke et al (2004) used rhBMP-7 and bone marrow-derived MSCs were added to a degradable polylactite scaffold, which had been loaded in a titanium mesh tray as an external scaffold. The patient served as their own bioreactor, as the graft was implanted inside the patient's latissimus dorsi muscle initially. After seven weeks the construct was transplanted to the patient's mandible. Bone scintigraphy and CT analysis showed that greater osteoblastic activity and bone formation were detected

in all parts of the mandible during the 38th week rather than in the 4th week. The authors concluded that transplantation could have been performed at a later stage, as osteoblast activity and bone remodelling remained highly active over at least the first 8 months. Histological examination for the formed bone was made during transplantation as a biopsy was taken from the outer surface of the transplant. There was viable young cancellous heterotopic bone surrounded by muscular tissue. The authors also pointed out that there was no evidence of malignant transformation, but unfortunately the patient died as a result of a cardiac arrest 15 months after implantation. There was no clear methodology regarding the aspiration of mesenchymal cells and of their culture expansion and seeding onto the scaffold or on the method used for adding BMP to the scaffolds.

Lee et al (2010a) reconstructed a 15 cm segmental mandibular defect following removal of a central haemangioma in a 14 year old male, using bone marrow stem cells. The resected jaw was freeze dried for 48 hours then perforated using surgical burs. Autogenous bone MSCs were aspirated, isolated and cultured in vitro. Seven months after the resection, the autogenous bone tray loaded with the differentiated MSCs and fibrin glue was repositioned in the mandibular defect area. One year postoperatively, the mandible showed good clinical and radiographic evidence of bone regeneration. Due to lack of adequate vertical height for future dental implant placement, a vertical distraction osteogenesis with simultaneous injection of differentiated MSCs was performed 7 months later the patient was re-treated with guided bone regeneration, titanium mesh with seeding of differentiated MSCs, fibrin glue and dental implant placement. A bone biopsy was taken upon implant placement which showed remodelled lamellar bone with abundant viable osteocytes in the lacunae within the distraction zone. Dental CT was carried out after 4 month which showed mineralised bone in the augmentation zone. The authors in this paper

presented a full scenario on how tissue engineering–based bone regeneration can resolve problems of large bone reconstruction, as well as overcome vertical bone deficiency prior to the placement of dental implants. On the other hand, the authors did not perform any assessment of the quantity and the quality of the newly generated bone. The method of cell isolation was not presented in this paper.

Hernandez-Alfaro et al (2010) managed a 33 year old patient who presented with recurrent ameloblastoma in the left side of the mandible. Following segmental resection with a 1 cm safety margins, a titanium mesh, Bio-Oss (Geistlich) infused with 2 g of rBMP-7 and 5 mL of concentrate from a bone marrow aspirate were placed in the defect and a collagen membrane (Bio-Gide, Geistlich) was used to cover the graft and prevent fibrous tissue ingrowth. Nine months later, re-entry for implant placement allowed for harvesting of two cores for histological analysis which revealed new bone formation around the particles of xenograft material. Four months later, the implants were loaded with a fixed prosthesis and at 1-year follow-up, the implants remained stable. The paper did not mention which type of ameloblastoma was diagnosed but this would have been useful as it may have affected the successful reconstruction. Also, optimization of the dose of BMP-7 was not discussed.

Ciccio et al (2012) presented the immediate reconstruction of a mandibular defect following en bloc resection of a dentinogenic ghost cell tumour. An inferior titanium plate was placed and rhBMP-2, Absorbable Collagen Sponge (ACS) and bone allograft were placed in a titanium mesh within the defect. At 9 months the titanium mesh was removed and dental implants were placed in the regenerated bone. The authors did not discuss the pathophysiology of the dentinogenic ghost cell tumour, its prognosis or the current different treatment modalities. The fast bone regeneration in

this case could have been related to the nature of disease in the first place with regards to increased angiogenesis and vascularity.

Zamiri et al (2013) reported on 3 patients with critical-size mandibular defects following tumour resection and who were managed with allogenic mandibular bone and autogenous MSCs. Fresh-frozen cadaveric mandibular bone was customized according to the individual 3D CTs of the patients, decorticated and sterilised. The defect was exposed and the bone allografts, loaded with MSCs in fibrin glue, were placed. Scintigraphy showed normal perfusion and increased uptake in the grafted side of the mandible in two cases. But the third case showed reduced perfusion and delayed uptake and was removed and replaced with an autogenous bone graft. Testing the antigenicity of the prepared graft bone may have been useful. Testing cells to scaffold interaction would have been advisable. Long term follow-up had not been carried out and no bone biopsies were performed. Histological analysis of the removed failed bone graft would also have allowed determination of the cause of the failure.

Marx et al (2013) compared two types of grafts in large vertical maxillary defects (1 cm vertically and 1 cm horizontally) in 40 patients; a composite graft of 1.05 mg rhBMP-2 and acellular collagen sponge (rhBMP-2/ACS), crushed cancellous freeze-dried allogeneic bone (CCFDAB), and platelet-rich plasma (PRP) (group 1, n=20), or size-matched 100% autogenous grafts (group 2, n=20). All grafting material was contained within a titanium mesh crib. At 6 months the titanium mesh was removed and implants were placed. Two grafts in each group were lost as a result of early mesh exposure and infection. Three grafts in each group developed a late exposure of the mesh that did not affect bone regeneration. All the successful autogenous grafts regenerated sufficient bone for implant restoration compared to 97.4% of the

composite grafts. The composite grafting technique resulted in less blood loss and shorter surgical time but greater and longer-lasting oedema. The author did not demonstrate what the inclusion criteria in this clinical trial were. Moreover, the use of autogenous cancellous bone was not justified in the discussion. The use of cortico-cancellous bone graft would have an advantage over cancellous bone alone as it could be fixed with screws only and would remove the need for the titanium mesh.

Kim et al (2013b) described mandibular reconstruction managed with autologous human bone marrow stem cells BMSCs and autogenous bone graft in patients with plexiform ameloblastoma. Following complete resection of a plexiform ameloblastoma in the right side of the mandible in a 26 year old patient, the defect was reconstructed with a cortical block which was harvested from the opposite buccal area and autologous BMSCs were injected in the graft. Autologous osteoblasts mixed with fibrin-glue and 3 months later were injected again into the mandibular defect area for the acceleration of bone formation. Six months later implant placement was performed and the prosthesis was retained at 3 years follow up. The author commented that BMSCs may be used as an alternative to autologous bone grafts. No bone biopsy was performed at the time of implant placement.

Wolff et al (2013) used adipose stem cells (ASCs), BMP-2, and β-TCP scaffold combined with CAD/CAM techniques for mandibular reconstruction in three patients with recurrent ameloblastomas requiring segmental mandibular resection (2 males, one female, mean age 49.3y). The defects ranged from 6.0 to 10.0 cm in length with a mean defect size of 8.2 cm. Prior to planning the operation, 3D stereolithographic medical skull models (Planmeca, Helsinki, Finland) were fabricated using the patients' preoperative CT. These images were used to reverse-engineer patient-specific guides and reconstruction plates using computer-aided additive manufacturing. The

constructs (ASCs, β- TCP granules, BMP-2) were implanted into the defects inside the custom-made titanium mesh. Two of the three patients opted for reconstruction with dental implants. The three patients were followed-up for an average of 28 months (range: 19-43 months). Bone biopsy was performed on implant placement and mesh removal. Histological analysis of the core bone showed signs of bone formation and remodelling. The β-TCP granules were interconnected by bridges of vital newly formed bone. Although the results are promising, the limited number of cases in the study means the methods need to be further investigated.

Sàndor et al (2013) treated a 55 year old patient after resection of a recurrent ameloblastoma (10 cm defect) using ASCs obtained using Good Manufacturing Practice (GMP) that were combined with 40 mL of β-TCP granules (porosity 60%; granule size, 1.4 to 2.8 mm, Chronos1, Synthes, Oberdorf, Switzerland), 48 hours before the operation. The defect was spanned by a titanium mesh and reconstruction plate. The ASCs/β-TCP granules were combined with BMP-2 and were placed into the mesh. 6 dental implants were placed 10 months after surgery. Bone core biopsies were retrieved from the implant placement sites. This revealed signs of bone formation and remodelling. The β-TCP granules were interconnected by bridges of vital newly formed bone. Histomorphometric analysis showed that the bone consisted of woven bone (36.7%), osteoid (32.4%), fibrous tissue (23.3%), and residual scaffold (8.6%). An implant-retained partial overdenture supported by a bar attachment was installed on the successfully osseointegrated dental implants. The patient was followed-up uneventfully for 3 years. The paper presented interesting data including in vitro cells characterization for the ASCs to scaffold interaction. The resorption rate of the scaffold in relation to bone formation was not discussed. A CT scan image was not considered during the follow up period, this would have been ideally been done before implant placement.

2.3.3 The application of Injectable scaffolds for the reconstruction of bone defects

Abramo et al (2010) tested the feasibility of using biphasic injectable bone substitute in grafting the radius bone after osteotomy of mal-union fracture cases in a non-controlled prospective study. Fifteen consecutive patients, with a mean age of 52 (27–71) years were included. All had a mal-union after a distal radius fracture and underwent an osteotomy. A fragment specific fixation system, TriMed1 (TriMed, Valencia, CA), consisting of a Buttress Pin1 and a Radial Pin Plate1 were used for fixation and a calcium sulphate/calcium phosphate mixture was used as a bone substitute. There were no adverse events correlated to the bone substitute at follow up, neither by clinical examination nor in the blood samples. There were seven adverse events correlated to the surgery or to the fixation device. Grip strength increased from 61 (28–93)% of the contralateral hand to 85 (58–109)%, p < 0.001. The preoperative pain at rest as measured on a visual analogue scale (0–10 cm) was 5.5 (3–10) and decreased to 2.4 (1–6) at 1 year (p < 0.001). Radiographically all osteotomies healed. The paper introduce the use of the biphasic bone substitute CS/HA in the treatment of malunion cases. The study was a single cohort and was not controlled. Data for assessment of bone healing and bone regeneration was not provided. A quantitative assessment tool using a scoring system to assess the radiograph at different time points would have been helpful.

Rauschmann et al (2010) conducted a prospective, non-randomized multicenter study assessing the efficacy and safety of a partly resorbable composite of calcium sulphate and hydroxyapatite (Cerament[TM] Spine Support). All the recruited patients were osteoporotic with vertebral compression fractures (n=15). These underwent percutaneous bioceramic vertebral augmentation under fluoroscopy. The patients were allowed to mobilize 2 hours after the intervention. The injected volume of the

composite material ranged from 2.8 to 9 mL (mean 4.2 mL). The pre-operative VAS score mean was 70.3 (I95% ±8.7) with an immediate post-operative pain relief, which was maintained at the 4-week visit (mean 26.4 with I95% ±16.1) and 8-week visit (mean 18.0 with I95% ±13.5). Eighty percent of the patients demonstrated clinical improvement. The pain relief was maintained over 18 months and no adjacent fractures were observed. There was a statistically significant improvement of physical components in the QoL assessment. No extra-vertebral leakage or neurological deficits were reported in this series.

Marcia et al (2012) evaluated injectable calcium Sulphate/HA cement (Cerament ^{TM} Spinal Support, CSS) in the management of vertebroplasty patients. Thirty-three patients with historical and clinical evidence of symptomatic compressive spine fractures caused by osteoporosis and trauma with fracture types A1–A3 (AO classification) were included in the study. A 10–13 Gauge needle was introduced into the vertebral pedicle through a small skin incision, one for each level. The CSS was then instilled under close imaging guidance until the anterior two-thirds of the vertebral body were filled and cement was equally distributed inside the bone. CT scanning was carried out post-operatively to assess intra-osseous cement distribution and signs of any cement leakages. 66 vertebral bodies underwent percutaneous vertebroplasty. The VAS pain score demonstrated a significant decrease from 8.61 (SD 19.8) pre-operatively to 2.48 (SD 2.36) at 1 month. The score was 2.76 (SD 2.68) at 6 months and 1.36 (SD 1.33) at 12 months. Oswestry Disability Questionnaire (ODI) score dropped significantly from 58.86 pre-op to 26.94 at 6 months and further down to 7.61 at 12 months. No re-fractures or adjacent level fractures were reported.

Masala et al, (2012) also evaluated the injectable calcium Sulphate/HA cement (Cerament^{TM} Spinal Support, CSS) bone substitute. The cement was employed in the fluoroscopic vertebral augmentation of osteoporotic collapse cases. The study was prospective observational non controlled study in 80 patients. Preoperative and postoperative imaging studies were performed. No intra-procedural or peri-procedural complications were reported, except for a cement leak in one case. Pain intensity was evaluated on a VAS, and quality of life was evaluated with an ODI. There were significant changes in pain intensity post-operatively ($p<0.001$). The ODI score dropped significantly from 54.78% to 20.12% at 6 months. At the end of the 1-year follow-up, no cases of new adjacent vertebral fractures were reported. In four cases (all women) with mono level involvement, a new incidental fracture per person occurred at a distant level. The first early vertebral collapse occurred 7 months after the procedure, the last at 9 months; all four cases were augmented with traditional PMMA cement. The authors concluded that the results strongly suggest that CSS can be an effective alternative to PMMA. They also suggested that the sustained pain relief during the 12-month follow-up period was due to a new bone ingrowth.

The above three studies (Rauschmann et al, 2010; Marcia et al, 2012 and Masala et al, 2012) were all non-controlled single cohort studies. The authors had performed several investigations (plain radiography, CT, MRI, and DXA scanning), however, assessment of the bone regeneration was not considered. One key problem with these papers is that the conclusion of the studies was based on two subjective measures (VAS and ODI) only.

2.4 Summary

This chapter showed that the reconstruction of critical-sized mandibular defects using induced pedicled muscle flaps seemed promising. Gene therapy was suggested to

induce muscle osteogenesis in free skeletal muscle flaps by one group and was only used to repair calvarial bone defects in rats (Liu et al, 2012). Several alloplast and allograft materials have been used alone or in combination to reconstruct large defects in the craniofacial region and different success rates were reported, possibly because of several different variables including different species, sizes of the defect, surgical techniques, timing of the grafting, follow up periods and anatomical sites used. Neovius and Engstrand (2010) compared biomaterials, bone grafts and combinations in non-load-bearing areas in the craniofacial complex, published between 1999 and 2008 (83 studies) and concluded that there was a significant difference in outcomes but mainly due to the size and location of defects rather than bio-material used.

In human trials the use of osteoinductive growth factors has gained wide support among clinicians, as seen by most of the included human and animal trials (Herford et al, 2007; Warnke et al, 2006). Yet, growth factors especially BMP need further refinement in their use for the reconstruction of large complex defects in the cranio-maxillofacial region (Neovius and Engstrand, 2010). In a systematic review by Herford et al (2011) it has been shown that BMP was associated with 13.9% failure rate and therefore, cannot replace autogenous bone grafts.

The use of osteoprogentor cells (MSCs or osteoblasts) in combination with alloplast/or allograft and growth factors has been studied, the reported success rate was variable (summary of studies are in table 2, appendix 1.3). Seeding and survival of the cells are dependent on the vascularity of the construct. Most research on osteoprogenitor cells have highlighted the lack of vascularity as the cause of cell death (Henkel et al, 2005; Alfotawei et al, 2010). A pedicled muscle flap should

overcome this obstacle and provides the necessary blood supply for survival of the osteoproginator cells to induce bone formation (Evan et al, 2009).

Table 2.1 and appendix 2 show the studies of using MSCs, BMP and scaffolds to reconstruct large mandibular defects. The majority of the studies used two methods for the assessment of bone formation; micro-CT & histomorphometry. The gold standard assessment tool remains the histological analysis which includes dynamic or static histomorphometry and/or immunohistochemistry. Sixty papers out of the 68 that were reviewed demonstrated two or more assessment methods (Table 2.2). However, in only 8 studies (11.7%) a comprehensive assessment of bone formation was considered which included plain radiography at multiple time points, CBCT, micro-CT, mechanical testing, and histological assessment. Most of these methods of assessments were applied in the research project of this thesis.

Chapter 3

The research hypothesis and study methodology

Table of Content

3 The research hypothesis and study methodology

3.1 Aims and hypothesis

The aim of this study was the reconstruction of a critical size mandibular defect in rabbits using bone cement (Cerament ™,, Bone Support, Sweden), loaded   with rBMP-7 and seeded with rMSCs injected into muscular tissue to stimulate osteogenesis.

In this study two hypotheses were tested:

a. The application of injectable cement loaded with BMP-7 and seeded with rMSCS could stimulate osteogeneis inside a pedicled muscle flap.

b. Bone formation within muscle tissue would be sufficient to reconstruct the surgically created mandibular defect.

The rational of this study was based on the fact that the main obstacle of bone regeneration with grafting is the lack of vascularity at the recipient site as a result of peripheral vascular disease and following radiotherapy. A local pedicled muscle flap, with its intact blood supply, would act as a vehicle for biomaterials to induce bone formation.

The rationale for injectable cement with mesenchymal stem cells and appropriate cytokines is to maximise the potential of bone formation and to minimise the risk of failure due to bacterial proliferation of non-vascularised implant. This is a common scenario in the head and neck region following cancer resection or traumatic bone loss which precludes the use of a non-vascularised bone graft. The injectable bioactive cement would provide an opportunity to reconstruct inaccessible and biologically challenging surgical defects which are currently left without adequate anatomical restoration. The application of bio-material loaded with cytokines and seeded with undifferentiated mesenchymal cells for maxillofacial reconstruction has not been considered before and the suitability of injecting the material into

muscle flap in one stage construction of mandibular bone defect has not yet been tested. Figure 3.1 illustrates the experimental design study.
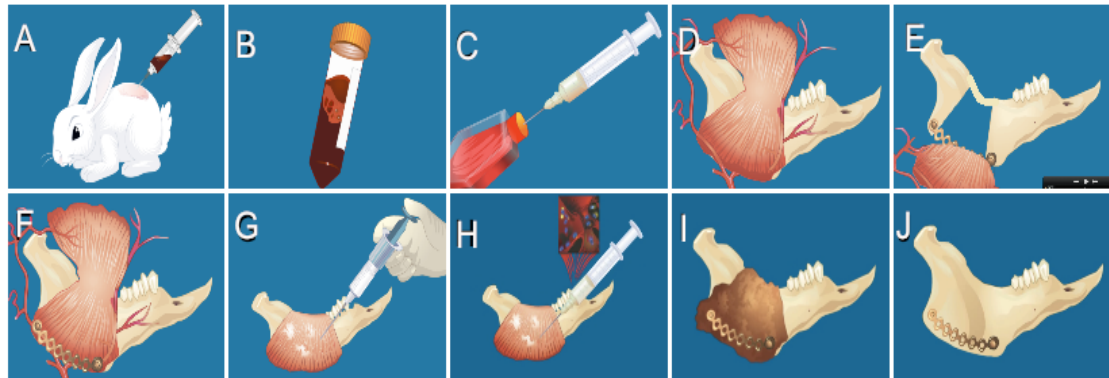
Figure 3.1:   Schematic representation of the step of the proposed in vivo study A) Aspiration of bone marrow from the posterior iliac crest. B) Preparation of the aspirate for expansion, C) Laboratory procedure for culture of the rMSCS. D) The anatomy of the masseter muscles and the associated blood supply. E) The created critical size defect in the mandibular ramus and plating of the inferior border F) Adaptation of the muscle flap into the defect, G) Injection of the cement loaded with BMP-7 into the muscle tissue, H) Seeding rMSCs suspension around the cement, I) The expected radiographic appearance throughout the course of the study. J) Ideal scenario of complete regeneration of the created surgical defect.

3.2 Material and Methods

3.2.1 The study design

3.2.1.1 Cadaveric study

This part of the study was carried out on 2 cadaveric rabbits; the procedure was performed immediately after the animals were euthanized by an overdose of intravenous Phenobarbitone. The main objectives of this phase of the study were to test the technical feasibility of creating the surgical defect in the mandible and the bone marrow aspiration from the posterior iliac crest for in vitro processing (Chapter 4) to optimise the manipulative variables of injecting the cement into the muscle. Plain X-ray radiographs, CBCT scan and histological analyses were under taken to test their validation.

3.2.1.2 The study population

3.2.1.2.1 The animal model

Rabbit was chosen as a representative model in this experiment for the following reasons; firstly the rabbit is a small animal with adequate jaw size supported by a well developed masseteric muscle, which is important for the experimental design of this study. Rabbits are the most popular animal models in health science research in particular tissue engineering (Matos et al, 2001). The conditioning and cost of the animals allow the research studies to be carried out on with a minimal impact on their welfare (Mastos et al, 2001). The bone structure and histology pattern of the rabbits are similar to humans, which is an important advantage in terms of extrapolation of results and transfer of findings for application in humans (Nunamaker, 1998).

 The surgical procedures were performed under general anaesthesia after obtaining the approval from the Home Office under the Animals (Scientific Procedures) Act 1986 to carry out regulated procedures on living animals.

3.2.1.2.2 The size of the surgical defect
The dimensions of a critical size defect in the mandible are varied in literature. There is a considerable debate over the definition of critical-size defects for bone bioengineering. Schmitz and Hollinger (1986) defined a critical-size defect as the smallest osseous defect in a particular bone and species of an animal that would not heal spontaneously during the lifetime of the animal. This has been re-defined as a defect, which demonstrates less than 10% bone regeneration throughout the lifetime of the animal (Hollinger and Kleinschmidt, 1990). The absolute value of the critical-size defect depends on the breed, age and the phylogenetic order of the animal. Ren et al (2005) showed that a defect of 12 mm× 5 mm in the mandible was of a critical-size and did not show any sign of bone union which was

confirmed by Kim et al (2013b). Li et al (2010) reported on a critical size defect of 12 mm x 8 mm at the inferior border of rabbit mandible. In a controlled trial by Jiang et al (2006) a defect of 15 mm x 6 mm in the mandibular ramus of rabbits was considered of a critical size. Guo et al (2012) confirmed in their study that a defect of 15 mm × 8 mm [at] ramus of the rabbit's was of a critical size when investigating bone regeneration. Similarly, Fu et al (2009) considered 15 mm x 15 mm a critical size defect at a ramus of the mandible in rabbits. Therefore, according to the published data, in this study a 25 mm x 15 mm was considered a critical size defect at the ramus of the mandible.

3.2.1.3 Duration of the study

With regard to the termination time, 3 months was considered an optimal period for complete bone regeneration in rabbits when critical size defect was created (Ren et al, 2007). Studies that have investigated bone regeneration in rabbit`s mandible terminated the experiments at same time points (Liu et al, 2010; Fu et al, 2009; Su et al, 2013; Guo et al, 2012). On the other hand, studies that investigated bone regeneration for a longer time (16 weeks) reported no significant difference with bone regeneration when compared with those terminated at 8 weeks (Li et al, 2010).

Plating the inferior border (the compression band) of the mandible using 2 mm titanium plate and screws was undertaken to reinforce the mandible that would take over a part of the functional load in the initial phase of treatment thus reducing the stress resulting from the masticatory forces and providing a preliminary stability (Merkx et al 2004; Nagasao et al, 2002). Mandibular plating allows more rapid resumption of oral functions which is essential for the animal

welfare.   The plate at the inferior border of the mandible allows maintenance of the facial contours (Jędrusik-Pawłowska et al, 2013).

3.2.2 In vitro characterization of rMSCs and bone cements

This part of the study involved rMSCs characterization including targeting common cell surface markers and testing the cell multipotentiality.

Two bone cements were evaluated; namely Cerament^{TM} Spine Support (CSS) and Cerament^{TM} Bone Void (CBV). Cell viability and the best seeding protocol of the cells into the cement's were explored. The details of the findings are provided in section (4.2.6; 4.2.7; 4.2.8).

3.2.3 In vivo pilot study

This study was carried out on 3 rabbits. The surgical procedures were performed under sedation and general anaesthesia after obtaining the approval from the Home Office under the Animals (Scientific Procedures) Act 1986 to carry out regulated procedures on living animals to evaluate the impact of the surgical procedure on the animal welfare, assessment of possible surgical complications and finalise the surgical protocol.

3.2.3.1 Bone Marrow aspiration

The following medications were used to sedate the rabbits before aspiration of bone marrow from the posterior iliac crest. A 12.5 µg Fentanyl (opioid) transdermal patch which was applied the night before the surgery, Meloxicam (NSAID) 0.2 mg/kg subcutaneous (S/C), 1 hour pre-operatively and Hypnorm (Fentanyl citrate & Fluanisone) 0.5 ml/kg intra-muscular (IM), 30 minute pre-operatively. Isofluorane N_2O & O_2, inhalation in a facemask was kept till the end of the procedure with close monitoring of the vital signs.

Bone marrow aspiration was done under sedation, the hair over the left posterior iliac crest of the hip bone was shaved and cleaned using Betadine, and then Marcain 0.5 % (0.5 ml) local anaesthesia was injected locally into the surgical site. The rabbits were maintained with isoflurane and O_2 inhalation gases throughout the procedure using facemask. A 16-gauge needle was used to penetrate the cortex of the posterior iliac spine. Bone marrow aspirate was collected using 20 ml syringes which contained 3000 units of heparin. The aspirate was divided into centrifuge tubes, 5-7 mls aspirate per tube then 20 ml of Dulbecco`s modified phosphate buffered saline (DPBS) was added. All samples were transferred to the

main laboratory at the Centre of Cell Engineering of the University of Glasgow for the laboratory investigation. After recovery, the rabbits were given 0.26 ml/ Kg Carprofen a sub-cutaneous prophylactic for pain.

The processing of the bone marrow processing is discussed within the cell culture section.

3.2.3.2. Cement preparation

Injectable bone cement (Cerament^{TM}, Bone support, Sweden) was used; details of cement composition and characterization are discussed in section 4.2.4. At the time of the operation, 3 g of Cerament^{TM} Spine Support powder was mixed with 0.4 mg of freeze dried BMP-7 and 1.26 ml of Iohexol liquid. The mix was loaded in 5 ml syringe, and made ready for injection at the surgical site.

3.2.3.3 The surgical procedure

A 2 cm long skin incision was made extending along the inferior border of the mandible at the ramus region involving the skin and the subcutaneous tissue. The masseter muscle was exposed and cut through its inferior attachment at the pterygo-masseteric sling. The muscle was reflected superiorly to explore the ramus of the mandible. A ramus ostectomy was then performed on the right side of the mandible, the first cut was made a few millimeters posterior to the last molar tooth, and the second cut was made 15 mm posterior to the 1st cut (Figure 3.2a). The segment of bone was removed together with the associated periosteum. A titanium plate was adapted along the inferior surface of the ramus, bridging the created defects. The plate was fixed on the body of the mandible with one titanium screw and another screw at the condylar unit (Figure 3.2b and 3.2a). The deep layer of masseter muscle was then adapted into the created defect, and secured in place with holding sutures. The cement was mixed with 0.4 mg rh-BMP-7 and then

loaded into a 5 ml syringe; a 16-gauge needle was used to inject the mix into the deep layer of muscle (Figure 3.2b). The material was injected at a full depth of the muscle, the injection was maintained while withdrawing the needle. In an attempt to standerdize the injection procedure, the injection of the cement was carried out through the holes of 1mm titanium mesh.
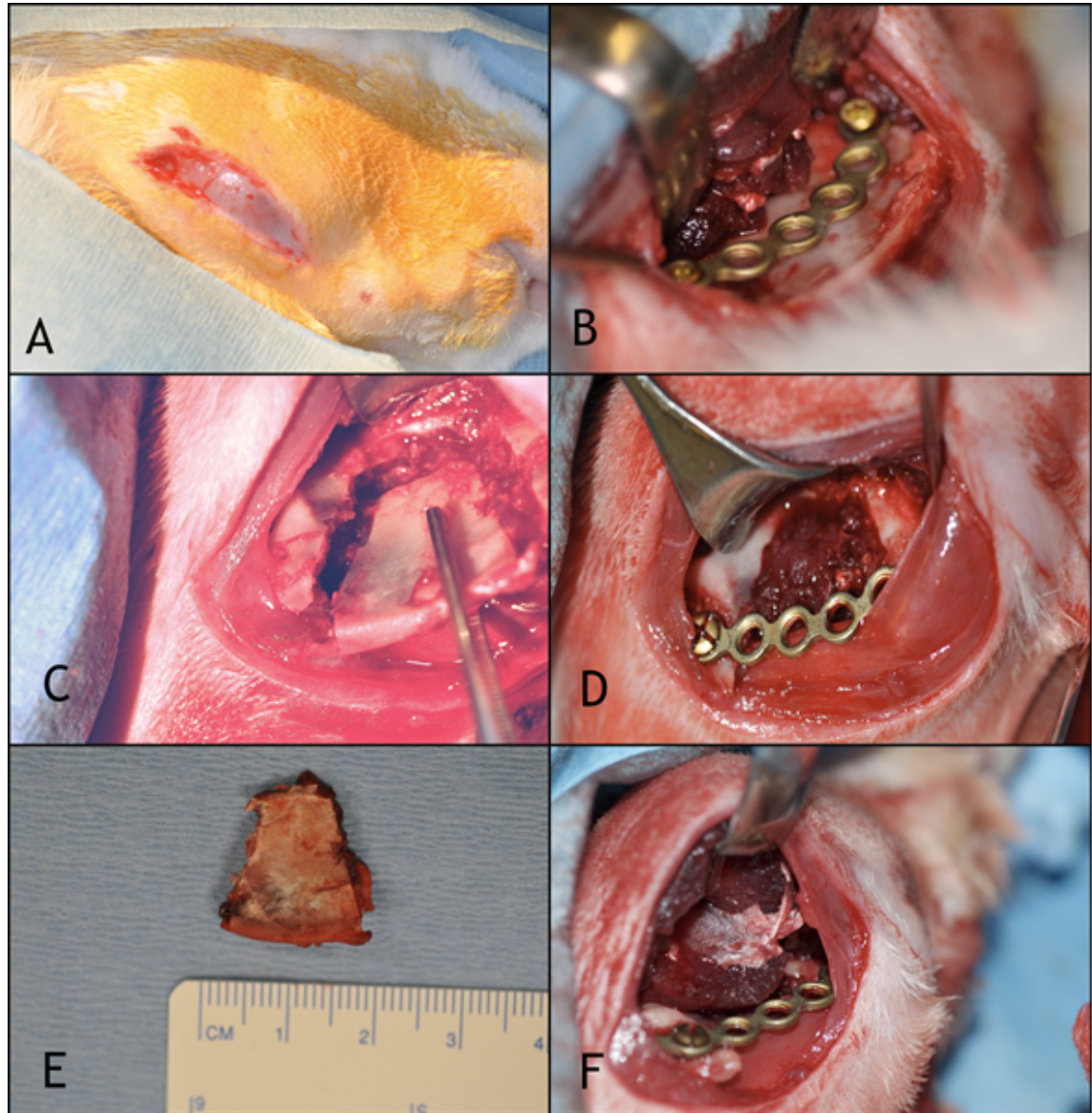
Figure 3.2a: Images of the surgical procedure, A) shows the 2 cm sub-mandibular skin incision, B) Reflection of masseter muscle at the angle of the mandible and checking the extension and adaptation of the bone plate, C) Exposure of the ramus of the mandibular and removal of the bone segment, D) Adaptation of the titanium plate in place after the bone cut was carried out. E) The size of the bone segment which measured about 15 mm × 25 mm, F) Adapation of the deep layer of the muscle into the created defect.
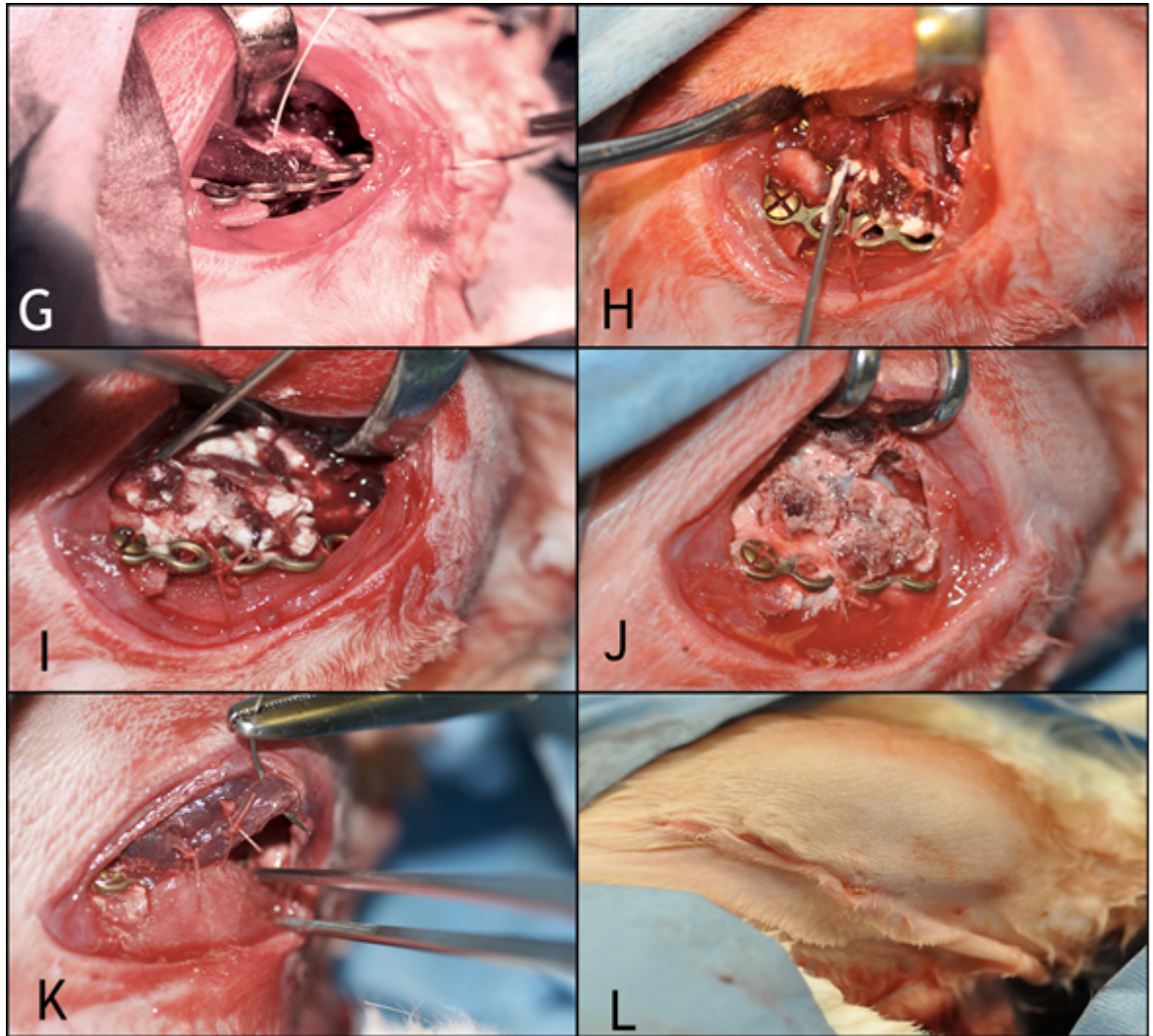
Figure 3.2b: G) Muscle is adapted in the defect and ready for injection, H) Starting the injection of the cement; I) shows the deep layer of the masseter muscle loaded with the injected cement J) Initial setting of the cement within the muscle; K) suturing of the deep layer of the masseter muscle; L) Complete closure of the wound with subcutaneous suture.

3.2.4 Results of the pilot study

All the animals completed the course of the study with minimal impact on their welfare. Technical difficulties have been encountered which includes the dislodgement of the anterior screw and displacement of the plate laterally which led to infection in one case. Titanium mesh proved impractical and interfered with the flow of the injected cement. The injection of the deep layer of the muscle was technically difficult to ascertain.

Therefore, as a result of the pilot study, to maximise the stability of the mandible following the creation of the surgical defect and to minimise the loading on the

inferior border plate, the upper border of the ramus of the mandible was kept intact at the surgical site(Kimsal et al, 2011)(Figure 3.3).   This did not compromise the size of the created defect which was kept at 15 mm× 20 mm (Fu et al 2009, Guo et al 2012). To obtain a homogenous injection of the deep layer of the masseter muscle, it was dissected into a superficial layer and deep layer. This facilitated the direct injection of the deep layer of the masseter muscle which was adapted to fill the created surgical defect.
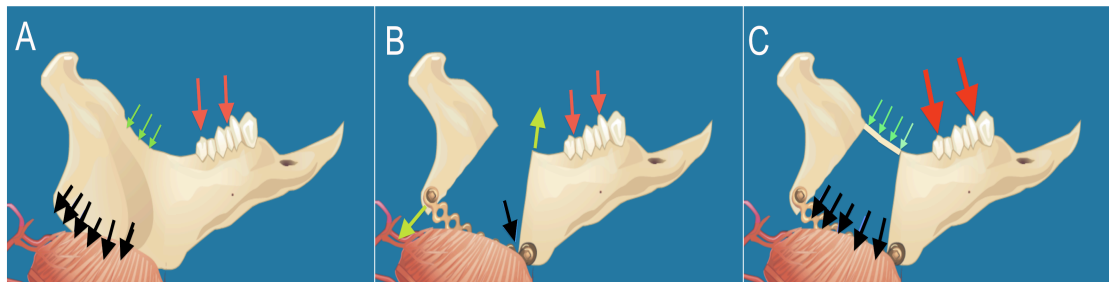
Figure 3.3: Critical analysis of the loading patterns during function in rabbit mandibular defect. A) Shows the effect of normal occlusal force (red arrows), peak compressive (black arrows) and tensile strains (green arrows) were created during function. B) When continuity defect was created and plated with single bicortical plate the occlusal force (red arrow) produces rotation (cantilever) forces (the green arrow) with centre of rotation around the posterior margin of the defect (black arrow) which lead to stress concentration and eventually to failure of the plate and instability of the graft. C) Shows the modification of the surgical design by leaving the superior boney ledge which act as a tension band (green arrow) together with inferior plate compression band which absorb the compressive forces(black arrows), which restore the mechanical stability of the mandible.

3.2.5 The main study

The main study was carried out on 10 New Zealand rabbits, all the surgical procedures were performed under general anaesthetic. The surgical protocol was similar to the one tested in the pilot study. It was decided that all the cases would receive the injectable cement (Cerament^{TM} Spine Support), BMP-7 followed by the seeding of rMSCs after the initial seating of the cement which was about 15 minutes, this was based on the outcome of in vitro investigation (Chapter 4). Quality and quantity of the regenerated tissues were assessed using, plain radiographs, CBCT, mico-CT, histology, and histomorphometry analysis.

3.2.5.1 Method of assessment of bone regeneration during the life-time of the animals

3.2.5.1.1 Assessment using plain radiographs

This was carried out by taking external oblique plain radiographs immediately following surgery, and at 1 month, 2 months and the day of euthanasia at 3 months after surgery. During radiographic capture the rabbits were sedated using Hypnorm 0.16 ml/kg IM 30 minute before radiographic imaging. Dental occlusal film (Kodak ultra-speed DF-50, Eastman Kodak Company, 3NY, USA) was used. The validation of the exposure setting was carried out on cadaveric model to evaluate the radio-density of the injected material compared to the adjacent bone and evaluate its diffusibility into the muscle tissue (Figure 3.4). The latter assessment confirmed the radio-opacity of the injected material and has reached the deeper layer of the muscle flap

The rabbit was placed on the side with the head stretched backwards. The occlusal film was placed opposite to the cheek area of the surgical side. The x-ray tube was positioned perpendicular to the film about 25 cm away from the film and was directed from the opposite sub-mandibular region.

  A step metal wedge plate was used in every X-ray film to scale the exposure time, film processing, and standardise the assessment of the comparative radio-opacity of the radiographs.
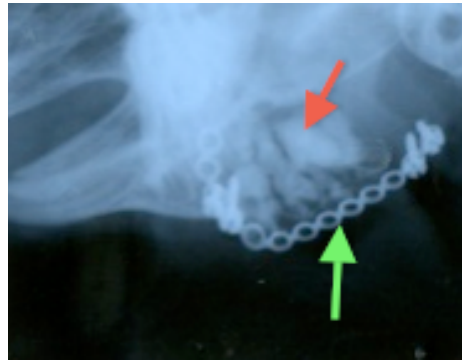
Figure 3.4: Shows lateral oblique x-ray film has been taken for the right ramus of the mandible immediately after injecting the cement (red arrow) into the masseter muscle, the plate that is holding the mandibular segment denoted with green arrow.

3.2.5.1.1.1 Qualitative scoring for of bone regeneration

To translate the qualitative data into numbers, a scoring system described by Cook et al (2005), as shown in Table (3.1) was applied. The grading system validated on rabbit model by Santic et al, (2009). The method was applied to the plain radiographs, the surgical defect was sub-divided into thirds, anterior, middle, and proximal (Figure 3.5). Each third was scored according to the grading system and the lowest score was considered the overall grade for the whole radiograph.

Table 3.1: The grading system used for assessment of the quality and quantity of bone regeneration, Cook et al (2005)

Extent of bone formation	Description
Grade 0	No change compared to the immediate post-operative appearance.
Grade 1	Trace of radio-dense material in the defect
Grade 2	Flocculent radio-density with flecks of calcification
Grade 3	The defect is bridged at least at one point with radio-dense material
Grade 4	Defect bridged on both medial and lateral sides with a uniform radio-density, the margins of the cortices remains visible.
Grade 5	Same as Grade 3; at least one of the cortices is Obscured by the new bone
Grade 6	Defect is bridged by uniform new bone; the margins of both cortices are no longer visible.

3.2.5.1.1.2 Quantitative assessment

The quantitative scoring (QS) was calculated for the overall bone formation in each surgical defect. ∑QS is the average percentages of the three scores of the anterior, the middle and the posterior thirds taken for each surgical defect (Figure 3.5). This was calculated according to the following equation (3.1) See Table (3.2).

∑QS={% GRADE anterior + %GRADE middle+ %GRADE posterior}

$$\frac{}{3}$$ Equ(3.1)

This method was successfully applied in previous study (Abu-Serriah et al., (2004). All the radiographic measurements were repeated for the non-operated side (control data). The median percentages for all the examined cases were considered for analysis.
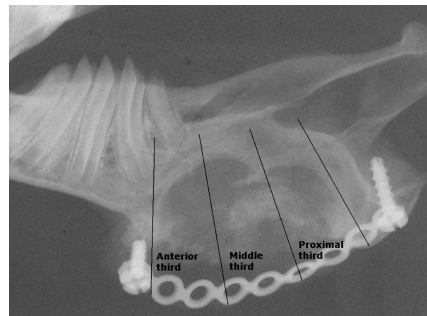
Figure 3.5: Radiographic image of the ramus of the mandible after 3 month from the day of the surgery shows the anatomical section are the anterior one third, the middle third, and the proximal third that were evaluated.

Table 3.2: Scale used in calculating quantitative score (ΣQS) and its interpretation(Abu-Serriah et al, 2004)

Grade	%Grade	Interpretation
0	0	0% radio-opacity
1-2	25%	25% radio-opacity
3-4	50%	50% radio-opacity
4-5	75%	75% radio-opacity
6	100%	100% radio-opacity

3.2.5.1.1.3 Reproducibility and reliability

The radiographs were selected randomly and the examination was repeated twice, one week apart, on each occasion the order of the radiographs was altered to minimise the potential effect of bias on the assessment. The rabbits ID numbers was concealed using paper tape. Standardised viewing conditions were maintained on each occasion i.e. the same dimmed-light room, with same viewing box, and the same distance apart for each examination.

3.2.5.1.2 Injection of Fluorochrome stain for assessment using UV light (Dynamic Histomorphometric)

According to a well established protocol on rabbit (Hing et al, 1999), injection of fluorochrome was carried out to test the rate of bone deposition and mineralization. Under sedation, 0.5 mg/kg Oxytetracylcine was injected at a concentration of 20 mg/ml one month from the day of surgery; at a dose of 0.2 mg/kg. Calcein blue (Sigma Aldrich, UK) subcutaneous injection at concentration of 50 mg/ml was given after 2 months from the day of surgery; at a dose of 0.5 mg/kg. Alizarin complexone dihydrate (Sigma Aldrich, UK) subcutaneous injection at concentration of 30 mg/ml was given at 7 days before the animals were euthanatized.

All the animals were euthanatized three months post operatively with an overdose of Lethobarb IV (Pentobarbitone sodium BP 20% W/V, Fort Dodge Animal Health, Southampton, UK), 140 mg/Kg. The death of the animals took place in seconds, which was confirmed by cardiac arrest and cessation of involuntary reflexes. Extra-oral radiographs were taken. The mandible was immediately harvested together with the attached soft tissues, which were carefully dissected out, including all the remaining attachments of the surrounding muscles and rinsed with saline and kept in a saline-soaked sponge. The mandibles were then transferred into properly labelled special plastic containers, and kept in -80°C deep freeze for

CBCT scan which was done on the same day at Glasgow Dental Hospital and School. The samples were fixed into a container containing 100 ml of 10% buffered formalin prepared from paraformaldehyde (Fisher-Scientific, UK) and phosphate buffered saline (Sigma-Aldrich, UK). All safety precautions for the handling of formaldehyde were carried out which includes the use of nitryl gloves, the material was only used in a well-ventilated area and the breathing of fumes or splashing skin and clothes were carefully avoided. Finally the specimens were transferred to special laboratory service for further analysis.

3.2.5.2 Method of assessment of bone regeneration after animal`s euthanasia

3.2.5.2.1 Cone beam computerised tomography (CBCT)

The explanted mandibles underwent CBCT scanning using i-CAT (imaging sciences international) scanner. The following setting was applied: 6 cm field of vision (FOV) scan, 120 kV for 20 sec, 0.3 mm pixel/voxel size, at 23.87 mA. The mandible was mounted on a rubber base material holding the muscle and the bone in a stable position during examination; the fixation plate and screws were kept in place during the radiographic examination. The CBCT setting was validated at Glasgow Dental Hospital and School (Weldon et al, 2008).

The mandibles were mounted on a stable plastic mounting table especially designed to fit over the metal frame gate to stabilise patient's head during CBCT scanning, small rounded latex blocks were placed under the mandible to provide a satisfactory contrast for the bones, providing a flat base and allowing the mandible to reach an appropriate position to face the X- ray beam. Fixation plate and screws were kept in place during the CBCT scanning.

All data were stored in a digital format on optical discs, then the captured images were analysed to assess the nature of tissue regeneration, its cross-sectional area analysis, linear measurements and volumetric analysis were also carried out.

Each surgical defect and its associated tissues were divided into three sections (anterior, posterior and middle). From each section 3 coronal slices were retrieved of the CBCT scans. In each section, the average recorded surface area was estimated by importing the CBCT coronal image into a computer-aided image analysis software system (Image J version 1.36b; NIH, Bethesda, MD) the analysis of each section was carried out as described by Honma et al, (1999) (Figure 3.6). Each image was converted to a binary image and the areas of radio-opacities where analysed by counting the related number of pixels/µm. The summary of the results showed the number of measured areas, the measurement of total surface area, the average size of the measured areas, and the percentage of the counted pixel in relation to the total surface area of the examined field of view. The median values of percentage of radio-opacities "bone formation" were estimated.
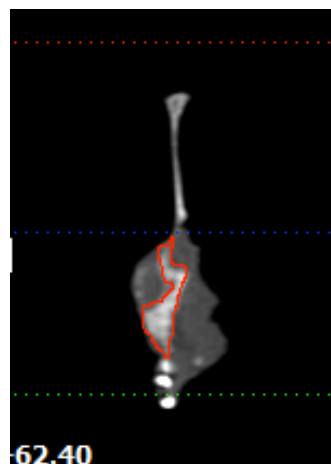
Figure 3.6: Coronal slice from i-CAT implant screen for sample 151, shows the examined tissue surface area per coronal slice is highlighted with red line

3.2.5.2.1.1 Volumetric analysis

The volume of the regenerated bone was calculated from the coronal section surface area multiplied by the thickness of the slice. The mean and standard deviations of the volume of bone formation were estimated by multiplying the radio-opaque area of each coronal section by the thickness of the section as explained by Honma et al (1999). The reproducibility of the method was carried out by repeating the measurements, three times, one week apart and the differences were assessed using the paired Student t-test. The median value and range were calculated for all the examined cases. The same measurements were carried out on the contralateral non-operated side for comparison.

The fixation plate and screws were carefully removed after the CBCT scanning without disturbing the newly formed tissue and to avoid micro-fractures or cracks of the regenerated tissue. The mandible was then separated into two halves.

3.2.5.2.2 Micro-CT scans

Following the CBCT scanning the mandibular samples were sectioned into halves. Only 4 experimental sides and one control non-operated side were included in this part of the study. This was predominantly to reveal the nature of the micro-structure of the regenerated tissue. The hemi-mandibles with area of interest were transferred into 120 ml cylindrical sample containers filled with 10% formalin to the Mellanby Centre for Bone Research, University of Sheffield. The container was placed inside the Sky scan 1172HR micro-CT machine (SKYSCAN, Aartselaar, Belgium) (Figure 3.7).
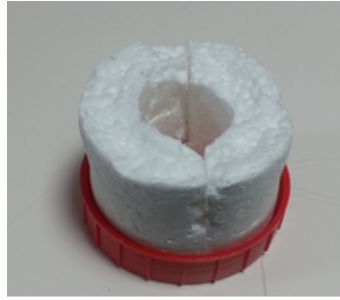
Figure 3.7: The polystyrene roller designed to hold the specimen while carrying out the examination inside the SKYSCAN machine.

The scanner was calibrated following standard procedure using Skyscan 1172 HR micro-CT (Skyscan, Aartselaar, Belgium). The optimal scan setting was empirical by trying a small range of voltages with the test sample (Figure 3.8), and then chose the setting that provided the best possible contrast. A 1.00 mm aluminium filter which is one of the standard filters supplied with the Skyscan 1172 system was used to get rid of low energy rays that negatively affect the sample contrast of the bone samples.

Figure 3.8: Photograph for the dry hemimandible with muscle tissue filling the defect, injected with cement prepared for micro-CT scanning.

Due the nature of our samples (muscle, cement and bone), the micro-CT settings were adjusted as follows: voltage 100 kV; current 167 µA; exposure time 120 sec; Field of View (FOV) = 2000 x 1024 pixel; isotropic voxel size 17 µm. The acquired data were reconstructed using N-Recon Software, GPU and (Skyscan, Belgium). For data archiving and storing, a high speed, high capacity tape system (LTO4 Ultrium) was used. The Field of View (FOV) was identified in all samples, which

contained the regenerated tissue at the area of the created defect. The selected volume of interest (FOV; 3 cm × 1.59 cm) was located in the ramus of the mandible at the site of the created defect (Figure 3.9). All the images were binarized using the same parameters. This investigation aimed to evaluate the newly regenerated tissue architecture and the interphase between the native bone and the regenerated tissue.

The bone tissue was separated from the suurounding soft tissue using a thresholding method. This process was based on matching the binary and the row images and the thresholds were then selected accordingly. The global thresholding procedure as explained by Gauthier et al (2005) was also adapted. A threshold higher than 68% of the maximal X-ray attenuation was used to identify the un-dissolved remaining of the Biphasic Calcium Phosphate (BCP) biomaterial, a threshold between 50% and 68% signified bone and thresholds below 50% represented marrow and soft tissue properties. The actual threshold value depends on settings during the scan and the reconstruction stages. Once the threshold has been chosen, the same value was applied for all samples. Thresholding was improved by applying noise reduction filter frame averaging to the images before the threshold operation. A median filter (radius size 1) was used as this effectively suppresses noise without affecting the edges of structures.

The area at the region of the defect (ROD) was defined and determined. Then calculation of bone volume fraction (BVF) which represented the volume of the mineralized bone (BV) over the total volume (TV) was carried out. Due to the pattern of tissue regeneration, volumes of calcified areas were determined inside the muscular tissue (medial or lateral to ROD) as well as within the ROD.

Three different locations were selected around the border as representative areas to assess interface between regenerated tissues and the surrounding native bone.

The 3D images were reconstructed using CT Vol Software (Skyscan, Belgium), micro-CT also determined the pattern of bony ingrowth within area of the defect.

(a)   (b)
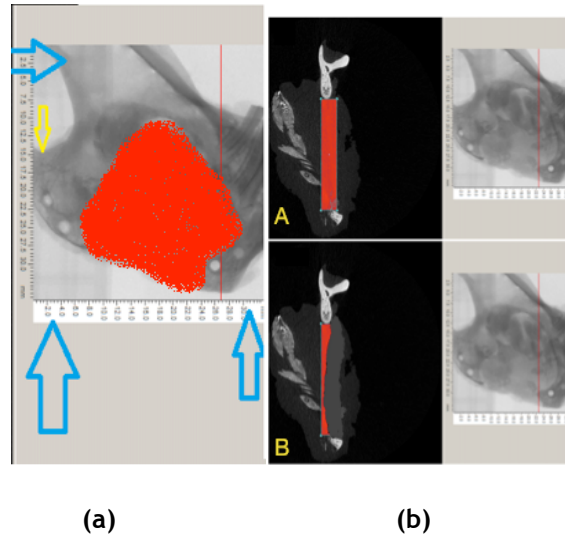
Figure 3.9: Screen shot from Micro-CT scanning for the right ramus area, showing the FOV that was selected for all the samples; red area indicate area of the defect, blue arrows indicate the limitation of FOV, a) shows the sagittal view of FOV, b) Coronal sections, the medio-lateral thickness was determined to be 2.5 mm thick as in (A). B) The thickness of the ROD adjusted based on the bone on the contralateral side.

3.2.5.2.2.1 Data analysis

The radiographic voxel data were used for the analysis of the volume of the area of interest (4 mm × 4 mm × 4 mm) which corresponding to 286 voxels. The gray-value images were segmented using a low-pass filter to remove noise and a fixed threshold was used to extract the mineralized bone phase. Bone surface area (BS) was evaluated using a marching cubes algorithm to triangulate the surface of the mineralized bone phase. Bone volume (BV) was calculated using tetrahedrons corresponding to the enclosed volume of the triangulated surface. The total volume (TV) was the volume of the whole examined sample. The specific bone surface or bone surface-volume-ratio BS/BV was measured. BV/TV was also analysed using the images retrieved from the sagittal cuts through the defect using Imag J software (Das et al, 2013). The results provided the number of counted areas, measurement of total surface area, average size of the areas, and the percentage of the counted pixel in relation to the total surface area of the

examined field of view. The median value from BS/TS was correlated to the quantitative plain radiographic scoring ΣQS as explained in section 3.2.5.1.1.2.

Trabecular thickness (Tb.Th) was determined by the thickness of the trabeculae of the regenerated bone, the average was calculated to give Tb.Th. Trabecular separation (Tb.Sp) was calculated by measuring the diameter of the pores, which represent the marrow cavities, between the trabeculae. Trabecular numbers (Tb.N) were also calculated for each part of the regenerated bone. The measurement of the mineral density as the gray scale from the micro-CT provided the mineral content of the regenerated tissue.

For each sample 10 reading of each of the micro-CT parameters were recorded and averaged, the median was calculated for the examined cases. All the measurement was repeated three times with one week apart to minimise the assessment errors.

3.2.5.2.3 Histology

3.2.5.2.3.1 Protocol for preparation and cutting the samples for decalcified histological assessment

Samples were then transferred in special container in 10% buffered formalin to specialized histological preparation (Oral Pathology Department, Kings College London). The area of regenerated bone was sectioned including 3 mm margins of the surrounding native bone (Figure 3.10). The cut was performed using a diamond-grinding disc under copious irrigation EXAKT-Micro-Grinding system, Norderstedt, Germany). All cuts were kept in plastic containers, which contain 10% buffered formalin w/v, and kept for 2 weeks before preparation (to ensure minimal exposure to light as fluorochrome is light sensitive). The histology sections run horizontally from anterior to proximal border of the defect, including the native bone on either side of the cuts (Figure 3.10a). The cut divided the section into

superior, middle, and inferior compartments. Each section was divided into two smaller sections (Figure 3.10b). From each section, undecalcified, and decalcified slides were prepared. One of the undecalcified sections was stained with Sanderson`s–Van Gieson or Goldener`s trichrome stains (stain mature and osteoid bone differently), and the other was left without staining to allow for fluorochrome bone label analysis and the evaluation of the rate of mineralization of the regenerated bone. The decalcified sections were prepared then stained with (H & E). Three slides were prepared from the contra-lateral (control side) for comparison.
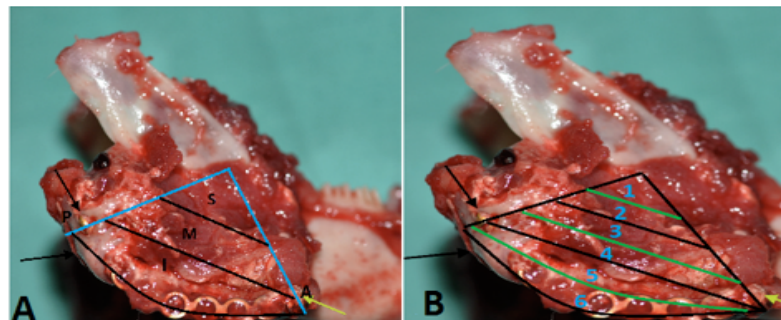
Figure 3.10: Images for the explanted mandible showing the divisions of the sample for histological examinations. A) The black horizontal lines representing the section cut lines that divid samples into superior (S), middle (M) and inferiors (I). B) The six horizontal cuts which were obtained by dividing each of the the three main sections (green lines) into upper and lower segments.

3.2.5.2.3.2 preparation of the undecalcified sections

The specimens were dehydrated in a graduated ethyl alcohol solution. Then, infiltrated and embedded in Technovit 7200 VLC (Heraeus Kulzer, Wehrheim, Germany). Ground sections were prepared using the EXAKT- Micro-Grinding system, Norderstedt, Germany) and polished sections of 75 µm thickness were obtained. The sections were then stained with Sanderson`s-Van Gieson stain and Glodener`s trichrome; (stain mature and osteoid bone differently) and mounted on glass slips for assessment

Slides were examined under light microscopy (Zeiss, Germany), five random areas were chosen using 2X objective, then the representative area were captured at different objectives 10X, 20X, 40X using Axio-Vision Camera, and was saved as tiff -File format. Moreover, serial images were captured at 5X magnification and exported to software (Microsoft ICE) which allowed the "stitching" of several images to be examined together.

3.2.5.2.3.3 Data Collection
3.2.5.2.3.3.1 Qualitative Decalcified histology slides assessment

The superior, middle and inferior decalcified sections were examined to explore the type and maturity of the regenerated bone, development of cortices, the presence of residual scaffold material and related inflammatory cells. The quality of bone regeneration was scored using a semi-quantitative scale according to Reikeras et al (2011) as in (Table 3.3). The median score was considered for overall scores of the examined cases.

Table 3.3: Semi quantitative scoring for qualitative assessment of bone regeneration and graft incorporation (Reikeras et al, 2011)

Description	Grade
Cortex development	
No cortex	0
One cortex intact	1
Both cortices intact	2
Residual implant (cement)	
No residual implant	0
Less than 50% of implant area	1
Cement remnant > 50% of implant area	2
Marrow fibrosis/ Collagen fibres	
No marrow spaces	0
>5% occupied with marrow area	1
>20% occupied with marrow area	2
Inflammatory cells	
less than 20 cells at high power field	0
One focus > 20 cells at high power field	1
Two or more focui	2

3.2.5.2.3.3.2 Analysis of the undecalcified sections

3.2.5.2.3.3.2.1 Static Histomorphometry

The ground sections were subjected to histomorphometric analysis to assess the percentage of the regenerated bone, the residual cement, and the surrounding fibrous or muscular tissue. The contralateral-non operated side was also examined for calculation of average surface area and the trabecular spaces for comparison. The images were exported to a computer-aided image analysis software system (Image J version 1.36b; NIH, Bethesda, MD). The scale bar was calibrated with the software, and the image changed into to grayscale at 8 bites. The image was

processed to binary code and the relevant areas where analysed by counting the

pixels/µm to measure areas of bone formation. Percentage of bone was calculated

according to Abu-Serriah et al, 2005, the following equation (3.2) was applied:

% of bone =

$$\frac{\sum \text{area of the microscopic field} - (\text{area of cement} + \text{area of the soft tissue}) \times 100}{\sum \text{area of the microscopic field}} \qquad \text{Equ(3.2)}$$

3.2.5.2.3.3.2.2 Dynamic Histomorphometry

The undeclacified unstained specimens were viewed by fluorescence microscopy

(Zeiss Axioskop, Germany) using R/G light filter (HBO 100, LEj, Germany). The

images were captured and exported in "image J" software for measurement.

Before the analysis, the scale bars of the images were calibrated and the distance

between bands of different label was measured. For each case 10 linear

measurement per subject were recorded for calculation of the mineral apposition

rate (MAR). The average MAR in (µm/day) of bone ingrowth was determined and

compared with the corresponding MAR on the contralateral side. The calculation

was carried out according to a well established protocol (Frost et al, 1981) which

was validated in rabbit model by Hing et al (1999)(Equation 3.3).

$$\text{MAR} = \frac{0.73 \sum_{x=1}^{x=n} Dx}{n \times t} \qquad \text{(Equ 3.3)}$$

We determined three variables before calculating the MAR, these variables

were: the distance between two fluorochrome labels in micro meter (D);

determine number of measurement (n); time interval between the

administration of fluorochrome (t); 0.73 is the correction error of trabecular

orientation.

Chapter 4

In vitro Investigation

Assessment of cellular viability on calcium sulphate/hydroxyapatite injectable scaffold

Table of Contents

4 In vitro Investigation

4.1 Introduction

Bone marrow aspiration is a common source of MSCs and thus it was selected in this research. There is evidence to show that the bone marrow contained more osteogenic stromal cells than peripheral blood that makes transplanted bone-marrow aspirate a promising tool for enhancing bone regeneration (Smiler et al, 2008). Furthermore, a reasonable volume of marrow may be obtained and the harvest of cells can be performed with less time and cost. On the other hand, selection of MSCs based on their multi-potential and the plastic-adherent population seems to be the most scientifically popular descriptor without implying unproven biologic or therapeutic potential (Friedenstein et al, 1966; 1970; Owen and Friedenstein, 1988; Kaiser et al, 2007). Therefore, the protocol of CFU-F formation, a well-known method for testing the differentiation potential technique of the cultured MSCs was adapted to confirm the identity of the cultured cells. Immunofluorescent staining, and reverse polymerase chain reaction (PCR) tests were used for assessment of the multi-potential of the cells using osteogenic markers including osteopontin and osteonectin. Therefore, the study plan was to harvest bone marrow stromal cells from the posterior iliac crest and the decision was made to expand heterogeneous MSCs colonies for two reasons; Firstly to ensure that all cells that will be implanted have an osteogenic potential, secondly, to allow BMPs to enhance the osteogenic potential of MSCs. Specific surface markers for rabbit MSCs namely CD166, CD44 positive and CD34 negative were tested using an immunofluorescent assay, based on common MSCs surface markers that have been tested in the literature (Oswald et al, 2004; Kaiser et al, 2007; Huang et al, 2009).

Cerament[TM] cement is available commercially for spinal fusion (Cerament[TM] Spine Support) and as filler for bone cavities (Cerament[TM] Bone Void Filler) with different formulations, setting speeds and mechanical properties (Nilsson etal, 2003; Masala et al, 2012; Karr etal, 2011; Rauschmann et al, 2010; Hatten et al, 2012). To our knowledge, there are no published data testing these two materials at the cellular level. The biocompatibility testing was carried out by implanting the material at ectopic and orthotropic sites using rat model (Nilsson, 2003). The application of injectable scaffold (loaded with cytokines and seeded with undifferentiated mesenchymal cells) for maxillofacial reconstruction was not considered, and the suitability of the material for this application has not been tested yet. This in vitro study is part of a comprehensive research programme to take the material from the laboratory to clinical maxillofacial application. This is an essential step before applying the material in a preclinical model (chapter 5). Thus, after performing all cell characterization, a study was conducted to investigate the interaction between Cerament [TM] and the undifferentiated rabbit mesenchymal stromal cells (rMSCs) and to inform the optimum surgical approach.

4.2 Material and Methods

4.2.1 Bone marrow aspiration

A 16–gauge needle was used to penetrate the cortex of the posterior superior iliac spine. Rabbit bone marrow was collected in a tube containing 3000 units of heparin. These were collected in centrifuge tubes 5-7 mls per tube with 20 ml of culture medium Dulbecco's Modified Eagle's Medium (DMEM, Sigma-Aldrich, UK) which contains 10% filtered fetal calf serum FCS (Life Technologies, UK), 2% mixture of streptomycin, penicillin, fluconazole, and glutamine (Life Technologies,

UK), 1% Sodium pyruvate (Sigma-Aldrich, UK) and 1% non-essential amino acid (Sigma-Aldrich, UK)).   The samples underwent a centrifugal force of 1400 rpm (376 g) for 10 minutes at room temperature to remove the fat, debris, and lysed cells. The formed pellet was resuspended into 10 ml of DMEM and centrifuged for 10 minute at 1400 rpm. The medium was discarded and the pellet was resuspended in a further 10 ml DMEM. The suspended cells were loaded into 7.5 ml Ficoll-paque ^{TM} premium gradient media (GE Health care, Life Sciences, Buckinghamshire, UK) slowly down the side of the universal tube then centrifuged at 1513 rpm (445 g) for 45 minute and decelerated slowly. The top layers including the interface, which includes the nucleated cells fraction with rMSCs around 3 ml, was placed into another tube for two further washing cycles using DMEM for 10 minute and centrifuged at 1400 rpm.

Finally, cells were cultured in complete DMEM as described previously and incubated at 95% humidity at 37°C and 5% CO_2 for 2-3 weeks. The medium was changed twice a week. When the cells, with a typical fibroblast like morphology, had reached semi-confluence, they were passaged from the tissue culture flasks; this involved removal of the culture media, and washing the cells in Dulbecco's phosphate buffered saline (DPBS, Sigma-Aldrich, UK) twice before removing the cells with a trypsin/EDTA solution (Sigma- Aldrich, USA) for 5 minutes at 37ºC. The trypsin was inactivated by the addition of an equal volume of Dulbecco minimum essential medium (DMEM, Sigma-Aldrich, UK) supplemented with 10% FCS and the cells were collected by centrifugation. At this point, the cells were re-suspended in 5 ml of DMEM supplemented with 10% FCS, and counted using a Neubauer haemocytometer before performing cell assessments.

4.2.2 Cell culture and preparation

Triplicate samples for each planned test was prepared. The glass cover slips were sterilised with 70% ethanol (Life technologies, UK) followed by a rinse with HEPES (sigma-Aldrich, UK) twice before cell seeding. The suspended cells rMSCs were seeded onto glass coverslips (13 mm diameter) in 24 well plates. The seeding cell density was at 1×10^4 cells/ml (2 ml per well). Immunofluorescence staining for a three surface marker proteins were carried out at days 7, 14 and 28 (Table 4.1)The examination was carried out using fluorescent microscopy (Leica-Letiz DM IRB, Germany), 5 random fields of view were imaged per well using an Axiovision camera (Zeiss, Germany). Image superimposition and processing was carried out using Adobe Photoshop (version 8 software). Low magnification imaging (5 X) was used for cell counts by detecting the nucleus stains (DAPI) in blue which get excited at 360 nm, and emitted at 460 nm wavelength; this was repeated at different time points: 3, 7, 14 and 21 days. The cell count protocol was achieved by using a grid sheet adjusted on the microscope eyepiece. Five random areas of each cover slip were selected. The mean cell count per coverslip was calculated.

4.2.3 Immunofluorescent staining for cell characterization

Immunostaining was undertaken to test different phenotypical proteins (Table 4.1). The following materials were prepared for the immunofluorescent staining. A fixative solution was prepared by adding 10 ml formaldehyde (Fisher Scientific, UK) into 90 ml of phosphate buffered saline PBS (Sigma-Aldrich, UK) then 2 g sucrose (Fisher Scientific, UK) was added and dissolved. 1% Bovine serum albumin (BSA)/PBS (Sigma-Aldrich, UK) solution was prepared by dissolving 1 g

bovine serum albumin into 100 ml PBS (Sigma-Aldrich, UK). Then a 0.5% Tween 20/PBS solution was composed of 0.5 ml of Tween 20 (Fisher Bioreagent, UK) in 100 ml PBS which was made to wash the samples after staining. Permeablisation buffer (Perm buffer) was prepared by adding the following: 10.3 g sucrose (Fisher Scientific, UK), 0.292 g NaCl (Prolabo, UK), and 0.06 g $MgCl_2$ –hexahydrate (Prolabo, UK) 0.476g Hepes (Fisher Bioreagent, UK) in 100 ml PBS. The pH of this solution was adjusted to 7.2 by adding 0.5 ml Triton X 100 (Sigma-Aldrich, UK). The fixative, 1% BSA/PBS, 0.5% Tween20/PBS (v/v) and perm buffer was warmed up to body temp (37 ℃) before use. Secondary biotinylated anti-mouse (Vector Lab, UK) antibody was prepared, which was made up 1:50 with 1% BSA/PBS, i.e. 20 μl of secondary antibodies in 1 ml of 1% BSA/PBS. Then a tertiary, streptavidin (Vectorlab, UK) was prepared by a dilution of 1:50 i.e. 20 μl of tertiary antibodies in 1 ml of BSA/PBS.

Following the removal of the culture medium, cells were rinsed once with PBS then cells were fixed by adding 1 ml of the fixative 10% formaldehyde (Fisher-Scientific, UK)) into each well and kept at 37℃ for 15 minutes. The permeabilisation buffer was added to the cells after removal of the fixative, and this was kept at 4℃ for 5 minutes. The perm/buffer was removed and 1% BSA/PBS was added-then incubated at 37℃ for 5 minutes. Next, the primary antibodies prepared in PBS (1:100 in 1% BSA/PBS) (Table 4.1) were added to the phalloidin (1:100 in 1% BSA/PBS) (Invitrogen, USA). The well plate was wrapped with aluminium foil and incubated at 37℃ for 1 hour. The primary antibodies and the phalloidin were removed then washed 3 times using 0.5% Tween 20/PBS. The secondary antibody was then added and wrapped with aluminium foil and

incubated at 37 ºC for 1 hour. The antibody was removed and washed 3 times for 5 minutes with PBS/0.5% (v/v) Tween 20. The streptavidin-Fluorescein IsothioCyanate (FITC) was added after discarding the washing detergent then wrapped with the aluminium foil and incubated at 37ºC for 30 minutes. Finally, streptavidin was removed and washed 3 times for 5 minutes with PBS/0.5% (v/v) Tween. A small drop of Vectroshield-DAPI stain was mounted on a labelled microscope slide and each cover slip was inverted (on which the cells were grown) onto the Vectorshield drop. The slides were then ready for examination under inverted fluorescent microscope. The examination was carried out on the same day using fluorescent microscopy (Leica-Letiz DM IRB, Wetzlar, Germany), 5 random fields of view were imaged per well using an Axiovision camera (Zeiss, Jena, Germany). Once the images were taken, they were processed using Adobe Photoshop (version 8 software).

Table 4.1: Shows all antibodies that were used for immunostaining

Primary antibody	Location
CD44 (Abbiotec, CA, USA)	MSC surface marker
CD166 (Abcam, UK)	MSC surface marker
CD34 (Abbiotec,San Diago, USA)	Surface marker for hematopoitic MSCs
Osteocalcin (AbD serotec,USA)	Osteogenic differentiation marker
Vinculin (Antibodies-online.com)	A membrane-cytoskeletal protein for focal adhesion plaques
Peroxisome proliferator-activated receptor gamma (PPARG, Antibodies-online.com)	Transcriptional regulator of adipocyte differentiation

4.2.4 Cell differentiation potential

MSCs were cultured in defined osteogenic and adipogenic media for assessment of osteogenesis and adipogenesis differentiation ability of the cells respectively. After the 1st cell passage, a cell count was performed and then cells were divided into three groups. The first two groups of cells were seeded at cell density of 1×10^4 per 2 ml of cell suspension into two 24 well plates over glass cover slips. The last group was seeded into a 25 cm^2 flask at 5×10^5 cells/ml density and was kept to test the gene expression of osteogenic markers osteocalcin (OCN) and osteopontin (OPN) and the housekeeping gene glyceraldehyde-3-phosphate dehydrogenase (GAPDH).   Cells were left for 3 days in the basal culture medium DMEM before being changed into either an osteogenic medium or an adipogenic medium; they were then kept for 28 days before assessment was performed. The osteogenic medium was prepared by using 500 ml of α-MEM (Sigma-Alrich, UK) supplemented with 10 % FBS (Life Technologies, UK), 100 nmol/L dexamethasone (Sigma-Aldrich, UK) and 50 µmol /L -ascorbic acid-2phosphate (Sigma-Aldrich, UK). The medium was replaced twice a week for 3 weeks. Cell differentiation was examined by immunofluorescent staining for osteocalcin (OCN, AbD serotec, USA) and gene expression for both osteocalcin OCN and osteopontin OPN (Invitrogen, USA), see section 4.2.3.1; 4.2.3.2.   For adipogenic differentiation, cells were seeded in a new 24 well plates and cultured for 28 days in the adipogenic medium. This medium was prepared by using 500 ml of DMEM supplemented with 10% FBS, 1µmol/L dexamethasone (Sigma-Aldrich, UK), 0.5 mmol/L 3-isobutyl-methylxanthine (Sigma-Aldrich, UK), 0.2 mM indomethacin (Sigma-Aldrich, UK) and 10 µmol/L Insulin (Sigma-Aldrich, UK. After 28 days of cell culture the cells were subjected to immunofluorescent stains for peroxisome proliferator-activated receptor gamma (PPARG, Antibodies-online.com).

4.2.4.1 Reverse Transcriptase polymerase Chain Reaction (RT PCR)

4.2.4.1.1 RNA Extraction

This assessment aims to recognize the gène expression for osteogenic markers namely osteopontin (OPN, Invitogen, USA) and osteocalcin (OCN, Invitogen, USA) in cells which were cultured 28 days in the osteogenic medium. GAPDH, (Invitogen, USA) gene was considered as a control which is housekeeping gene because the GAPDH gene is often stable and constitutively expressed at high levels in most tissues and cells. The gene-specific primers were synthesised commercially (Invitrogen, USA); the genes, accession numbers, primer sequences, size, and annealing temperatures are listed in (Table 4.2).

Cells that grew in the osteogenic cell culture medium for 28 days were trypsinized. This process was started by removal of the culture medium then the cells were washed with HEPES a biological buffer (Sigma-Aldrich, UK). Afterwards, 1-2 ml of 0.1-0.25% Trypsin-Versene (Sigma-Aldrich, UK) was added to the cells, and these were incubated for 2-5 minutes at 37 ºC until the cells detached from the flask. Medium was then added immediately to the flask to inactivate the trypsin. Cells were transferred to a polypropylene centrifuge tube (RNAse free) and centrifuged at (300 g= 1800 rpm) for 5 minutes. The supernatant was completely discarded and then cell pellets were disrupted by flicking the tube and adding 350 µl Buffer RLT (RNeasy Mini Kit, Qiagen, Germany). The lysate was then pipetted and collected into a 1.5 ml collection tube, and centrifuged for 5 minutes at 300 g. 70% ethanol was added to the lysate and mixed well by pipetting. The samples were transferred to an RNeasy MinElute spin column placed in a 2 ml collection tube. The tube lid was closed gently and centrifuged for 15 seconds at > 8000 x g (> 10,000 rpm). The flow through was collected in the collection tube and discarded.

350 µl of Buffer RW1 (RNeasy Mini Kit, Qiagen, Germany) was added onto the membrane which was placed in a new collection tube (RNeasy MinElute spin column) and then centrifuged for 15 second at >8000 g (> 10,000rpm); to wash the spin column membrane. The flow through was discarded afterwards, then, 80 µl of DNase incubation mix (RNeasy Mini Kit, Qiagen, CA, USA) was added directly to the RNeasy MinElute spin column membrane, the mix was placed on the bench top (20-30 °C) for 15 minutes. The added DNase was used to digest any DNA contaminant inside the tubes. The tubes were subjected to another centrifuge cycle. Afterwards 350 µl buffer RW1 (RNeasy Mini Kit, Qiagen, Germany) was added to the RNeasy MinElute column and centrifuged for 15 seconds at > 8000 ×g (> 10,000 rpm); the flow through the membrane and the collection tube were discarded.

New collection tubes were placed into the RNeasy MinElute Spin column; a 500 µl Buffer RPE (RNeasy Mini Kit, Qiagen, Germany) was added and centrifuged for 15 seconds at ≥ 8000 to wash the spin column membrane. The flow-through was then discarded; 500 µl of 80% ethanol was added to the RNeasy MinElute spin column, this was centrifuged for 2 minutes at 8000 g. After centrifugation, the columns were removed carefully from the collection tubes, and placed in new collection tubes. The tube lids were kept open and centrifuged at full speed (≥ 10,000 rpm) for 5 minutes for drying. Finally, the RNeasy MinElute µ spin column was placed in a new 1.5 ml collection tube; and 14 µl RNase-free water (RNeasy Mini Kit, Qiagen, Germany) was added directly to the centre of the spin column membrane, and centrifuged for 1 minute at full speed (≥ 10,000 rpm) to elute the RNA.

4.2.4.1.2 RNA to cDNA

The next step was to convert the RNA into cDNA. Firstly, the concentration of RNA was measured using a nano-drop reader; the reading of this machine was in ng/µl. Adjustment of RNA concentration was considered according to the least RNA concentration among the samples. Thus 4µl of RNA was added to 7 µl of water into the RNase tube mix. Then it was incubated in the thermocycler (Master Cycle personal, Eppendorf, Germany) machine at 65°C for 5 minutes then cooled down to 4°C. This was to break the H-bonds in RNA samples. 9 µL of reaction mix was made by mixing the following (2 µl of 10x Buffer RT (RT kit, Qiagen, Germany), 2 µl of dNTP (RT kit, Qiagen, Germany), 2 µl random Primer (Invitrogen, UK) 500 ng/reaction, 0.25 µl of RNase inhibitor (40U/µL), 1 µl of Ominscript R transcriptase (RT kit, Qiagen, Germany) and 1.75 µl H_2O). The reaction mix was added to the RNA mix with a total volume of 20 µl. The whole mix was then centrifuged at 8 g for 1 minute to ensure that all liquid reached the bottom of the tubes. Then it was incubated into the thermal cycler at a set program of 3 cycles first, 37°C for 60 minutes, then to 93°C for 5 minutes, and finally cooled down to 4°C.

4.2.4.1.3 PCR

The preparation for the polymerase chain reaction (PCR) was conducted by preparing a master mix. The master mix was prepared in bulk with an extra 10% in small tubes: 5 µl GoTaq® buffer (Promega, UK), 0.2 µl GoTaq® enzyme (Promega, UK), 0.75 µL of 100 µM foreword primer, 0.75 µl of 100 µM reverse primer (table2), 2 µl MgCl (Promega, UK), 2 µl dNTP (RT kit, Qiagen, Germany), and 13.8 µl H_2O. Next 2 µl of the cDNA was added to the master mix in each tube. The tubes were arranged into the thermal cycler (Master Cycle personal, Eppendorf, Germany) and then the following program was run which included: 95ºC for 2 minutes for initiation then the three consecutive cycles run 30 times:

95°C for 30 second denaturation followed by 50ºC for 30 seconds for annealing, then 72ºC for 30 seconds to gain elongation. Lastly, the final elongation was achieved at 75 ºC for 30 seconds; the machine was then cooled down at 4°C. The above process aimed to amplify DNA. The final step was to assess the reaction and screen the presence of the gene of interest. Two important constituents were prepared, the agarose gel (Roche, UK) and the ladder mix preparation: The agarose gel was prepared by mixing 20 ml TBE buffer, 21.8 g Tris (Boehringer Mannhem), 11.9 g Boric acid (Fisher Scientific, UK), 1.86 g EDTA (Riedel-deHaën) + 2 L of H_2O, 0.3 g agarose (Roche, UK), 2 µl Sybr safe DNA gel stain (Invitrogen, UK). The ladder mix was prepared by mixing 2 µl ladder (Biolabs, UK), 6 µl H_2O, and 2 µl gel loading dye (Invitrogen, UK). The gel constituent was mixed and placed in the microwave until the agarose completely dissolved, the gel was then poured inside the small tank (Xcell sure lock, Bio-RAD), and a comb was inserted inside the gel. After 15-20 minutes the gel was set, and the comb was withdrawn, the tank was filled completely with x1 TBE. The formed wells were loaded with the amplified DNA and the first and the last wells were left for the molecular weight ladder mix. Afterwards, the electrophoresis generator was connected and started at 100 volts. After about 20 minutes the yellow band with dye started to move slowly along the gel until it reached ¾ of the way along the gel, then the generator was stopped and the gel was moved and viewed using a UV light machine reader (using Gene snap software, UV syber save).

Table 4.2 shows the primer gene sequence for the assessed gene, their size and annealing temperature.

Genes	Primer Sequence(5`-3`) (forward/reverse)	Product size(bp)	Annealing temperature
OPN	forward: G A C A G C C A G G A G A A G G A C A G reverse: T C T T C A C T C T T C G G C T C G A T	169	50
OCN	forward: G T G C A G A G T C T G G C A G A G G reverse: G G T T G A G C T C G C A C A C C T	153	50
GAPDH	forward: T G C C C T G G G G T G G G A A T G G A reverse: A G G G G T G A G G G A C A C G A G G C	200	45

4.2.4.2 Immunofluorescence for osteocalcin - osteogenic extracellular component

This technique was undertaken to test osteocalcin (OCN, Serotec, UK) which is a late osteogenic protein secreted by osteoblasts into their extracellular environment. In addition to the actin filament stain (rhodamine phalloidin, invitrogen) a nucleus stain, DAPI (Vector Lab, UK), was undertaken. The same protocol was used as explained in section 4.2.2. However, the secondary antibody was biotinylated anti-mouse (Vector Lab, UK) and the tertiary layer streptavidin (Vector Lab, UK)-FITC were used. The slides were then ready for examination under an inverted fluorescent microscope.

4.2.5 Characterization of Injectable calcium sulphate based cement

The scaffold was formed by mixing 60% α-calcium sulphate hemihydrate (α-CSH) with 40% hydroxyapatite HA (Cerament[TM] Bone Support, Sweden),a commercially

available product, consisting of a powder and a liquid phase. The liquid phase was an iodine-based water soluble, non-ionic radio-opacity enhancing component containing two different concentration of iohexol (Cerament^{TM}|C-Tru, Bone support, Sweden). When the powder was mixed with the liquid phase, an easily injectable paste was formed. The paste provided easy administration and good visibility during injection. During the experiment two subtypes of CS/HA cements were used. The Cerament^{TM} Bone Void (CBV) filler which was mixed with Cerament^{TM}|C-Tru using an iohexol concentration of 180 mg /ml, with a powder to liquid ratio of 1g/0.43 ml of liquid. However, Cerament^{TM}Spine Support (CSS) powder was mixed with Cerament^{TM}|C-Tru at an iohexol concentration of 300 mg /ml, with a powder to liquid ratio of 1 g/0.5 ml. The α-CSH showed large, rectangular shaped primary crystals that were compact and well formed with sharp edges after mixing with the liquid phase (Figure 4.1 and 4.2).
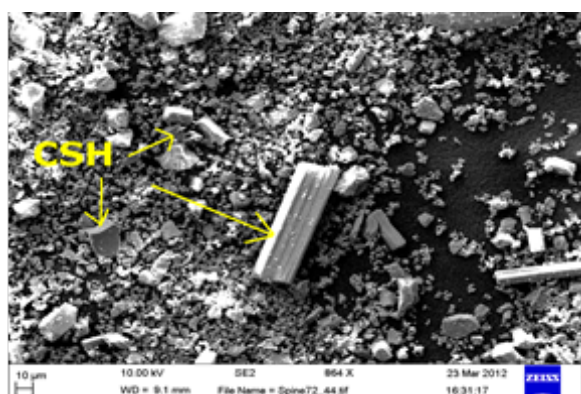
Figure 4.1 SEM of CSH/HA powder of Cerament ^{TM}, shows CSH in rectangular and rod in shape (arrows), and the smaller particulars are HA, scale bar= 10 µm.
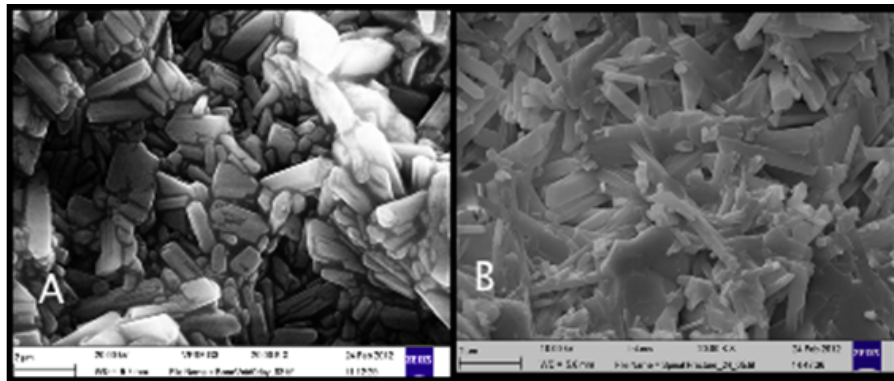
Figure 4.2 SEM of the mixed Cerament^{TM} which attained compact structure of well interconnected crystal, HA crystals are longer than CSD crystals, a) shows CSD of Cerament^{TM} Bone Void, b) CSD of Cerament^{TM} Spine Support, scale bar= 2 μm .

α-CSH has high density (ρ = 2757 kg/m^3) compared to a β-CSH form (ρ = 2637 kg/m^3). The solubility of α-CSH in water is 0.67% at 20°C. The material is metastable below 40°C under atmospheric pressure and will hydrate in contact with water to form calcium sulphate dihydrate CSD (Equation 4.1). The size of the crystals of CSD which were long and flat in shape were about 4-6 μm in length, and spread in every direction forming a matrix of well interconnected crystals. The formed cement was not macroporous, but rather microporous with the average size of micropores being 5 μm (Figure 4.3). CSD has a very high resorption rate, the advantage of this fast resorption rate of CS was to enhance pore formation and therefore allow angiogenesis and bone ingrowth. It has been observed that two thirds of CSD was resorbed after one week from implantation of the material in the muscle in vivo (Nilsson et al, 2003).

$$CaSO_4. 1/2H_2O + 3/2\ H_2O \rightarrow CaSO_4\ .2H_2O. \qquad \text{(Equ 4.1)}$$
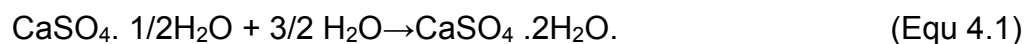
The other component of the cement is 40% HA $Ca_{10}\ (PO_4)_6\ (OH)_2$ which is a calcium phosphate compound with a calcium /phosphate (Ca/P) ratio of 1.67. It has a similar chemical composition to the mineral phase of bone. However, it is

stoichiometric and has no ionic substitution like biological apatite. The crystallinity of this heat treated HA was high and renders the HA non-resorbable (Nilsson, 2003). The HA crystals were longer than CSD crystals at about 6-8 μm in length and it was possible to distinguish it from the CSD-matrix (Figure 4.2). The delay in resorption of HA makes this material reconstruct bone in a natural way. Therefore, HA particles were added to provide osteoconductivity and to get integrated with newly formed bone and to provide sufficient strength at the early healing phase (Nilsson et al, 2003).

The compressive strength of the CSD/HA scaffold depends on the amount of water added, the morphology of HA, the HA content and the amount of accelerator used. This was estimated to be 31.0 ± 6.1 MPa based on HA morphology. However, a liquid to powder ratio of 0.43 ml/g, decreased the compressive strength to 20 MPa (Nilsson et al, 2003). It has been reported that the compressive strength for this cement was similar to that of cancellous bone when implanted. Moreover, this cement has been designed to have stiffness close to that of cancellous bone in order to avoid stress shielding effects while conserving the natural healing and the mechanical properties of cancellous bone. It has been found that new bone in growth into this scaffold occurs as early as 3 to 6 weeks and HA was embedded within the new bone (Nilsson, 2003). Moreover, an in vitro study for the calcium-sulphate based material showed that once the material was soaked in simulated body fluid (SBF) it creates calcium phosphate precipitates on the material surface. These precipitates are formed by the reaction between released calcium ions from the samples and phosphate ions in the solution. The layer of precipitate is only loosely adherent and sloughed off in sheets with time. These reactions between calcium and phosphate will proceed until no more calcium sulphate is left (Nilsson, 2003). Interestingly, the Ca/P ratio

of the precipitates is similar to bone mineral and this was reported to stimulate bone in growth in vivo. More rapid bone contact was obtained on surfaces treated with bone like apatite (Yan et al, 1997; Kokubo et al, 1996).
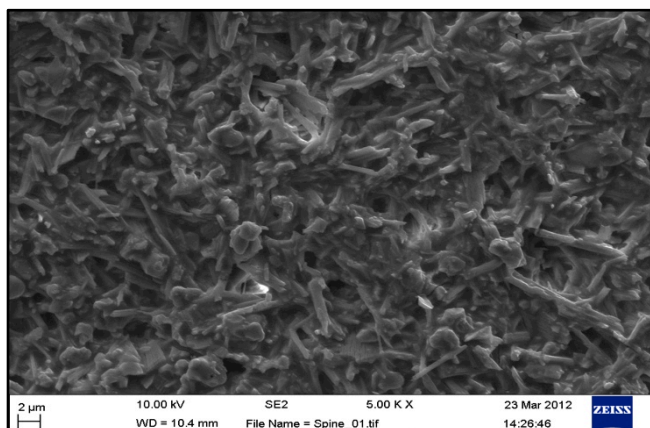
Figure 4.3: SEM of Cerament^{TM} shows the microstructure for CS-HA was mainly compact and the range for pore size was 10-5 μm when the ratio of liquid to powder was 0.425 ml/g. SEM for CSD after setting reaction, scale bar= 2 μm.

Element composition and mapping of the cement powder using SEM composition and mapping the cement powder was undertaken using energy-dispersive X-ray analysis (Zeiss Sigma SEM, Germany). The results showed the presence of three key elements: sulphur, calcium, and phosphorus at different concentrations and with different shapes. The percentage of sulphate-calcium which was present in the form of rectangular and rod crystals were given a red colour code by the computer software. The small grains were composed of calcium-phosphate which was presented as green in colour. Data indicated that the percentage of the calcium sulphate (red) to calcium phosphate (green) colour was 60%, 40% respectively (Figure 4.4).

Finally, samples were prepared by embedding the sample into a metallurgical resin to quantify the percentage of porosity and the size of micropores. Samples were sputter coated and viewed by SEM. Under SEM, black areas represent the

pores that were filled with resin, whereas the rest of the cement appeared as grey in colour (Figure 4.5). In general, the cement appeared compact which inhibited the quantification of the percentage of porosity using wavelength-dispersive X-ray analysis (WDX), this would have allowed quantitative microanalysis against standard software. The pore size was measured using a calibrated measuring tool. The maximum pore size was 10 µm and the minimum was 5 µm.

(a)

b)
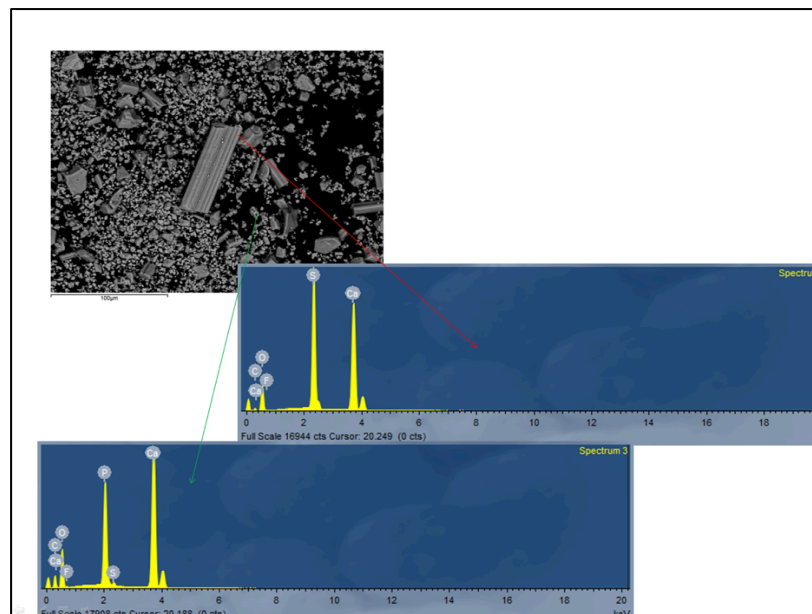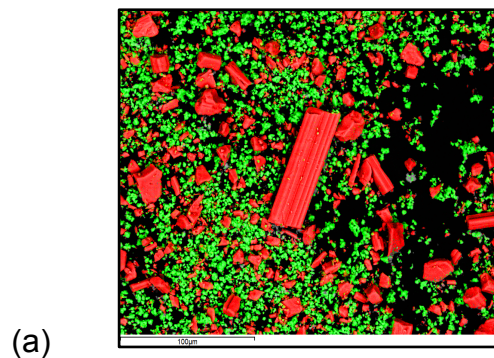
Figure 4.4 (a) Photomicrograph showing a microanalysis for the Cerament^{TM} powder composition using wavelength-dispersive X-ray detectors the red area indicates the CSH particles, whereas the green is the small grain composed of calcium-phosphate (HA), the scale bar = 100 µm. (b) Graph showing the mineral composition of the red crystals which were made of calcium sulphate (60%), graph showing the mineral composition of the green crystals which were made of calcium phosphate (40%), scale bar= 100 µm.
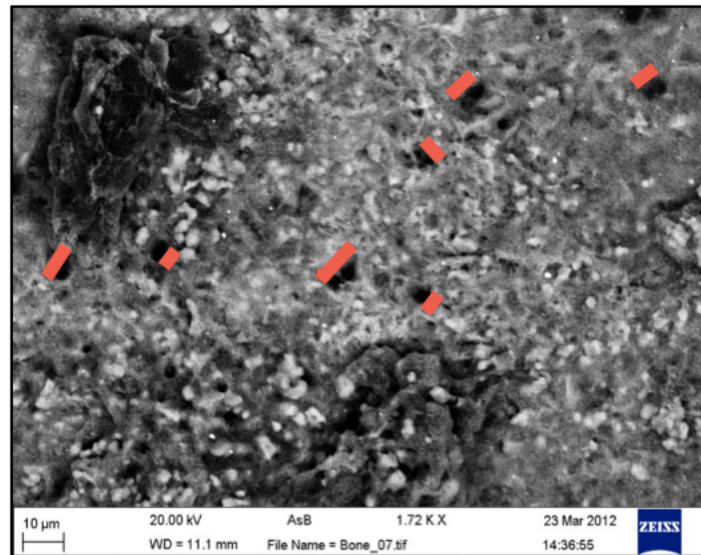
Figure 4.5: Photomicrogrph of SEM for Cerament^{TM} samples that was prepared by embedding the sample into a metallurgical resin, showing the size of the pores (red lines) ranged from 10 μm to 5 μm, scale bar=10 μm.

4.2.6 BMP-7 (OP-1)

BMP-7, like all other sub-groups of BMPs are part of the transforming growth factor (TGF) -superfamily (Abu-Serriah, 2005). Recombinant DNA technology has revealed that BMPs are synthesised as larger precursors that undergo proteolysis before secretion. The active molecules of BMP-7 are dimeric polypeptides bound to each other by disulphide bonds. This material is best presented in heterodimer form which makes it more biologically active providing a broad range of effects on target cells than a homodimeric compound. The BMP-7 used in this study was highly purified and freeze dried. Recombinant human BMP-7, comprised of vacuum dried type-I bovine bone collagen produced by Chinese hamster ovary cells in culture and purified from culture media. The BMP-7 (rhOP-1) implant vials containing 3.5mg of powder were used (Stryker BIOTECH® MA, USA). 0.4 mg of freeze dried powder was added to 3g of calcium sulphate/HA

powder which was mixed with 1.26 ml of iohexol solution to form a construct for rMSCs tests at different time points.

4.2.7 Biocompatibility assays using MG-63

4.2.7.1 Live and dead staining for cell cultured with Cerament^{TM}

Developing a reliable method for seeding cells into CSH/HA cement for tissue engineering approach was attempted. This process involved seeding cells onto the cement. Two constructs were made, the MG-63 cell line was made ready for seeding on the top of the scaffold or mixing cells with the CSH/HA powder and iohexol solution.

MG-63 cells were cultured and before they reached semi-confluence, they were washed with DPBS twice before removing the cells with a trypsin/versene solution (1/10) for 5 minutes at 37°C. The trypsin was inactivated by the addition of an equal volume of DMEM supplemented with 10% FCS and the cells were collected by centrifugation. At this point, the cells were suspended in 5 ml of DMEM supplemented with 10% FCS (Life Technologies, UK). Once the cement paste was prepared it was loaded into 5 ml syringes and then was injected into 24 well plates. The suspended cells were seeded onto the surface of freshly mixed cement (CSS, CBV) in each well plate at a density of 1×10^4 in 2 ml of the culture medium for the first construct and mixed with cement for the second construct. The plates were incubated at 37°C and 5% CO_2. Cell viability assessment was carried out using live and dead assay kits (Bioscience, UK) at different time points, namely 24 hours, 72 hours and 7 days from the day of seeding.

The live / dead stain assay was performed for all samples; samples were divided into three groups depending on the day of assessment, and each group consisted

of 4 well plates. This assessment was performed to quantify the percentage of dead and live cells. To perform the live and dead test two types of stains were used: calcein AM (Bioscience, UK) to stain the cytoplasmic esterases of live cells green (esterase cleave the calcein so it fluorescence), and ethidium homodimer (Bioscience, UK) which stained the compromised cells with red (it can only enter the nuclei of compromised cells); the stains appeared green and red under fluorescent light respectively. Dye dilution was prepared by adding 1 µl/ml DMEM for both stains. The old culture media was removed from the scaffold construct first and then the dye and medium was added to each well. The construct was then left inside the incubator for 30 minutes; afterwards the dye was removed and replaced with 1 ml of DMEM. The examination was carried out immediately using fluorescent microscopy (Leica-Letiz DM IRB, Germany) under low power objective (5 x), five random fields of view were imaged per well using an Axiovision camera (Zeiss, Germany), and images were processed on computer using Adobe Photoshop, Version 8.

The live and dead cells test was also considered for the cells that have been cultured around different cements. The percentage of living cells was estimated by dividing the number of live cells over the number of total cell counts and multiplied by 100(Equation 4.2).

% of viable cells =   no. of vital cells   × 100   (Equ 4.2)
                  Total number of the examined cells

4.2.7.2 MTT- 3-(4, 5-Dimethylthiazol-2-yl)-2, 5 diphyenyltetrazolium assay

3-(4,5-dimethylthiazol-2-yl)-2,5-diphenyltetrazolium bromide (MTT) (Sigma-Aldrich, UK) is a colorimetric assay for measuring the activity of mitochondrial enzymes

(yellow) that reduce MTT to form insoluble purple formazan crystals giving a purple colour. The main application allows the assessment of the viability (cell counting) and the proliferation of cells (cell culture assays). It can also be used to determine the cytotoxicity of potential medicinal agents and toxic materials, since those agents would stimulate or inhibit cell viability and growth.   The MG-63 cell line was made ready for seeding on the top of the scaffold. The scaffold was prepared by mixing calcium sulphate/hydroxyapatite powder with iohexol the liquid phase (powder to liquid ratio were 1g/0.43 ml, 1g/0.5 ml for CSS and CBV respectively).   Once the cement acquired a paste-like consistency it was spread over the glass slip with thickness of 2 mm. Before the material was set, it was divided into equal squares, these were placed in to each of the 24 well plates. The prepared cell suspension was seeded on the surface of the prepared squares of different type of cement as explained in section (4.2.4). Cells were seeded at density of 1×10^3 cells/cm^2 after 15 minutes of mixing the cement. Wells containing cells only (no cement) were used as controls. The plates were incubated and maintained at 95% humidity at 37°C and 5% CO_2. Cell viability was determined after 24 hours, 72 hours and 7 days of culture using the standard colorimetric MTT assay to detect the presence of living cells. The reduction of the yellow MTT substrate only takes place when mitochondrial enzymes are active, and therefore conversion is often used as a measure of viable (living) cells. 100 μl of methyl thiazoly tetrazlium (MTT, Sigma Aldrich, UK) was added into both (the experimental and control) wells in the plate. The plate was incubated for 1.5 hours. Then the supernatant of each well was removed and 200 μl dimethyl sulfoxide (DMSO) was added into all wells. An optical density (OD) reading was obtained to correlate directly with cell number and was used to determine the relative number of live cells on each cement i.e. the light absorbance is directly proportion with the

cell numbers. The plate reader (Dynatech MR7000, Channel Islands) was adjusted to a wavelength of 550 nm.

The light absorbance of this coloured solution can be quantified by measuring the adjusted wavelength (usually between 500 and 600 nm). The percentage of viability was calculated according to (Equation 4.3)

% of cell viability= <u>Absorbance of treated cells</u> ×   100   (equ 4.3)
                                    Absorbance of control cells

4.2.8 Cellular response upon direct cell seeding

4.2.8.1 Seeding of the rMSCs and cytoskeleton immunostaining

Both cements were prepared as described in section 4.2.4 once the cement acquired a paste like consistency; it was spread over the glass coverslip at a thickness of 1 mm. Before the material set, it was divided into equal squares. The squares were placed in each well of the 24 well plates. Parallel to this, rMSCs were made ready for seeding on the top of the scaffold. The resuspended cells were directly seeded onto the surface of scaffold in each well plate at a density of 1×10^{4} in 2 ml of the culture medium. The plate was incubated at 37°C and 5% CO_2.Cell culture assessment was carried out at 24 hours and 72 hours. Immunofluorescent staining was conducted using a primary antibody against vinculin, an adhesion associated protein and a phalloidin actin probe was also used (Invitrogen, USA), with DAPI (Vector lab, UK) as described in section 4.2.2. The aim was to observe the stress fibre (actin microfilament) and focal adhesion formation as well as the size and shape of the cells on the surface of the different scaffolds. Cells cultured at the sides of the wells were used as a positive control.

4.2.8.2 Scanning Electron Microscope Examination

The scanning electron microscope (SEM) examination used in this research was a Carl Zeiss (Sigma VP Oxford Micro-analysis, Germany). This is a field-emission SEM that produces images at high and low operating voltages.   The machine has secondary electron and backscattered electron imaging with high-resolution in-lens. It also enabled uncoated specimen characterisation using a low vacuum mode. The machine allows use of Energy-dispersive X-ray analysis (EDX): 80 nm detector for rapid determination of elemental compositions and structural mapping. The use of a wave length x-ray (WDX) allowed for quantitative microanalysis. The other specification which allowed determination of crystalline orientations was the electron backscatter diffraction (EBSD), SEM based technique that was used to identify crystalline material and determine their crystallographic orientations (Payton and Nolze, 2013). EBSD mapping could also be combined with simultaneous X-ray microanalysis for complete sample characterisation.

4.2.8.2.1 Sample preparation for SEM examination

Both bone cements were prepared as described in section 4.2.4. The suspension of rMSCs was seeded on the surface of the prepared constructs.

After 1 or 3 days of cell culture, rMSCs on the test material were prepared according to a standard protocol for SEM examination to allow the viewing of individual cells (Dalby et al, 2002). All samples were fixed using 1.5% gluteraldehyde (Sigma-Aldrich, UK) in 0.1M sodium cacodylate buffer (Agar Scientific Ltd, UK). The fixative was warmed up to 37°C immediately before pouring onto the cells and fixed at (4°C) for an hour. The samples were then rinsed with 0.2 M sodium cacodylate buffer (Agar Scientific Ltd, UK) at pH 7.4 and left overnight in the fridge (4°C). 1% Osmium tetroxide (Oxkem Ltd, UK) made up

in 0.2M sodium cacodylate buffer was used to postfix the samples for an hour. The samples were then rinsed twice for 5 minutes using sodium cacodylate buffer. Samples were then immersed into 1% tannic acid (TAAB Laboratories Equipment Ltd, USA) in 0.1M sodium cacodylate buffer for 60 minutes. They were then rinsed twice for 3 minutes with 0.2 M sodium cacodylate buffer then washed eight times using alcohol of different concentrations (20%, 30%, 40%, 50%, 60%, 70%, 90%, and 100%) (Ethanol – BDH, UK), each washing cycle lasted for 3 minutes and each cycle repeated twice. The samples were dried using 100% alcohol and the process was repeated three times for 5, 10, and 15 minutes. Finally, the samples were rinsed with hexamethyldisilazane (HMDS, Sigma-Aldrich, UK) in a glass container, the procedure was repeated, which took 2 minutes each. Samples were sputter coated, and then left to air dry for SEM examination.

4.2.9 Cell seeding into a collagen model

4.2.9.1 Collagen preparation

Collagen gels were used to mimic clinical tissue into which the material will eventually be injected. Collagen was prepared by using a Type I collagen from rat-tail which has been treated with chloroform at a protein concentration of 2.05 mg/mL added to 0.6% acetic acid (Millipore Ltd, Temecula, CA, USA); 0.5 mL of DMEM was added to 0.5 mL FCS, and then, 2.5 mL of the collagen was added simultaneously with 1 mL of 0.1 M NaOH. The addition of 0.1 M NaOH was needed to adjust the acidity of the collagen mixture to neutral until the colour turns to red; the universal tube was placed on an ice bath. Then, 1.5 mL of the mixture was poured in each well plate, triplicates were made for each experiment. The mixture was then incubated at 37°C before cement/cell injection.

4.2.9.2 Injection of MG-63 and cement into collagen

For scaffold preparation, Cerament ^{TM}Spine Support was prepared by mixing 3 g of the calcium sulphate/hydroxyapatite (CS/HA) (60:40) powder with 0.629 mL Cerament |C-Tru (opacifier, Bonesupport, Lund, Sweden) solution and 10^3/0.6 mL cells suspension in culture medium, the resultant formed paste was loaded into a 5-mL syringe. The liquid scaffold was injected into the prepared collagen using an 16-gauge needle (Figure 4.6). The scaffold inside the collagen was then incubated at 37°C and 5% CO_2 overnight, and the collagen was detached from the sides of the well using a needle; fresh media was then added to feed the cells. A live/dead stain was performed as described earlier.

4.2.9.3 Injection of cement into a collagen construct

Cerament ^{TM}Spine Support powder was mixed with Cerament |C-Tru, with a powder-to-liquid ratio of 1 g/0.5 mL, and immediately injected into the collagen. After 15 min, 0.6 mL of rMSC suspension was injected between the CS/HA bone cement and incubated at 37°C and 5% CO_2 overnight. Then, live/dead staining was carried out using calcein-AM to stain viable cells and ethidium homodimer to stain compromised cells (Biolab, UK), following the same protocol described earlier. A set of experiment was repeated using rMSCs (Figure 4.7).

Figure 4.6: Image for collagen construct, shows the well plate which contain the prepared collagen constructs and the injected cement; collagen construct (red) and the injected scaffold with cells (white).
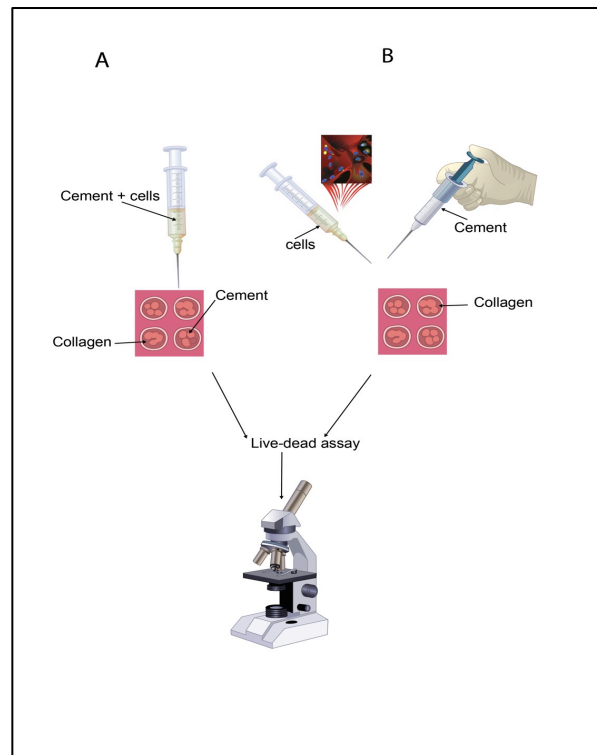
Figure 4.7 A) shows cement and cells are mixed together in one syringe then injected into collagen, live and dead assay was carried out after 24 hours of cell culture, B) shows the sequential seeding of cells and cement into the collagen, followed by live and dead stain after 24 hours of cell culture.

4.2.10 Testing of the osteogenic impact of calcium sulphate/HA on rMSCs differentiation potential using collagen model

The collagen construct was prepared as described in section 4.2.8.1. Then 1.5 ml of the collagen mixture was poured in each well plate in triplicate which was used for different experiments. The mixture was then incubated in 95% humidity at 37°C and 5% CO_2. After 24 hours 3 g of CSS was mixed with 1.5 ml iohexol. Then the mix was loaded in a 1 ml syringe, the cement was injected using a 16 gauge needle into the seeded collagen at different areas around the constructs (Figure 5.6), followed by injection of the suspended rMSCs around the CSS. The constructs were kept for 21 days inside the incubator, maintained in 95% humidity at 37°C and 5% CO_2; the culture media was changed twice a week. At day 21, the immunofluorescent stain was carried out on rMSCs seeded on collagen using an

osteocalcin antibody (OCN, AbD Sertec, USA) to assess the osteoinductive potential of cement on the seeded cells as described in section (4.2.2).

4.3 Results

4.3.1 Immunofluorescence staining of rMSCs surface markers

Positive staining was reported using CD166, CD44 surface markers which indicated the cells were rMSCs (Figures 4.8& 4.9). Staining for CD34 were negative as expected as CD34 is a hematopoietic marker. Furthermore, CD44 showed intense positive expression in the early stages of the culture, whereas CD166 showed increased expression in the cells that were in the culture for a longer time. Interestingly, staining for CD44, and CD34 at 7 days showed positive uptake in some of the flasks that were left for 4 days before changing the first media after cell isolation, it showed variable size of cells and nucleus which may indicate the heterogencity of the cell colonies (Figure 4.10). Small rounded cells were observed to take both stain CD44 & CD34 (Figure 4.10).

Composite   Actin fibre   CD44   DAPI
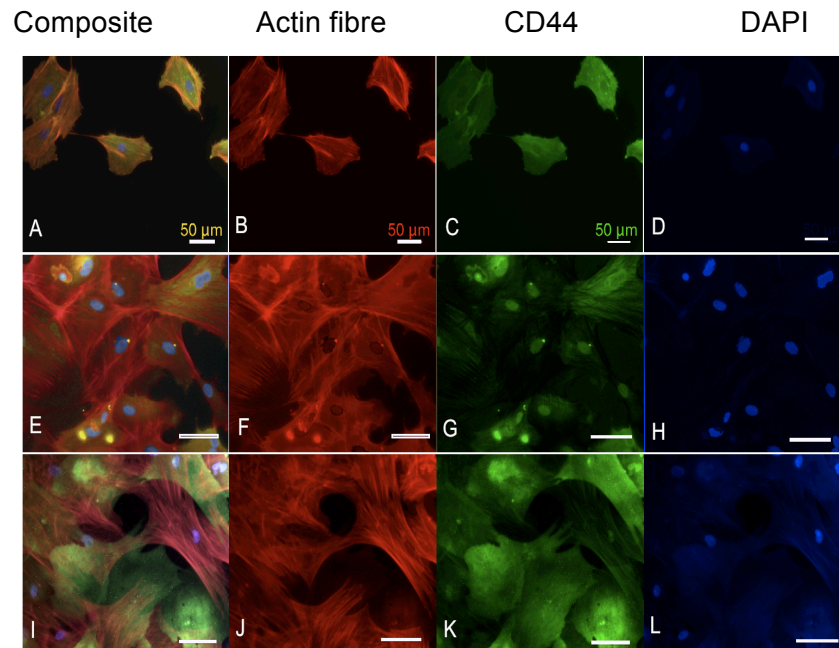
Figure 4.8: Photomicrographs of immunofluorescent stains of rMSCs using primary antibodies (CD44) at different time point. A, E & I shows composite stains for CD44, Phalloidin, and DAPI at days 7, 14 & 21 in cell culture respectively, B, F & J shows phalloidin stain for actin cytoskeleton fibres at 7, 14 & 21 days in cell culture, C, G, K show intense positive intake for CD44 antibodies at 7, 14 & 21 days in cell culture, D, H & L shows DAPI staining for the nucleus at 7, 14 & 21 days in culture. Scale bar for A, B, C, C, D = 50 μm whilst scale bar for E, F, G, H, I, J, K, L = 100 μm.

Composite   Actin fibres   CD166   DAPI
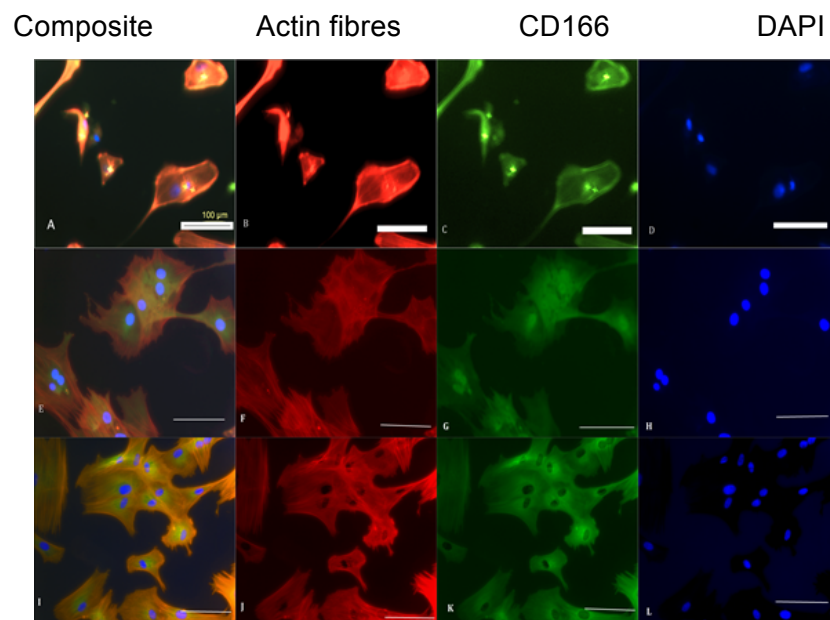
Figure 4.9: Photomicrographs of immunoflourescent stains of rMSCs using primary antibodies at different time point. A, E, I shows composite stains for CD 166, phalloidin, and DAPI at 7, 14 and 21 days respectively in cell culture. B, F, J shows phalloidin stain for actin cytoskeleton fibre at 7, 14 and day 21 respectively in cell culture, C) shows weak positive intake for CD 166 antibodies at day 7 of cell culture, but a strong uptake at days 14 & 21(G,K) respectively   D, H, L shows DAPI stain for nucleus at 7, 14 and 21 days in culture scale bar= 100 μm.

CD34
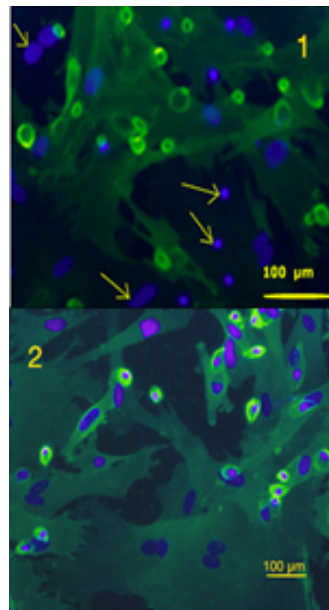
Figure 4.10: Photomicrograph of immunoflourescent stains for CD44, CD34 & DAPI for rMSCs which were left for 4 days before change the medium for the first time after cell isolation process, the stain was carried out at day 7. 1) shows mixed population of cells in flask, variable size of nucleus and unstained cells denoted with (arrows) and positive expression of large number of cells at this field of view at day 7 of cell culture, scale bar= 100 μm, 2) shows variable positive expression to CD44 antibody at day 7 of cell culture, scale bar 100 μm. The images confirm that the mixed populations of rMSC were positive for CD34 and CD 44 if the culture medium was left for 4-5 days.

4.3.2 The rate of cell growth

For cell growth, a cell count was performed for the adherent cells at day 3 and it was found that the cell density was $1 \times 10^4/cm^2$ into a 24 well plate. At day 7 the mean cell count was $2.0 \times 10^4/cm^2$ and the cell count reached 20 times that at day 14 ($220 \times 10^4 /cm^2$). At day 21, the mean cell count was $3.81 \times 10^6/cm^2$. Data showed that the growth rate was higher during the second week of cell culture (Figure 4.11). However at the 3rd week the mean cells count was reached approximately double the number at day 14. Therefore, the rate of growth was $0.25 \times 10^3/day$.
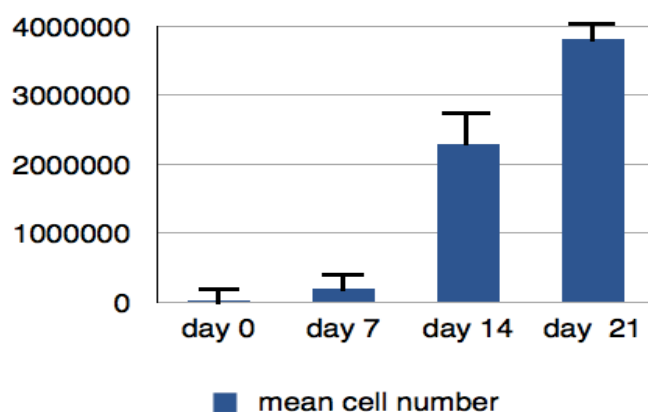
Figure 4.11: Graph shows cell growth rate from day of cell harvesting (day 0), 7, 14, 21 days of cells culturing into 24 well plate. The X–axis represent the different time point, bars =mean cell count per cm^2 error bar= the standard deviation SD, (n=3).

4.3.3 Testing cell differentiation potential

The rMSCs were induced to differentiate along osteogenic and adipogenic lineages under a specific cultured condition after 3 weeks of induction. Immunofluorescent stains for osteocalcin showed a positive expression on day 21, which indicates late protein specific marker for osteoblastic expression (Figure 4.12 A). Osteogenic differentiation was further confirmed by strong expression of osteoblastic-specific gene osteocalcin using RT-PCR (Figure 4.12 B). On the other hand, adipogenic differentiation was expressed by positive stain to PPARG as well as the cells attaining an adipocyte typical morphology (Figure 4.12 C).
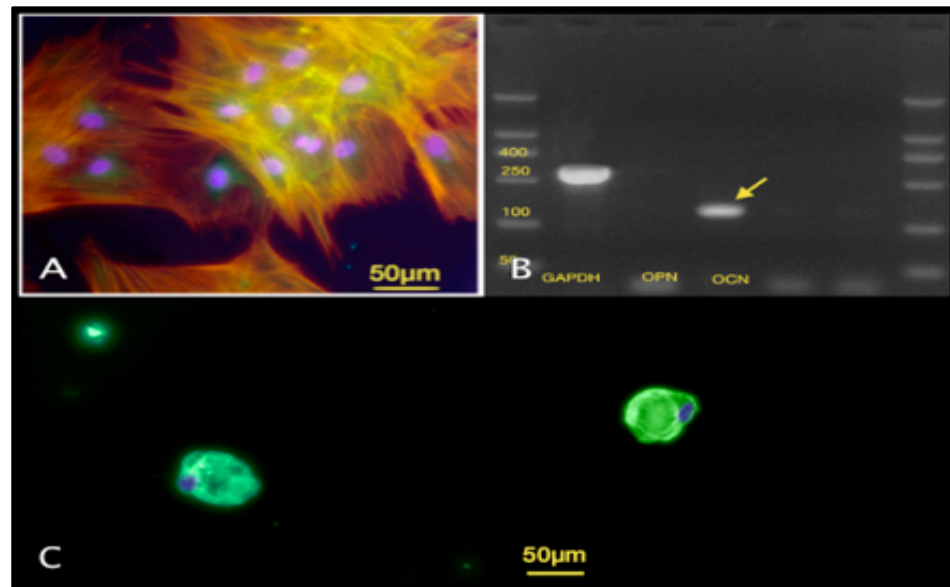
Figure 4.12 : Photomicrograph of cytoskeleton staining and polymerase chain reaction for cDNA of marker protein transcripts, A) shows positive immunofluorescence photomicrography for rMSCs for osteocalcin antibody OCN, Actin (red), and DAPI (blue) stains at 21 days of rMSCs culture (marker bars = 50µm). B) a scanned image of gel RT-PCR of osteogenic lineage marker expression in rMSCs where RNA was harvested after 21 days of cell culture showing a strong signal for osteocalcin (arrows), and GAPDH is housekeeping gene to control the test C) Immunofluorescence image shows positive intake to PPARG antibodies which indicate the adipocytic differentiation of rMSCs. All confirmed the multipotential of the test of rMSCs after 21 days of cell culture.

4.3.4 The biocompatibility test

4.3.4.1 Live and dead staining of the cells cultured on Cerament^{TM}

In the construct made of cement mixed with cell suspension, nearly all the cells were dead with a small percentage of living cells observed (Figure 4.13 A). However, cells that were seeded on the surface of the cement were easily visualised and were mostly viable (Figure 4.13 B). Live and dead assays were performed for the cells indirectly seeded and cultured around the two different versions of the same scaffold (Figure 4.14). Cells were counted to determine the percentage of live cells and the mean numbers were evaluated and statistical analysis was performed. Data showed that the presence of viable cells was 85% ± 15 and 82% ± 25 in the first 24 hours for Spine Support (CSS) and Bone Void

cement (CBV) respectively. The percentage of viable cells was 89%±8 and 84% ±

7.0 after 7 days of culture around CSS and CBV bone respectively (Table 4.3),

(Figure 4.15). The number of live and dead cells that have been cultured around

the two tested cements was also calculated. A statistically significant difference

was seen for the mean of cell count around both cements (P <0.01) on day 7 data

shown in (Table 4.4; Figure 4.15).
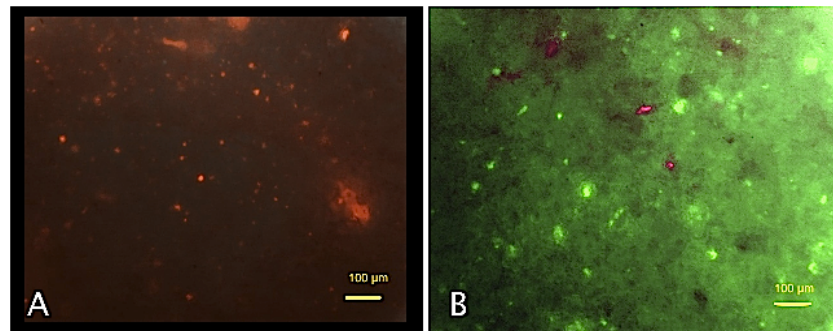
Figure 4.13: Photomicrographs showing live / dead stain (Calcein ^{AM}**, Ethidium homodimer). A) shows assessment of cell viability after MG-63 cells were mixed with Cerament**^{TM} **Spine Support which shows presence of dead cells only (red stain), B)   shows the presence of live (green) and dead cells(red) when cells were seeded on the surface of the scaffold, Scale bars= 100 µm, n=3.**
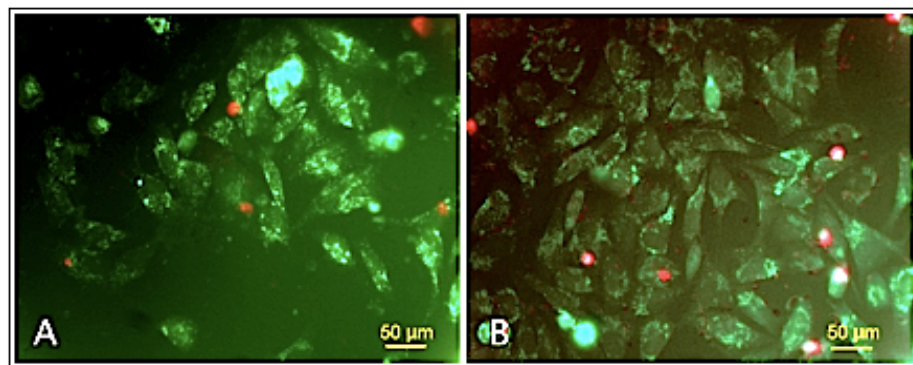
Figure 4.14: Photomicrograph for Live and dead assays of MG-63 cell proliferation and growth around A) Cerament^{TM} **Bone Voidfiller and (b) MG-63 cell proliferation around Cerament**^{TM} **Spine Support, mean cell count shows statistical difference (P< 0.05), Scale bars = 50 µm, n=3.**

Table 4.3: The percentage of live cells cultured on different cements (Cerament [TM], Bone Void "CBV" and Cerament[TM] Spine Support "CSS" at different time points.

Scaffolds	24 hrs	72 hrs	1 week
CSS	85±15	75±23	89±18
CBV	82±25	81±26	84±17
CBV (control)	84±19	93±18	94±13
CSS (control)	91±18	97±11	95±11

Table 4.4: Data showing the live and dead assay results, data shows the mean values of the cultured cells (MG-63) and their standard deviation with different treatment (Cerament [TM]Bone Void CBV/ Cerament [TM]Spine Support CSS) at different time points

Mean cell number			
Cerament[TM]	24 hrs	72 hrs	1week
CBV	57.2±5.5	71.6±13.4	105.2±34.9
CSS	49±21	75.2±19.7	145.3±15.9
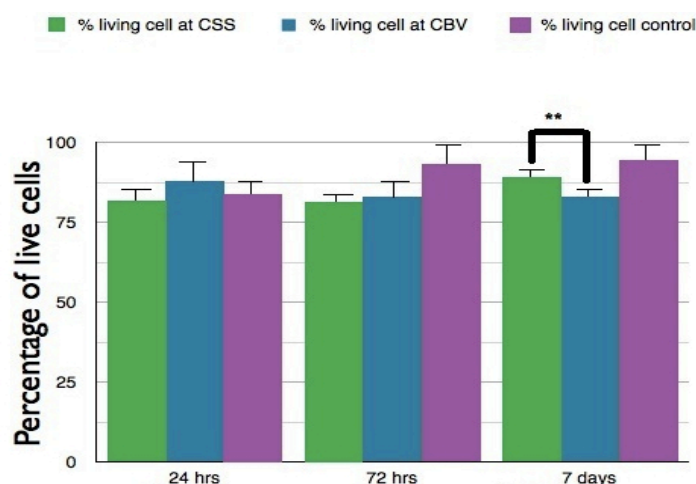
Figure 4.15:   Graph of live and dead assay using MG-63 cell line, shows the percentage of MG-63 live cells seeded on both Cerament [TM]Spine Support CSS, Cerament [TM]Bone Void CBV in respect to control cells that were cultured at the same times without cement.

4.3.4.2 Cell viability assay MTT

MG-63 were incubated with the two versions of the Cerament[TM] (CBV, CSS) material. Percentage of viable cells was determined by MTT assay (Table 4.5). In all samples the mean cell proliferation was determined by colour difference at each time point. On day 7 of cell culture, the cell numbers increased three fold compared to day one for both groups (Table 4.5). The percentage of viable cells

was equal for both cements in the first 24 hours. However, after one week of cell culture the percentage of viable cells were 90%±18 and 77%± 8 for CSS and CBV respectively (Table 4.6). However, this difference in cell proliferation was not statistically significance (p=0.08). Similarly, cell proliferation at 24 hours and 72 hours reported no statistical difference between MTT readings when compared using independent t-test for the different versions of CSH/HA cements tested (p=0.05)(Figure 4.16). The results for both live and dead staining and MTT assay were constant in the first 24 hours and at 7 days when means values were compared. At 1 week of cell culture there was a difference in mean reading however this difference is not statistical significant between CBV,and CSS(p>0.05) as analysed using student t-test on SPSS software (Figure 4.17).

Table 4.5: Data shows the mean values of MTT readings which reflect the amount of active proliferating cells (MG-63) present with different cements (Cerament ^{TM}Bone Void "CBV"and Cerament ^{TM}Spine Support "CSS" at different time points

Mean MTT values			
Cerament^{TM}	24 hrs	72 hrs	1week
CBV	0.097±0.002	0.1±0.08	0.31±0.14
CSS	0.12±0.03	0.097±0.007	0.37±0.16

Table 4.6: Data showing the results from the MTT readings from which were calculated the percentage of the number of the proliferating and hence active cells present within the different cements (Cerament ^{TM} Bone Void CBV/and Cerament ^{TM}Spine Support CSS), at different time points

(Cerament^{TM})	24 hours	72 hours	7 days
CBV	67±15	79±12	77±6.0
CSS	66±16	70±11	90±18
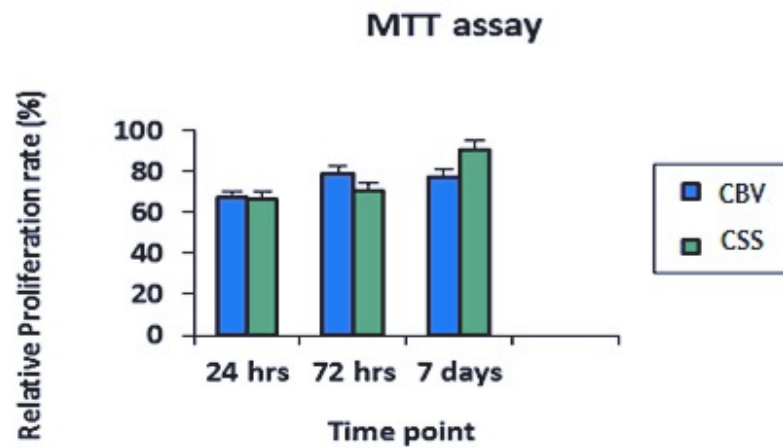
Figure 4.16. MTT toxicity assay, using MG-63 cell line, the graph shows the percentage of proliferating cells based on mitochondrial enzyme activity of the cultured MG-63 live cells seeded on both Cerment^{TM}; Cerament ^{TM}Bone Void (CBV) and Cerament ^{TM}Spine Support(CSS) at different time points.
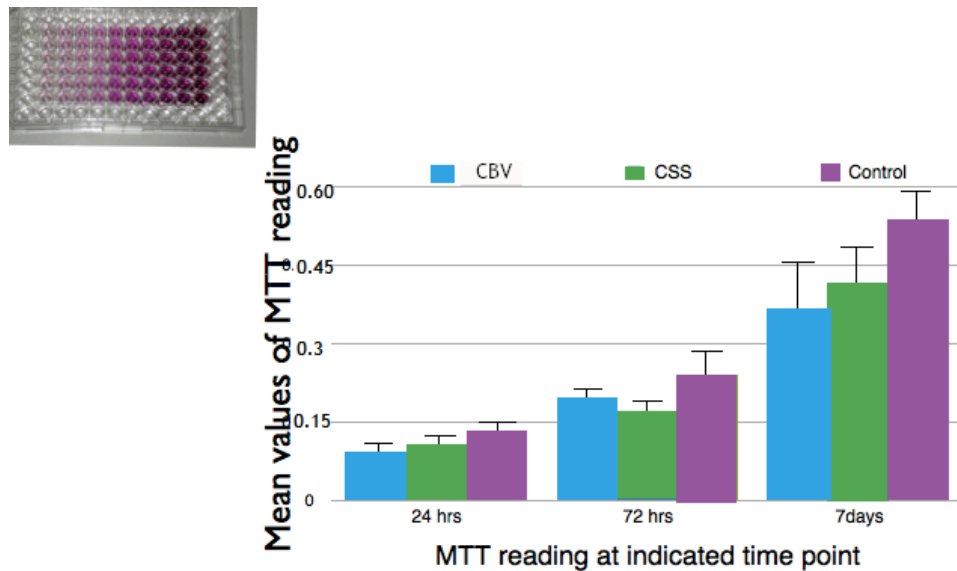
Figure 4.17: MTT toxicity assay, the graph shows the mean reading of MTT for MG-63 live cells seeded and the on both cement Cerament ^{TM}Bone Void CBV and Cerament ^{TM}Spine Support CSS. Blue and green bars represent CBV or CSS respectively.

4.3.5 Cell response upon direct cell seeding on the cement surface

4.3.5.1 Cytoskeleton staining on surface of Calcium-sulphate/HA cement (Cerament^{TM})

Cytoskeleton staining was carried out for the rMSCs seeded on the surface of

CSS and CBV. Phalloidin was used to stain actin filaments red, DAPI was used to

stain the nucleus and an anti-vinculin antibody was used to stain focal adhesions. The stains were applied at two time points of 24 hours and 72 hours (Figure 4.18; Figure 4.19). In general there was a change in shape and size of rMSCs on the surface of the cements. There was a reduction in cell adhesion and reduction of lamellipodial and filopodia extension of cells seeded on CBV cement. Cells become rounder in morphology as a result of reduced ability to adhere and spread (Figure 4.19 A). However, MSCs on CSS attained a more spread morphology, larger size and better adherence on the surface of the material (Figure 4.19 B). Imaging of cells on surface of the cement was not so bright and clear when cells were cultured for a longer times; this was due to the fast dissolution of calcium-sulphate and the deposition of apatite crystal on the cells as described in section 4.2.2 (Figure 4.19 B). Cell cytoskeleton size and shape were compared with rMSCs cultured on the glass slips.
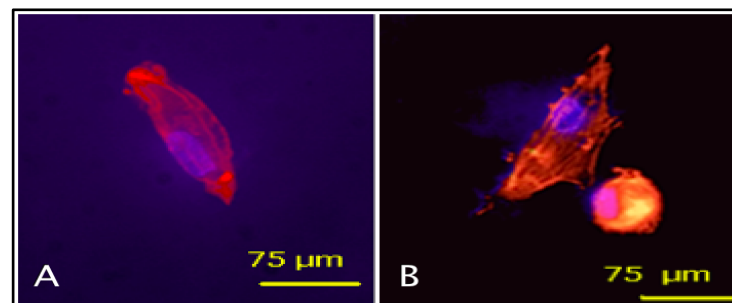
Figure 4.18: Photomicrographs of cytoskeleton staining of rMSCs after 24 hours of cell culture following the seeding on the surface of Cerament [TM]Bone Void "CBV" in figure A and on the surface of Cerament [TM]Spine Support in figure B. (scale bars = 75 µm).
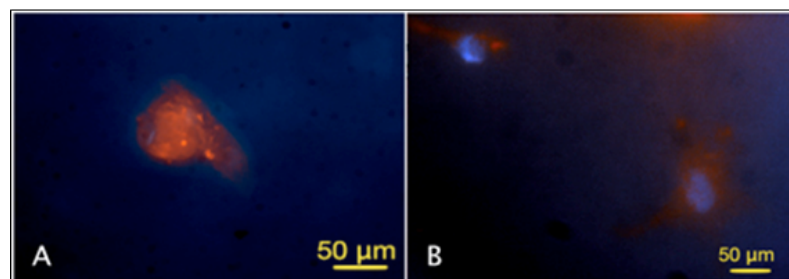
Figure 4.19: Photomicrographs of cytoskeleton staining of rMSCs after 72 hours of cell culture following the seeding on the surface of Cerament [TM]Bone Void "CBV" in figure A and on the surface of Cerament [TM]Spine Support in figure B, scale bars = 50 µm.

4.3.5.2 Scanning electron microscopy (SEM)

The cell morphology of rMSCs seeded on the different CSD/HA cements were observed with SEM. Samples that were prepared by mixing cells with the cements showed only damaged cells inside this scaffold (Figure 4.20). However, cells seeded on the surface of both versions (CBV and CSS) of CSD/HA cements were viable after 24 hours and 72 hours of cell culture. Marked numbers of cells were adhered on the surface of the CSS at the various time points (Figure 4.21), whereas, there were few rMSCs observed on the surface of the CBV cements (Figure 4.22). The rMSCs on day one were observed to adhere to the surface of the material by advancing their pseudopodia over the micropore surface or growing into the pores and adhering to various parts of the cement (Figures 4.23, 4.24). This phenomenon was observed more frequently on the CSS version scaffold more than on the CBV scaffold. Two days later, SEM examination of the rest of the prepared samples of CSS showed more rMSCs between the CSD/HA crystals or the apatite crystals and were precipitated on the surfaces of the rMSCs. Moreover, the rMSCs were found on the flat top surfaces rather than within grooves or clefts. Some areas of CSS showed rMSCs had adhered and spread on the top of the surfaces that has been covered (Figure 4.23 A, B). Cells attained normal size (60-100 μm) and they were polygonal or fusiform in shape (Figure 4.24 B, D). These cells had pseudopodia attached advancing over the crystal of CSD/HA cement and advanced over the filamentous fibres (Figure 4.25 A, B). Furthermore, the appearance of an uneven outer surface of the cells showed rounded indentation on some rMSCs which could indicate cells conforming to the shape of the cement (Figure 4.24 C, B).
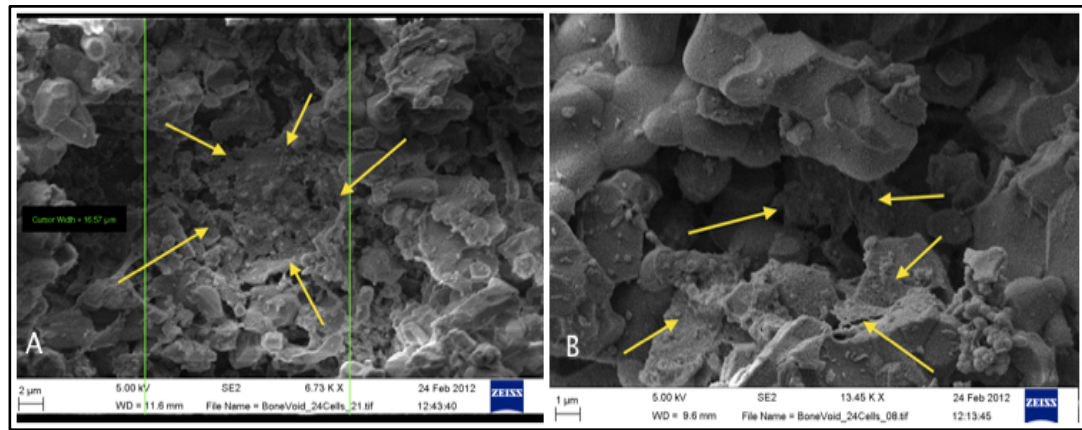
Figure 4.20 Photomicrograph SEM images assessing cell spreading when rMSCs were mixed with Cerament ᵀᴹSpine Support, a) damaged cells (denoted with arrows) inside the cement when cells were mixed with cement at day 24hrs, (marker bars = 2 μm), b) remnant of biological tissue after mixing the cells with cement.(scale bar= 1 μm).
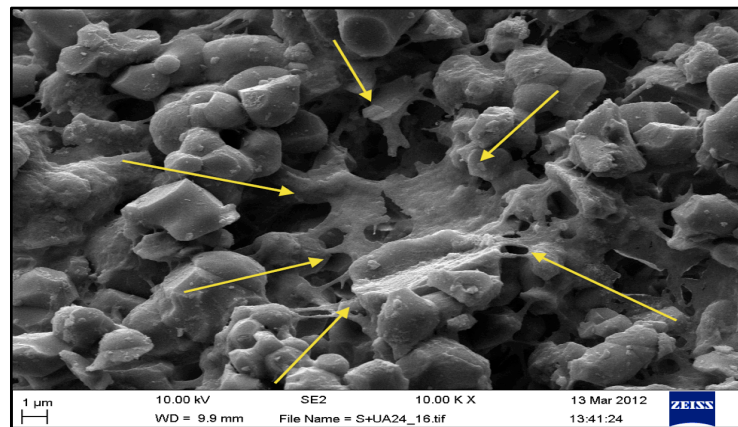
Figure 4.21 Photomicrograph of SEM for rMSCs seeded on surface of Cerament ᵀᴹSpine Support, shows rMSCs spread on the surface of the cement intermingled between the CSD/HA crystals at 24 hrs, marker bar = 1μm.
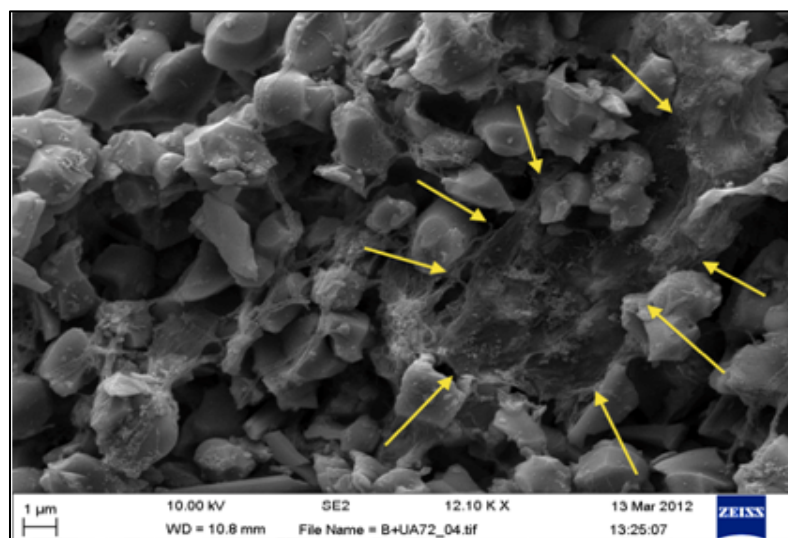
Figure 4.22 Photomicrograph SEM images for assessing cells survival when rMSCs was seeded on Cerament ᵀᴹBone VoidCBV after 24 hrs, it shows rounded cells (denoted with arrows) inside the cement crystals (marker bar = 1μm).
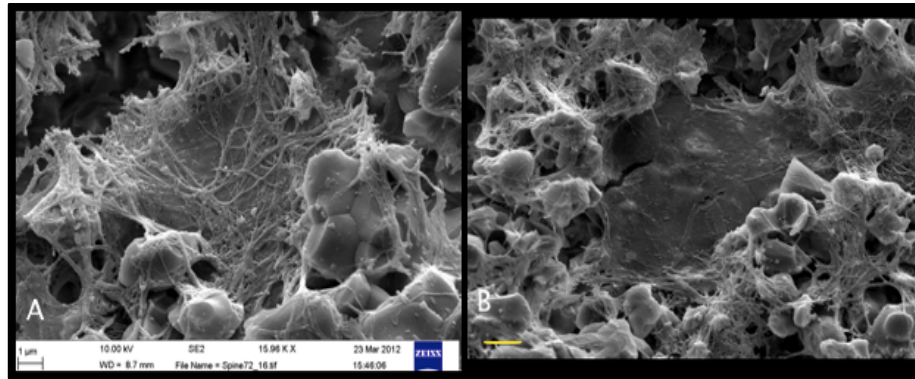
Figure 4.23 Photomicrograph SEM images for assessing cell spreading when rMSCs were seeded on Cerament[TM]**Spine Support after 24 hours, A) SEM showing cells adhered and stretched on the surface of the cement with their filamentous fibres on surface of CSS at 72 hours. b) shows rMSCs on surface of cement, the cell covers the pores on the surface on cement and spread in all the directions, (scale bars= 1µm)**
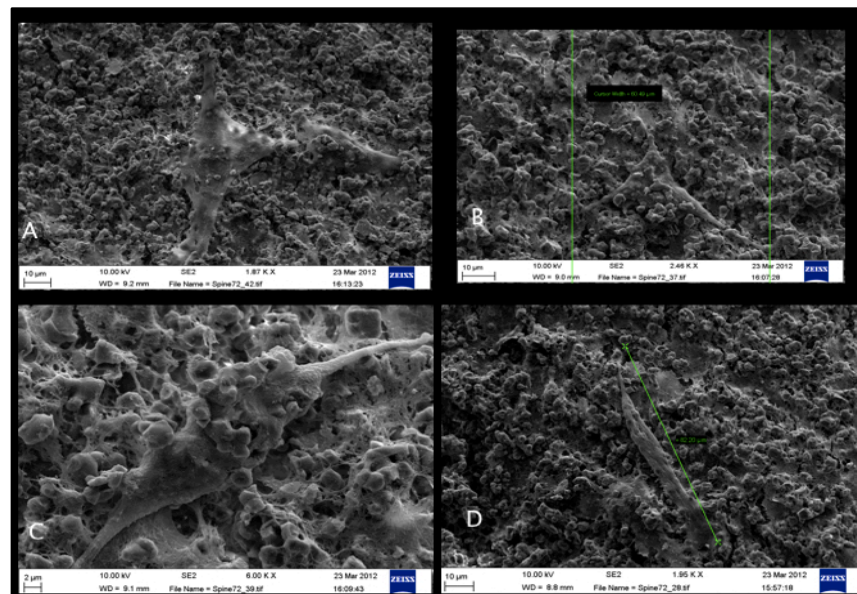
Figure 4.24 Photomicrograph SEM images for rMSCs on Cerament[TM]**Spine Support at different areas, images show the cells attaining normal size (60->100µm) and shape (polygonal and fusiform) on the surface of CBV after 3 days of culture (Scale bars (a), (b), (d) = 10µm, and c) 2µm).**
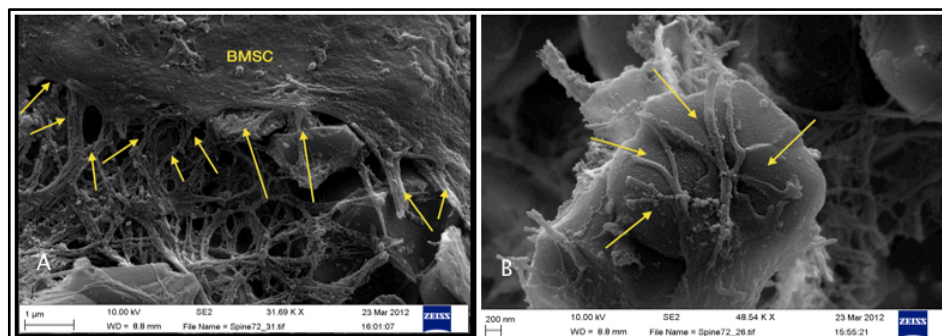
Figure 4.25 A, B. Photomicrographic SEM images showing filopodia and lamellipodia of rMSCs denoted with arrows on Cerament **[TM]Spine Support (Scale bar = 200 nm).**

4.3.6 Assessment of cell seeding into a collagen construct

The constructs were designed to mimic tissue into which the material will eventually be injected. Calcium sulphate/HA was seeded with MG-63 cells and this was then repeated using rMSCs. The other constructs were prepared by injecting calcium sulphate/HA followed by a second injection with the cell suspension once the cement was cured. The first construct showed the escape of cells into the surrounding collagen where live cells (green) could be detected i.e. away from the scaffold. Closer to the scaffold all cells were dead. The second construct showed live cells in collagen with a more even cell distribution when the cell suspension was injected into the collagen after the cement cured (live cells appeared blue in colour (Hoechst stained) (Figure 4.26). A repeat experiment using rMSCs showed similar results, that live cells were observed when cell suspension was injected around the cement only (Figure 4.27). The control for this experiment showed a construct was made by injecting cells only into collagen which also showed an even distribution of cells inside collagen.
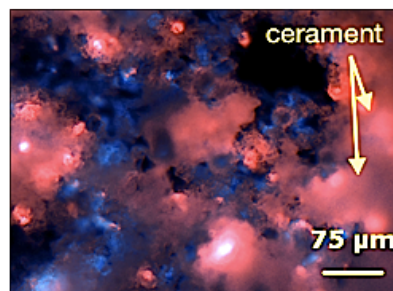
Figure 4.26 Photomicrograph for collagen construct and live/ dead assay (Hoechst stains DNA stain (blue), Ethidium homodimer (red). It shows the presence of dead cells inside the cement denoted with yellow arrows (red colour) and presence of live cells around the cement (blue), scale bar=75 μm.
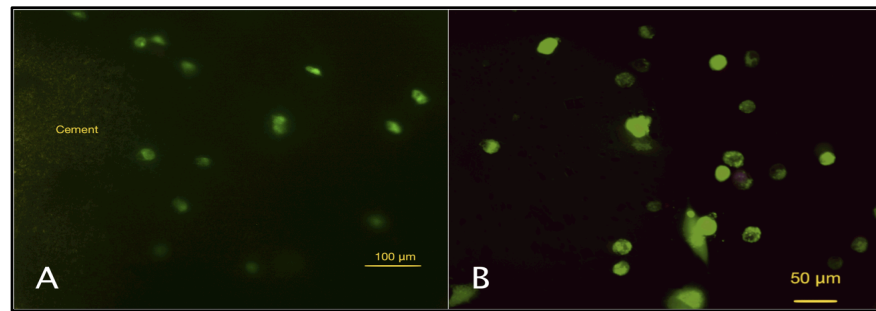
Figure 4.27 Photomicrographs for live and dead staining (Calcein AM and ethidium homodimer) respectively for rMSCs in collagen after 24 hours of cell culture, A) shows presence of live rMSCs around the CSS (green) (scale bars=100 µm), B) shows live cells inside rat tail collagen without cement (control) after 24 hours of cell culture.scale bars=50 µm.

4.3.7 Testing the osteogenic potential of calcium sulphate dihydrate/hydroxyapatite cement

In this collagen construct the cement namely (Cerament^{TM} Spine Support) was prepared and injected, the rMSCs suspension was injected 15 minutes later. The cells were assessed after 21 days in the construct by staining for osteocalcin (OCN). The surviving cells showed positive staining for OCN which indicates an osteogenic effect of the calcium-sulphate/HA on rMSCs (Figure 4.28).
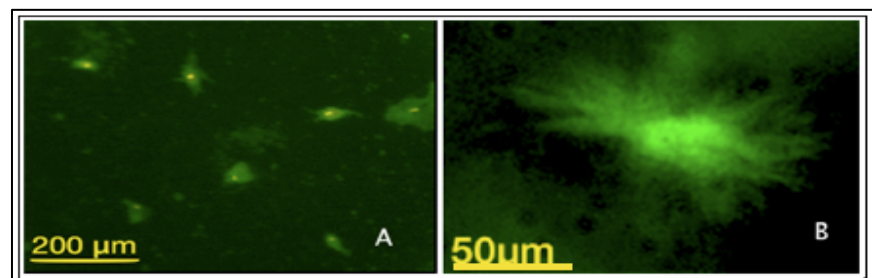
Figure 4.28 Photomicrography showing immunofluorescent staining for rMSCs seeded into collagen construct and Cerament ^{TM}Spine Support,which shows positive staining to the OCN antibody, A) rMSCs with positive intake to OCN antibodies, scale bars= 200 µm, B) at higher magnification,scale bar=50 µm which indicates the pre-osteoblast differentiation of the rMSCs after seeding into the collagen and the CS/HA cement.

4.4 Discussion

In this chapter, the protocol of cell aspiration, isolation and culture (Haynesworth, 1992) was validated for rMSCs, however variable rates of cell growth were noted among the samples. The mean initial yield was 1×10^4 cells/cm^2, and it reached 20 times this number after 2 weeks of cell culture (2.2×10^5), in the third week the number was almost double that at 2 weeks. Cell growth has been previously found to be site specific and dependent on the volume of the harvested marrow (Pittenger et al, 1999). The initial yield of MSCs from the mandibular marrow was 3 times less than that of the iliac bone aspirates as reported by Lee et al, 2011. In the same study, they have found that the relative percentage of MSCs among the mononuclear cells isolated from the mandible was 1%-7%. This was much higher than the average value reported previously which was 0.01-0.001% of the total nucleated cells within the pelvic bone marrow (Pittenger et al, 1999). This may suggest that mandible marrow may represent a more predictable and consistent source of MSCs compared to iliac bone. Similarly, Akintoye et al (2006) reported that the MSCs from mandibular marrow bones showed proliferative activity superior to those from iliac marrow.   However, iliac bone has been considered the most popular anatomic location for obtaining bone marrow aspirate (Ohishi and Caplan, 2010; Sen and Miclau et al, 2007). The number of MSCs cells isolated is dependent on three factors; the method of bone marrow harvest, individual constitution of the aspirate, and the efficiency of isolating stem cells (Gan et al, 2008). These facts could explain the variable growth rate among our samples in this research. Authors have claimed that repeated attempts at aspiration would directly have positive influence on the enrichment and improve the quality of monocytes, and MSCs isolate (Huibregtse et al, 2000). This finding was in

agreement with our previous work which showed that out of the 3 samples obtained the cell enrichment had improved in the second aspirate (AlFotawi et al, 2014).

In this experiment, cell induction using osteogenic media has been achieved before the in vivo cell implantation. The induction was carried out after 10 days from culturing cells in conventional medium. The same protocol has been used in several studies to improve osteogenesis after cell seeding (He et al, 2007; Kon et al, 2000, Torroni, 2009).

We conducted immunofluorescent staining for detecting specific surface markers positive for MSCs namely, CD166, CD44 whilst CD34 was negative as expected. We tested their differentiation potential. These fulfilled the standard criteria of MSCs as approved by the international society for cellular therapy (ISCT).

In this research, heterogeneous rMSCs colonies were expanded as was confirmed with the recognition of variable size of cells that expressed positive surface marker to CD44 & CD166. Our protocol was in agreement with other studies that used heterogenous MSCs colonies in reconstruction of maxillofacial bone (Mao et al, 2006). It is well known that MSCs are immune modulating cells; they lack the expression of MHC-II. These properties are retained even after the osteogenic induction in vitro and in the allogenic transplantation of MSCs for tissue engineering (Niemeyer et al, 2007). Therefore, the protocol for bone marrow aspiration, the isolation of rMSCs and induction of the cells was successful. This step was necessary before carrying out further cell characterization on the cement and in vivo experimentation. The estimated time for cell proliferation to reach the desired number was also optimized which is essential to estimate the schedule for in vivo implantation.

The decision was taken to proceed with the in vivo studies using Cerament[TM] Spine Support cement as the preferred material due to the associated greater cell viability. The direct mixing rMSCs with the calcium sulphate cement/HA has caused cell damaged, this could have been either due to the exothermic setting reaction. It is important to note that CSS has more liquid to powder ratio (1g/0.5ml). Mechanical damage could be another possible cause of cells death while mixing, the formed HA crystals were needle-like in shape. The lack of macroporosity may have contributed to the early cell death. Our wavelength-dispersive X-ray analysis (WDX), showed that Cerament[TM] was microporous (Figure 4.5). The pores ranged from 5-10 µm which were small in size to allow cells such as rabbit MSCs (up to 100 µm) to migrate to the deep layers. The simultaneous application of the rMSC was therefore ruled out.

The approach of testing the materials by injection into collagen constructs has shown the importance of timing of the application of both a CS/HA–injectable cement and rMSCs into soft tissue. This illustrates the need to use sequential injection, starting by the cement first followed with the expanded rMSCs.

Finally, the in-vitro study showed that CSD/HA cement has induced rMSCs to pre-osteoblastic cells, hence it showed positive signal to OCN antibody after 21 days of cell culture. Similar findings were reported by Lazary et al (2007), when they studied the proliferation and gene expression of mouse pre-osteoblastic cells on CS and reported that the cells exhibited increased alkaline phosphatase activity and expressed genes associated with bone healing (e.g., type II collagen, fibronectin).

Chapter 5
Results of the in vivo experimentation

Table of Contents

5 Results of in vivo experimentation

This chapter summarizes the results of the in vivo experimentation. The first part includes the preliminary data of the pilot study which was conducted on 3 rabbits. The section includes gross clinical examination, radiographic, and histological analysis. Based on the findings and in discussion with the named vet surgeon, some modifications were made before conducting the main study as it isexplained in section 3.2.4. The second part of the study was conducted on 10 New Zealand white rabbits. The assessment of bone regeneration was carried out using plain radiographs, CBCT, micro-CT, histology and histomorphometry.

5.1 Pilot study

One rabbit died one month postoperatively due to complications from anaesthesia unrelated to the surgery. In the remaining two rabbits one developed a fluctuant swelling three days postoperatively in the right sub-mandibular area. Fine needle aspiration revealed a yellowish serous fluid content. Culture and sensitivity showed no bacterial growth. A week later another collection of yellowish fluid appeared and was discharging extraorally though a sinus. This was diagnosed as pus, and Oxytetracycline 0.5 mg /kg was administered, the site was debrided under sedation, no further recurrence was noted.

5.1.1 Gross Examination

After animal sacrifice, the mandibles were harvested with the attached muscles. In one case, upon dissection of the masseter muscle, a cheesy whitish material was

observed and this had the appearance of residual bone cement. Cement was also

detected inside the muscle tissue (Figure 5.1). This might have resulted from using

a small needle gauge to inject the material. In the other case upon harvesting the

mandible, the proximal segment was found to be mobile with the anterior screw

dislodged and the plate positioned laterally. It was obvious that preservation of the

bone at the superior margin of the defect would have helped the stabilization of the

mandibular segments without compromising n the size of the created surgical

defect. An area of necrotic tissue was also observed around the plate (Figure 5.2).
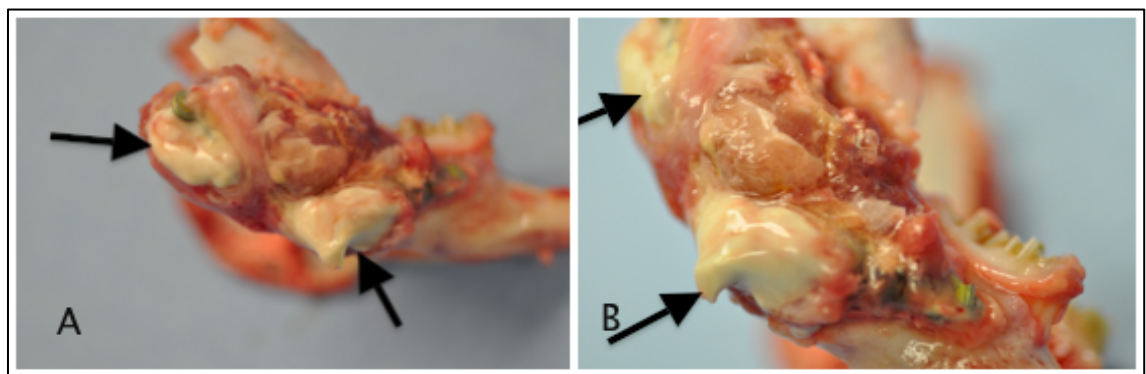
Figure 5.1: Clinical photographs of the explanted mandible of one of the pilot study cases showing the residual cement (black arrows).
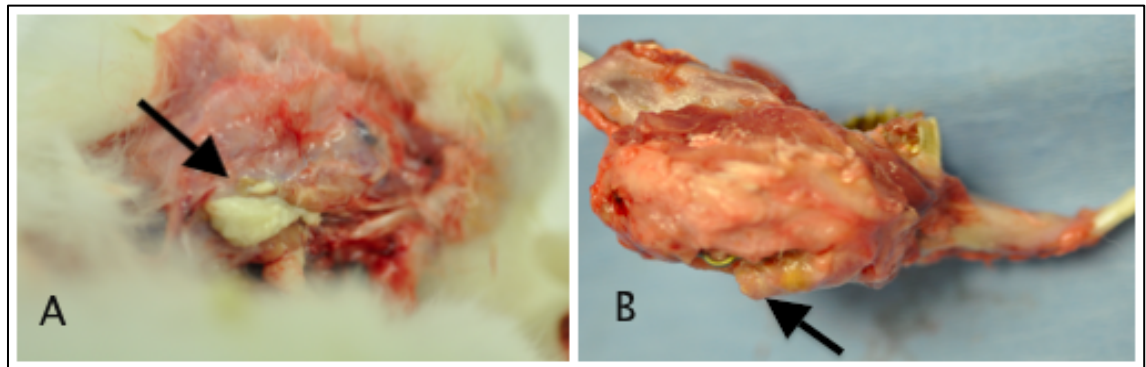
Figure 5.2: Clinical photographs of the mandible of one of the pilot study cases, A) A thick yellow discharge at the site of operation, B) Aras of necrotic tissue around the plate inferiorly (arrow).

5.1.2 Radiographic examination

5.1.2.1 Plain extra-oral film

The immediate post-operative radiographs showed a reasonable amount of injected scaffold (bright radio-opaque patches) inside the masseter muscle within the defect. Due to the radio-opacifier in the Cerament^{TM}, the immediate post-operative films were not used as baseline for comparisons, instead the 1 month postoperative radiographs were used for the assessment of tissue regeneration as the radio-opacifier iohexol would have been fully absorbed.

The pilot cases showed a range of radio-opaque patterns within the muscle tissue in the three months following surgery. It was not possible to use a scoring system to objectively quantify the regenerated tissue.

5.1.2.2 Analysis of the CBCT images

CBCT scans shoed heterogeneous areas of radio-opaque tissue occupied the centre of the created defect (Figure 5.3 A). The coronal sections confirmed radio-opacity at the centre of the defect that was thicker than the native bone in the bucco-lingual direction (Figure 5.3 B). The surface area and volume of the radio-opaque tissue in Rb1 was 70.6 % ± 2.8 of the control side (Table 5.1).

Complete dislodgment of the anterior screw and displacement of the segment was seen (Figure 5.4). The surface area and the volume of the radio-opaque tissue was 34.70 % ± 3.4 (Table 5.2).
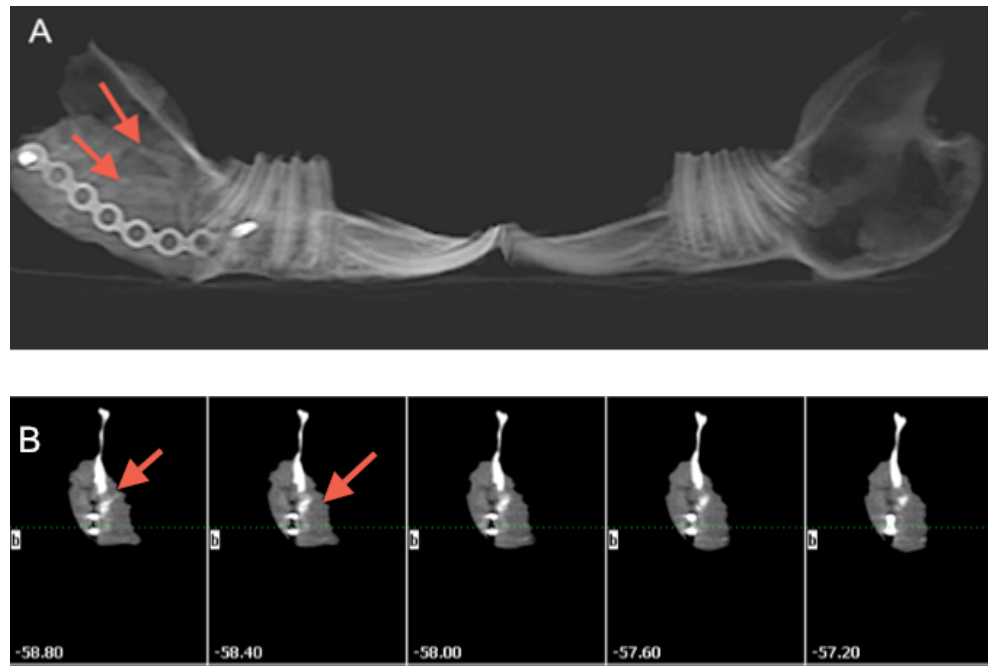
Figure 5.3: CBCT scans showing the pattern of the radio-opacities within the muscle at the site of the surgical defect in one of the pilot study cases, A) shows sagittal views with area of diffuse radio-opacity bridging the surgical defect (red arrows), B) Consecutive coronal sections through the defect; from anterior to posterior displaying the radio-opacities of the regenerated tissue.
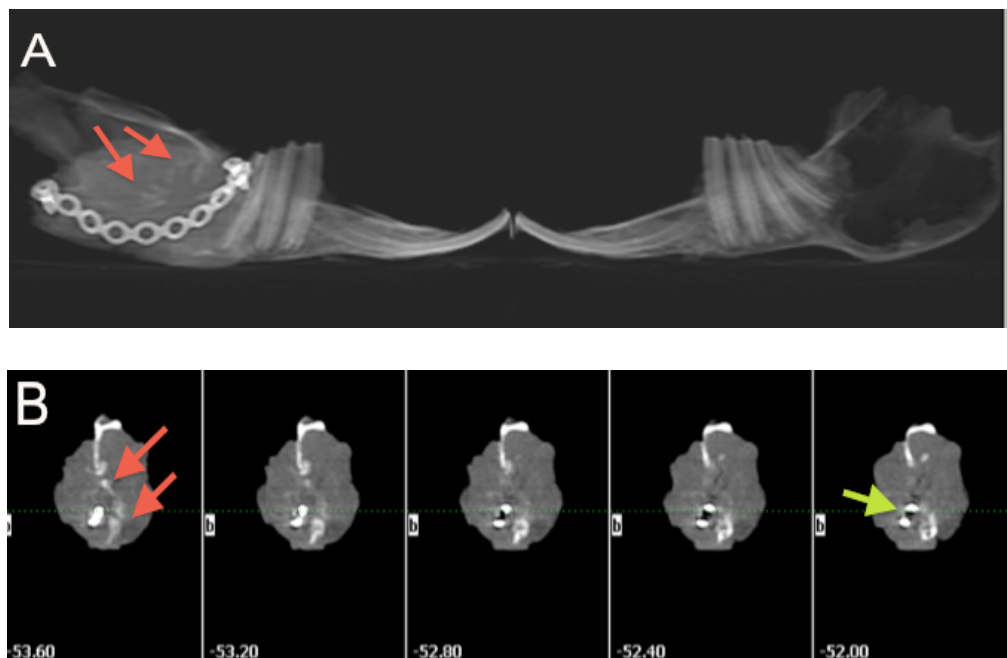
Figure 5.4: CBCT scans showing the pattern of the radio-opacities within the muscle at the site of the surgical defect in one of the pilot study cases, A) shows a sagittal view for the mandible, B, Areas of radio-opacity at the centre of the muscle tissue almost bridging the surgical defect (red arrows),and the laterally displaced plate (green arrow).

Table 5.1: Cross section surface area and volumetric measurements of a series of coronal sections of the CBCT scans   (thickness = 1.6 mm) for one of the pilot cases, with the non-operated side for comparison.

1.6 mm coronal sections	Surface area of radio-dense material experimental side (mm^2)	Volume of radio-dense mass of experimental side (mm^3)	Surface area control side (mm^2)	Volume of bone control side (mm^3)
1	0	0	17.9	28.7
2	0	0	15.8	25.3
3	11.5	18.4	17.2	27.5
4	6.9	10.9	11.5	18.4
5	11	17.9	26.4	42.2
6	22.5	36	24	39.9
7	23.6	37.8	28	45
8	26	41.6	22.4	35.9
9	26	41.6	22.5	35.9
10	20	32	22.	35.5
Total	147.7±12	236 ±19	208.9± 4	334.3± 7

Table 5.2:   The cross section surface area and volumetric measurements of a series of coronal sections of the CBCT scans (thickness = 2 mm) for another case of the pilot sudy, with the non-operated side for comparison.

2 mm thickness coronal sections	Surface area of radio-dense material of experimental side (mm^2)	Volume of the radio-dense mass experimental side (mm^3)	Surface area Control side (mm^2)	Volume of bone control side (mm^3)
1	0	0	24.	50
2	3.2	6.4	28.6	57.3
3	0	0	25	50
4	2.2	4.4	19.5	39
5	24.8	49.8	35.3	70.7
6	22	44	25.3	50.7
7	12.3	24.8	27.5	55
8	15	30	24.4	48.9
9	3.2	6.4	22.9	45.8
10	8.2	16.3	28.4	56.8
Total	90± 11	182± 14	262± 5	524± 7.5

5.1.3 Histology

In the case that died before the full term of the study there was a large amount of cement between the muscle fibres, the muscles showed signs of degeneration, hyalinisation and fibrosis with minimal vascularity (Figures 5.5, 5.6, 5.7). The muscle tissue appeared to start organising into rounded structures resembling osteons (Figure 5.7). Areas of sporadic immature bone were visible at the centre of the defect and these were surrounded by fibrous tissue (Figures 5.8). No inflammatory cells were detected. In the case that showed remnant cement, areas of highly cellular fibrous tissues were noted (Figures 5.9). Islands of bone

formation surrounded with fibrous tissue were visible at the centre of the defect (Figure 5.10).

The case which developed infection showed areas of tissue necrosis, with multinucleated inflammatory cell infiltrates (Figures 5.11). Remnants of cement were observed between the muscle fibres. There were areas of bone regeneration found in close proximity to the cement that were separated by bundles of fibrous tissue.
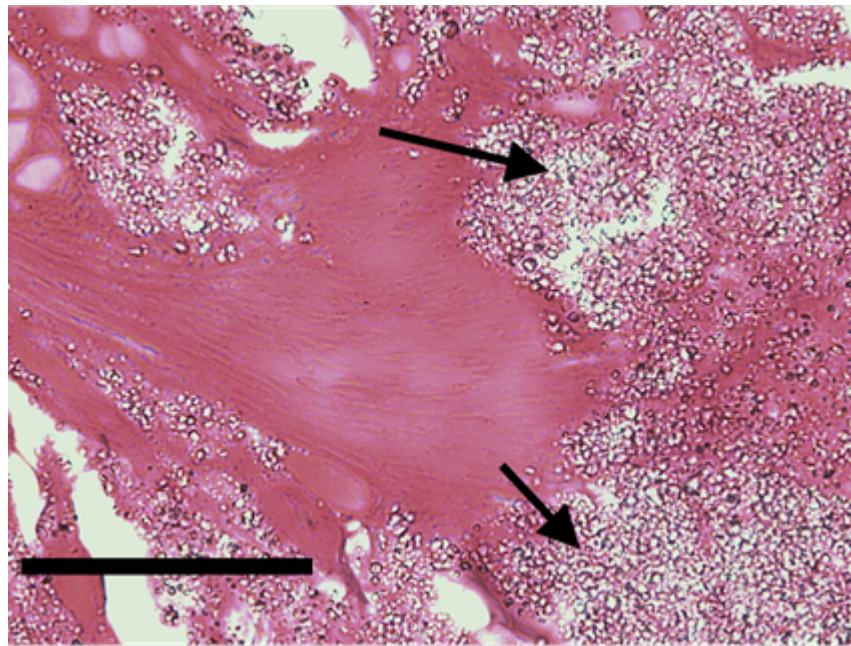
Figure 5.5: Photomicrograph of a decalcified section stained with H&E, visualised under light microscopy (Zeiss, Germany), showing large areas of cement between muscle fibres (arrow), scale bar= 100 µm.
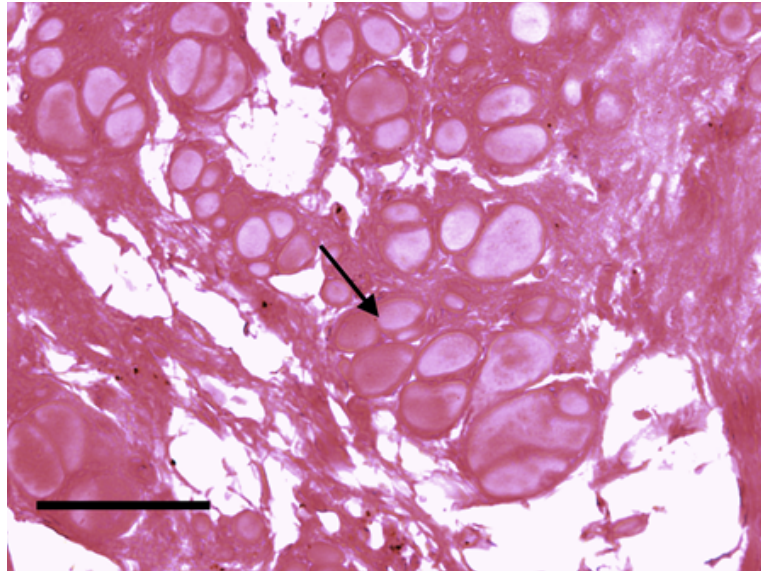
Figure 5.6: Photomicrograph of a decalcified section stained with H&E, shows areas of muscle degeneration, which look less cellular, the vacuoles (arrow) shows hyalinization stained pale pink in colour. Scale bar = 100 µm.
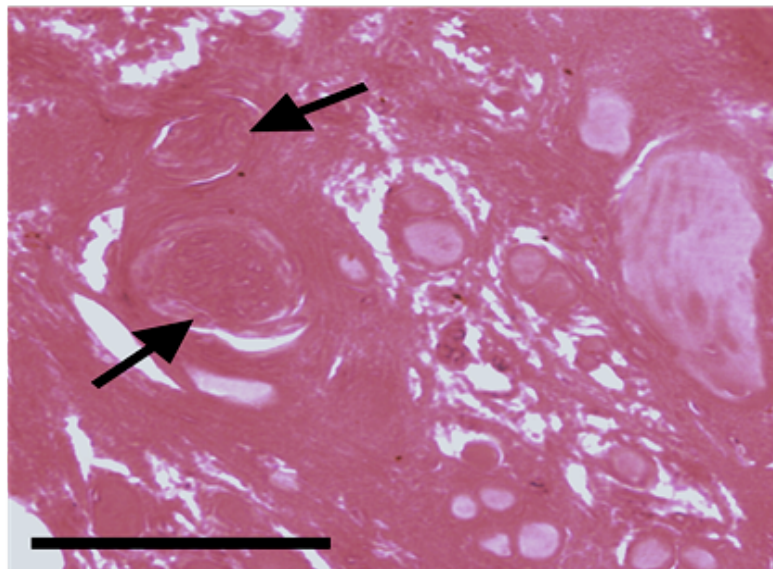
Figure 5.7: Photomicrograph of a decalcified section stained with H&E, shows areas of muscle degeneration visualised under light microscopy (Zeiss, Germany), showing muscle degeneration and hylainization, and organisation of rounded structure (arrows) inside the muscle fibres. Scale bar =100 µm.
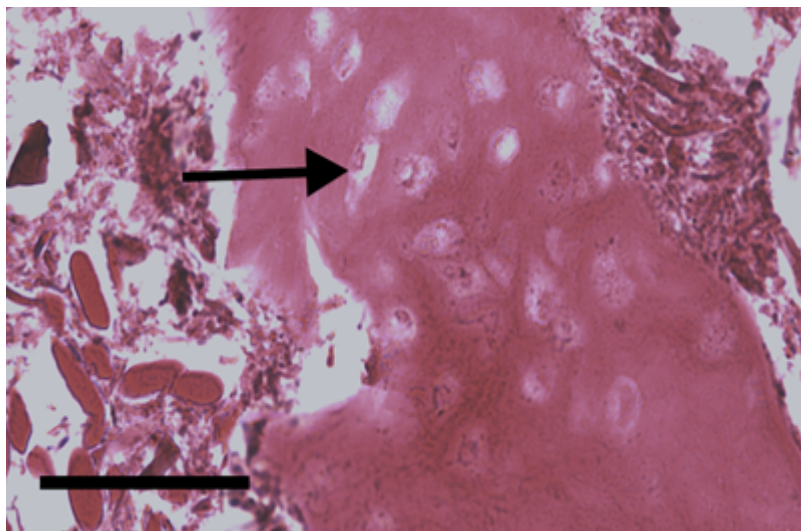
Figure 5.8: Photomicrograph showing histology of a decalcified section stained with H&E, visualised under light microscopy (Zeiss, Germany), islands of immature bone (arrow) surrounded with fibrous and muscular tissue are visible. Scale bar = 100 µm.
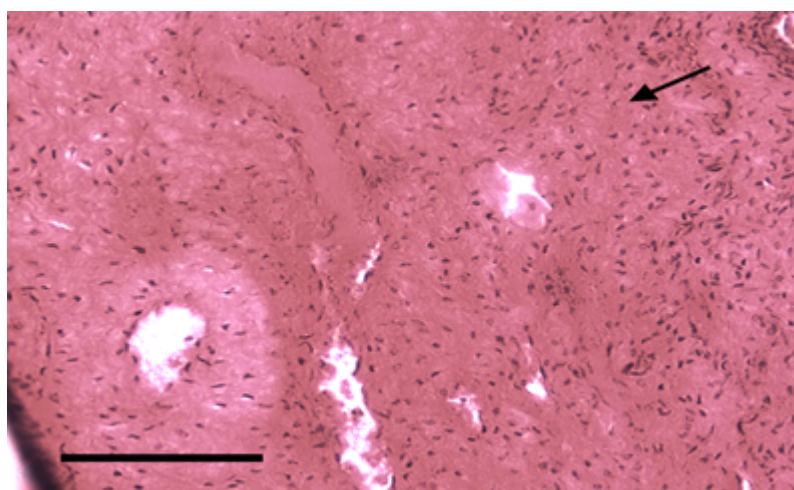
Figure 5.9: Photomicrograph showing histology of a decalcified section stained with H&E, visualised under light microscopy (Zeiss, Germany), cellular fibrous tissue (arrow) replacing the muscle fibres is seen. Scale bar = 100 µm.
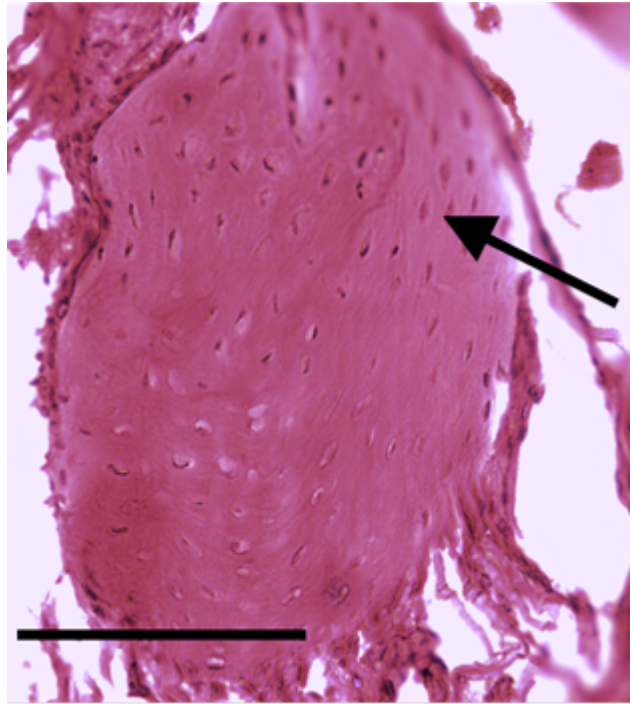
Figure 5.10: Photomicrograph showing the histology of a decalcified section stained with H&E visualised under light microscopy (Zeiss, Germany), an island of bone at the centre of the defect (arrow) is visible, the bone is cellular and surrounded with fibrous tissue. Scale bar = 100 µm.
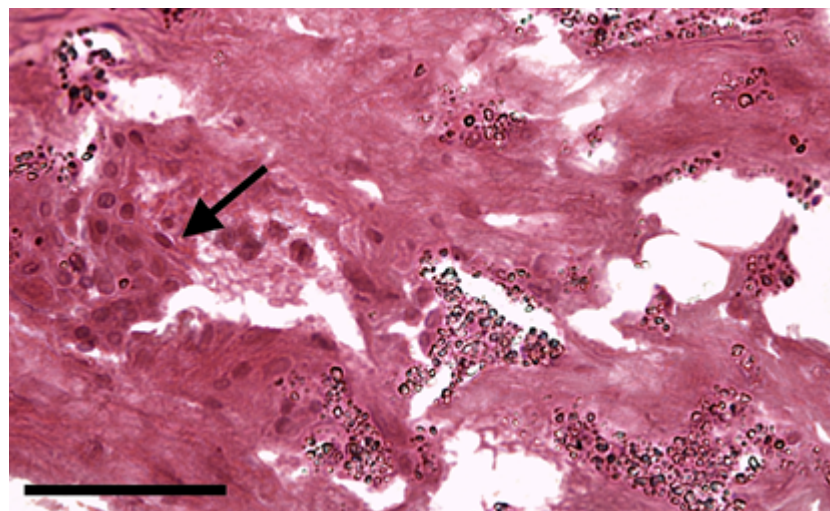
Figure 5.11: Photomicrograph showing histology of a decalcified section stained with H&E visualised under light microscopy (Zeiss, Germany), from the third case with areas of necrotic tissue and remnants of cement and giant cell (arrows). Scale bar = 100 µm.

5.1.4 Conclusions of the pilot study

In spite of the various complications encountered in this pilot study, the histological assessment confirmed the presence of new bone regeneration at the site of the created defect. Based on these outcomes, modifications were considered before conducting the main study as explained in section 3.2.4.

5.2 Results of the main study

In the main study group, all rabbits tolerated the surgery, and no significant change in body weight was noticed post operatively. All animals were euthanised after finishing the full term of the study which was 3 months. No infection was reported. However, a seroma was noted in three cases about 3-6 days after surgery. Surgical aspiration of the serous fluid was required in two of these cases, the seroma in the third case resolved spontaneously (Figure 5.12). In one case there was displacement of the fixation plate buccally due to dislodgment of the anterior screw, this was noticed in the radiograph 1 month postoperatively.
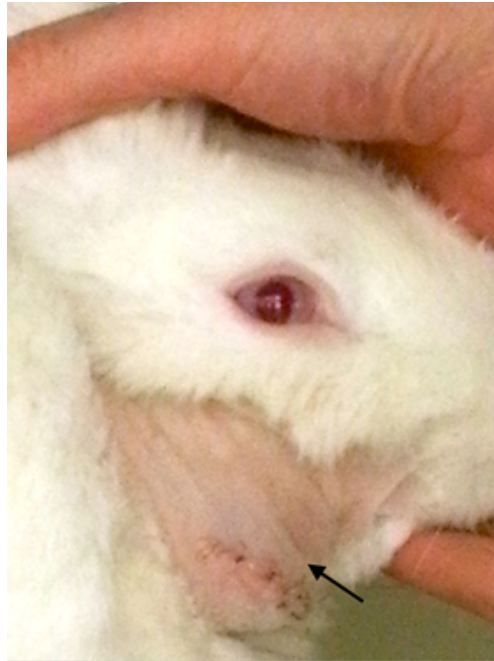
Figure 5.12: Photograph showing the right submandibular area with the arrow showing the swelling caused by the seroma.

5.2.1 Clinical examination

Following mandibular explantation, the colour and texture of the tissue appeared

normal indicating their viability. In all the cases the inferior mandibualr palte

maintained the unity of the mandible. It was difficult to dissect the deep layer of the

masseter muscle to expose the ramus of the mandible due the presence of a

tenacious fibrous layer covering the surgical site. Fibrous tissue was also found

around the titanium plate (Figure 5.13). The tissue that occupied the area of the

defect was mobile bucco-lingually. A thin layer of hard tissue was also seen at the

most inferior part of the surgical side which was also surrounded by fibrous tissue.

In most of the cases an area of bone overgrowth was also observed around the

site of the proximal screw. Remaing parts of the injected cement were detected in

the outer layers of the muscle fibres (Figure 5.14). The area of bone over growth

was more marked in cases no. 218 and 151. It was estimated to be double in size

medio-laterally when compared to the contralateral side (Figure 5.15). Case no.

241 showed topographical changes at the superior margin of the defect, the

irregular rough bone was observed immediately next to the remaining residual

cement (Figure 5.16). Table 3, appendix (1.4) summarises the main gross clinical

findings for all experimental animals, including postoperative complications.
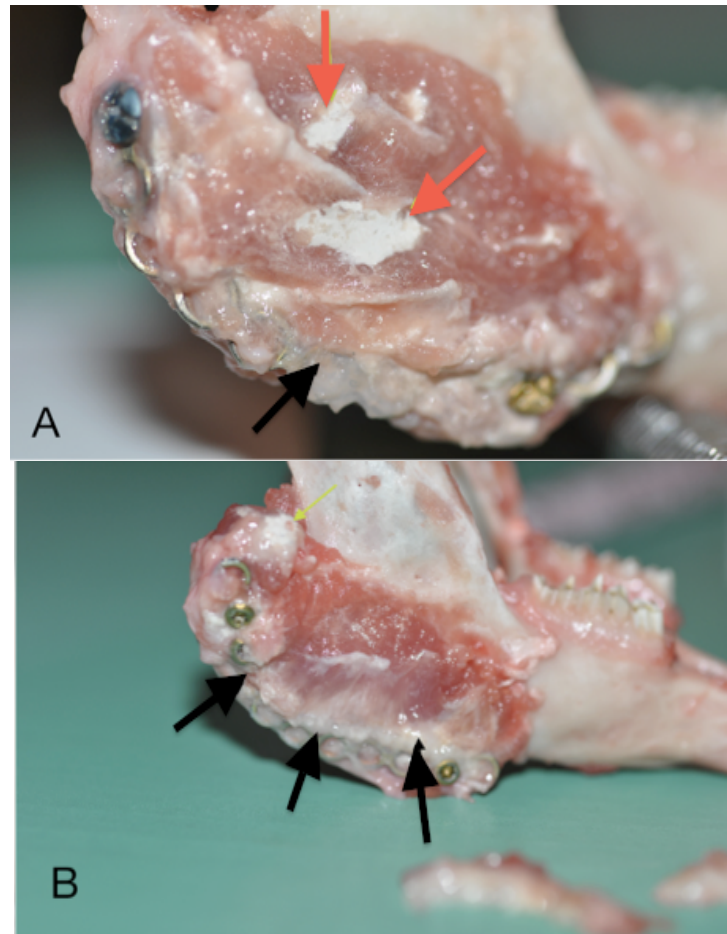
Figure 5.13: Photographs of sagittal views showing the explanted mandibles for Rb 215 & 214. The fibrous tissue capsule around the titanium plate is visible in image A (black arrow) and the yellow arrows show remnants of the cement. B) Black arrows show fibrous tissue around the plate and extended in a fan shape over the masseter muscle.
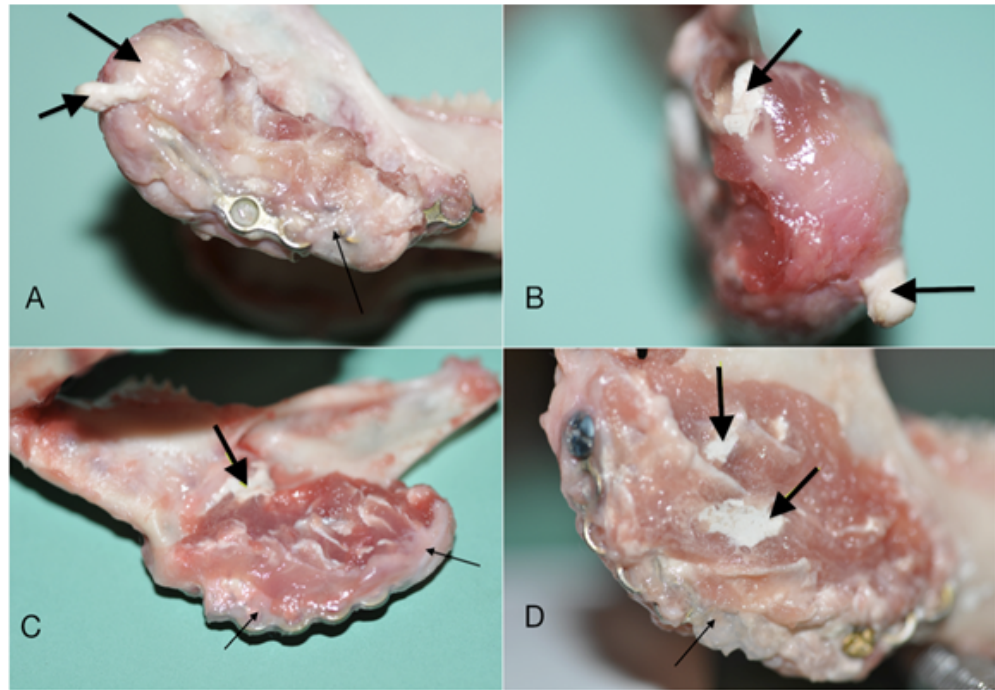
Figure 5.14 Photographs of the explanted mandibles of Rb 218 (A,B), 215 (C) & 214 (D) showing areas of whitish rubbery material of the residual cement (black arrows) in the outer layers and between the muscle fibres.   Images show the titanium plate covered by the muscle tissue.
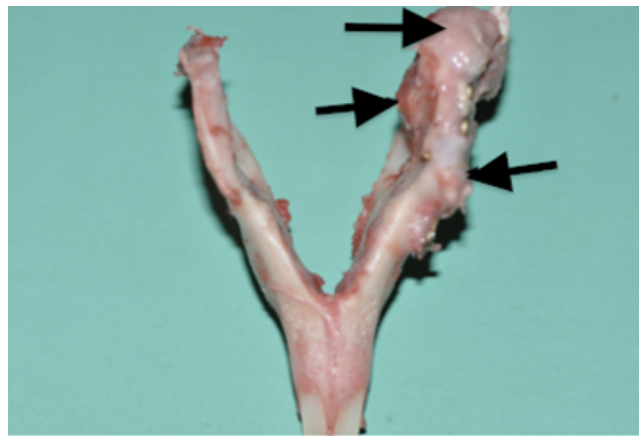
Figure 5.15: Photograph of the explanted mandible of case Rb 218 showing areas of bone overgrowth on the operated side (black arrows).
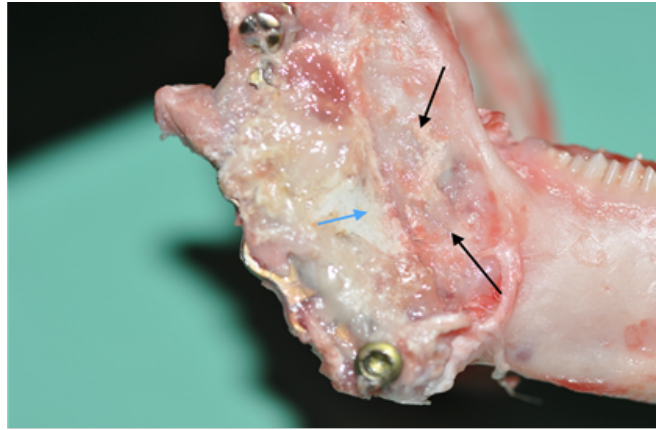
Figure 5.16: Photograph showing the sagittal view of the operated side of the explanted jaw of case Rb 239. Topographical changes are visible at the superior margin of the defect with irregular rough bone surfaces (black arrows) that are found in close proximity to the area of cement (blue arrow). The plate and proximal screw are covered with a fibrous capsule.

5.2.2 Radiographic examination

5.2.2.1 Plain extra-oral film

Radiographs were taken one month followng surgery showed complete disappearance of the bright radio-opaque patches due to the adsorption of the iohexol (the cement opacifier) into the circulation. In general there were sporadic radio-opaque areas which had similar density to the surrounding bone. These areas are likely to be either the HA of the injected cement or areas of initial calcification (Figure 5.17).

The radiographs taken two months postoperatively showed heterogenous radiopaque masses in the surgical defect surrounded by relatively radiolucent tissues. These were in close proximity to the defect borders and areas of bone bridging were visible in the anterior, superior and/or at the proximal border of the defect (Figure 5.18). Three months post-operatively the radiographs showed more radio-opaque areas visible within the defect; however the radio-opacity did not show complete bridging of the surgical defect (Figure 5.19). There were sporadic

areas of radio-opaque mass along the margin of the defect and these were more radio-dense when compared to the second month radiographs. In most of the cases the radio-opaque mass extended from the centre of the defect to the proximal (Figure 5.18; Figure 5.19). There was also a uniform radio-opaque shadow at the margin of the surgical defect due to the increased thickness of the bony border (cortication). Details description of all radiographic findings for all the experimental animals are summarised in table 4, appendix (1.4).

These initial findings appear to reveal a relationship between the distribution of the injected cement and the amount and location of the visible radio-opaque tissue. A scoring system was used to reveal the estimated quantitative scoring for the regenerated tissue for all the examined cases and is summarized in Table 5.3. The median percentage of radio-opaque tissue present in the created defect was found to be 45.8% (Range 66.6-25.2%).
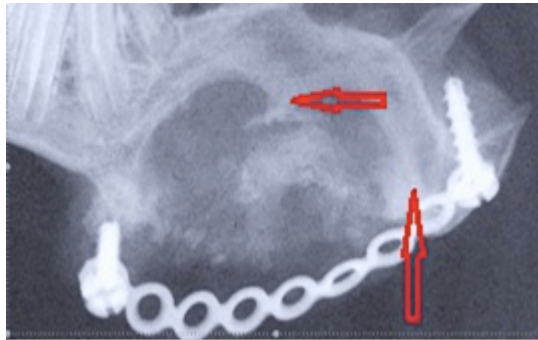
Figure 5.17 An extra-oral radiographic image taken at one month showing an island of radio-opaque tissue at the centre of the defect which is in continuity with the proximal and superior and inferior margins of the defect area (red arrows).
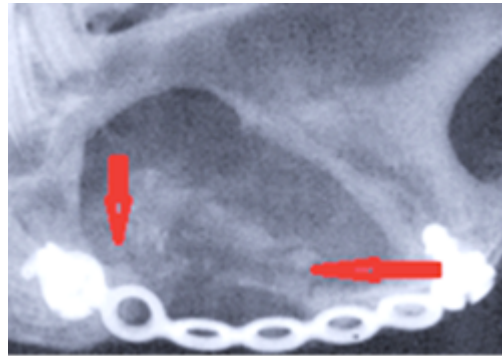
Figure 5.18 An extra-oral radiograph taken at 2 months showing islands of radio-dense mass at the centre of the defect, the anterior mass bridged the anterior and the inferior margins of the defect (red arrows).
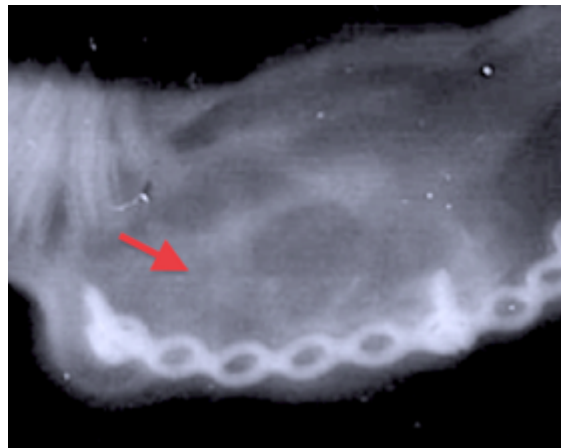
Figure 5.19: An extra-oral radiograph taken at 3 months showing a homogenous radio-opaque mass bridging the anterior third of the surgical defect (red arrow).

Table 5.3: Table illustrating the estimated quantitative radiographic scoring of the different anatomical sections of the surgical defects.

Rabbit no.	The grading of the radiographic examined sections and the average percentage of the quantitative scoring			
	Proximal	Middle	Anterior	∑QS
Rb1 (151)	75	50	75	66.6± 8.4
Rb2 (152)	75	50	50	58.3± 12.7
Rb3 (214)	50	25	0	25± 20
Rb4 (215	25	25	25	25± 19
Rb5 (218)	75	75	50	66.6± 8.9
Rb (217)	75	25	25	41.7 13.8
Rb (216)	75	50	75	66.6± 7.9
Rb (239)	50	25	75	50± 20
Rb (240)	0	0	50	25±10.9
Rb(241)	25	50	50	41.7±17.6
Median value(range)				45.8(66.6-25.19)

5.2.2.2 Radiographic findings of the CBCT scans

At 3 months following surgery radiopaque tissue occupied the centre of the created defect with bridging in at least two points to the adjacent borders. Calcified radio-opaque areas were seen in most cases at the proximal one third of the defect, with absence of clear demarcation between the regenerated tissue and the native proximal and superior bone. In 8 cases, the regenerated tissues were located either medial or lateral to the Region of the Defect (ROD). The results of

surface area measurements of the CBCT images are shown in Table 5.4. The volume of the estimated radio-opaque tissue was more than the volume of bone at the ROD in 4 cases, with an average of 35% ± 15. The three dimensional radiograph models demonstrated the location of the calcified mass in relation to the ROD. The other six rabbits showed variable results, the median value of generated tissue volume was 361 mm^3 (range 196.3 - 871), which was 84% (range 39 - 160) with respect to the contra-lateral side, as shown in Table 5.4.

There was remarkable hard tissue thickening of the borders of the mandible adjacent to the created defect. These dimensions were measured from 10 random areas of the coronal sections of the i-CAT scans for all cases and were compared with the contra lateral side (Figure 5.20, 5.21). The ratio of thickness medio-laterally was 2:1 in comparison with the contra lateral side. Consecutive CBCT coronal images for all cases involved in the main study are presented in figue (1), appendix (5.3). The density of the regenerated tissue was calculated at the centre and the peripheries of the surgical defect using the Hounsefield unit (HU) (Table 5.5). Six cases showed an increase in density of the regenerated tissue at the centre of the defect, which was laid either medial, lateral, or within the ROD. The estimated median reading was 20 % (range 9 - 75) more dense than the contralateral side. However in the other 4 cases the median HU reading was 621 (range 575 - 748), which constituted 64% (57-98) of the bone density of the contralateral side. The median value for the radio-density of the thickened bone at the margin of the defect including the bony bridging was reported to be 40% (range 96 - 130) denser than the contra-lateral side.
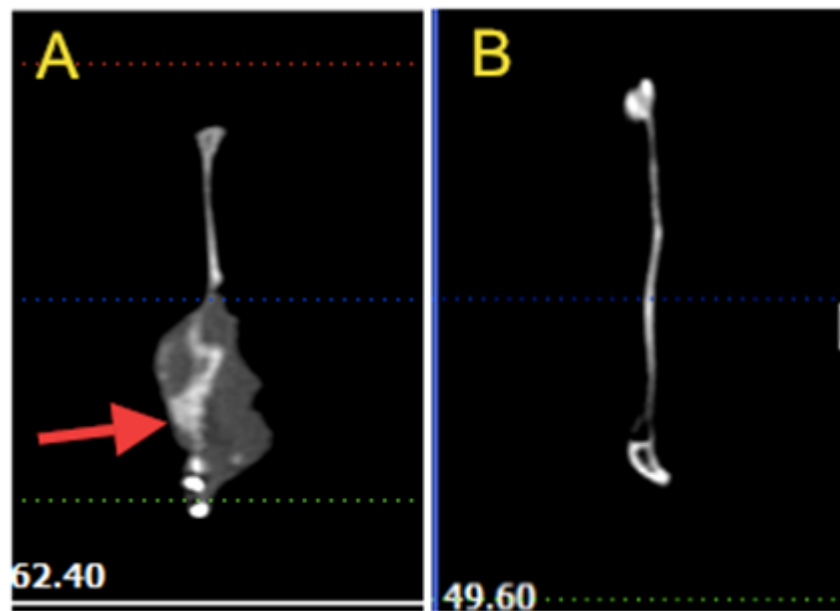
Figure 5.20 Coronal sections of the CBCT through the ramus of the mandible for case 151; A) shows the area of bone regeneration (red arrow). B) Shows the contralateral side, the thickness of the slices is 2 mm.
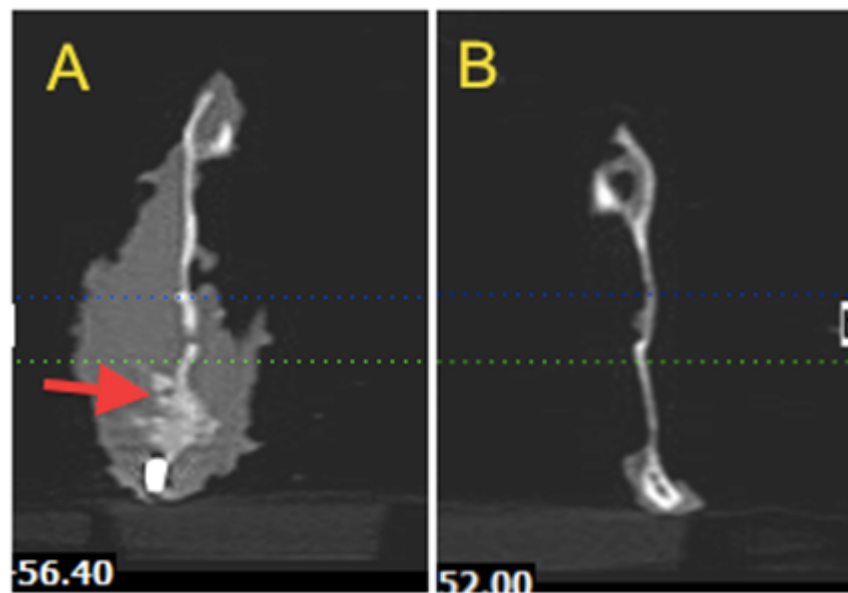
Figure 5.21 Coranl sections of the CBCT scans through the ramus of the mandible for case 240; A) shows the area of bone regeneration (red arrow. B) Shows the contralateral side, the thickness of the slices is 2 mm.

Table 5.4: Table showing the data of all the examined cases at 3 months showing; the average surface area of radio-density per coronal section for the iCAT scanning, the volume of the radio-dense material per defect, and the average thickness of the borders of the defect for operated and non-operated sides.

Rabbit ID	Average surface area for the radio-opaque tissue (operated side)	Average volume of the radio-opaque tissue (operated side)	Average surface area bone (non-operated side)	Average volume of bone (non-operated side)	Average thickness of the bony margin at the defect (mm)	Average thickness of bone at non-operated side (mm)	Percentage of radio-opacity mass	Remarks
Rb 151	99.2	871.2	26.2	524.3	3.3	1.6	+ 60%	Area of bone over growth at the distal end of the fixation plate
Rb 152	14.8	236.3	20.8	334.3	2.84	1.8	70%	–
Rb 214	8.7	181.2	21.3	445.6	2.5	1.4	40%	Cortical thickening at all borders of the defect by 20%
Rb 215	13.58	315	20.2	470	2.5	1.9	67%	–
Rb 217	12.27	196.3	31.3	499	2	1.4	39%	Radio-opaque mass was located more laterally in relation to ROD
Rb 218	35.5	456.5	23.8	380	4.6	1.5	+ 20%	Bone overgrowth medial and distal to the defect
Rb 216	30.97	486.7	30.4	495.5	2.2	1.3	98%	Radio-opaque mass located buccally, marked thickening of the bone medio-laterally at the anterior and proximal border of the defect.

Rb 239	41	656.4	33.6	537.6	3.45	1.52	+ 22%	The radio-opaque mass was located more buccal, and the proximal segment of ramus bone was deviated more medially possibly due to the position of the plate.
Rb 240	47.7	686.8	32.2	492.8	5.6	1.35	+39%	Radio-opaque mass located in line with the ramus, marked thickening of bony borders anterior and proximal to the defect. Bone at the superior border.
Rb 241	25	400	36.4	582.4	2.2	1.2	68%	Most of the radio-opaque mass was in line with the ramus, a small mass was medially located.

Table 5.5: Table of the density readings in Hounsfield units (HU) of the radio-dense tissue that was detected in the coronal sections of the CBCT scans, and the average bone density for the thickened   borders of the defect at the operated and contralateral sides.

Rabbit no	HU of the regenerated tissue	HU at the border of the defect	HU at the control side	% of tissue density in relation to the control side	% of bone density at the border of the defect in relation to control side
Rb 151	748.2 ± 285	1821±294.2	761± 250	98%	+ 130%
Rb 152	527.7 ± 126.8	1305±653	705.6 ±345.3	74%	+25%
Rb 214	575.8±165	1235±271	1002.6±242	57%	+ 23%
Rb 215	666.2±159.7	1581.6± 347.4	930.5±232.7	71%	+ 69.9%
Rb 218	918.2±234	1173.5±196.6	824.3±268.8	+11 %	+ 42%
Rb 217	1056±222.7	1694.6±368	968.1±285	+ 9%	+75%
Rb 216	1470± 234.4	1621±431.7	835.9± 299.7	+75%	96%
Rb 239	1412±263.6	1598±281.7	989.9±325	+40%	+9%
Rb 240	1390±240.5	1559.8±232	1153±281.6	+20%	+45%
Rb 241	1293.6± 253.3	1584.8±264.3	1066± 321	+21 %	+ 38%

5.2.2.3 Micro-CT analysis

The region at the interface between the regenerated tissue and the native bone

was determined. This was achieved at three positions; 1) Offset from reference

point by 9.0 mm. VOI = 5.0 x 3.0 x 4.0 mm^3 (Figure 5.23A), position 2, the VOI =

5.0 x 5.0 x 3.5 mm^3 as shown (Figure 5.22B), position three was estimated to be

VOI = 10.0 x 7.0 x 4.0 mm^3 as shown (Figure 5. 22C). In addition a reference point that could be detected in both the control and the experimental sample was determined. The boundary between the regenerated tissue within the defect and the surrounding host bone was indistinguishable in two areas of bony bridging. The regenerated tissue was located either medial or lateral in relation to the surrounding host bone; this was consistent with the CBCT findings. The surface morphology of the regenerated tissues was rough compared with the contra-lateral side (Figure 5.23). Coronal cross sectional views at the area of bone interface with the native bone revealed that the cortices of bone were displaced and replaced with trabecular bone rendering the area thicker than the contralateral site (Figure 5.24, 5.25).
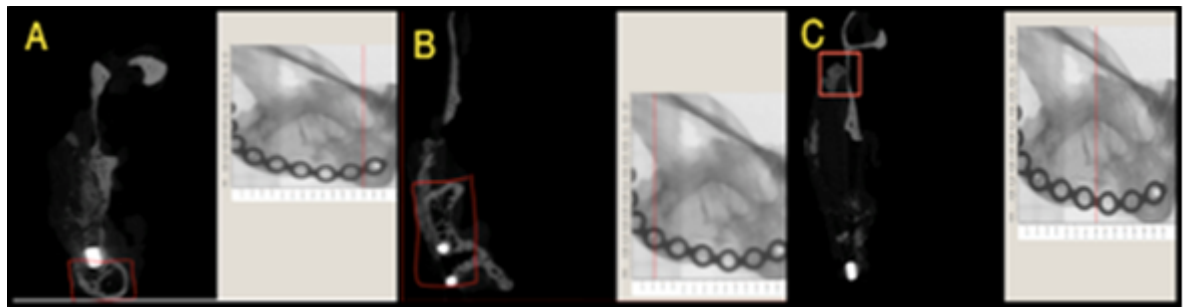
Figure 5.22: The coronal sections of micro-CT images through the area of the defect showing bone bridging the gap (red box), A) shows areas of tissue regeneration located lateral to the defect (red arrow), the red boxed area at the inferior margin represents the second interface of the newly generated bone with the native bone (yellow arrow). B) Represents the contra-lateral non-operated side of the mandible (FOV = 10.0 x 7.0 x 4.0 mm^3 denoted by the red box).
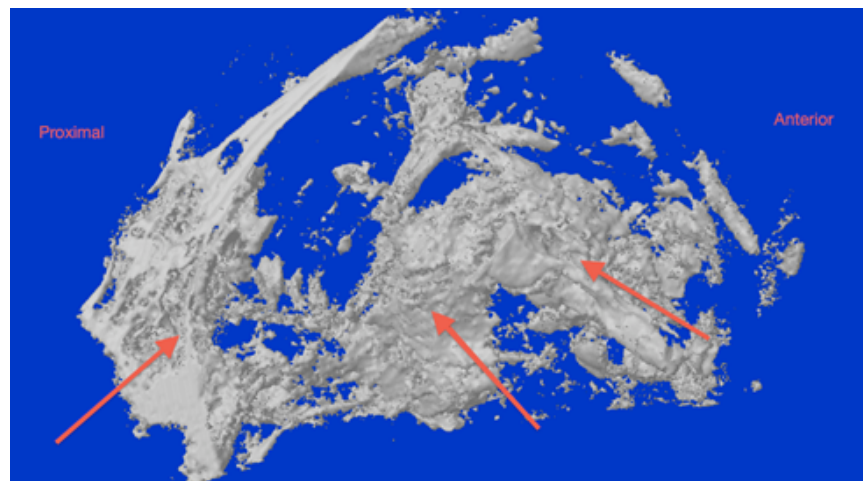
Figure 5.23: Images of a sagittal section of the 3D model for case 151 showing the area of the defect filled with a radio-dense material which appeared irregular in shape (red arrows).
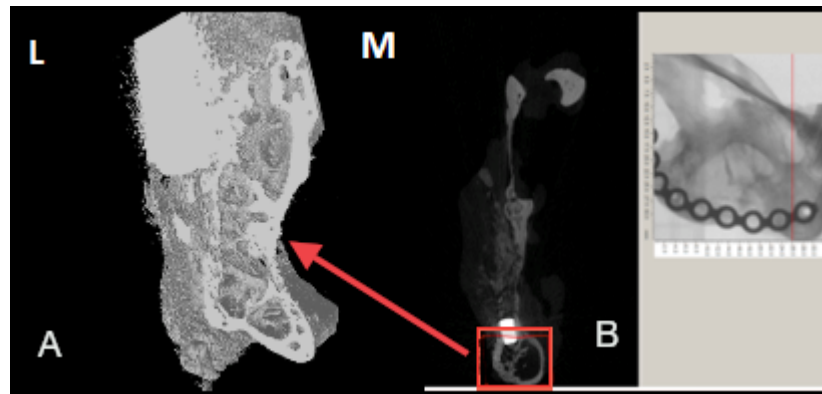
Figure 5.24 the micro-CT scan of the area of bone bridging of the surgical defect, A) 3D model of the area of interface between the regenerated tissue and the native bone (the red box in image B) which shows the displaced cortices and their replacement with a characteristic trabecular pattern, (L & M represent lateral and medial sides of the 3D model).
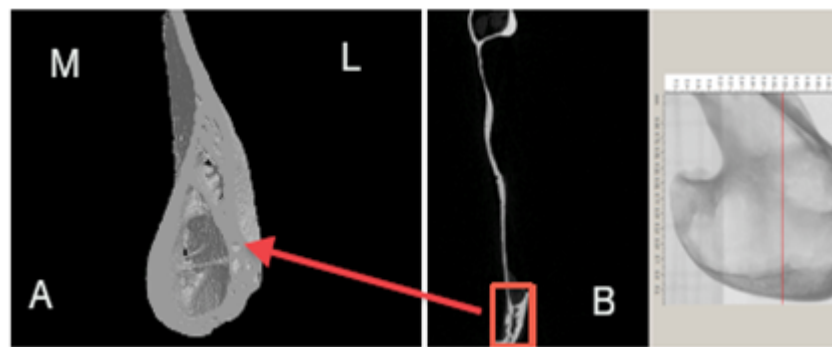
Figure 5.25 The micro-CT scan of the contralateral side (non-operated side) A) 3D model which shows the normal trabecular pattern of the bone at the inferior border of the ramus of the mandible (the red box in image B)   (L & M represent lateral and medial side of the 3D model).

The Micro-CT images distinguished the volume of bone from the cement, the threshold of the micro-CT slices was optimised, a threshold higher than 68% was of the cement biomaterial, while between 50% and 68% signified bone and a threshold below 50% represented marrow and soft tissue (Figure 5.26). Accordingly, it was estimated that the cement volume ranged from 21% to 0.1% at the ROD, and the BV/TV median value was 66% (range 15-145) inside the defect. The median volume of the new bone formed outside the ROD was 166 mm^3 (range 26.9-320). All direct 3D measurements, including bone volume fraction (BV/TV), bone density (BD), and bone architecture are presented in (Tables 5.6). Due to the nature of bone healing in this animal model, the bone volume fraction

was calculated for the amount of the regenerated tissue inside and outside the region of the defect. Bone outside the region of the defect was 5 times the bone volume inside the ROD.   At the interfaces between the regenerated tissue and the native bone, 3 random areas were chosen, as explained above, the median BV/TV was 27.5% (range 23-34), which was double the volume of bone on the same representative anatomical region at the non-operated side(18%). This finding was consistent with the CBCT analysis.
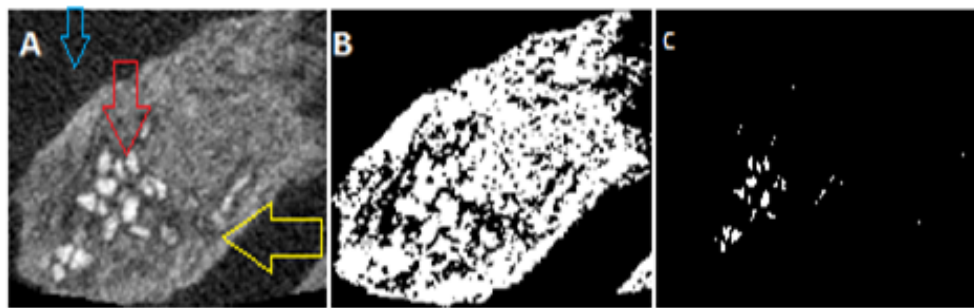
Figure 5.26 Image of the Axial-view of a micro-CT section of the surgical defect of case Rb 216 A) shows the threshold image of the micro-CT slice, bone appears grey (yellow arrow) soft tissues appear black (blue arrow) and the cement appears white (red arrow), B) Binary image for image (A), C) shows the white particles which represent areas of cement.

For the case which showed complete tissue regeneration in 2D assessment, micro-CT examination showed the tissue was located lateral to ROD, 3D modelling for this case showed details of the pattern of bone formation and integration in relation to the defect and the native bone (Figure 27, appendix 1.5). With regard to architecture of the regenerated bone, the average TbN was double that of the contralateral side. TbTh and TbSp were only 63% ± 44, and 73% ± 7 compared to the contralateral side, respectively. The degree of anisotropy (DA), and bone density were 75%± 0.4 and 85% ± 50 respectively, compared to bone in the contralateral side.

The newly formed bone attained more volume than the ROD, it showed thinner trabeculea but more than the average trabecular number and a smaller degree of

anisotropy when compared with the non–operated side. This suggests that the bone formation was associated with a fast deposition rate and active remodelling process.

Data from the 2D analysis of the sagittal micro-CT images using image analysis software (ImageJ, 1.46h, Wayne Rasband, National Institutes of Health, USA) revealed that 59.7% ± 14 of the ROD was occupied by calcified tissues. This was close to the plain radiographic quantitative assessment of bone formation which provided a median score of 62 % ±14 (Figure 5.28).   Schematic representation of the pattern of bone regeneration at the border of the ROD and at the centre, medial or lateral ends is illustrated in Figure 5.29.

Table 5.6: Table demonstrating the micro-CT variables measured for the regenerated bone for 4 samples and the control side 3 months after surgery. The presented values show mean percentages (and SD) of the new bone formation, for control sides, and trabecular analysis at area of interface between the regenerated tissue and the native bone (n=3).

Micro- CT variables	Rb 151	Rb152	Rb 216	Rb 239	Control
TV mm^3	71.8±32	65.9±21	95.6±34	57.3±10	40.9±9.8
BV mm^3 (inside ROD)	59.4±12(1.6)	47.7±9.0(1.29)	44.3±14(1.2)	36.9±10(1)	36.9±1.2
BV mm^3 (outside ROD)	84.9±13.4	26.9± 7.0	320.7±23	249.1±29.9	-0
CV	8.6±0.6	7.6±2.3	0.07±0.06	0	-
% BV/TV in ROD	145 % ± 59	117 % ±48	15 %±2	15%±8	99±58
% BV/TV at area of interface	23± 4.0	32±13.9	34± 20 (2.7)	23±7.0	18± 7.0 (1.00)
Bone Surface area (BS)mm^2/Total surface area (%BS/TS) [*]	51%± 11	52%±8.9	99%±7.1	59%±12.6	100%
Tb Th mm	0.19±0.04	0.39±0.06	0.38±0.2	0.22±0.1	0.58±0.14
Tb N mm^{-1}	0.99±0.9	0.75±0.2	0.64±0.02	0.94±0.22	0.37±0.2
Tb Sp mm	0.87±0.1	1.35± 0.5	1.71±0.2	0.99±0.2	1.97±0.09
DA	1.57±0.9	1.65±0.34	1.88±0.33	1.59±0.4	1.98±0.51
Bone density(gray scale g/cm^2	99.25±2.2	98.3±	162.8± 24.6	94.7± 7.1	167.7±29.2

*Analysis of bone surface area using ImagJ, (ImageJ, 1.46h, Wayne Rasband, National Institutes of Health, USA)
BV= Bone Volume, ROD=Region of the defect, BV/TV= Bone Volume fraction, TV= Tissue volume, BS= Bone surface area, CV= Cement Volume, BS/TS= Bone surface area fraction, Tb Th=Trabecular thickness, Tb N= Trabecular number
Tb Sp=Trabecular separation, DA= degree of anisotropy, Rb=Rabbit.
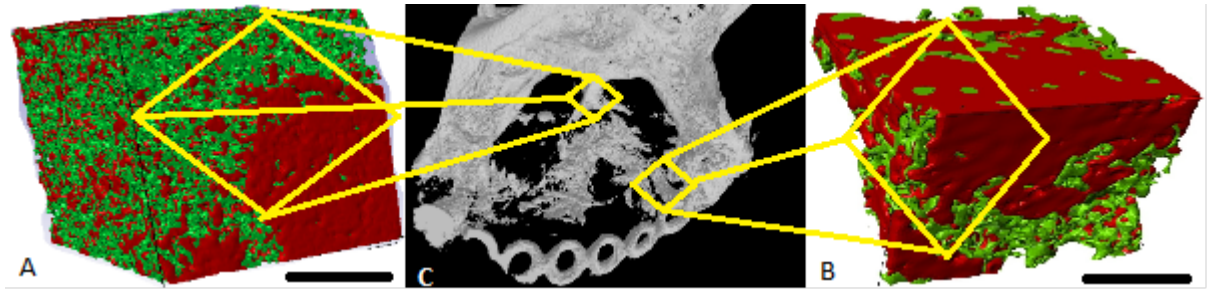
Figure 5.27: Micro-computed tomographic image, A) shows a 3D model of a representative area of the superior margin of the defect at an area of bony bridging of the gap as shown in figure C, B) shows the second area of bony bridging with the regenerated tissue at the proximal border as shown in figure C. The red colour indicates more radio-dense tissue while green indicates less radio-dense tissue (bars = 1 mm).
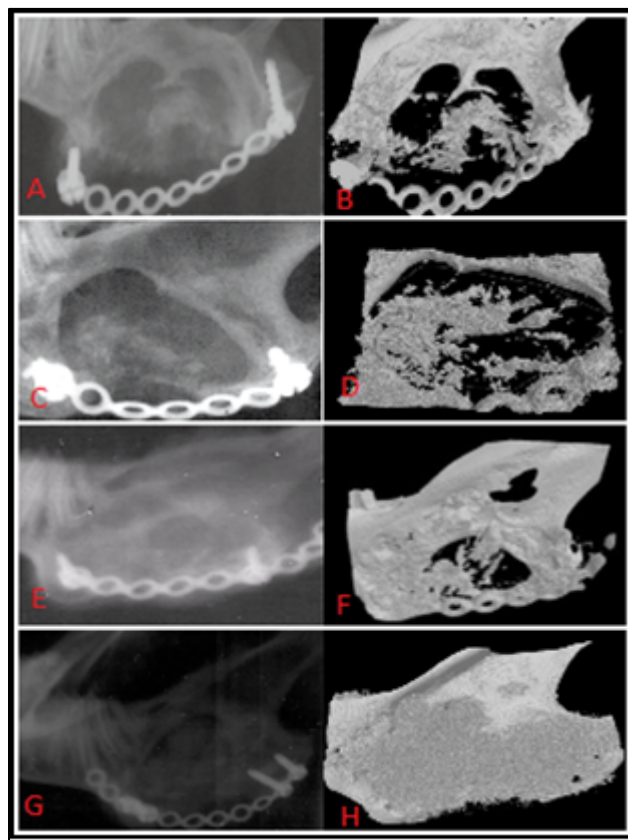
Figure 5.28 Images of sagittal views of plain photographs and micro-CT images. A, C, E & G are plain radiographs adjacent to their corresponding micro-CT images B, D, F & H. Image analysis showed 65.4% ±14 occupied by calcified tissues, which was consistent with the quantitative assessment of the plain radiograph using the scoring system which was 64.4 % ±14.9.
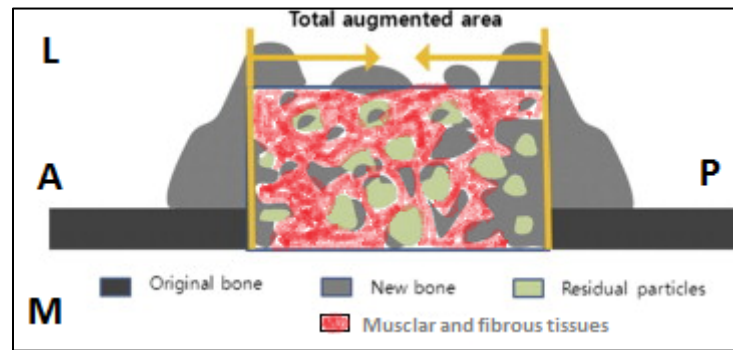
Figure 5.29: Schematic representation of the pattern of bone regeneration of an axial section through the defect 3 months after surgery. The red area represents the bulky muscle or fibrous tissue which occupies the surgical defect and extends beyond the limits of the original bone defect, the residual particles of the cement (HA) present inside the muscle fibres and areas of bone formation are more apparent at the borders of the defect. L, M, A, & P represent the lateral, medial, anterior, and proximal walls of the defect.

5.2.3 Histology

5.2.3.1 Nature of bone regeneration

Six sections were examined for each sample, two decalcified and four undecalcified. The decalcified histology slides were 75 µm in thickness. The amount of the regenerated bone at the created defect was different between sections in comparison to the control side. Photomicrographs for the decalcified sections (H&E) demonstrated areas of bone regeneration at the surgical defect for all study cases (Figure.3 and 4, appendix 1.5). Sections that showed areas of bony union were few, the union occurred with less mature osteoid bone (Figure 5.30, Figure 5.31). Bone was noted in the borders and at the centre of the defects (Figure 5.32). The new bone showed both lamellar and woven morphology both of which contained large lacunae for osteocytes with mosaic appearance due to the irregular reversal cement lines that separated the woven bone from the lamellar bone (Figure 5.33). The lamellae were either parallel to the surface of the marrow spaces or encircled blood vessels forming mature Haversian systems (Figure

5.34). There were nascent bone trabeculae with relatively regular alignments; new cortex was formed in the outer layer of the regenerated bone which was found covered with periosteum (Figure 5.35).   There were numerous bone marrow cavities, but regular osteon and marrow caves were observed more on the non-operated side (Figure 5.36). It was noted that in some areas less organised woven bone was located next to loose connective tissue which was rich in blood vessels and was highly cellular. The cell populations consisted of osteoblasts and preosteoblasts, possibly from metablastic changes of fibroblasts or myoblasts (Figure 5.37). The borders of the defect in all sections showed highly remodelled bone that exhibited trabecular patterns which caused expansion and displacement of the lingual cortex (Figure 5.38). The soft tissues surrounding the area showed horizontal layers of loose connective tissue that was highly cellular; this may indicate the formation of new periosteum (Figure 5.39, 5.40). Moreover, some areas at the border of the defect showed different directions of lamellar bone. The newly formed bone ran parallel to the periosteum layer, whereas the remodelled older lamellar bone (native bone) was running in a vertical direction (Figure 5.40). In some area of bone remodelling a scalloped appearance was visible in the bony border with the presence of multinuclear osteoclastic bone cells that indicate active bone resorption (Figure 5.41). This may have been triggered by the injected cement which was deliberately placed in close approximation to the border of the defect.
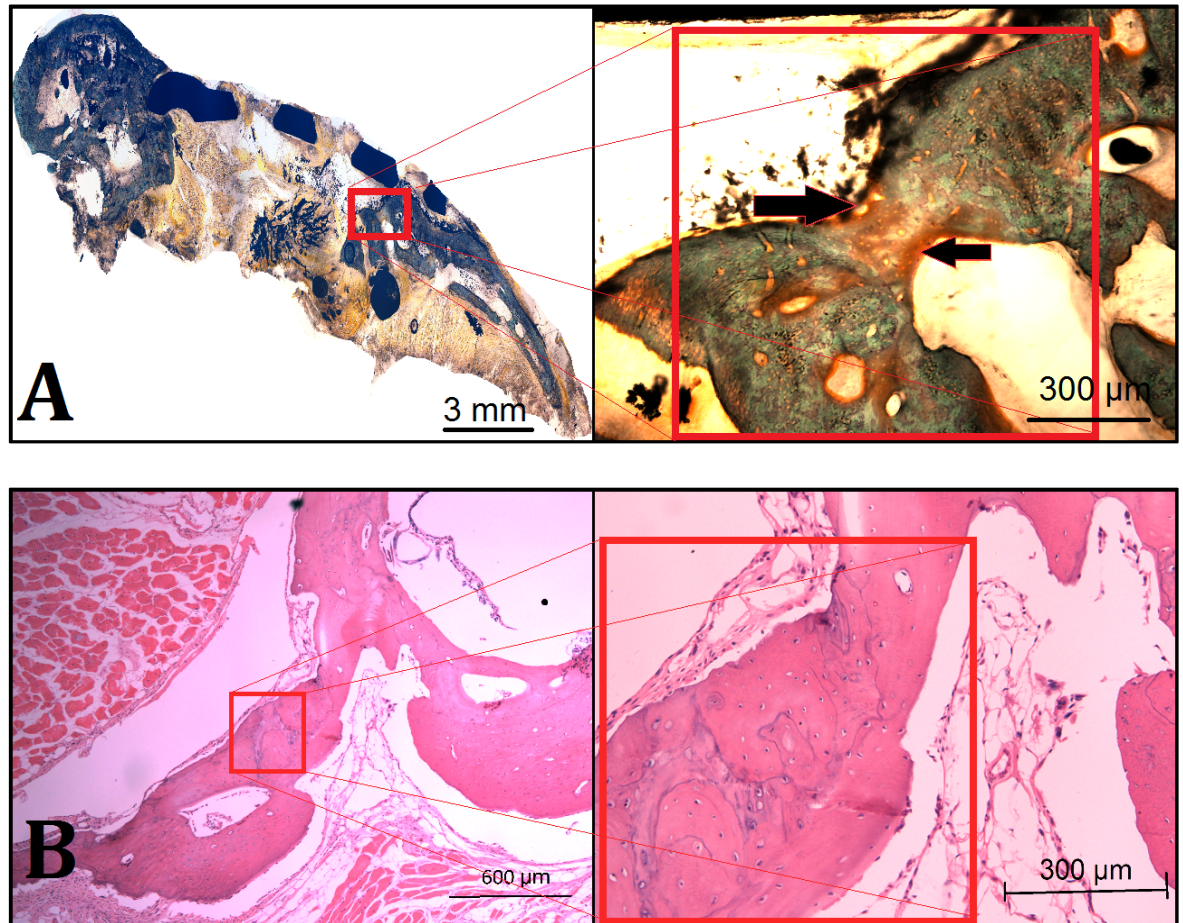
Figure 5.30: Photomicrographs showing areas of bone union (red box) between the native bone and the regenerated bone, A) shows an undecalcified section stained with Goldner`s trichrome taken from the lower section of the defect. Right image shows a magnification of the red box, scale bar = 3 mm and 300 μm, respectively, B) shows a decalcified section of the area of bone union (marked in red box), the right image shows a magnification for the area in the red box. The bone at the interface appeared less mature.
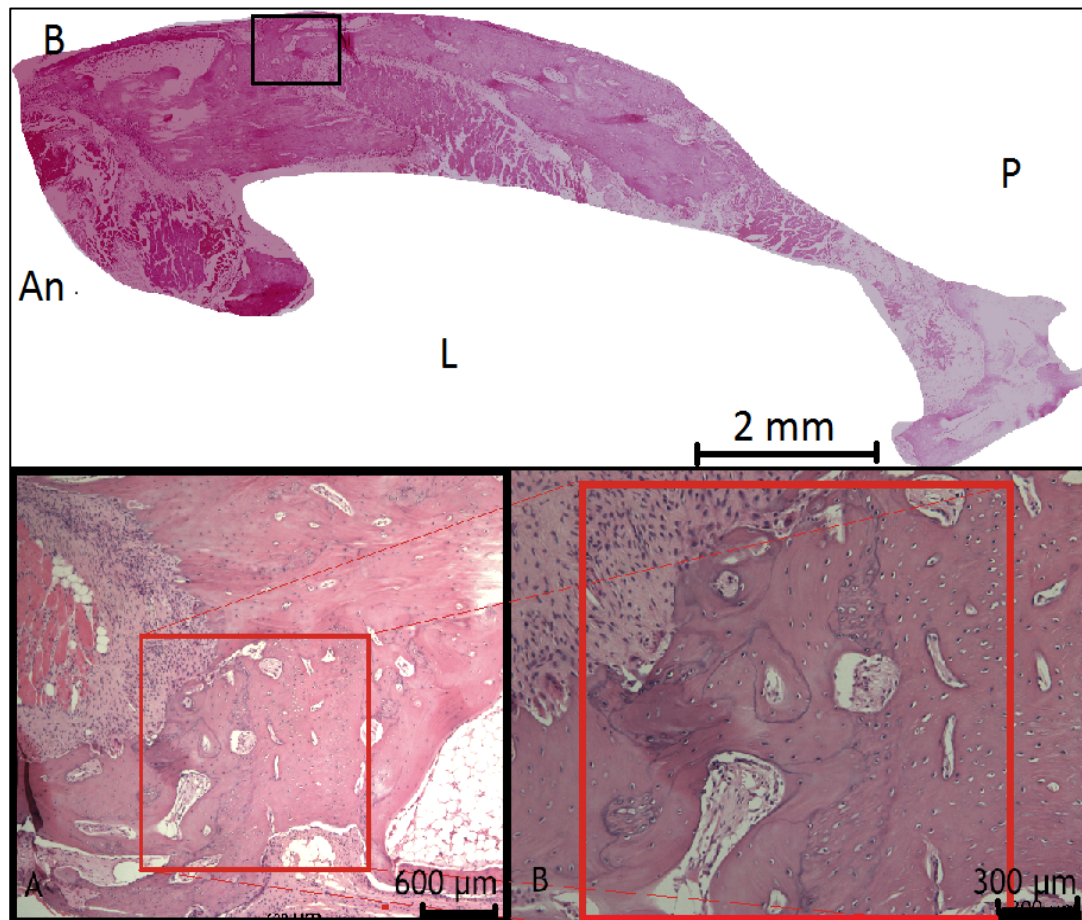
Figure 5.31: Photomicrographs showing decalcified sections stained using (H&E), which demonstrate the area of bony interface (boxed), A) shows a magnification of the black box in the superior image, scale bar = 600 μm, B) shows a higher magnification of the area of the interface (red box) which is occupied by woven bone, scale bar = 300 μm. B, An, P and L refer to buccal, anterior, proximal and lingual.
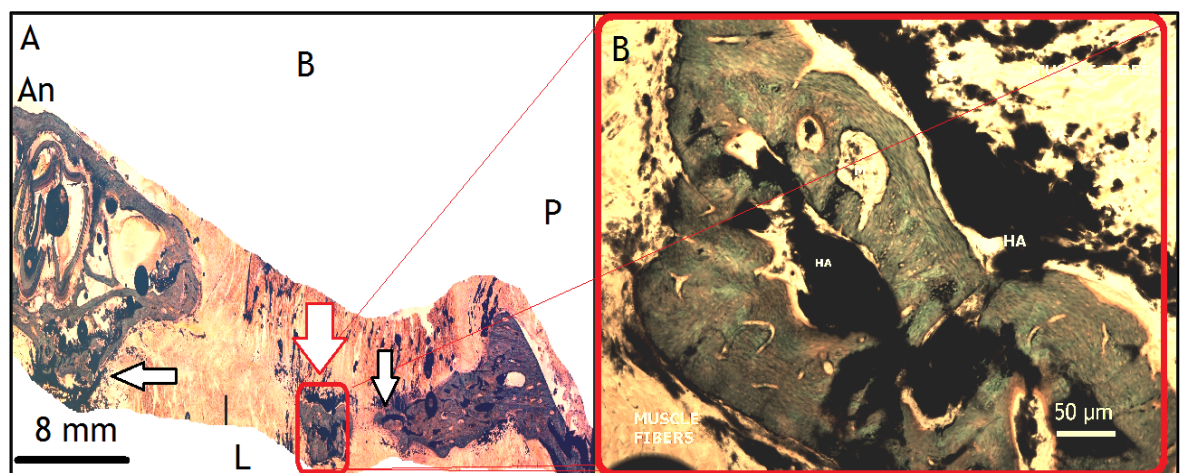
Figure 5.32 Photomicrographs showing undecalcified sections stained with Goldner`s trichrome for case 151, A) shows an overall view of the site of regenerated bone at the centre (red box) and borders of the defect (black arrows), scale bars = 8 mm, B) shows a magnification of the red box, illustrating the close relation of the remnants of the cement to the regenerated bone, scale bar = 50 μm. An, B, P and L refer to anterior, buccal, proximal and lingual boundaries for the defect respectively.
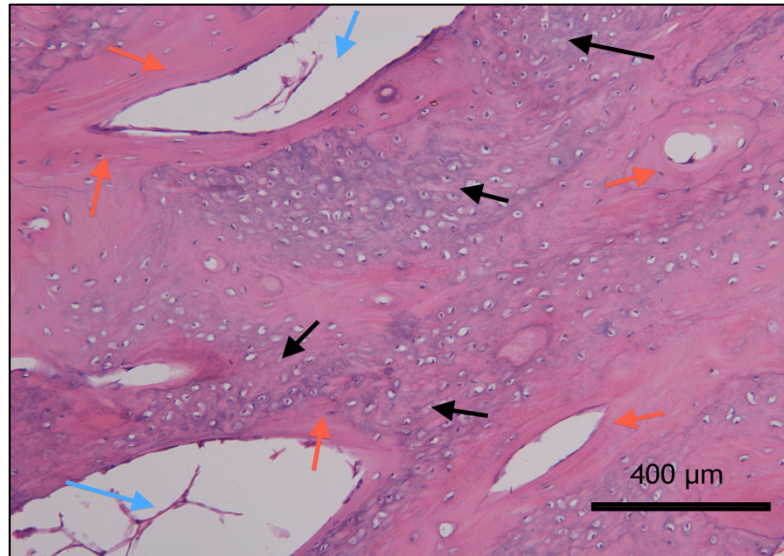
Figure 5.33 Photomicrograph of a decalcified histological slide stained with (H&E), showing the heterogeneous nature of bone formed at the regenerated site, consisting of lamellar bone (red arrows) close to marrow spaces, caves (blue arrows) and woven bone (black arrows), scale bar = 400 µm.
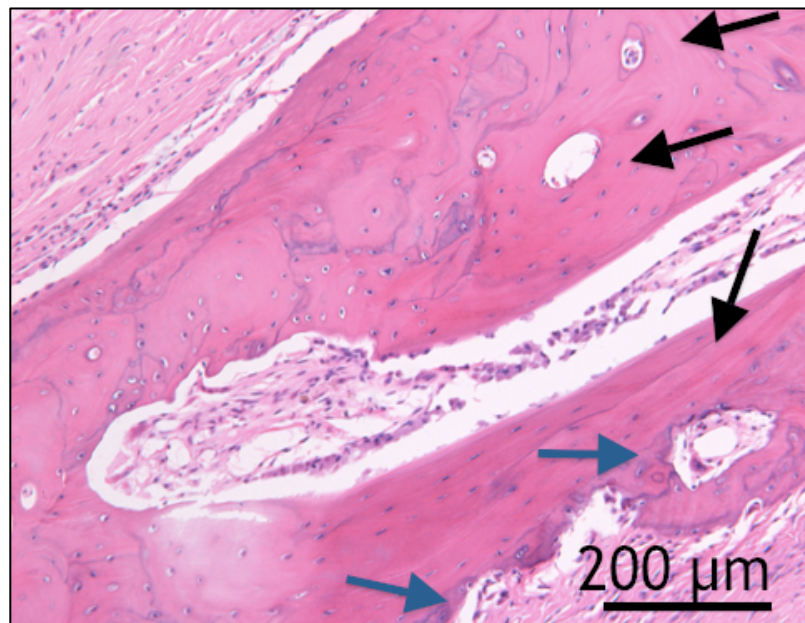
Figure 5.34 Photomicrograph showing a decalcified section stained with H&E, demonstrating new bone with lamellar structure close to bone marrow and vascular channels (black arrow) with adjacent loose connective tissue (blue arrow), scale bar = 200 µm.
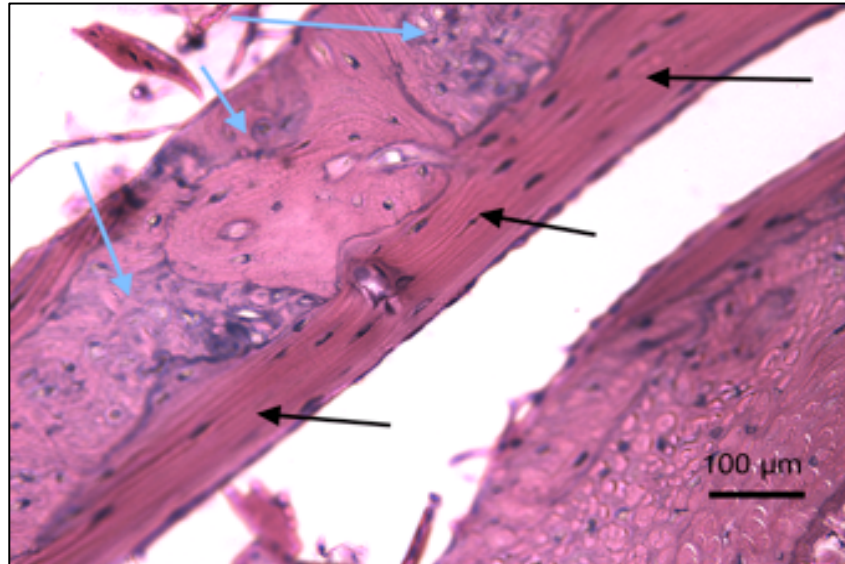
Figure 5.35 Photomicrograph showing a decalcified section stained with H&E, demonstrating mature lamellar bone (black arrow) on the outer surface close to the periosteum, less mature bone with more collagen appears purple in colour (blue arrow). Scale bar = 100 μm.
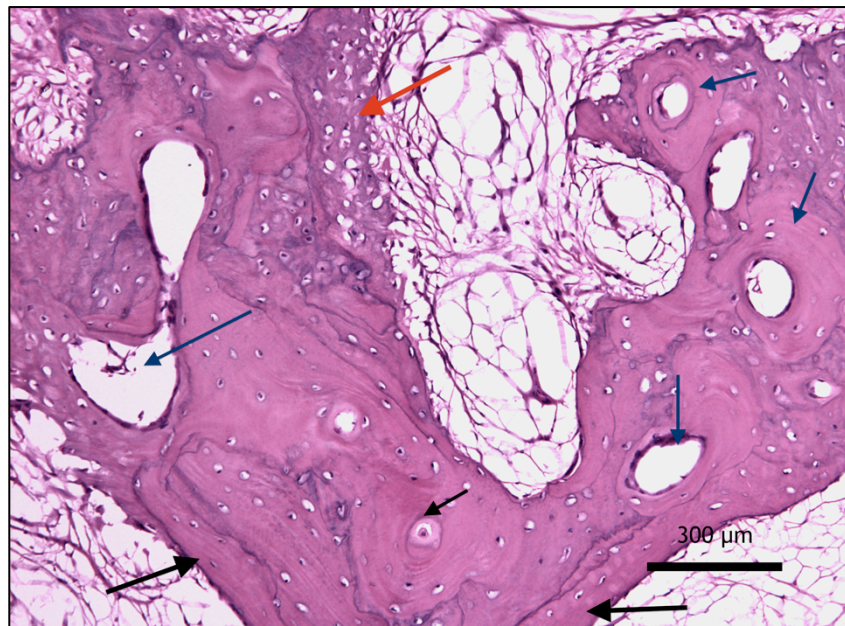
Figure 5.36 Photomicrograph showing a decalcified histological section stained with H&E for the regenerated bone showing bone marrow cavities, regular osteons and marrow caves (blue arrows), lamellar bone (black arrow) is present next to periosteum, whereas woven bone (red arrow) is visible next to the loose connective tissue. Scale bar = 300 μm.
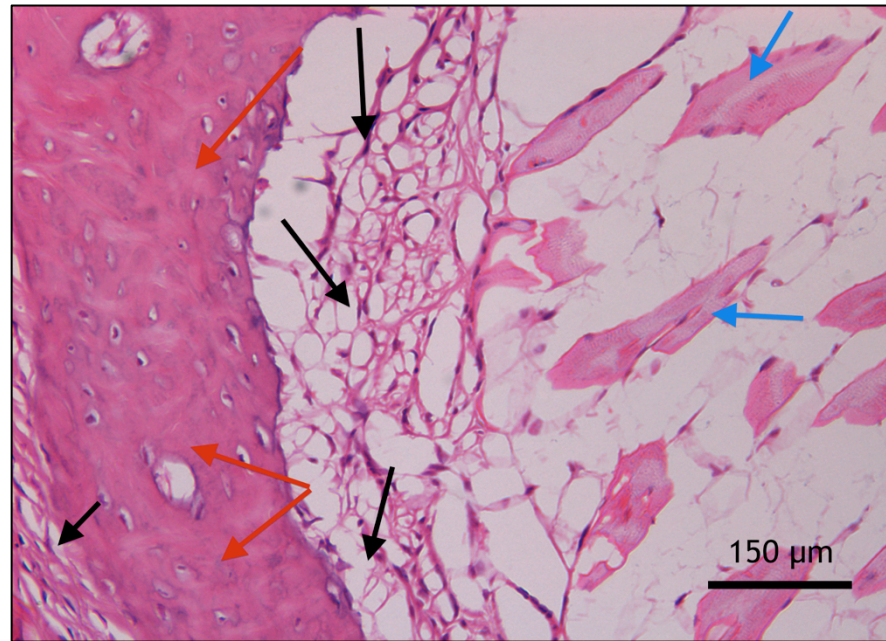
Figure 5.37 Photomicrograph showing a decalcified section stained with H&E illustrating the newly formed bone (red arrow) adjacent to the muscle fibres (blue arrow) which are separated by loose fibrous tissue forming a periosteum-like membrane (black arrows) indicating metablastic changes of the tissues, scale bar = 150 μm.
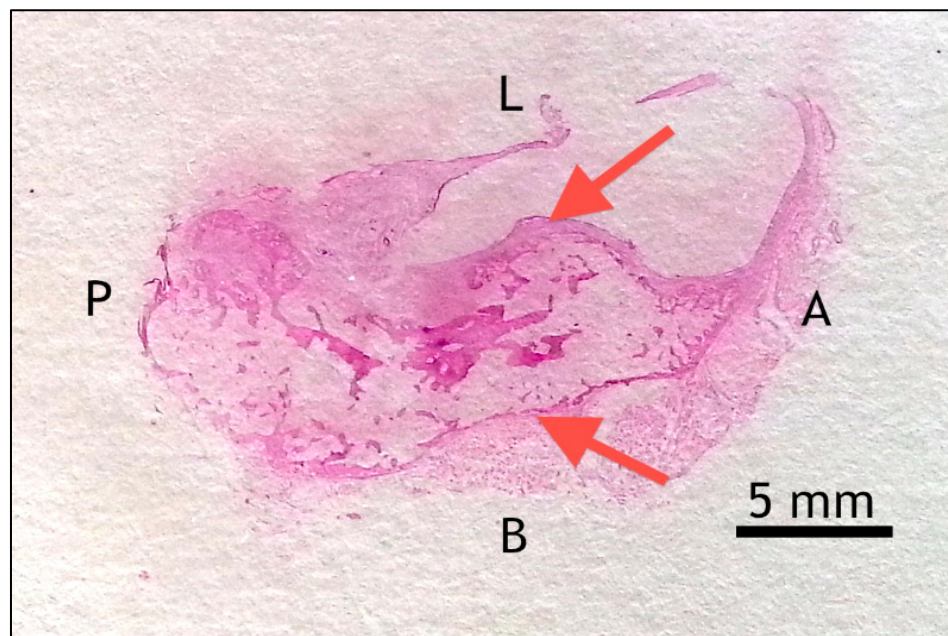
Figure 5.38 Photomicrograph showing an undecalcified section stained with H&E of the proximal border of the defect, showing the cortices (red arrows) displaced buccally and lingually due to trabecular bone formation. L, B, P and A refer to the lingual, buccal, proximal and anterior wall of the defect, respectively, scale bar = 5 mm.
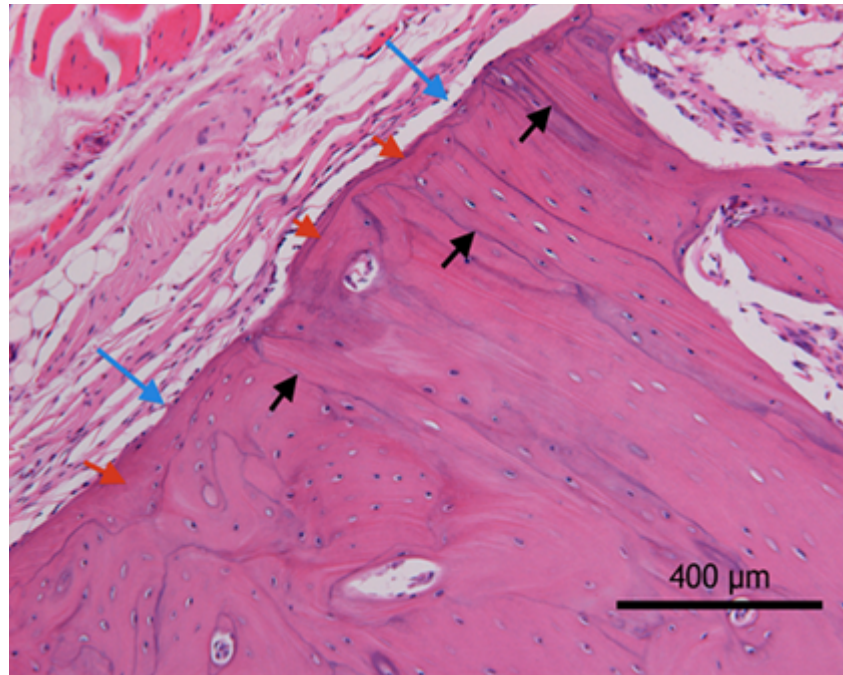
Figure 5.39 Photomicrograph showing a decalcified histological slide stained with H&E, the section shows the border of the surgical defect illustrating the different directions of lamellar growth, horizontal (red arrows) next the periosteum layer (blue arrows), and vertical (black arrows), scale bar = 400 μm.
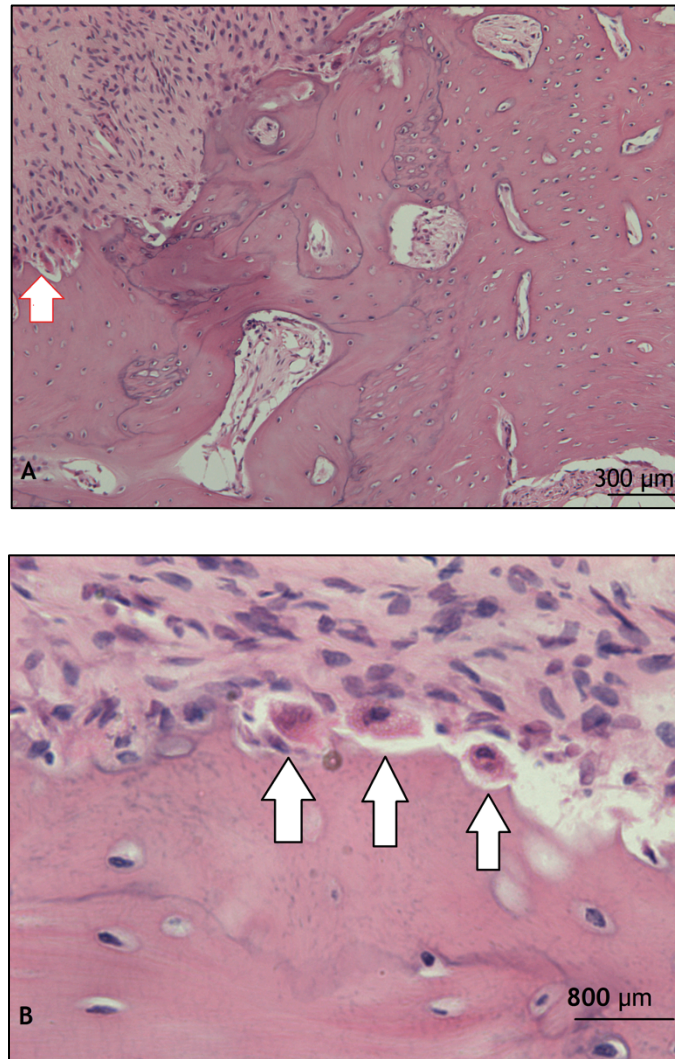
Figure 5.40 Photomicrograph showing decalcified histology slides stained with H&E, A) shows areas of active bone remodelling next to highly cellular connective tissue, with scalloped bone surface containing multinucleated osteoclastic cells (arrow), scale bar = 300 µm, B) shows a higher magnification of the osteoclastic cells (arrows), scale bar = 800 µm.

In the decalcified sections, most of the residual cement was washed out during processing; however, few a sections showed areas of undefined pale tissue which was noticeably associated with mild to moderate inflammatory cells. This tissue could be the remnants of the cement seen clinically. The bone / marrow ratio was similar to that of the most inferior part of the ramus and the marrow spaces were filled with blood-forming tissue and/or fatty tissue.

Eight out of the ten experimental animals underwent semi-quantitative scoring as shown in Table 5.7. The examination revealed that, more than half of the cases

showed development of at least one cortex, but both cortices were noted only in three cases. Residual cement was spotted in only four of the examined cases, however there were empty spaces around the new bone and between the loose connective tissues which might be areas of bone cement that were removed during the decalcification process for histology. The cellular infiltrate was mild (less than 20 cells) to moderate (more than 20 cells); more than 20% of the spaces were filled with marrow fibrosis or collagen fibres.

Table 5.7: Data of the semi quantitative scoring of the decalcified slides for 8 cases.

Case ID no.	Cortex Development	Residual Scaffold	Marrow fibrosis/collagen fibers	Inflammatory cells
214	1	0	2	0
215	1	0	1	0
216	2	0	1	0
217	2	1	2	0
218	1	1	2	0
239	1	1	2	1
240	1	1	2	1
241	2	0	2	0

Un-decalcified sections showed bone formation with an intricate network of woven bone trabeculae within the cement (Figure 5.41). The regenerated bone was formed from the bone border of the defect as well as sporadically within the muscle tissue.   In general the regenerated bone appeared to be thicker in the bucco-lingual direction compared to the non-operated side. The presence of bone cement may explain the expansion of the bony borders. Bone regeneration at the centre of the defect was clearly demonstrated with Sanderson`s Van Giesion stain which appeared as sporadic red areas surrounded with loose fibrous tissue (blue) forming a periosteum like structure (Figure 5.42, 5.43, 5.44). Interestingly, some

areas showed bone regeneration intermingled with fibrous tissue (Figure 5.43 D; 5.45 B, C).

An area of bone regeneration was seen in close contact to the HA granules. The regenerated bone did not follow the same bone contour as the normal non-operated side (Figure.5, appendix 1.5). No evidence of cartilage tissue or chondrocytes was observed indicating that the bone regeneration was by intramembraneous ossification.
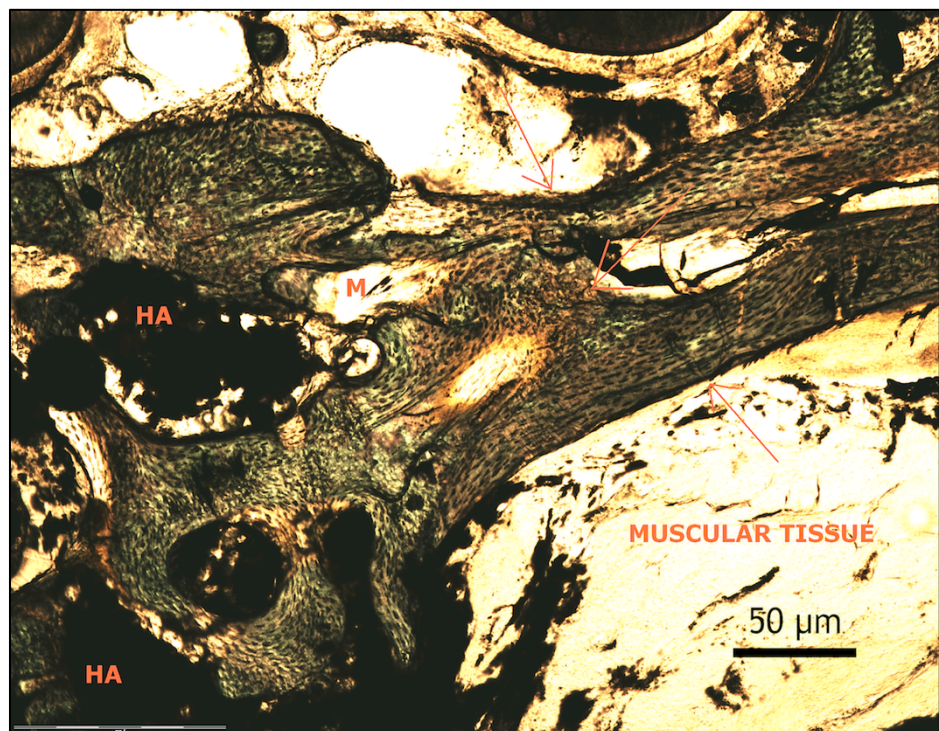
Figure 5.41: Photomicrograph showing an un-decalcified section stained with Goldner`s trichrome illustrating the pattern of the newly formed bone between the muscular tissue and the remaining part of the cement at the anterior border of the defect (red arrows). M - marrow spaces, HA - remnant of cement, scale bar= 50 μm.
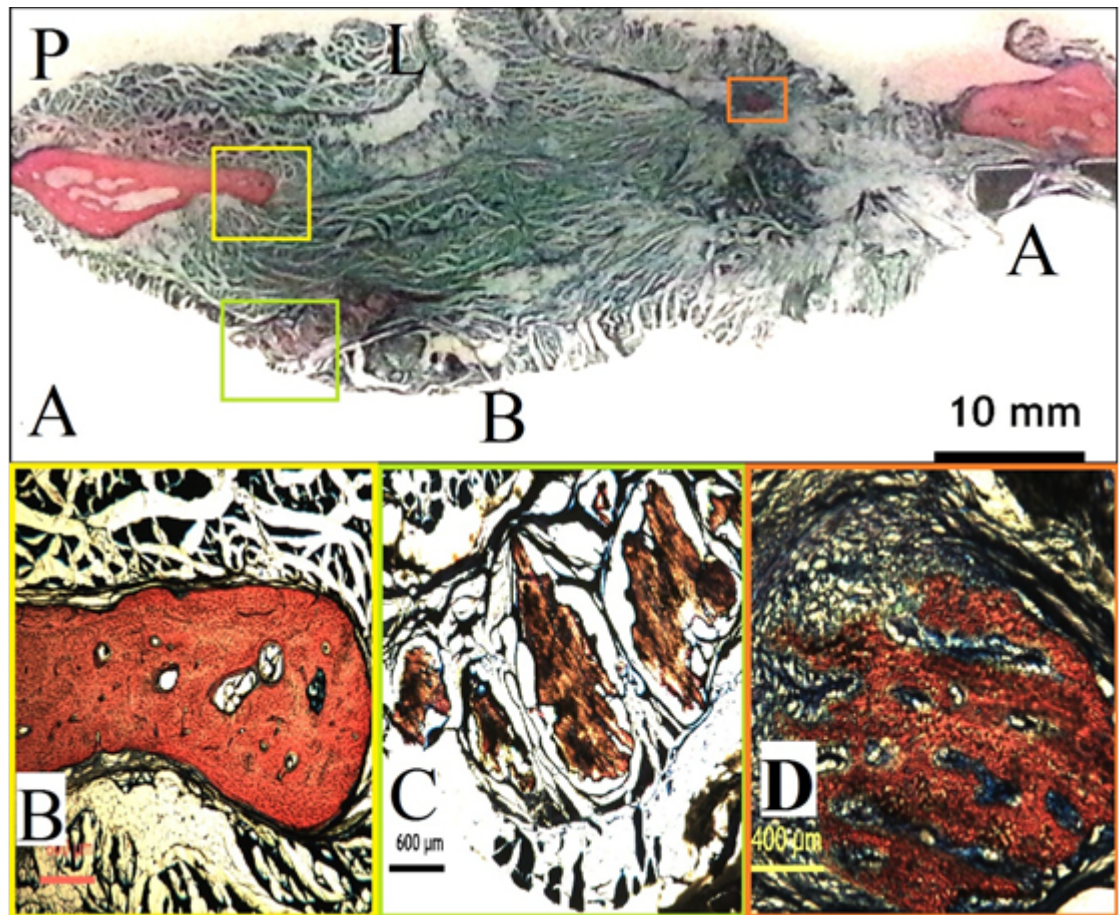
Figure 5.42: Photomicrographs showing undecalcified histological sections using Sanderson`s Van Gieson Stain for case 217. A) The top image shows an overview for the defect area, the muscle (blue) and the regenerated bone (red) at the site of the created defect, there was sporadic bone formation inside the muscle fibres (green and red boxes) and at the border of the defect (yellow box), scale bar = 600 µm. B) shows that the bone is surrounded with loose fibrous and periosteum like tissue, scale bar = 600 µm, C) shows an island of calcified tissue formed buccal to the defect area, scale bar = 600 µm, D) shows regenerated bone (red) in-between the fibrous tissue (blue), less mature bone is also visible (yellow, green), scale bar = 400 µm. A, P, L, B indicate anterior, proximal, lingual, and buccal borders of the defect area.
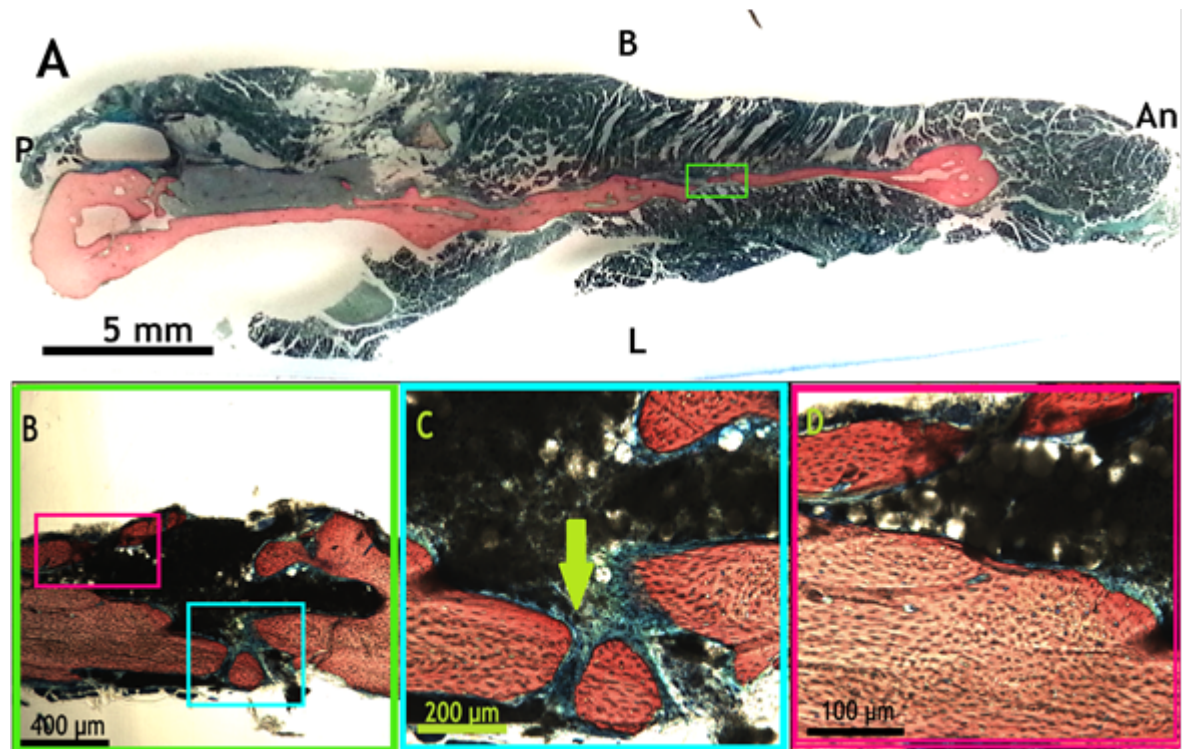
Figure 5.43: Photomicrographs showing an undecalcified histological section using Sanderson's Van Gieson Stain for case 240. A) shows an overview of the surgical defect showing bone bridging (boxed), scale bar = 5 mm, B) shows a magnification of the area in the green box in A showing cement close to the newly generated bone (black area), scale bar = 400 μm, C) a higher magnification (blue box) showing cortical bone surrounded with periosteum-like fibrous tissue (arrow), scale bar = 200 μm. D) shows a magnification of the red box in B with sporadic bone regeneration buccally close to the remnant cement, scale bar = 100 μm. An, P, L, B indicate anterior, proximal, lingual, and buccal borders of the defect.
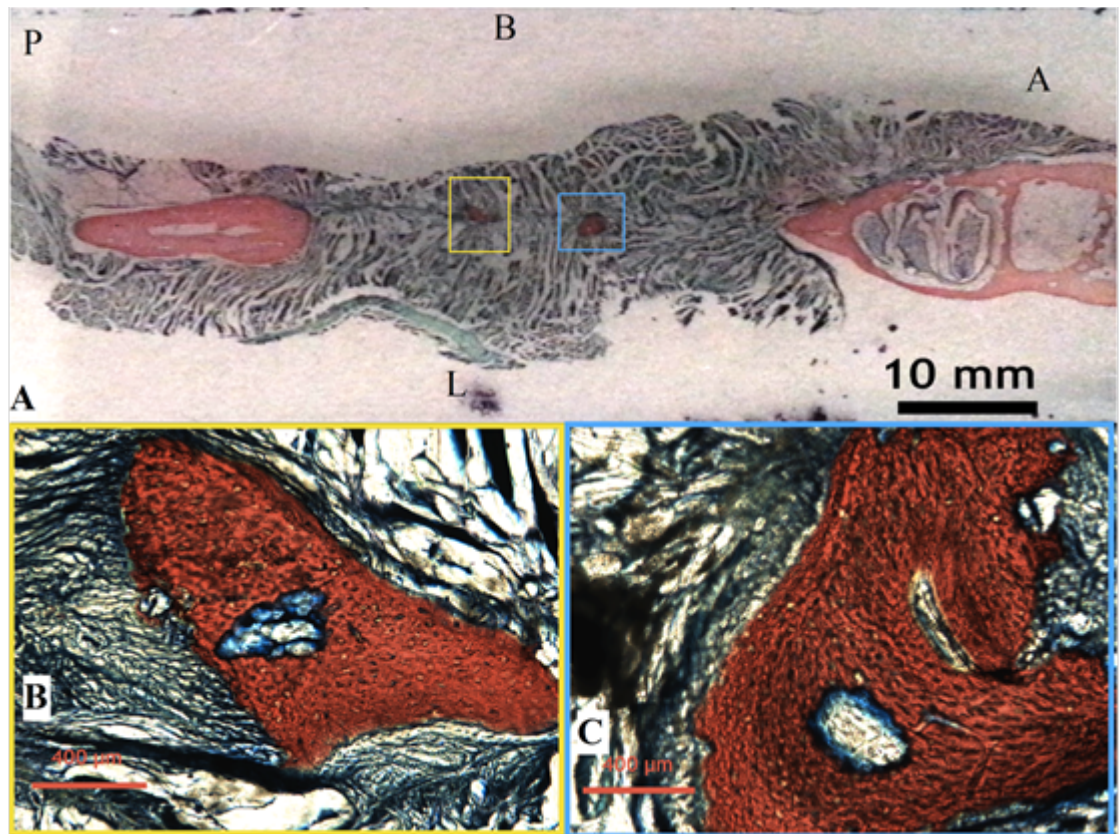
Figure 5.44 Photomicrographs showing an undecalcified histological section, stained using Sanderson's Van Gieson Stain, for case 214, A) shows sporadic bone regeneration at the centre of the defect (boxes), B) shows an island of bone formation (red) surrounded with loose fibrous tissue and marrow spaces at the centre of the defect, C) shows bone regeneration close to the cement on the left side. A, P, L, B indicate anterior, proximal, lingual, and buccal borders of the defect area. Scale bar = 400 µm.

5.2.3.2 Histomorphometric analysis

The process of histomorphometric analysis was carried out as explained in the previous section (3.2.5.2.3.3.1). The joined "stitched" images were used for the calculation of the average bone surface (Figure 5.45). Table (5.8) summarise the average surface area per side in mm^2 and the bone percentage in relation to the control side. The estimated median value was 14.5 mm^2 (range 8-47) at the experimental sides which constituted 78.8% of the bone at the non-operated side. The mean percentage of bone, residual HA, soft tissue and marrow spaces are shown in Table (5.9). The median percentage of bone regeneration, residual cement and soft tissue/marrow spaces were 37.5% (range 22-49), 22% (range 8-33) and 37% (range 31-66), respectively.
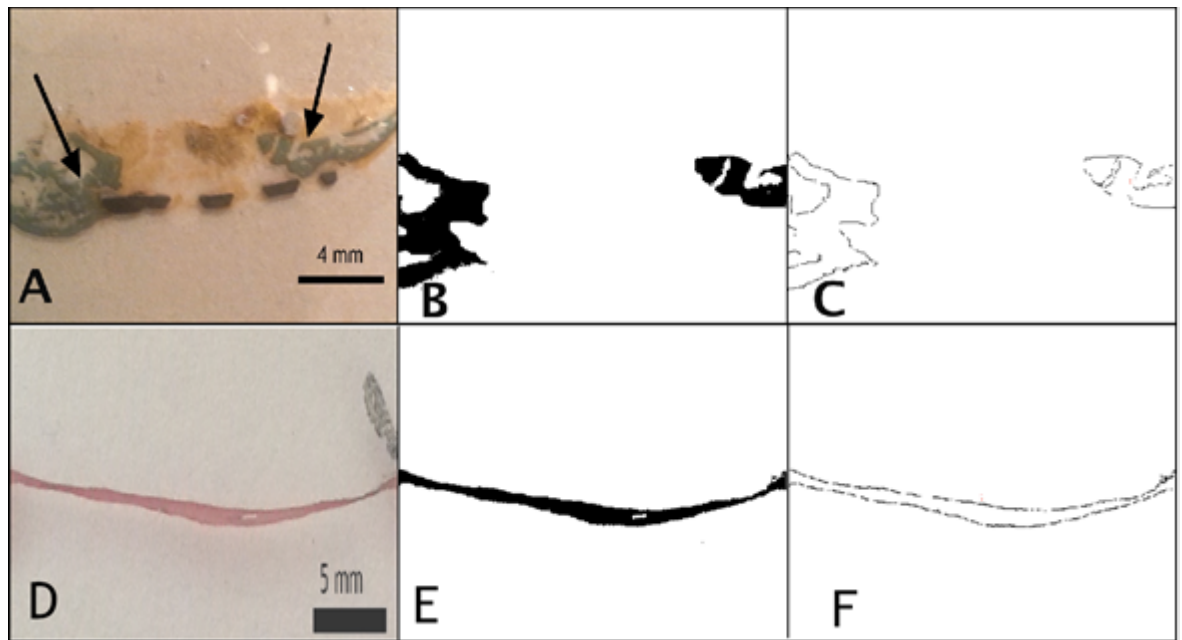
Figure 5.45 Photomicroradiographs illustrating the steps used in the histomorphomteric analysis to quantify the surface area of the regenerated bone, A) shows undecalcified histological slides stained with Goldner`s trichrome, the areas of bone regeneration are indicated with arrows, B) shows the created binary image for the regenerated bone, C) shows an outline of the binary image to allow analysis of the pixels/µm. D, E, F illustrate the same steps in A, B, C but for the non-operated side.

Table 5.8 The average surface area of the regenerated bone (mm^2) and the percentage of bone regeneration for the experimental sides.

Rabbit ID	Average surface area (mm^2)	Percentage of bone formation (%)
151	20.85±10.15	+13%±5
152	12.25±3.25	66%±17
214	12.11±1.19	72%±7
215	10.5±1.6	59%±11
216	8.25±0.9	42±4
217	10.3±1.5	62%±9
218	47.5±9.6	+37±27
239	17.03±9.2	92±5
240	35.68±10.2	+93±13
241	37.9±17.3	+99±20
Median value of surface area for the experimental sides	14.5	78.8 %
Control	18.4±2.1	100

Table 5.9:   Summary of the histomorphometry data for the operated sides, the average percentage of regenerated bone, residual cement and soft tissue/space ratio.

Case number	% of bone regeneration	% of residual cement	% of soft tissue/ marrow spaces
151	33±9	32±6	32±7
152	49±12	23±8	31±16
214	45±5.1	9 ±7.8	48±12.6
215	22±6	12 ±5	66±32
216	34±2	14±7	50±5
217	38±15	30±9	35±11
218	47±11	8±1	37±3
239	29±13	33±5	34±32
240	38±21	22±4	40±18
241	36±14	25±13	37±23
Median	37.5	22.5	37

5.2.3.3 Fluorochrome bone label assessment

Two of the fluorochrome bone labels (given at 8 and 11 weeks) were clearly distinguished. The fluorochromes used were Calcein blue and Alizarin (Figure 5.46). They were found forming either eccentric lines which would be consistent with bone osteons or appeared as parallel lines indicating mature lamellar bone (Figure 5.47, 5.48).   Areas of woven bone were also noted as a network-like structure was seen with both labels (Figure 5.49). The bone labels followed either an outward or inward direction with mature lameller bone noted on the outer layer and woven bone found on the inner layers (Figure 5.50A), this might illustrate the remodelling process. Areas of woven bone were found next to loose connective tissue (Figure 5.50B). The latter may indicate osteogensis which as a result of the injected rMSCs or the metablastic changes of the fibroblasts or myocytes induced by the BMP-7 or the cement.

The average mineral apposition rates (MAR) were calculated for both the experimental and the control sides and are summarised in Table (5.10). The average rate of apposition was 1.93 µm/day for the experimental sides and 1.1 µm/day for the control sides. These findings indicate active mineralization due to fast deposition of bone matrix and were consistent with findings of the micro-radiographic analysis
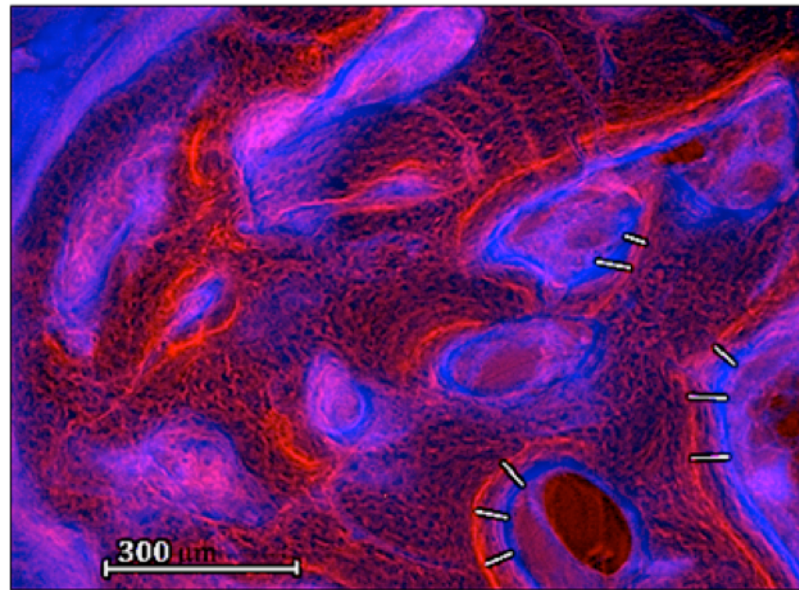
Figure 5.46 Phomtomicrograph showing an undecalcified, unstained section used to detect the mineralization rate with fluorescent microscopy (Zeiss Axioskop, Germany) and a R/G light filter (HBO 100, LEj, Germany). The fluorochrome bone labels (Calcein blue and Alizarin complexone) given at 8 and 11 weeks are clearly demonstrated, scale bar = 300 µm .
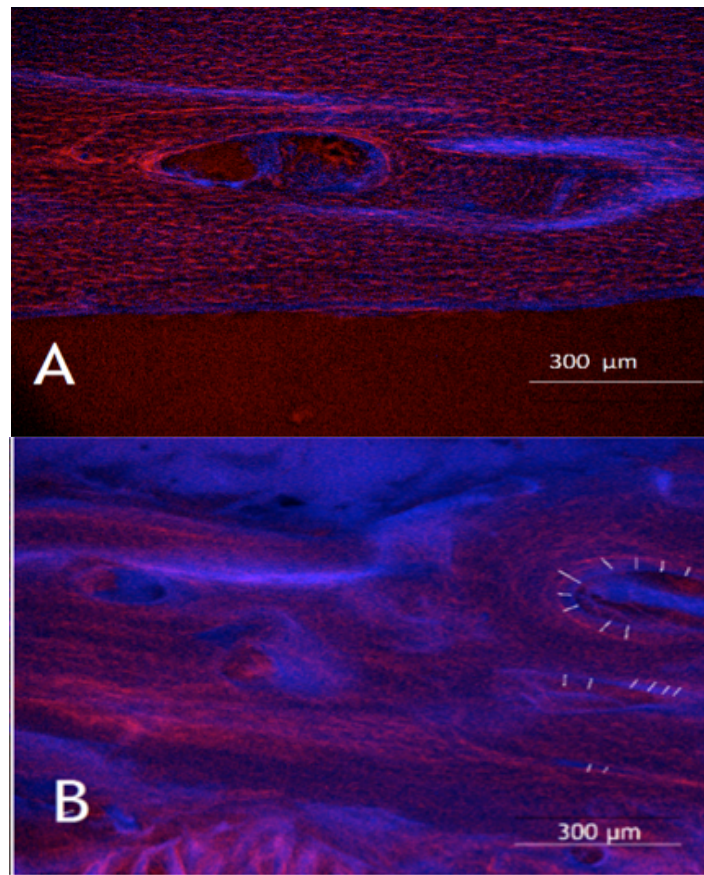
Figure 5.47 Photomicrograph showing an undecalcified, unstained section viewed under fluorescent microscopy (Zeiss Axioskop, Germany) with a R/G light filter (HBO 100, LEj, Germany). A) Shows the non-operated side with circular lines around the vascular channels at the centre and parallel lines at the periphery indicating the lamellar structure of mature bone, B) shows the experimental side with osteon structures, the measurement is made from the blue to red line as indicated (white lines). Scale bar= 300 μm
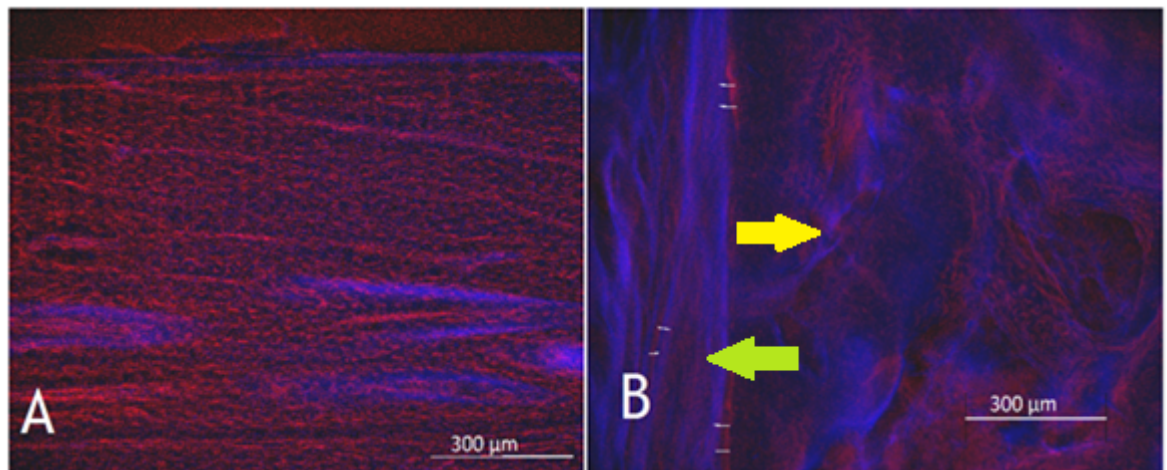
Figure 5.48 Photomicrographs showing undecalcified, unstained sections under fluorescent microscopy (Zeiss Axioskop, Germany) with a R/G light filter (HBO 100, LEj, Germany). A) Shows the non–operated side with parallel lines indicating lamellar bone (calcein blue) and red (Alizarin complexone) bone labels, B) shows the experimental side with parallel lines (green arrows) which indicate lamellar bone and web like lines (yellow arrow) indicating woven bone, scale bar = 300 μm.
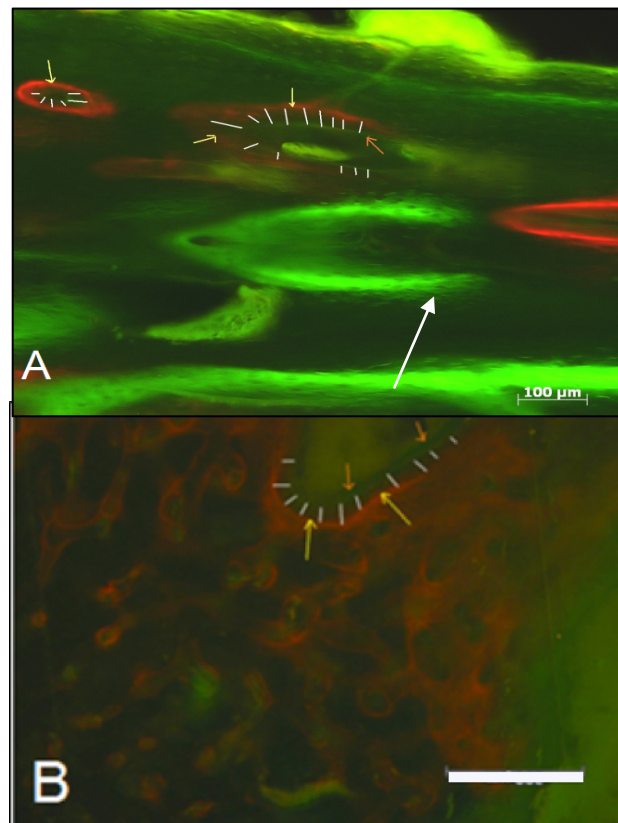
Figure 5.49 Photomicrograph showing undecalcified, unstained sections under fluorescent microscopy (Zeiss Axioskop, Germany), with a R/G light filter (HBO 100, LEj, Germany). A) Shows calcein blue bone label (green), and Alizarin complexone (red colour) in the control side, scale bar = 100 µm. B) Shows the experimental side with red lines (Alizarin complexone) and green lines (calcein blue), areas of woven bone were clearly identified, scale bar = 200 µm.
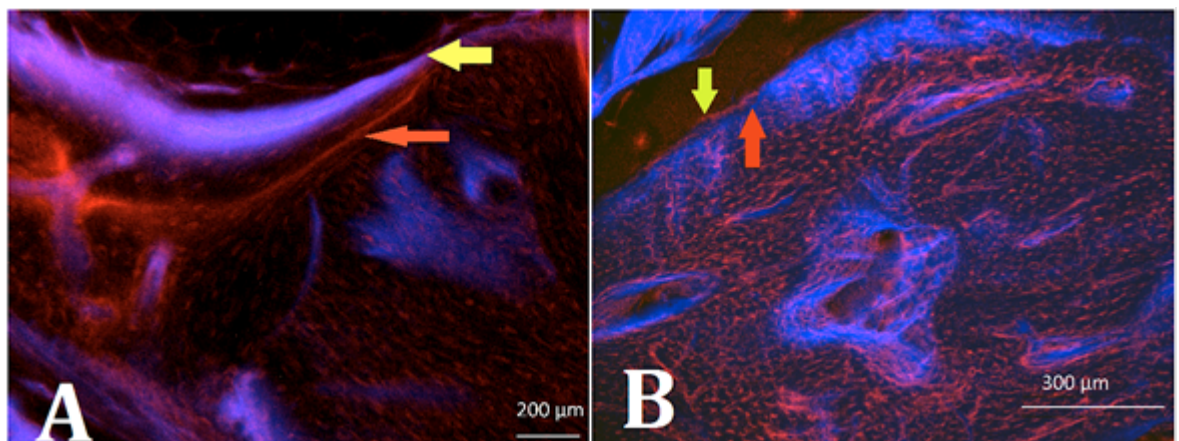
Figure 5.50 Photomicrograph showing undecalcified, unstained sections under fluorescent microscopy from different areas of the regenerated bone, A) shows blue and red lines (arrows) located in between the woven bone superiorly and lamellar bone inferiorly, calcein blue (yellow arrow), alizarin complexone (red arrow) are located closer to the mature bone inferiorly, scale bar = 200 µm, B) shows regenerated bone next to loose fibrous tissue superiorly, alizarin complexone red lines (green arrow) are next to the loose fibrous tissue and blue lines (calcein blue, red arrow) are present inferiorly, scale bar = 300 µm. The two images indicate different directions of bone deposition.

Table 5.10: Table summarising the average reading for the mineral apposition rates (MAR) for the experimental sides.

Case number	Experimental side MAR (µm/day)
151	1.99±0.3
152	1.74±0.31
214	2.24±1.2
215	1.8±0.2
216	3.1±0.9
217	2.9±1.2
218	1.55± 0.6
239	1.48± 0.6
240	1.23±0.4
241	1.35± 0.3
Average	1.93±0.60
Control	1.1±0.3

5.3 Discussion

The results have demonstrated the potential for the use of facial muscle flaps, injectable cement and rMSCs for the regeneration of bony defects. It is likely that the muscle flap provided the required blood supply for bone regeneration and acted as a bioreactor for the rMSCs, alongside the injected cement and BMP-7 that induced bone formation.

The animals tolerated the surgery well, there was no dramatic weight loss or infection with the normal diet reinstated 3-4 days after surgery. The only complication reported in 3 cases was the formation of a seroma, which was detected 3-6 days post-operatively. To avoid an increased risk of infection, needle

drainage was carried out in two cases but some seromas can resorb

spontaneously as happened in one of the cases. A similar finding was reported by

Truedsson (2010) in a study on rats using Cerament^{TM}. They reported seroma

formation in one third of the experimental cases. This may indicate the hyper

tonicity of the calcium sulphate when its starts gradually dissolving. Seroma

formation also occurs with the use of BMP in animal and in clinical applications

(Jovanovic et al, 2007; He et al, 2010; Shields et al, 2006; Smucker et al, 2006).

This complication was due to a high dose of BMP which caused more cellular and

free water transudation to the surgical site, even in spite of giving high doses of

steroids in some studies (Marx et al, 2013). This complication could be avoided by

using the protocol suggested by Kim et al (2011), or clinically, by inserting an extra

oral stent to drain any seroma or hematoma collections, as suggested by Marx et

al (2013).

Clinical assessment of the harvested mandibles showed that half of the samples

demonstrated the presence of a whitish rubbery material between the muscle

tissues and around the defect. Similar finding was noted during the pilot study.

Histological examination revealed the presence of compact mineral crystals with

fibrous tissues in between. This could be due to the HA crystals and the

degenerated muscle fibres. A 16 gauge needle was used to inject the cement as

recommended by the manufacturer to avoid the filter pressing phenomenon.

Residual cement may have persisted due to changes in the viscoelastomeric

properties of the material that can be affected by the powder to liquid ratio (PLR),

the use of additives and the mixing methods (Lewis, 2011). The PLR was kept

constant for all the experimental cases; however the addition of 0.4 mg/ml of BMP

did decrease the setting time of the cement. A manual mixing method was used in

this project so the material was subjected to low shear strain compared to

automated mixing which led to a more viscous cement mix. The observed residual cement was found intermingled between the muscles tissues and around the periphery of the defect, this could be due to large amounts of cement being injected initially where the excess cement leaked into the surrounding spaces; this phenomenon was common when injectable cement was used for vertebral surgery (Nakano et al, 2005).

Our data analysis showed that, complete bone integration or incorporation was not achieved. This is partially due to the physical nature of the injected cement that prevented the diffusion of the material at a micro level between the fibres of the muscle tissue. This point will be further explored and discussed in detail in Chapter 6. Alternative ways to deliver the growth factors and cement within the muscular tissues in a more controllable manner are discussed. Another factor that could impair the process of integration of the regenerated bone with native bone is the size of muscle flap which obliterated the created surgical defect making it clinically difficult to ensure that the injected scaffold had uniformly reached the desirable site. It may have been easier to apply a thinner pedicled muscle to reconstruct the created defect, to assure the regenerated bone will form within the vicinity of the ROD, or inject the cement into the reflected flap first then adapt into the created defect before suturing it in place (Figure 5.51). However, we could argue that use of a more bulky muscle flap would provide more osteoprogenitor cells or endogenous growth factors to the grafted site. Liu et al (2012) claimed that the volume to surface area of the muscle flap affects the amount of bone regeneration.

Studies on factors affecting bone incorporation showed that with the most optimal bone graft (autograft) several aspects are crucial for its success which includes stability of the mechanical environment, the presence of adequate vascularity and

an intimate contact with native bone (Stevenson et al, 1996; Feiertag et al, 1996; Emery et al, 1994; Boden et al, 1995). In our experiment we injected the bone cement, BMP-7, and rMSCs all around the bony border of the defect as well as inside the muscular tissue to ensure intimate contact with bone. The pedicled muscle flap provided the vascularity throughout the defect as seen from the histological examination. With regard to stability, a titanium plate and two screws were used to bridge the created defect and maintain the jaw integrity. Since the muscle flap is a dynamic tissue the contraction of this muscle would affect the pattern of bone regeneration. The latter observation could induce more bone formation at the periphery of the defect which was observed in all examined samples.
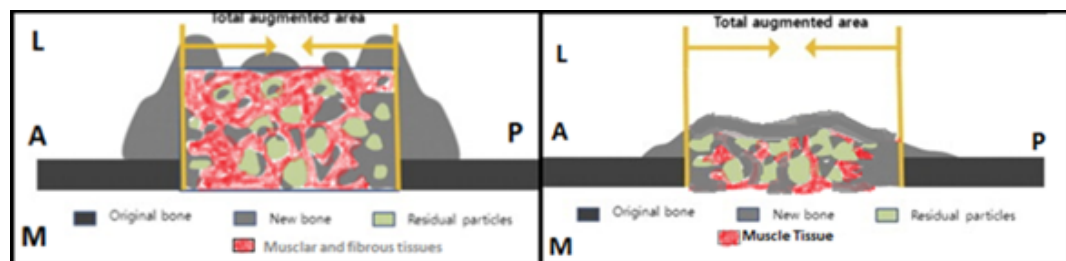
Figure 5.51 Schematic representation of the pattern of bone regeneration based on micro-CT and histological investigation which shows the bulky muscle occupies and extends beyond the limits of the surgical defect. The red area represents the residual particles of cement inside the muscle fibres, and areas of bone formation (grey colour) at the borders of the defect. The illustration on the right side shows that a thinner muscle flap would enhance the process of bone formation in the ROD. (L, M, A, & P denote the lateral, medial, anterior, and proximal walls of the defect).

We believe that it was important to investigate the nature of the interface between the regenerated calcified tissue and the surrounding native bone, CBCT imaging alone was not enough for this. Micro-CT disclosed the nature of this interface and also revealed the trabecular pattern of the regenerated bone (Muller et al, 1998). It also helped in distinguishing the structure of the remaining undissolved cement and the regenerated calcified tissue in 3D by adjusting the threshold. Adaptation of the global threshold for the biphasic calcium phosphate cement was successful in

our experiment as in other studies (Muller and Ruegsegger, 1997). The estimated median value of the new bone volume was 46 mm^3 (range 36.9-59.0) inside the ROD in all assessed cases. The median volume of the new bone formed outside the ROD was 166.9 mm^3 (range 26.9-320.7) which was more than 3 times the bone volume inside the ROD. This agreed with the histomorphometric findings. The remaining cement constituted an average percentage of 22.5% (range 8-33). This was expected, as the resorption rate of the Calcium sulphate component of the Cerament^{TM} is faster than the hydroxyapatite. The new bone showed a thinner trabecular pattern but the number of trabeculae exceeded the average of the contra-lateral native bone. These findings imply that the bone had a fast deposition rate and active remodelling process (Frost, 1999). Turner et al (1995) tested the trabecular pattern of less mature bone and observed a reduced extra cellular matrix deposition which led to less anisotropy compared to the mature bone. These findings were consistent with the histological findings; the undecalcified sections showed the presence of an intricate network of woven and mature bone trabeculae within the residual cement. Similarly, the flurochrome bone label indicated the mineral apposition rate (MAR) was 1.93 µm/day for the experimental side compare to 1.1 µm/day for the contralateral side. The regenerated bone was a mixture of immature osteoid and woven and mature cortical bones were detected toward the centre of the defect. The estimated average bone surface area was 21.2 ± 6 mm^2 and 18.4 ± 2.1 mm^2 for the experimental and non-operated sides respectively. This difference was due to the expansion of the bony cortices at the border of the defect.

Histological assessment did not reveal cartilage tissue nor were chondrocytes observed. This suggests an intramembranous ossification pattern which agrees

with a general consensus about direct bone formation inside calcium phosphate ceramics implanted into extra-skeletal sites (Le Nihouannen et al, 2008; Ripamonti et al, 1996; Yuan et al, 1999).

Bone morphogenetic proteins (BMPs) induce bone regeneration by endochondral ossification when it has been implanted in hetrotopic or orthotopic sites (Geiger et al, 2003; Abu-Serriah et al, 2002). This paradox in the pattern of bone formation between BMP and bone cement and the results of our analysis indicate that bone cement, BMP-7 and rMSCs most probably induce bone regeneration via intramembranous ossification. The suggested mechanisms for osteoinduction were described by Le Nihouannen (2008). The micro-pores greatly enlarge the surface area of the material and this favours the adsorption and entrapment of exogenous BMPs (De, 1998). These proteins on the surface of the material could promote both the adhesion and differentiation of rMSC cells into osteoblasts. Osteogenic cells attach to this biological apatite layer and produce an extracellular matrix composed of collagen, non-collagenous proteins, and growth factors such as BMP (endogenous) (Le Nihouannen et al, 2005). This extracellular matrix is then mineralized by osteoblasts forming a cement line. Micro particles measuring <5 μm are dissolved and released around the biomaterial. This release of micro particles might provoke an inflammatory reaction (Lu et al, 2004; Laquerriere, 2003). The local release of inflammatory cytokines (tumour necrosis factor-alpha, interleukin-6, IL-10, IL-18) stimulates the circulating stem cells to differentiate into osteoblastic cells, thus producing bone tissue. In this study, the use of exogenous BMP-7 and autogenous rMSCs have promoted the process of bone formation and in turn enhanced the proliferation and differentiation of mesenchymal stem cells at the site of surgery (Yamada et al, 2003).

Further scopes of discussion on the study methodology and the outcome will be

presented in the next chapter6.

Chapter 6

Discussion

Table of Contents

6 Discussion

6.1 Pattern of bone regeneration

In this study the histology and radiographic findings of bone regeneration were in agreement. The assessment showed that a significant amount of bone was formed outside the region of the defect ROD and the volume of the regenerated bone inside the muscle flap was 5 times the volume of the ROD. Radiographic and histological findings showed insufficient bone formation to bridge the surgical defect in all cases. It seems that the bone regeneration was limited to the areas where cement and BMP-7 or/and rMSCs were injected inside the muscle flap. The radiographic and histological findings provide compelling evidence of the osteoinductive bone regeneration within the muscle flap which provided the necessary blood supply for bone formation. It is well documented that the presence of vascular bed and angiogenic factors are imperative for bone regeneration when muscle flaps are used to reconstruct large cranial defects (Liu et al, 2012). The pedicle muscle flap provided a sustained vascular perfusion which is essential for osteogenesis.

The main factor that influenced the location and the pattern of bone regeneration was the distribution of the injected cement. The material set within 10-15 minutes between the muscle fibres and did not diffuse at a micro-level within the muscle tissue. The design of this study would not separate the impact of BMP-7 and rMSCs on bone formation. The achieved bone regeneration was the result of the cumulative effect of cement, cytokines andMSCs.

To our knowledge there is only one report which showed complete bone regeneration in long bone by injecting adenovirus vector of BMP-2 inside a muscle flap (Evans et al, 2009). The same technique was not successful when adenovirus vector of BMP-2 was injected into a skeletal muscle flap for the reconstruction of

large cranial bone defects (Liu et al, 2012). It has been claimed that the lack of vascularity and the known differences in the mechanism of bone formation between the partial bone and the long bone could be the reason behind the reported suboptimal results.

In this study several factors were taken into consideration on deciding on the size and the anatomical location of the created mandibualr defect. The defect was of a critical size, bicortical, 20 mm vertically and 15 mm antero-posteriorly. Reconstruction of this defect is challenging, the ramus is paper thin, about 1.5 mm thick, and the bone marrow content of the adjacent bones is limited. Therefore, it was the objective of this study to investigate the cumulative effect of the injected cement, BMP-7 and rMSCs in stimulating bone formation within a pedicled muscle flap to reconstruct the surgical defect. We acknowledge that the design of the study did not allow the assessment of the osteogenic potential of each factor separately, but, this was not the objective of the study. The direct injection of the cement into the surgical defect was not considered as the material lacks the mechanical strength to bridge the created gap. The application of the muscle flap was crucial in this study to ensure the adequacy of the blood supply at the surgical defect and to maximise the potential for bone formation.

Two mechanism of ossification take place in bone regeneration, endochondral which favours the hypoxic condition and usually occurs at an early stage of bone repair. It is associated with the presence of the hypertrophic chondrocytes that secrete angiogenic factors which are essential for bone regeneration (Gerber, 1999). Intra-membranous ossification is based on the presence of mesenchymal cell clusters that transform into osteoblasts forming an ossifying centre, which secrets osteoid that becomes mineralised within a few days, and so a rich vascular bed is required from the early days of bone formation. In our constructs the blood

supply could have been jeopardised in the early days after cement injection. However, the histological assessment did not show chondrocytes or cartilaginous tissues.

In this study the possible mechanism of bone formation is based on the inflammatory reaction at the surgical site and the presence of cement which reinforced and amplified the signalling of the added BMP-7, thus triggering the MAPK pathway as explained by Hassel et al (2003). The effect was more marked at the bone border of the defect which could be due to the dynamic motion of skeletal muscle that stimulates more osteoblasts, and hence more bone thickness was observed. Other possible reasons include specific post translational modifications undergone by the endogenously synthesised molecule, a potent paracrine and autocrine signaling that triggered a response (Liu et al, 2012).

There were many manipulative variables that led to the reported different results. The methodology of the study will be discussed, the previous published papers on similar methods will be appraised. The results and limitation of both the in-vitro and in vivo parts of this study are presented.

6.2 The study Methodology

6.2.1 In Vitro study

6.2.1.1 Availability, isolation, culture, and expansion of rMSCs

It is well documented MSCs have been successfully used for bone regeneration at the critical size defect created in the rabbits' mandibles. In our study we used bone marrow as a source of MSCs; the protocol used for bone marrow aspiration from the posterior iliac spine of the rabbit was developed by our team (Alfotawi, 2014; Busuttil, 2012). The problems reported were the variable rate of initial yield which affected the overall number of stem cells expanded and cultured for application in the created surgical defect. To overcome the low initial yield of themarrow`s cells, isolated volumes of the harvested marrow was maximised by collecting more than one aspirate at a time. A similar technique has been suggested by Lee et al (2011). Therefore, both the right and left posterior iliac crests of the rabbits were used to obtain around 5 ml of marrow. Expansion of the cultured cells for up to 4 days produced a more hetero-tropic population of cells.

An examination of the in-vitro rMSCs attachment, adhesion and the proliferative ability were assessed on the surface of Cerament ^{TM} (CSS and CBV). It was found that the rMSCs attached and adhered on the surface of CSS only, this was due to various reasons; such as the chemical composition of CSS which did not affect cell survival or expression of transgenes as demonstrated by Bianchi et al (2001). Also the cement composition provided a suitable microenvironment for rMSCs which supported their attachment, adhesion and proliferation (Figure 1.1). Moreover the cement guides the fate of the seeded rMSCs by selecting sub-populations and influencing their fate, an area studied by Bianchi et al (2001). Our

findings suggest that rMSCs found their niche in the putative perivascular area, interacting with various other differentiated cells by means of cell-adhesion molecules. The extracellular matrix (ECM) is deposited by the niche`s cells under the influence of integrin receptors, and other signaling molecules, including autocrine, paracrine, and endocrine factors. Another variable is O_2 tension, together with pH, ionic load, and glucose strength also associated with the rMSCs in the bone marrow niche. These factors could be important reasons for the less promising results that were obtained when Cerament Bone Void was used in vitro.

On other hand, It has been found that rapid new bone in-growth into cement surface (Ceramet^{TM}) occurs as early as 3-6 weeks. This is due to the precipitation of apatite on surface of cement which improves cells to cement attachment and adhesion as seen during SEM examination (Figure 4.24). This was previously confirmed, in vitro, when the same material was soacked in SBF (Nilsson, 2003). Similar result was obtained by Kokubo et al, 1996; Yan et al, 1997, they reported on the rapid bone contact on surfaces treated with bone like apatite. The relationship between the number of seeded cells and the quality of the bony union cannot be ruled out in this study. Around 3×10^6 / ml cells were seeded per defect in our experiment. Van Gaalen et al (2010a) suggested that cell concentration upon seeding is important for bone fusion rate. Similarly, Minamide et al (2005) reported different results for lumber spine fusion based on cell concentrations seeded at the defect side in the rabbit's model.

6.2.1.2 Seeding rMSCs into calcium sulphate bone cement

To model in vivo application, two constructs were made. In the first, cell suspensions were added on the surface of the freshly mixed cements and in the

second, cells were mixed together with cement and the viability of rMSCS was evaluated. In the second method, virtually no cells survived. This result was attributed to one or more of the following factors. The reacting calcium sulphate could have caused local fluctuations in pH or ionic strength, or the setting of the cement is exothermic which is unfavourable for survival of the cells, or the direct mechanical impact on the cells during mixing contributing to the cell damage. Therefore, the decision was made to seed the cells in vivo once the material had set.

To overcome the problem of direct contact between cells and bone cement biomaterials have been explored to serve as the temporary matrix. These biomaterials should be prepared in porous forms to offer a channel for the migration of host cells and/or seeded cells into the matrix and be biodegradable into non-toxic products once they have served their function in vivo. The introduction of hydrogel beads for cell encapsulation to protect them from un-reacted component of the cement is an example of current methods (Zhao et al, 2010; Weir et al, 2006). In fact, the introduction of the beads system to bone cement was interesting for two reasons; firstly, it protects cells during seeding and secondly, the beads introduce macroporosity to the cement which enhances cell survival by improving diffusion of nutrients and media into them and it allowed the wash out of ionic components of the end products of the setting reaction (Simon et al, 2004).

6.2.1.3 Bio-compatibility and cyto-compatibility tests

The rationale for conducting biocompatibility tests with a commercially known product is to assess the difference in the method of application and the

unprecedented use of the cement loaded with BMP and seeded MSCs within the maxillofacial region. In our investigation standard tests such as live and dead assay (calcein-AM and ethidium homodimer respectively), MTT colorimetric assay, and assessment of cell adhesion and attachment on the surfaces of the tested materials were conducted. Our results showed that there were clinical differences between different versions of bone cement upon direct cell seeding. Nilsson et al (2003) tested the bio-compatibility of same material in vivo, no foreign body reaction was noted, and there was close contact between material and bone without fibrous tissue or inflammatory reaction. In another in vivo test the same cement was implanted subcutaneously. Histological evaluation of the implanted cement was also carried out at different time points. The evaluation was designed to show signs of acute inflammatory response initiated by the implant i.e. neutrophils and monocytes. Inflammation was not detected at the interface between the cement and adjacent local tissue.

We can conclude that testing the cytocompatibility of the material at cellular level is a sensitive approach for our particular application. Similary, Zange et al(1998) suggested that in vitro cytotoxicity tests was seemed to be sensitive tests but cannot replace animal experimentation.

6.2.1.4 Use of indirect immunofluorescent staining for cytoskeleton analysis and testing the differentiation potential

Immunofluorescence staining was used in this study to assess the identity of rMSCs and to test their osteogenic potential. We targeted CD44, CD166, CD34 and osteocalcin (OCN) protein surface marker of rMSCs. Immunofluorescent assay (IFA) is a procedure using primary antibodies against markers of interest

present in cultured cells or tissue sections, followed by secondary fluorescent labelled antibodies against the appropriate antibody class and species in which the primary antibody was produced (Stewart et al, 2000).

The result showed positive staining for CD44 and CD166 and negative for CD34, which means the cells were not hematopoietic stem cells. Furthermore immunfluorescent stains for OCN showed positive stains for cells that were cultured in osteogenic medium for 21 days and the test was also positive for cells that were cultured in proximity to CSD/HA cement within the collagen model.

The drawbacks of the assays have been studied and documented. In our study in order to minimize the nonspecific staining of the antigen with the labelled globulins, the use of pre-treatment preparations for the cells with normal serum (bovine serum) was used to minimise the nonspecific reaction, as demonstrated previously (Stewart et al, 1999). Background fluorescence may be a problem if antibody specificity is not high enough or if there is non-specific binding of the antibodies due to inadequate blocking procedures (Stewart et al, 1999).

The use of confocal microscopy, in comparison to conventional microscopy allows additional information to be obtained, including co-localization of three or more separate fluorescent markers on separate channels and three dimensional constructs for intracellular localisation (Lindon et al, 1998; Cornelison and Wold, 1997). The available labelling compounds range in emission wavelength from the blue area of the spectrum at 420 nm with 4,6- diamidino-2-phenylindole (DAPI) as seen by Cornelison and Wold (1997), to the green areas of the spectrum at (520 nm) with fluorescein isothiocyanate (FITC) by Lindon et al (1998) and then into the red wavelengths with rhodamine (TRITC) at (570 nm) by Cornelison and Wold (1997) and Texas Red at (620 nm) as reported by VanderVen and Fürst (1997).

6.2.1.5 Using the collagen model construct

The assessment of rMSCs was carried out using the collagen model, which proved to be an effective model as a guide for the seeding technique to be used at the pre-clinical stage of this study. This construct mimics muscle tissue and predicts what might happen to the cells inside the scaffold when injected in vivo. The results showed rMSCs could not be applied simultaneously with the injection of Cerament^{TM}. The viability of the cells, however, could be successfully achieved after 15 minutes from injection of the scaffold as this allowed the injected material to start the setting process prior to cell seeding. It has been proved that collagen provides a microenvironment that is similar to that in vivo, so the resulting morphology of the cells differentiated from MSC in the 3D culture may be similar to that of cells in vivo (Naito et al, 2013). Collagen culture is a three dimensional medium that has been shown to be biologically more appropriate to mimic organogenesis in vitro when compared to 2D culture with cell morphologies that are different between culture conditions (Riccio et al, 2010; Friedl and Brocker, 2000). 3D culture media allow better understanding of cell morphology. Moreover, histological findings of the 3D reticular matrix in 3D cultures were similar to those of osteoid tissues observed in regenerating bones after fracture. It has been suggested that collagen construct provides an extracellular matrix (ECM) which plays key roles in guiding cell migration, proliferation and differentiation (Burdick and Vunjak-Novakovic, 2009; Boudreau and Jones, 1999; Ohgushi and Caplan, 1999; Naito et al, 2011). Matrix elasticity can affect the differentiation of MSC into osteoblasts (Burdick and Vunjak-Novakovic, 2009). Furthermore, it is clear that 3D culture increases Runx2 gene expression following osteoblastic differentiation

(Naito et al, 2011). There is a suggestion that there is a relationship between a 3D culture and Runx2 gene expression which is still unclear (Naito et al, 2011).

In our construct the cells were left in culture for 21 days prior to osteogenic assessment. Previous studies have reported that MSCs do not alter their osteoblastic differentiation capacity, surface marker profile and expression profiles during expansion (Kulterer et al, 2007). Our results were in agreement with this view, as we found that rMSCs still hold their surface markers after 3 weeks of cell culture. However, the debate remains about whether the effect of the collagen extracellular matrix resulted in the cell differentiation into pre-osteoblasts or if the normal fate of the cells was governed by other factors such as the rMSC niche or the Cerament^{TM} cement. A controlled experiment was performed as the cells were seeded into collagen only. However, it would have been ideal to estimate the effect of the cement on cells at different time points as well.

6.2.2 In vivo study

6.2.2.1 Biomaterial bone cement

Assessment of the regenerated tissue revealed the presence of an appreciable amount of un-degraded cement. This cement presented as patches inside the muscle fibres or was surrounded by regenerated bone. Regenerated bone was also detected inside the pores of the cement especially at the border of the defect. This finding warrants further investigation on the factors that control the degradation process of the cement.

6.2.2.1.1 The bio-chemical degradation of the bone cement (Cerament^TM)

The residual Cerament^TM Spine Support bone cement at 3 months following implantation was observed clinically and estimated to be 20% ± 12. This was assessed during the histomorphometric analysis, which suggested that one quarter of the created defect was still occupied with the cement remnants. This was mainly made of HA particles and fibrous tissue due to the fast dissolution rate of CSD. Generally it has been believed that the range of CS degradation was 40-80 days in defect size 2.5 cm (Peltier, 1961; Tay et al, 1999; Pietrzak and Ronk, 2000). A study has been carried out to test the dissolution of Cerament^TM composite both in vitro and in vivo (Nilsson, 2003). This study revealed that the method of dissolution of the material when implanted into rat muscle and in vitro by implanting the material into SBF occurred in a layer-by-layer process. Starting from the outer surface to the centre of the implanted cylinders of the cement the size of the samples decreased rapidly. They also noticed that the dissolution occurred faster in vivo than in vitro. The dissolution in vitro occurred passively by ionic exchange. However, it occurred actively in vivo involving both cells and ionic exchange. Another factor that may enhance the dissolution of material in our experiment is active muscle movement; this consideration is in agreement with Nilsson (2003). It has been found that CSD/HA materials lose their shape rapidly when implanted in rat's abdominal muscle, parts of the material (CSD) dissolved and formed slurry around the remaining HA particles. Once the material started to disintegrate, body fluid and cells penetrated the materials and caused further dissolution (Nilsson, 2003). Simultaneously, the fast dissolving of CSD increases the saturation of calcium and phosphate ions in the liquid phase surrounding the

cement and that would slow down HA dissolution (Nilsson, 2003). In this composite, CSD on the surface would quickly dissolve and form a number of micro-pores on the surface of the composite cement, which increases the contact area of cement with the solution of surrounding medium in vivo. Thus, our findings were in agreement with data reported in literature. Histomorphometry and 3D micro-CT assessment showed the volume of cement remnant after 3 months from the day of surgery could represent the 40 % HA that is present in Cerament [TM] Spinal Support. Similarly, Rawlings et al (1988) demonstrated that when HA granules were combined with calcium sulphate to reconstruct cranial defect in cats, the HA granules become surrounded by tissue composed of 65-69% bone and 31-35% fibrous tissue at 6 months. The authors suggest that HA granules remained as a permanent implant and formed the majority of volume of the reconstructed area.

6.2.2.1.2 Compressive Strength of bone cement (Cerament [TM])

An important parameter to be evaluated whenever bone cement is used for augmentation of bone defects is the compressive strength of the material, especially if it is implanted in a weight bearing area. However, this was taken into consideration at the initial stage of the study. Firstly, the cement was injected into skeletal muscles and secondly, the fixation of the defect was achieved by plating the inferior border and by maintaining the superior border of the defect intact. Therefore, the injected cement was not subjected to direct force in contrast to other experimental designs.

In our study a 2 mm titanium plate at the inferior border of the mandible and 2 screws on either side of the defect were placed to stabilise the surgically created defect and minimise the direct mechanical loading on the CS bone cement.

Insufficient stabilisation of the segment on either side of the defect would have led to undesirable movements which would have compromised the healing. In our pilot study, an infection developed which may have been as a result of the dislodgment of the fixation plate which caused undesirable mobility of the bony segments during function; thus creating an unfavourable bio-mechanical environment for tissue regeneration. This problem was however overcome by further modification of the surgical technique, and by maintaining a bony bridge at the superior margin of the defect (tension band), as illustrated (Figure 3.3).

It has been reported that the mean compressive strength of the cancellous bone of the rabbit jaw is 4.4±1.5 MPa and the modulus of elasticity is 153±69 MPa (Orr et al, 2001). Whereas, the compressive strength of cerement ^{TM} is between soaked (17 MPa) and non-soaked samples (27 MPa) as optimized by Nilsson (2003). However, using CS 60%-HA 40%, cement (Cerament^{TM}), the phenomenon of stress shielding was unlikely to happen due to the fast resorption rate of CSD and the low percentage of the remaining HA. The remaining HA would become embedded within the surrounding trabecular bone as seen in histological examination.

Factors that influencing the compressive strength of the injectable CS-HA cement (Cerament ^{TM}) were also studied by Nilsson et al (2003). They found that the largest factor that affects the strength of CS-HA injectable cement was the amount of water added to the powder. The strength increased linearly with the reduction in the added water. The second factor was the morphology of the HA crystals. The more porous the surface the more water adsorption was needed on the particle surface to mix the material, which ultimately resulted in a decreased strength (Nilsson et al, 2003). Another factor that has been studied is the amount of HA added by weight to the CSH mix.

6.2.2.1.3 Mechanism of bone formation by the injected construct (calcium sulphate cement, BMP, rMSCs)

Histological assessment of the regenerated tissue in this study gave interesting results. Firstly multiple small islands of bone formation were seen at the centre of the defect. These did not bridge the gap and did not unite with the native bone. Secondly, these islands were always surrounded by hydroxyapatite crystals and loose connective tissues. However, areas of more bone formation that bridged the gap were noted at the border of the created defect, where no fibrous tissue was observed. These findings warrant further exploration of the mechanism of bone regeneration using the CSD/HA, BMP-7 and rMSCs. The proposed mechanism was explained in detail in section (5.3). However, there were many variables related to the injected construct which need to be explored such as factors related to the role of different components of bone cement, BMP carriers and dose. It has been suggested that CS particles bind to adjacent bone and then resorb, providing a mechanism to guide bone growth (Coetzee, 1980). Others have shown that CS increases microvascular density in the CS treated defects, suggesting a positive effect on angiogenesis. The resultant increase in vascularity may, in part, account for the biological effects of CS bone cement (Strocchi et al, 2002). With regard to HA, Shindo et al (1993) shown that when the HA cement was placed directly onto bone, approximately half of the implant was resorbed and then replaced with bone and osteoid tissue after 9 months. The evidence suggests that HA cements undergo progressive replacement with new bone by a combination of resorption and osteo-conduction (Friedman et al, 1991; Costantino et al, 1992). However, the long-term fate of remnant HA particles are not yet known. It is reasonable, though to expect continued osseous deposition as the implants were found to be progressively replaced by bone over time (Friedman et

al, 1991). In other words, there would be the potential for the remaining 20% ±11 of HA found in our tested specimens to form more bone, if it was left for long enough.

BMP-7 has been used successfully in other studies for repair of critical size bone defects (Wang et al, 2004a). However limited bone formation in this experimental design could be due to incomplete transformation of muscle tissue into bone. Alternatively, the metablastic changes of muscle into fibrous tissue could inhibit the process of osteo-inductivity of BMP. A suitable carrier is essential to provide the optimal pharmacokinetics of the BMP. It should be biocompatible, have reasonable mechanical properties and should be resorbed in a suitable time period to prevent fibrous tissue ingrowth and simultaneously should not interfere with bone regeneration (Hollinger and Leong, 1996). Cerament ^{TM} proved to have optimal biomaterial characteristics that could allow it to act as a carrier for BMP. It consists of 60% CSH and 40% HA which last for a longer time. HA has a unique ability to adsorb different chemical structures on its surfaces (Thomas and Puleo, 2009; Ohura et al, 2000; Tiselius et al, 1956). In our experience, using BMP-7 that has been freeze dried with collagen type I, and mixed with Cerament ^{TM} (CSS) decreased the setting time. This may be due to an increased powder to liquid ratio. Thus a reduction of the liquid phase was carried out (0.1 ml). The combined effect of collagen CSD/HA has an advantageous effect with regards to the BMP half-life. To our knowledge there was no published data of using Cerament^{TM} with BMP. However, there evidence in literature stated that using BMPs on its own cannot induce regeneration of large tissue defects (Whang et al, 2000). This is due to the free BMP being quickly washed away from the site of application and degraded by proteolytic enzymes. The presence of a suitable carrier as a bone

cement will hold the material at the implantation site for a longer period of time (Whang et al, 2000). A series of investigations were carried out to evaluate various injectable osteogenic factor/carrier combinations in large animal models (Seeheman et al, 2004). Among all the carriers studied, a commercial resorbable CPC was considered to be the best carrier in terms of bone healing after 10 weeks in a fibular osteotomy of a non-human primate model. One of the main advantages of this carrier is that it can be implanted by a single percutaneous injection. Bone healing was accelerated by approximately 40%, as compared to untreated osteotomy sites. Ohura et al (2000) obtained analogous results by incorporating different amounts of recombinant human BMP (rhBMP-2) into cement formed by β-TCP monocalcium phosphate monohydrate (MCPM), calcium sulphate hemihydrate and granules of β-TCP, in a rabbit model. In conclusion, for this study CPC proved to be an adequate substrate for delivery of rhBMP-2. Similar results were also reported by Kamegai et al (1994).

Optimisation of the most effective dose of BMP is controversial. It has been reported that the dose of the BMP depends on the type of carrier and species of the animal (Marukawa, 2002). In our research we decided on the dose of BMP based on the size of the defect according to Kokubo et al (2003) and the outcome of the pilot study. Administration of a larger dose of BMP was reported by Barnes et al (2005), they showed that complete bony fusion was achieved with 10 mg per side (2.0 mg/ml) of BMP-2 which was applied via a calcium phosphate carrier and 3 mg per side (1.5 mg/ml) of BMP-2 on an absorbable collagen sponge. In contrast, 3 mg per side (1.5 mg/ml) of BMP-2 with the calcium phosphate carrier failed. However, there is a risk of seroma formation due to the high dose of BMP (He et al 2010 and Marx et al 2013). The logistics of our experiment did not allow for dosage optimisation.

It was observed that manual mixing of the Cerament[TM] powder with BMP-7 may not be an efficient way to achieve a homogeneous distribution of the BMP into the CS/HA particles, therefore refining the technique of mixing could be an important future development. This could be achieved by using a special dispensing tool that ensures uniform mixing of the BMP and Cerament[TM] powder as well as the liquid phase. Kim et al (2011) proposed a sophisticated way to deliver BMP to bone cement to overcome any inaccuracy regarding dose, handling or an uncontrolled flow. They suggested the stepwise lyophilizing method from –40°C to 20°C to coat ErhBMP-2 onto ceramics for convenient storage and easy handling at room temperature without requiring additional procedures. Additionally, this method would assure accurate doses and controlled flow in vivo.

6.3 Result of the main study

6.3.1 Clinical findings

After sacrificing the animals, the jaw was explanted and the site of the surgery examined carefully. Dissection through the deep layer of the masseter muscle to expose the ramus was difficult to achieve, due to the tenacious fibrous layer covering the site of the defect. Fibrous tissue was also found around the titanium plate. A thin layer of hard tissue, whitish in colour, was also seen from the most inferior part at the surgical side and surrounded by fibrous tissues. The presence of a fibrous tissue capsule could be due to either muscular tissue converted to fibrous tissue or a result of the physicochemical effect of the injected cement. Our previous study reported the presence of a fibrous tissue capsule surrounding the scaffold when β-tri-calcium phosphate scaffold and (rMSCs) were used to

construct the critical size mandibular defect in rabbits (Al-Fotawi et al, 2014). A trial by Khadaka et al (2011), reported the presence of tenacious fibrous tissue around the implant which was made of nano-hydroxyapatite/polyamide and bone marrow stem cells to reconstruct calvarial critical size defect in rats. Similarly, a study by Van Gaalen et al (2010b) showed the presence of fibrous tissue surrounding the scaffold which was made of porous calcium phosphate which was implanted at a postero-lateral lumbar spine in a goat. The patho-physiology for the fibrous capsule around the implant was explained by Dolores et al (2004), they examined the peri-implant fibrous capsule formed around the silicone implant, their findings support the fact that its formation was due to the activity of immune cells (CD4+/CD8+ T-cells, dendritic cells, CD44, CD45RO, CD45RA and CD25 expressing cells, macrophages), as well as the presence of collagenous and non-collagenous extracellular matrix (ECM) proteins including procollagen type I and type III, collagen type I and type III, laminin, tenascin, and fibronectin (Dolores et al, 2004).

Bostrom et al (1998); reported certain micro-motion stimulates the osteoinductive effect of BMP when used for bone regeneration of rabbit long bones, when compared with the static bone model. This theory could be applicable in our model because the induced pedicle muscle flap (IPMF) was an active dynamic muscle adapted into the created defect. This could explain the corticated bone noticed in all cases at the border of the defect. Abu-Serriah (2002) suggests that a lack of mechanical strength and the associated micro-movement of the scaffold as proposed earlier could lead to further diffusion of BMP which may result in an intense and strong osteoinduction that recruited excessive chemical and cellular machinery to the site of implantation. This could be what occurred in case 151 due to the fact that the plate was laterally displaced. Finally, another explanation for

the expansion of bone margins of the defect with immature active bone with high deposition rate, could be due to injection of a large amount of construct at the bony margin of the defect to enhance the chance of flap incorporation.

6.3.2 Radiological Examination

6.3.2.1 Plain Radiographs

The radiograph taken at one month following surgery seemed to be suitable for use as a baseline, it showed a homogenous radio-lucent area surrounded by the bone margin of the native bone that was easily distinguishable.

The shortcomings of plain radiographs were that the assessment of bone regeneration was in 2 dimensions. Also the radiograph did not show any distinction between bone and cement. Waitzman et al (1992) concluded that plain radiography had many drawbacks including that it provided poor volumetric information, and there were only a limited number of identifiable landmarks, all of which affected the quality of the images and their reliability. Using the Cook`s scoring system (2005) combined with the quantitative measurements provided comprehensive information regarding the quantity of bone formation in the created bony defect sites. It was felt that the use of a scoring system was mandatory for standardising the radiographic analysis but needs to be developed in a way that would accurately record the quantity of bone formed by considering the following factors. The degradation of the scaffold which was expected to be at the same rate as that of bone formation (Mulconry et al, 2008; Eck et al, 2000). Secondly, it must consider changes in bone formation such as resorption or excess bone formation.

We faced a problem in standardising the projection angulation for a sedated animal on the operating table, where we required the neck to be extended

backward to achieve the maximum exposure of the site of operation. In our case, the use of an occlusal stent was not applicable as we used an extra-oral radiograph and the use of a cephalostat on a sedated animal was not possible. We were also unable to use a computerised alignment technique to overcome the difference in projection angles due to the large geometrical differences noticed. The problem could have been avoided by designing a special film holder with occlusal registration, which could standardise the position of the film in relation to the occlusal plane. This could give a stable relationship between the X-ray tube, object, and film. However, film projection distortion may be unavoidable in clinical trials as reported by van der Stelt, (2008).

We decided to include the plain radiographic examination as it allowed the assessment of bone formation during the life of the animal. The principal investigator carried out the radiographic assessment and this may have introduced some bias into the results (Petrie et al, 2002, Mulconrey et al (2008)). In our study the rabbit's identification number was concealed and the assessment was repeated three times one week apart to try to minimise bias.

6.3.2.2 CBCT examination

The CBCT provides more precise information about the actual tissue formation in a three dimensional view when compared with 2D dental radiographic results (Oberoi et al, 2009; Hamada et al, 2005). In the current study, the radio-opaque mass was found to have a wider bucco-lingual dimension than the removed bone and located either buccally or lingually in relation to the native bone. The regenerated bone has formed at sporadic areas within the muscle flap. The total volume of these radio-opaque masses was estimated to be more than the volume of bone at the region of the defect (ROD).

With regard to bone density testing, Hounsfield units (HU) are used as a standard method for measuring the reconstructed attenuation coefficient in Medical CTs but the manufacturers for CBCT have not yet agreed on a standard system for scaling the grey level (attenuation coefficient), because of the low effective energy of the dental CBCT machine. However, the attenuation coefficient has been tested using different materials and this was determined with a less than 1% error (Mah and Mcdavid, 2012). It was suggested that improvements in cone-beam reconstruction algorithms and post-processing would eventually solve or reduce these problems (Vannier, 2003). The current recommendations are to use a reference object containing three standard materials (acrylic, water, aluminum) placed in the field of view to provide data for calibration before exposure (Vannier, 2003). Molteni (2013) discussed another limitation of CBCT in accurately determining the tissue density using HU due to possible image artefacts. The study also suggested careful interpretation of quantitative density measurements obtained with CBCT. On the other hand, Gonzalea-Garcia and Monje (2013) assessed bone density in CBCTs (i-CAT) and reported a strong positive correlation with volume fraction (BV/TV) measured by micro-CT at the site of dental implants in the maxillary bones. The author concluded that, CBCT is a reliable tool to determine objectively bone density. Langravere et al (2006) also suggested that CBCT provides an effective determination of material density. More than one method of assessment of mineral density was carried out in our research and correlation between the BV/TV and the bone density using micro-CT analysis was performed to avoid the potential inaccuracies in measurements (Bryant 2011; de Carvalho Crusoe Silva et al, 2012). The bone density of the regenerated tissue was calculated for the centre and the peripheries of the regenerated defect using HU from i-CAT images. These were then correlated with the calculated volume of regenerated bone of the same

site from the micro-CT. The volume of the bone regenerate calculated from the micro-CT was positively correlated to the bone density calculated from i-CAT scan using HU. In six cases, there was an increase in density of the regenerated tissue at the centre of the defect. The measurement proved that the regenerated bone was 29.4%± 25 more dense than the contra-lateral side, which was either due to increase of bone volume or due to the presence of remnant of HA cement. The histological analysis proved the presence of more bone than the contra-lateral control side. Similarly, the radio-density of the thickened bone at the margin of the surgical defect was 35% ± 25 more dense than the contra lateral-side.

The bone volume measurement was however inconsistent with bone mineral density assessment using Micro-CT. This due to the fact that the micro-CT measurement was limited to the density of the areas of bone formation only; while estimated mineral density from the CBCT was for any radio-dense tissue and it could therefore contain remnants of the cement and the newly formed bone together.

In conclusion, CBCT was able to capture the volumetric 3D model of the radio-opaque tissue, but it was not specific enough to measure the absolute bone volume.

6.3.2.3 Micro-CT Examination

Micro-CT allowed the investigation of the area of interface between the regenerated and native bone. The resolution of the images from the micro-CT was to 17 µm while it was only 0.3 mm for the CBCT images.

Using a desktop microtomographic imaging system (Skyscan 1172 HR micro-CT (Skyscan, Aartselaar, Belgium) equipped with a 10 mm focal spot microfocus X-

ray tube, the specimens were scanned using a 17 μm isotropic voxel size at 100

kV, a current of 167 μA energy, 120 secand integration time with approximately 99

μCT slices per specimen. This proved to be a satisfactory setting for this study. To

be able to achieve a difference in density between bone and cement, the images

were thresholded using an adaptive algorithm and morphometric variables were

computed from the binarized images using direct three dimensional techniques

that do not rely on any prior assumptions about the underlying structure. This

protocol was successfully able to distinguish between different materials (bone,

cement, soft tissue) in all analysed specimen in our study, it was consistent with

the study by Gauthier et al (2005) who reported on the application of micro-CT to

assess BCP biomaterial.

It was also found that the new bone showed thinner trabeculae but the number

exceeded the average of the contralateral side. These findings suggest that the

bone had a fast deposition rate and active remodelling process (Frost, 1999). The

result also reported less degree of anistropy of new bone compared to the non-

operated side; it could be due to bone being immature with less extra cellular

matrix deposits as suggested by Turner et al (1995), or due to the presence of HA

crystals attached to the bony trabeculae that led to a false reading. This result was

in agreement with the results of the dynamic histomorphometric analysis.

6.3.3 Histological assessment

The results of the histological findings were in agreement with the other

investigations. It was estimated that the mean surface area of bone formation per

examined slide was 21.2±6 mm^2 and 18.4±2.1 mm^2 for the surgical and the non–

operated sides respectively. The percentage area taken up by the remnant of

cement was estimated to be 20±12. The un-decalcified section stained with Goldner`s Trichrome, and or Sanderson's provided useful information. A systematic approach of assessment was used for examining the slides. It showed more bone formation around the bony border of the created defect which looked more spongy and porous while it was woven in appearance near the centre of the defect.   This wide variation in the histology findings was similar to previous reports by Truedsson et al (2010) who also used Cerament ^{TM}. That study reported the mean new bone thickness was 1258 ± 288 mm and trabecular in nature for the experimental group at 12 weeks, while the sham group demonstrated a cortical thickness of 591 ± 73 mm at 12 weeks. It seems bone formation at the border of the defect was due mainly to the osteoconductivity and the inductivity role of the cement and the vascularity of the host bone. The presence of intact periosteum in the surrounding bone might render the periphery more vascular compared to the centre. Similar findings were also reported by Abu-Serriah (2002) and Yudell and Block (2000).   However, in our samples the presence of an island of calcified tissue at the centre of the defect could be due to vascular muscular fibres in between the cement as well as the osteoinductive role of the IPMF that contains the BMP-7 and the autogenous rMSCs.

Remnants of cement (HA) were noticed around the regenerated bone because of the slow degradation rate of HA. The regenerated bone displayed a high degree of remodeling with an intricate network of woven bone trabeculae within the Cerament^{TM}. Some areas of thin cortices and several areas of trabecular bone were characterised by the haphazard organization of collagen fibres as seen in the undecalcified histology analysis using Goldner`s Trichrome. Similarly, Costantino et al (1992), Friedman et al (1991) and Mankani et al (2008) had reported the same pattern of bone regeneration around hydroxy apatite cement.

Unfortunately, we were not able to quantify the vascularity and track the fate of the implanted exogenous rMSCs (Wang et al, 2014).

Histomorphometry is a quantitative measurement of microscopic examination and has been used to provide information on cellular responses, tissue pathology, bone regeneration and remnants of bone graft. However, this technique has its limitation as it is a 2D assessment tool and the examination was carried out on limited representative slides only. Nevertheless, this was considered an important assessment to demonstrate different structural components under the microscope. Calculation of the percentage of bone or cement followed a standard protocol (Van Gaalen et al 2010b). The technique that has been adapted in this study was studied and validated against commonly available software (Egan et al, 2012).

In our study the mineral deposition rate appeared to be faster than the normal bone. The direct apposition of concentric lines representing lamellar bone of osteons was detected in parallel with the time of the injected bone label at, 8 and 11 weeks. The chronological order of the administration of the bone labels, from the implant surface to the bone surface were similar to that reported by Hing et al (1999). The findings were consistent with the micro-CT examination of bone architecture at the area of bone bridging which showed thinner but more condensed trabeculae per mm^3 and had a lower degree of anisotropy. This finding is different from those reported by Abu Serriah et al (2002) who reported that BMP did not influence the speed of the mineralization process during lamellar bone formation. This may indicate a difference in the mechanisms of osteogenesis and bone mineralization.

Chapter 7

Conclusions and Recommendations

Table of Contents

7.1 Conclusion

Within the experimental framework, the following are concluded:

• Rabbits are suitable experimental models to study bone bioengineering, because they have a well-developed marrow, which facilitated the aspiration process. The masseter muscle is well developed which allowed surgical manipulation and rotation, and adaptation into the created surgical defect. The level of anatomical variations among cases and the noted postoperative complications were acceptable.

•In the vivo study, using the injectable resorbable calcium sulphate cement, BMP and MSCs into rabbit`s masseter muscle indicated the potential of using this as a model for bone regeneration based on evidence from the wide range of investigative tools used that include micro-CT, CBCT, histology and histomorphometry.

• The regeneration of bone in the defect was established both by micro-CT examination and histology of the decalcified tissues, with both techniques being deemed as essential tools for the examination of bone quality.

• The concept of inducing bone formation within a local pedicled muscle flap is achievable. It is likely that the muscle flap provided the required blood supply for bone regeneration and acted as a bioreactor for the rMSCs, alongside the injected cement and BMP-7 that induced bone formation.

• Complete bony bridging of the created surgical defect was not achieved in all the cases. This is partially due to the physical nature of the injected cement that prevented the diffusion of the material at a micro level between the fibres of the muscle tissue or the design of our construct.

• The design of this experiment did not allow the study of the role of each of the injected components on bone regeneration

7.2 Recommendations

• The use of a cell tracking technique and testing the quantity of osteogenic markers would be useful in future studies. This would shed some light regarding the fate of the seeded exogenous cells population and its role in the regenerative process. Green fluorescent protein, the use of specific alu gene sequence and a digoxigenin-labeled probe could be utilised for this purpose.

• The use of a sophisticated imaging system including the bioluminescence method is a non-invasive system to monitor ongoing biological processes in small laboratory animals. This would provide an insight regarding the process of osteogenesis.

• The use of adenovirus that is encoded for human BMP cDNA (gene), to transduce the muscle flap or the rMSCs should be considered in future studies. There is a need to develop injectable scaffolding that has great diffusability between the muscle fibres, which probably could improve the pattern of osseous regeneration and its integration with the surrounding bone.

• A comparison between the rMSCs seeded and non-seeded scaffold with or without BMP for bone induction is desirable.

Appendices

1.1 Abstracts and Publications

Original research publications authored by the candidate on work relating to this thesis.

Randa Al-fotawi, Kurt Naudi, Matthew J Dalby, K Elizabeth Tanner, Jeremy D McMahon and Ashraf Ayoub.   Assessment of cellular viability on calcium sulphate/hydroxyapatite injectable scaffolds. Journal of Tissue Engineering 4: 2041731413509645, 2013

Randa Al-fotawi, Ashraf Ayoub, Neil Heath, Kurt Naudi, Matthew J. Dalby , J McMahon.2014 Radiological assessment of bioengineered bone in a muscle flap for reconstruction of a critical-size mandibular defect. PLoS ONE 9(9): e107403. doi:10.1371/journal.pone.0107403.

Randa Al-fotawi, Edward Odell, Kurt Naudi, K. Elizabeth Tanner, Matthew J. Dalby , K. Elizabeth Tanner, J McMahon, Ashraf Ayoub. Reconstruction of critical size boney defect: Histological assessment of a novel surgical approach in rabbit model. PLOS One

Parts of this study have been presented at scientific conferences:

- · A poster presentation in United Kingdom Society of Biomaterial(UKSB), 2013, Birmingham, UK

- · Oral presentation at UKSB 2012, Nottingham, UK

- · Oral presentation at Glasgow Orthopaedic Research Initiative, 2011, University of Strathclyde , Glasgow, Uk

Publication

Journal of Tissue Engineering

http://tej.sagepub.com/

Published by:
$SAGE

http://www.sagepublications.com

On behalf of:

ITR≡∏

Institute of Tissue Regeneration Engineering

PLOS | ONE

Radiological Assessment of Bioengineered Bone in a Muscle Flap for the Reconstruction of Critical-Size Mandibular Defect

Randa Al-Fotawei[1], Ashraf F. Ayoub[1]*, Neil Heath[2], Kurt B. Naudi[3], K. Elizabeth Tanner[4], Matthew J. Dalby[5], Jeremy McMahon[6]

1 University of Glasgow, Glasgow, United Kingdom, 2 Oral & Maxillofacial Radiology, Glasgow University Dental Hospital & School, Glasgow, United Kingdom, 3 Oral Surgery, Glasgow University Dental Hospital & School, Glasgow, United Kingdom, 4 Biomedical Materials, School of Engineering, University of Glasgow, Glasgow, United Kingdom, 5 Centre for Cell Engineering, University of Glasgow, Glasgow, United Kingdom, 6 Oral & Maxillofacial Surgery, Southern General Hospital, Glasgow, United Kingdom

Abstract

This study presents a comprehensive radiographic evaluation of bone regeneration within a pedicled muscle flap for the reconstruction of critical size mandibular defect. The surgical defect (20 mm×15 mm) was created in the mandible of ten experimental rabbits. The masseter muscle was adapted to fill the surgical defect, a combination of calcium sulphate/hydroxyapatite cement (CERAMENT™ |SPINE SUPPORT), BMP-7 and rabbit mesenchymal stromal cells (rMSCs) was injected inside the muscle tissue. Radiographic assessment was carried out on the day of surgery and at 4, 8, and 12 weeks postoperatively. At 12 weeks, the animals were sacrificed and cone beam computerized tomography (CBCT) scanning and micro-computed tomography (μ-CT) were carried out. Clinically, a clear layer of bone tissue was identified closely adherent to the border of the surgical defect. Sporadic radio-opaque areas within the surgical defect were detected radiographically. In comparison with the opposite non operated control side, the estimated quantitative scoring of the radio-opacity was 46.6% ±15, the mean volume of the radio-opaque areas was 63.4% ±20. Areas of a bone density higher than that of the mandibular bone (+35% ±25%) were detected at the borders of the surgical defect. The micro-CT analysis revealed thinner trabeculae of the regenerated bone with a more condensed trabecular pattern than the surrounding native bone. These findings suggest a rapid deposition rate of the mineralised tissue and an active remodelling process of the newly regenerated bone within the muscle flap. The novel surgical model of this study has potential clinical application; the assessment of bone regeneration using the presented radiographic protocol is descriptive and comprehensive. The findings of this research confirm the remarkable potential of local muscle flaps as local bioreactors to induce bone formation for reconstruction of maxillofacial bony defects.

Introduction

Loss of bone due to trauma, infection or resection of pathological lesions results in large, osseous, segmental defects of the facial skeleton which are difficult to reconstruct. Even in the best hands, inadequate vascularisation at the site of the bone defect (recipient site) has been the main obstacle for successful reconstruction with bone grafting [1]. Many strategies have been proposed for the management of mandibular surgical defects following bone loss, vascularized autogenous bone grafts are considered the most reliable method for reconstruction. However, this type of graft is not suitable if the patient has been subjected to radiotherapy or is suffering from peripheral vascular disease which compromises the blood supply to the surgical site. The harvesting of vascularised bone graft is associated with well documented

have investigated various ways to induce angiogensesis and arteriogenesis which are essential for the bone regeneration process [6,7]. The applications of vascular endothelial growth factors (VEGF), angiogenic proteins and hypoxia induced factor-1α to improve vascularity at the surgical site have also been reported [8–10].

More advanced surgical techniques were advocated to overcome the problems of the limited vascularity at the surgical defects "the recipient site" by utilizing local skeletal muscle flap to induce bone formation due to its reliable source of adequate blood supply [11–13]. The muscle has the propensity to induce bone formation because of its intrinsic osteogenic potential when exposed to osteogenic stimuli including bone matrix substitutes and bone morphgenic proteins (BMP) [14].

In clinical practice, plain radiographs are the most common

Appendix 1.2
Table 1: The most popular commercially available ceramic-based composite bone cements that are injectable, granules, blocks or putty (all have been used in human trials).

Materials	Company	Composition	Uses	Advantages	Disadvantages
Collagraft(Ilan and Ladd, 2003)	Zimmer/NeuColl	Bovine collagen, HA and tricalcium phosphate (TCP)	Grafting of long bone fractures and filling of traumatic defects	Osteoconductive, Osteoinductive when used with marrow	Requires aspirated marrow, Hard to confine to desired site
Allomatrix (Ilan and Ladd, 2003)	Allosource + Wright Medical	DBM + calcium sulfate as carrier: Putty (Custom) Block (DR) Injectable	Nonunion, delayed and potentially delayed unions, metaphyseal defects Periarticular fractures (DR)	Potentially osteoinductive and Osteoconductive Potential stability with DR form Potentially better carrier (inert, nonprotein) than other carriers for DBM	Human derived, lack of structural support for putty and injectable form.
Healos (Ilan and Ladd, 2003)	Orquest	HA coated bovine collagen sponge, approved in Europe	Replacement of autograft/ autograft extender for spinal fusion	Osteoinductive when used with marrow	No structural support, Potential immunogenicity, Requires aspirated marrow
Mimix (Ilan and Ladd, 2003)	Biomet/Lorenz Surgical	Synthetic hydroxyapatite tetra-tricalcium phosphate	Cranial defects	Osteconductive	Not tested in stress bearing sites/ Not reported in the orthopaedic literature, Reported infection due to delayed resorption (Verret et al, 2005)

Materials	Company	Composition	Uses	Advantages	Disadvantages
SRS (Skeletal Repair System)(Ilan and Ladd, 2003)	Synthes/Norian	Calcium phosphate + carbonated apatite injectable cement	Injection or insertion—distal radius fractures Studies also in spine, hip, tibial plateau, calcaneus; approved Jan 2002 general orthopaedic use	Osteoconductive, good compressive strength , Provides structural support for transverse metaphyseal fractures , Remodels. Sets in 10 min.	Poor shear/torsional strength (requires augmentation for complex fracture), Slow resorption/remodeling , , Setting time may be longer in cold/tourniquet environment , Not inductive.
Novabone (particulate form of Bioglass)(Ilan and Ladd, 2003)	US Biomaterials	Bioactive Glass (SiO_2 and minerals)	Reconstructive procedures and bone defect filling	Resorbable and eliminated by body, Allows cell ingrowth and remodelling, Can be combined with autograft	Silica is non-physiologic , Hard to confine to desired site , Little structural support , Resorption rate not yet established
Cerament ™ Spinal support, and Bone Void(Masala et al, 2012)	Bone support, Lund, Sweden	CSH 60%/ HA 40%	Vertebral augmentation of osteoporotic collapses, vertebroplasty, bone mal-union, filling bone voids resulting from surgical debridement of chronic infection	Injectable cement. Takes shape of any defect, Non-invasive surgery	Low mechanical strength, Orthotopic site.

Materials	Company	Composition	Uses	Advantages	Disadvantages
HERAFILL®bead sG (Franceschini et al, 2012)	Heraeus Medical.	Calcium sulphate dihydrate, calcium carbonate, hydrogenated triglyceride, gentamicin	Indicated to fill bone voids that result from surgical debridement of chronic, post-traumatic, post-operative and hematogenic osteomyelitis/osteitis, infected pesudo-arthrosis and infected osteosynthesis	Osteoconduction, drug delivery, Fully absorbable in few months, balances pH in case of infection due to presence of calcium carbonate and radioopaque	Little structural support, Limited application to site of infection, Long resorption time
Calcibon (Khan et al, 2005)	Biomet LTD, Turkey	alpha-tri-calcium-phosphate, calcium-hydrogen-phosphate, calcium-carbonate, and precipitated hydroxyapatite	Filling of metaphyseal, cancellous bone defects, tibial head fractures, distal radius fractures calcaneus fractures	compressive strength (up to 60 MPa), osteoconductive, malleable paste, hardens in-situ, biodegradation by cellular mediated processes	Accurate repositioning as well as fixation and stabilisation. Longer absorption time
BoneSave granules (Stallmann et L, 2006)	Stryker	80% tricalcium phosphate/20% hydroxyapatite	Use as bone void filler for defects not intrinsic to the stability of the bony structure	50% volume porosity. Radiopaque osteocinduction	Lack of structural support

Materials	Company	Composition	Uses	Advantages	Disadvantages
Pro Osteon (Bostrom and Lan, 1997)	(Interpore Cross International, Irvine, CA	Biologic hydroxyapatite + calcium carbonate	Primarily used to fill metaphyseal defects; interconnecting channels allow tissue ingrowth; slow resorption with variable strength.	Osteocondictive, porosity	Lack of structural support, Slow resorption rate and no osteoinductive effect
Triosite(Ransford et al, 1998)	Zimmer, France); BCP BiCalPhos (Medtronic Sofamor Danek, Memphis, TN	60% HA/40% TCP	Posterior spinal fusion, High tibiat osteotomy bone graft	Could be used in combination with bone marrow	Presence of material after long follow up (4 years)(Hooper, 2013)
JectOS (orthopedic list.com)(Obert et al, 2010)	Kasios(Injectable Bone Substitute)	55%DCPD (Brushite), 45%TCP	Bone void filling in trauma cases such as radius, tibial and calcaneus fractures, mal-union of distal radius, wedge osteotomy	Injectable cement	Lack of strength needing extenal fixation, long resorption rate (4-6 years)
JectOS+ (orthopedic list.com)	Wright Medical Technology	Calcium phosphate and Zirconia as a radiopacifier	The vertebral body following kyphoplasty on young patients with a stable and recent traumatic vertebral body fracture.	Radiopaque injectable bone cement synthetic	Not recommended in compression fracture of vertebra (Hao and Kuh, 2007)

Materials	Company	Composition	Uses	Advantages	Disadvantages
CopiOS(Bone void filler,(Bongio etal, 2010).	Zimmer, personla fit, renewal life.	CaP +Type I collagen+BMP in DICAL	Present in sponge and paste, used as bone filler material	Can be mixed with bone marrow	Cannot be used in stress bearing areas
PRO-STIM™ (Teufack et al, 2014	Wright Medical Technology	50%c Calcium sulfate and 10% calcium phosphate and 40 % DBM	Bone filler material	Osteinductive, osteoconductive, flowable, composite bone graft	Human derived. Lack of structural support in putty and injectable form
Genex(Orhopedic list.com)	Biocomposites Ltd, Staffordshire, UK)	Tri-calcium phosphate and calcium sulphate ratio of 1:1	Refilling the defect after tumour removal	Osteoinduction and osteoconduction	Soft tissue inflammation and destruction(Friesenbichler, 2013

Appendix 1.3

Table 2: Summarizes   the studies that tested the reconstruction of critical size defect in the mandible using osteoprogentor cells, BMP and bone scaffolds, also illustrated the assessment methds used, and the studies outcome, (+,++,+++) indicate the procedure was performed using one or more type from the same method, (-) indicate the assessment was not carried out.

Study	Anatomical site	Specious	Graft	Assessment Of Bone Regeneration				Day of assessment and follow up
				Histology/ histomorphometery	Micro CT	Radiographs	Mechanical	
Jiang X et al, 2009	Mandible	Rat	BMSCs+gene BMP-2+ MSS	Histology 57.79% ± 7.9 bone formation	Micro CT: 38.8± 7.6	-	-	8 weeks
Li J et al 2010	Mandible	Rabbit	MSCs+gene BMP-7+ n-HA/PA	120.67 % ± 6.4complete	-	+	+	4, 8, 16 weeks
Park et al 2003	Mandible	Rat	BMSCs+gene BMP-2+Collagen sponge	Complete	_	+	-	6 weeks
You-Chao, 2008	Mandible	Rat	BMSCs+cHA+GENE BMP-2	23.3 ±0.015% Incomplete	-	-	-	8 weeks
Warnke et al, 2006	Mandible	Human	BMSCs+BMP-7+POLYLACTITE	Complete		-	-	38 weeks

Study	Anatomical site	Specious	Graft	Assessment Of Bone Regeneration				Day of assessment and follow up
				Histology/ histomorphometery	Micro CT	Radiographs	Mechanical	
Arosarena et al, 2003	Mandible	Rat	BMSC+BMP+Collage+HA	19.3 ± 2.3 % in complete bone reg	-	-	-	8 weeks
Jiang et al, 2006	Mandible	Rabbit	MSCs+BMP-4+NNB	38.2 ± 9.4 in-complete bony bridging	-	-	-	8 weeks
Wolffe et al, 2013	Mandible	Human	ASCs/ BMP-2/ TCP	complet reconstruction and implanted loaded	-	+	-	28 month(19-38)

Appendix.1.4.

Table 3. Table demonstrating the gross clinical observations upon harvesting each specimen, the weight of animal at the day of sacrifice and any postoperative complications

Rabbit Number	Weight (Kg)	Postoperative complications	Gross clinical observation
R51	32.7	The plate was laterally positioned with dislodgement of the anterior screw.	Area of bone over growth over the proximal screw.
152	30.6	-	-
214	33.4	-	Presence of rubbery white material between the muscle fibres at most superior margin of the defect medially.
215	31.04	-	Presence of rubbery white material in between muscle fibres on lateral surface of the graft.
216	36.63	Developed seroma 6 days after surgery, subsided spontaneously after 5 days	-
217	32.29	-	-
218	32.04	-	Presence of rubbery white material between muscle fibres at site of graft. Area of bone over growth proximal to the defect. Marked increase in the width of the ramus medio-lateraly.
239	33.95	-	Presence of rubbery white material in between muscle fibres in more than one site
240	36.16	Developed seroma, aspiration done	Presence of rubbery white material between muscle fibres.

241	37.27	Developed seroma, which resolved after aspiration of 17 ml of serous fluid two weeks from the day of surgery.	Irregular rough surface over the superior margin of the defect, and white rubbery cement material at superior border of the defect.

Table 4: Table summarising of the qualitative assessment of plain radiographs taken at different time point for all the operated cases.

Rabbit. No	Descriptions		
	I month	2 months	3 months
Rb 151	The superior and proximal margins of the defect showed areas of radio-opaque mass extending from the margin toward the centre of the defect.	Displacement of the plate laterally due to dislodgement of the anterior screw, the radio-opaque mass in the middle 1/3 of the defect was in continuity with radio-opaque mass extending from the superior and proximal margins which means that the defect was bridged at least at two points with radio-opaque tissue.	Continuity of the radio-opaque tissue with the proximal, superior and inferior margins of the defect. More radio-opaque mass around the proximal border. Radiolucent shadow that was noted at 2 months following surgery was more defined and was surrounded by a radio-opaque mass at the middle of the defect.
Rb 152	Homogenous radio-opaque shadow at the defect area, it was difficult to trace any radiolucent areas at this stage.	The radio-opaque patches disappeared. Small areas of radio-opaque tissue noted emerging from the anterior and the inferior margin of the defect.	The radio-opaque mass became more radio-dense and bridged the gap at the anterior and the inferior margins of the defect.

Rabbit.	Descriptions		
No	I month	2 months	3 months
Rb 214	Radio-opaque mass occupying the superior proximal area, and the anterior superior margin of the defect.	The border of the defect appeared more radio- dense; the rest of the defect was occupied with homogenous but less radio-opaque tissues.	Radio-opaque mass near the proximal border. Areas of bony bridging extending from the inferior to the proximal margin of the defect. The margins of the defect appeared more radio-opaque compared with the rest of the bone.
Rb 215	Patches of radio-opaque shadows of the injected cement at the anterior, proximal and the central areas of the defect.	Less radio-opaque areas visible.	Traces of radio-opaque material appeared at the centre of the defect. Localised thickening at the margin of the defect in comparison to the surrounding bone.
Rb 216	Shadow of radio-opaque material obscured the defect border anteriorly, proximally and superiorly	Borders of the defect look more radio-opaque compared to the surrounding native bone. The rest of the defect occupied with homogenous radio-opaque tissues.	Uniform radio-opaque mass occupying the whole defect area. The opacity of the mass was similar to the surrounding bone. The defect was bridged at the proximal border with a radio-opaque mass and the cortices were obscured by the new tissue. At the anterior border of the defect, the cortices remained visible.
217	Shadow of radio-opaque mass was observed at the centre of the defect which corresponded to the site of injected cement.	Radio-opaque area noted at the border and less homogenous radio-opaque mass at the centre.	Flocculent radio-opaque areas with flecks of calcification noted at superior, anterior borders and the centre of the defect. Defect bridged at proximal border with uniform radio-opaque mass and the cortices were obscured by the newly formed radio-opaque tissue.

Rabbit. No	Descriptions		
	I month	2 months	3 months
218	Remnant of cement appearing as a radio-opaque mass observed at the superior margin of the defect.	The borders of the defect were more radio-opaque than surrounding bone.	The defect was bridged at the superior and proximal border of the defect with a radio-opaque mass. The proximal and anterior borders of the defect were more radio-dense with irregular margins. The residual defect was smaller in size compared to first month radiograph.
239	Remnants of cement present at the middle and anterior one third of the created defect.	Radio-opaque mass occupying the superior border of the middle one third of the defect. The proximal margin of the defect was more radio-opaque than the surrounding native bone.	A uniform radio-opacity occupying the anterior one third of the defect, bridged at the anterior border. Another radio-opaque mass at the inferior border which extended from the posterior one third of the defect to the centre. Flocculent radio-opaque areas in the middle one third of the defect. The superior margin of the defect was more radio-opaque than the surrounding native bone.
240	Remnants of cement appeared as a radio-opaque masses occupying the anterior one third of the defect.	The radio-opaque area at the anterior one third appeared more uniform. Rest of defect occupied by uniform radio opaque mass similar to the surrounding soft tissue shadow. The borders of the defect were not clear.	The radio-opaque mass showed more density than the surrounding bone, while the rest of the defect was covered with a uniform radio-opacity which was less dense than the mass seen at the anterior one third.

Rabbit.	Descriptions		
No	I month	2 months	3 months
241	Remnants of cement appeared as a radio-opaque masses in the centre of the defect.	Radio-opaque mass at the centre if defect in the same site where remnants of cement were observed at 1st month radiograph.	Radio-opaque mass at the superior border extending to the anterior margin. The density of the mass was uniform. Traces of radio-opaque mass occupying the defect at the proximal one third at the superior borders which appeared more opaque than the surrounding native bone.

Appendix 1.5
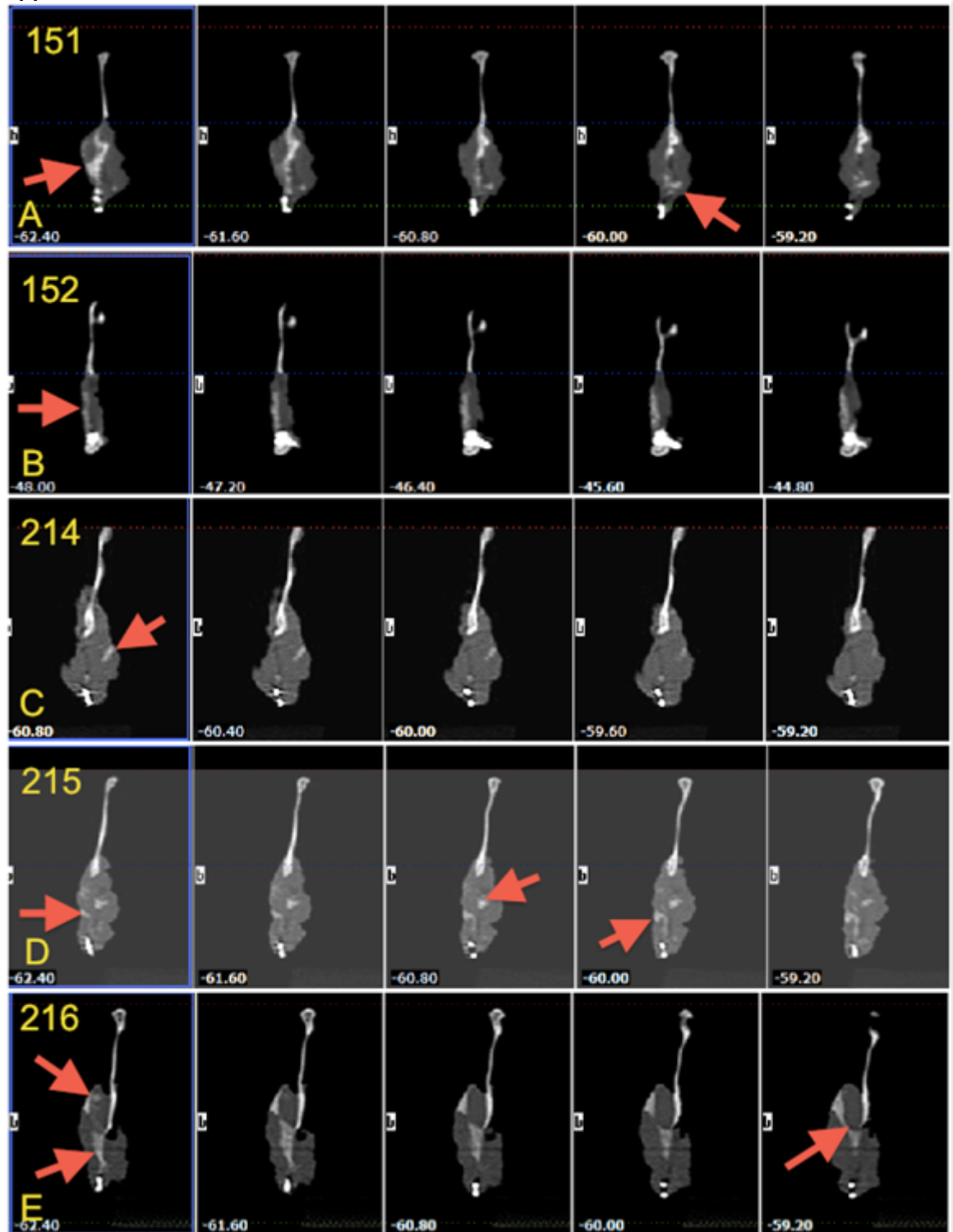
Figure 1a: Consecutive CBCT coronal images for all cases involved in the main study, A) shows case 151 and the continuity of the regenerated tissue (arrow), the radio opacity was medial to the ramus, B) shows case 152 with the radio-opaque line (arrow) in line with the native bone, and a gap in the superior margin of the defect, C) shows   case 214 with sporadic radio-opaque areas (arrow), and medially located, D) shows case 215, the radio-opaque tissues are continuous with the inferior border and displaced laterally (arrow), E) shows case 216 demonstrating a large bulk of radiopaque tissue (arrow) located lateral to the defect area, with no continuity with the inferior and superior border of the defect.
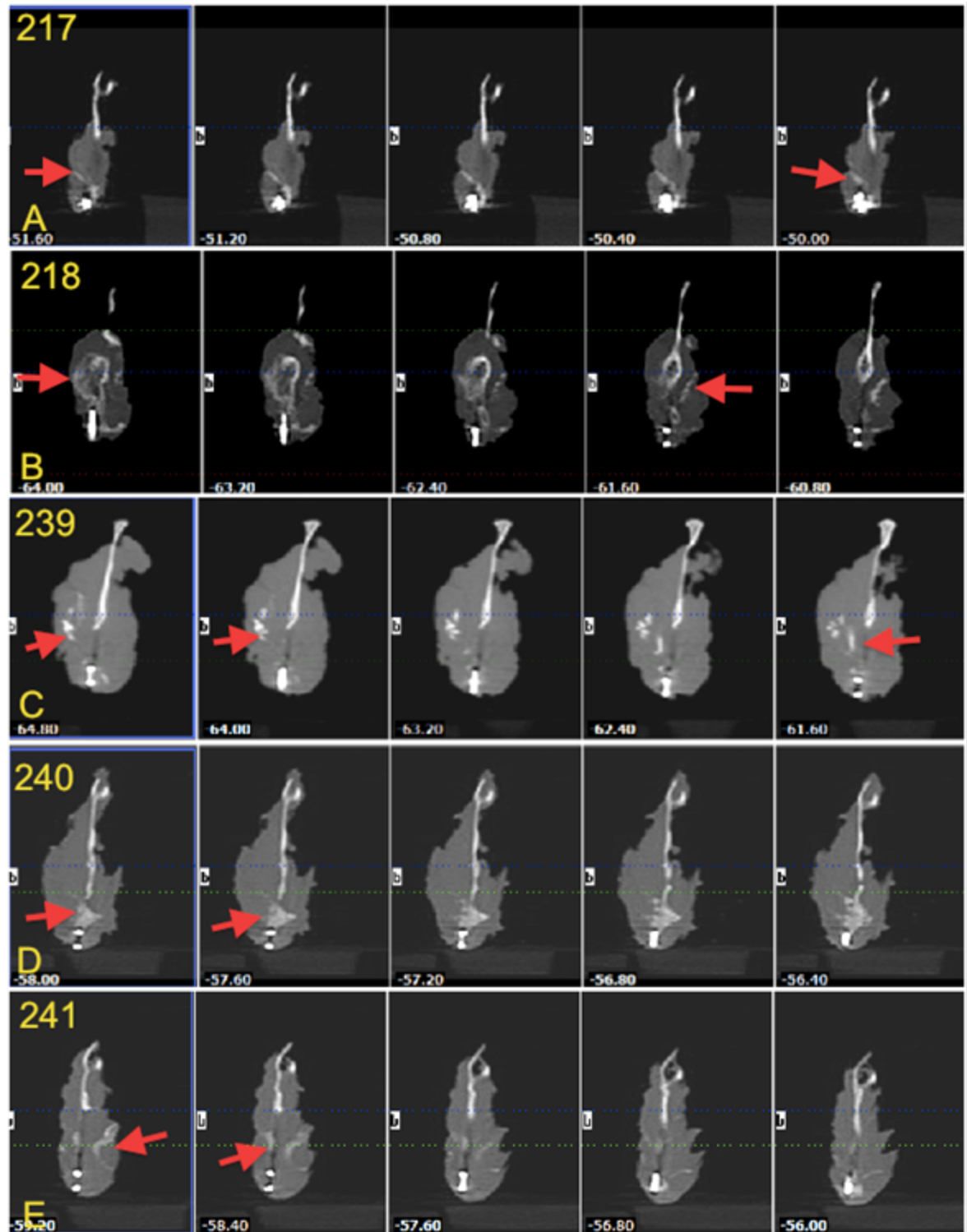
Figure1b: b: Consecutive CBCT coronal images for all cases involved in the main study, A) shows case 217, the radio-opaque tissue was located only inferiorly and directed laterally, B) shows case 218, radio-opaque tissue was located lateral to the defect and displaced, expansion of both cortices is denoted with red arrows, C) shows case 239, radio-opacity was sporadically located lateral to the defect area (arrow), D) shows case 240, with radio-opacity that appears continuous from the superior to the inferior   border that was wider medio-laterally (arrow), E) Case 241, sporadic areas of radio-opacity are located at the centre and medial side of the defect (arrow)
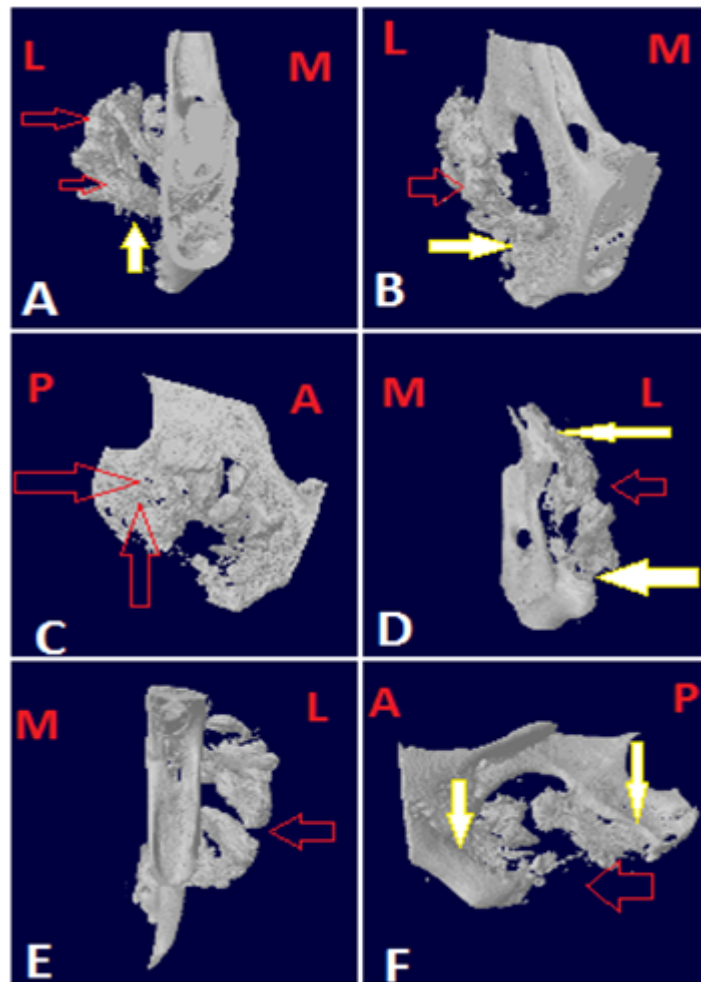
Figure2: Images of several consecutive screen shots for case 216 showing the pattern of bone formation (red arrows) and integration in relation to the defect and the native bone (white arrow), L, M, A and P represent Lateral, medial, anterior and posterior boundaries of the defect.
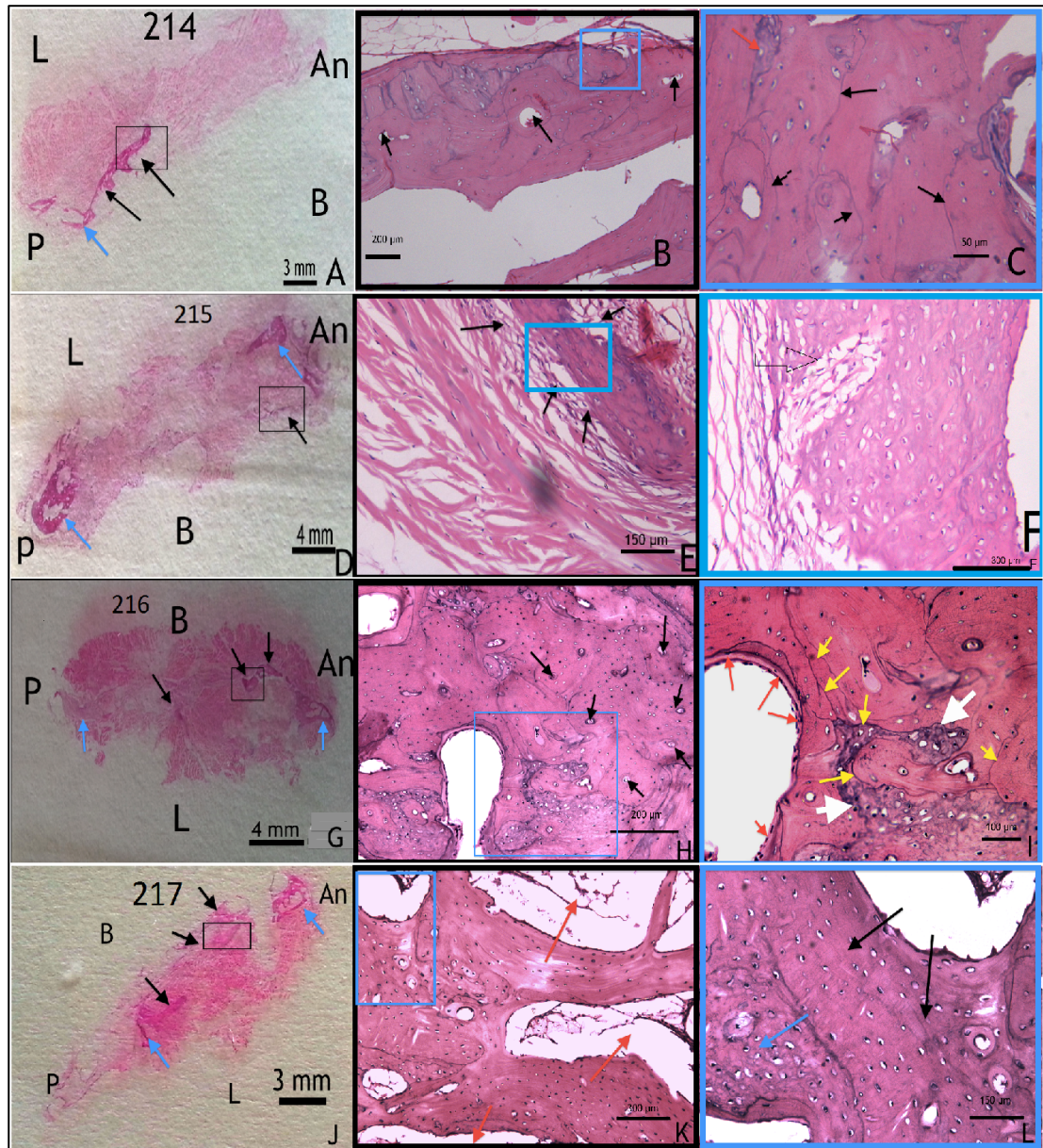
Figure3 a: Photomicrograph showing the decalcified sections (H&E) demonstrating areas of bone regeneration at the surgical defect for cases 214, 215, 216 and 217. A, D, G and J show an overall view for the defect from anterior to posterior margins of the defect (blue arrows) black arrow shows areas of bone regeneration, the black boxes highlight areas examined in B, E, H and K. The blue boxes in these images are magnified in C, F, I and L.   B) Shows bone regeneration toward the centre of the defect, the bone is surrounded by periosteum, scale bar= 200 µm, C) Shows the reversal lines (black arrows) which indicate remodelling of bone, less mature bone appears more purple in colour (red arrow) scale bar = 50 µm, E) Shows woven bone (arrows) next to loose connective tissue, scale bar= 150 µm, H) Shows Haversian structures (arrows) next to vascular channels (black arrow), scale bar=300 µm, I)   Shows osteoid (red arrow), woven bone (white arrow) mature lamellar bone and the reversal line in between (yellow arrow), K) Shows bone marrow spaces (red arrow), scale bar= 300 µm. L) Shows mature lamellar bone (black arrow) and woven bone (blue arrow) scale bar = 150 µm. An, P, L and B indicates anterior, proximal, lingual and buccal borders of the defect.
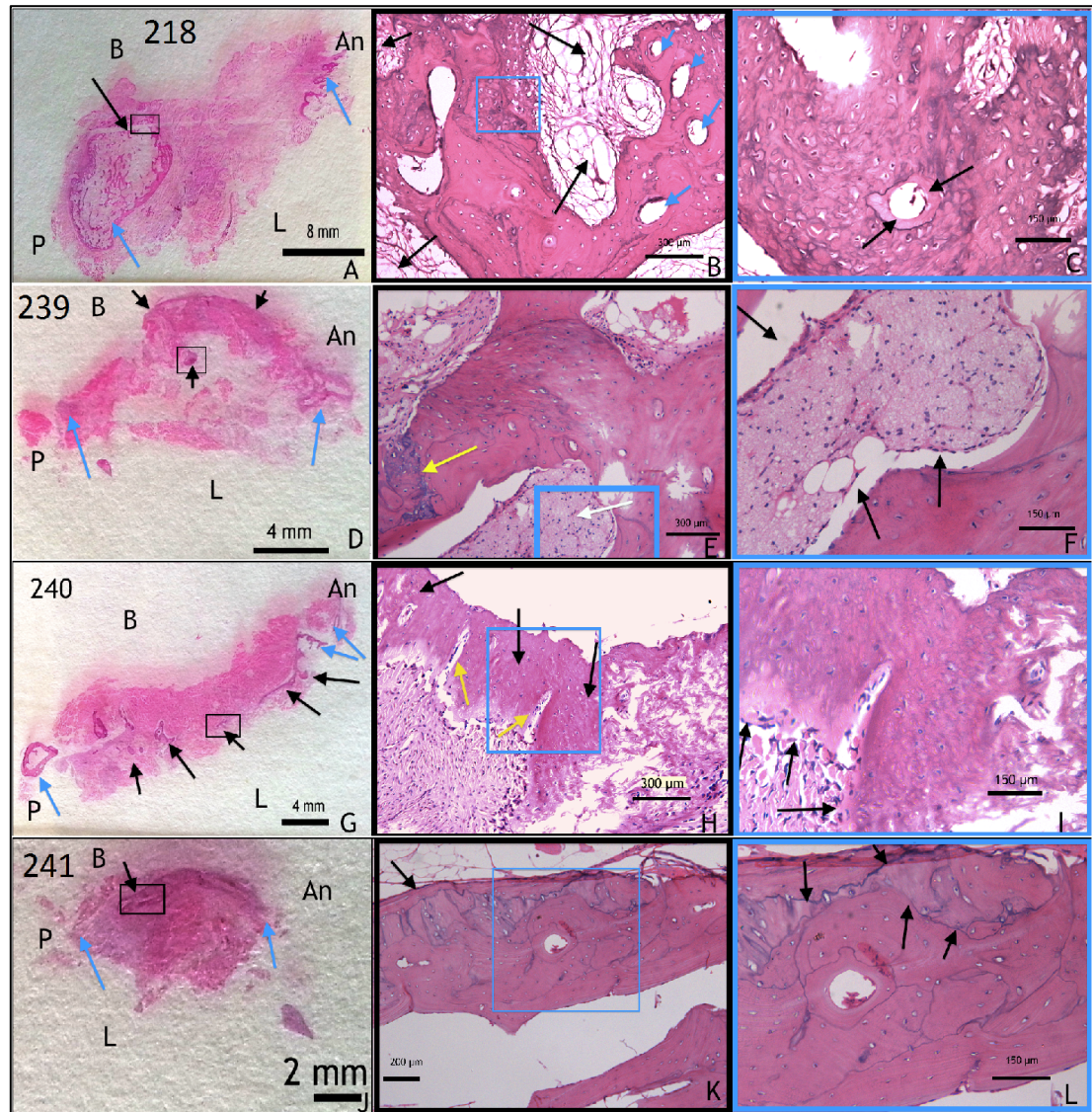
Figure 3b: Photomicrographs for decalcified sections (H&E) demonstrating areas of bone regeneration at the surgical defects for cases 218, 239, 240 and 241.   A, D, G and J show overall views from anterior to posterior margins of the defect (blue arrows) with areas of bone regeneration (black arrow), the black box highlights the areas examined in B, E, H and K. The blue box are magnified in C, F, I and L. B) Shows trabecular bone formation with large marrow spaces (black arrows) and mature osteons (blue arrow), scale bar=300 μm, C) Shows woven bone with large lacunae for osteocytes and osteoid around the vessels channels (arrow), scale bar = 150 μm, E) Shows bone formation surrounded by remnants of cement (white arrow), scale bar= 300 μm, F) Shows pale tissue with inflammatory cell infiltration, cement surrounded by fibrous tissue, and spaces between the material and the bone (black arrow), scale bar = 150 μm, (H) Shows areas of woven bone (arrow) and multiple narrow cavities (yellow arrow), scale bar = 300 μm, I) Shows the interface between the loose connective tissue and the bone with a periosteum-like membrane barrier (arrow), scale bar= 150 μm. K) Shows mature regenerated bone with large marrow spaces, covered with periosteum at the superior border (arrow), scale bar= 300 μm , L) Shows the bone with irregular reversal cement lines (arrow) which have separated the woven bone from the lamellar bone, scale bar = 150 μm.
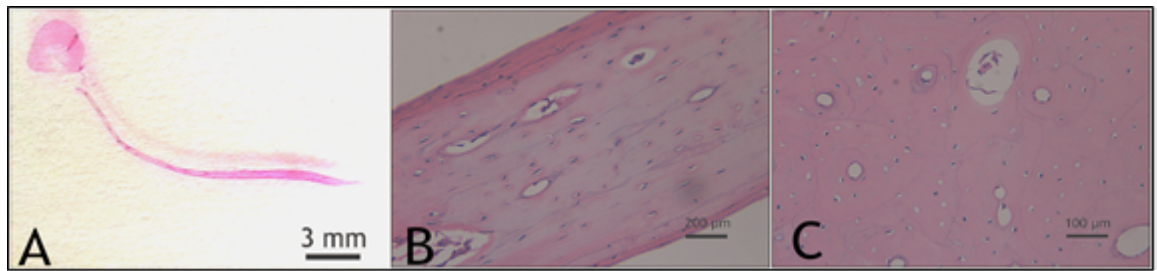
Figure4: Photomicrographs showing decalcified histological sections stained with H&E for the non-operated side. A) Shows an overall sagittal view through the ramus, scale bar = 3 mm, B) Shows well developed lamellar bone and osteocytes in lacunae arranged parallel to the bone lamella, scale bar = 200 μm, C) Shows closer magnification of the osteons, scale bar = 100 μm.
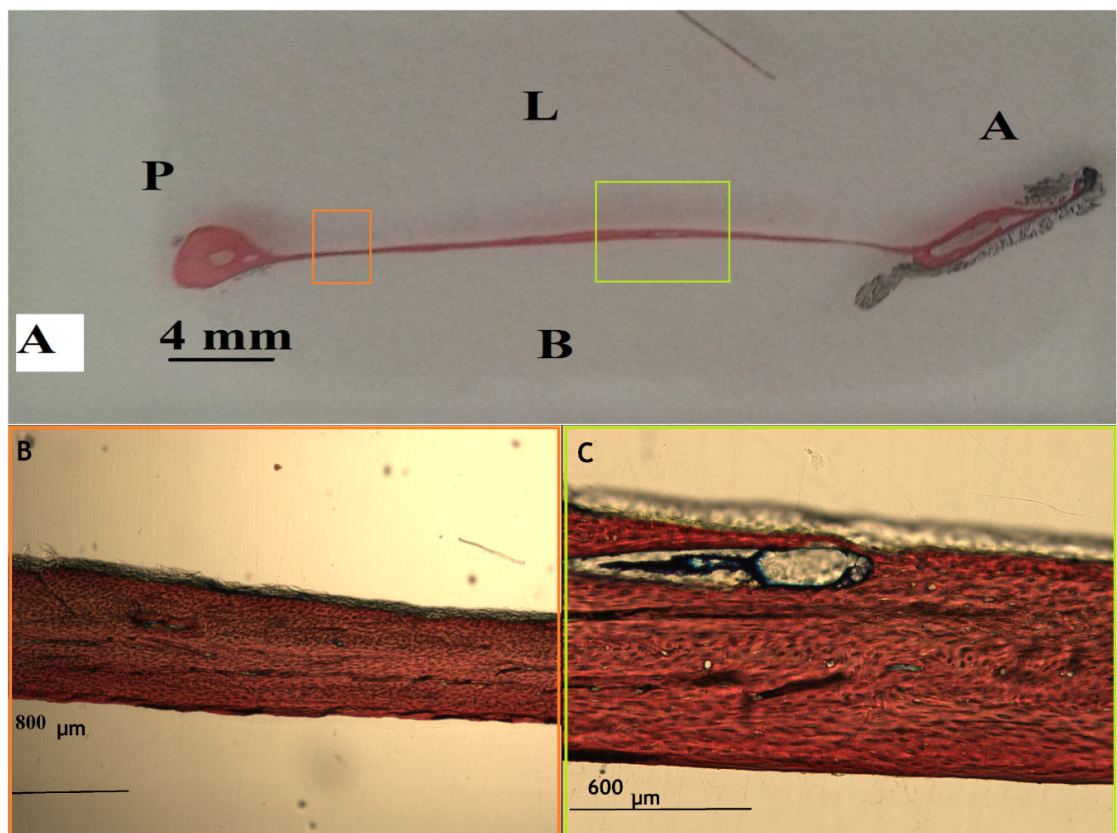
Figure 5: Photomicrographs for undecalcified histological section using Sanderson`s Van Gieson Stain for the non-operated side, A) shows normal bone histology and it`s thickness at the area of the defect (boxed) < 1 mm, B, C showing magnified images for the green and orange boxes, scale bar= 800 and 600 μm respectively. Using light microscopy (Zeiss Germany.

REFERENCES

Abramo, A., Geijer, M., Kopylov, P., & Tagil, M. 2010. Osteotomy of Distal Radius Fracture Malunion Using a Fast Remodeling Bone Substitute Consisting of Calcium Sulphate and Calcium Phosphate. Journal of Biomedical Materials Research Part B-Applied Biomaterials, 92B, (1) 281-286

Abu-Serriah, M. 2002. Reconstruction of osteoperiosteal discontinuity critical size mandibular defects using recent advances in bone bioengineering. University of Glasgow, Glasgow Dental Hospital and School

Abu-Serriah, M.M., Odell, E., Lock, C., Gillar, A., Ayoub, A.F., & Fleming, R.F. 2004. Histological assessment of bioengineered new bone in repairing osteoperiosteal mandibular defects in sheep using recombinant human bone morphogenetic protein-7. British Journal of Oral & Maxillofacial Surgery, 42, (5) 410-418

Abu-Serriah, M., Kontaxis, A., Ayoub, A., Harrison, J., Odell, E., & Barbenel, J. 2005. Mechanical evaluation of mandibular defects reconstructed using osteogenic protein-1 (rhOP-1) in a sheep model: a critical analysis. International Journal of Oral and Maxillofacial Surgery, 34, (3) 287-293

Abukawa, H., Shin, M., Williams, W.B., Vacanti, J.P., Kaban, L.B., & Troulis, M.J. 2004. Reconstruction of mandibular defects with autologous tissue-engineered bone. Journal of Oral and Maxillofacial Surgery, 62, (5) 601-606

Agrawal, C.M., Best, J., Heckman, J.D., & Boyan, B.D. 1995. Protein Release Kinetics of A Biodegradable Implant for Fracture Non-Unions. Biomaterials, 16, (16) 1255-1260

Akintoye, S.O., Lam, T., Shi, S.T., Brahim, J., Collins, M.T., & Robey, P.G. 2006. Skeletal site-specific characterization of orofacial and iliac crest human bone marrow stromal cells in same individuals. Bone, 38, (6) 758-768

Alfotawi, R., Naudi, K.B., Lappin, D., Barbenel, J., Di Silvio, L., Hunter, K., McMahon, J., & Ayoub, A. 2014 The use of Tri-Calcium Phosphate (TCP) and stem cells for the regeneration of osteoperiosteal critical-size mandibular boney defects, an in vitro and preclinical study. Journal of Cranio-Maxillofacial Surgery (0) available from:http://www.sciencedirect.com/science/article/pii/S1010518213003363

Alhadlaq, A. & Mao, J.J. 2003. Tissue-engineered neogenesis of human-shaped mandibular condyle from rat mesenchymal stem cells. Journal of Dental Research, 82, (12) 951-956

Alliotlicht, B., Gregoire, M., Orly, I., & Menanteau, J. 1991. Cellular-Activity of Osteoblasts in the Presence of Hydroxyapatite - An Invitro Experiment. Biomaterials, 12, (8) 752-756

Asahara, T., Bauters, C., Zheng, L.P., Takeshita, S., Bunting, S., Ferrara, N., Symes, J.F., & Isner, J.M. 1995. Synergistic effect of vascular endothelial growth factor and basic fibroblast growth factor on angiogenesis in vivo. Circulation, 92, (9S) II365-II371

Assael, L A. 2009. Mandibular Reconstruction: Expert Opinion and Outcome Studies Remain a Fragile Guide to Treatment. Journal of Oral and Maxillofacial Surgery, 67, (12) 2557-2558

Ayoub, A., Challa, S., Abu-Serriah, M., McMahon, J., Moos, K., Creanor, S., & Odell, E. 2007. Use of a composite pedicled muscle flap and rhBMP-7 for mandibular reconstruction. International Journal of Oral and Maxillofacial Surgery, 36, (12) 1183-1192

Baksh, D., Song, L., & Tuan, R.S. 2004. Adult mesenchymal stem cells: characterization, differentiation, and application in cell and gene therapy. Journal of Cellular and Molecular Medicine, 8, (3) 301-316

Ballen, K.K., Barker, J.N., Stewart, S.K., Greene, M.F., & Lane, T.A. 2008. Collection and preservation of cord blood for personal use. Biology of Blood and Marrow Transplantation, 14, (3) 356-363

Barnes, B., Boden, S.D., Louis-Ugbo, J., Tomak, P.R., Park, J.S., Park, M.S., & Minamide, A. 2005. Lower dose of rhBMP-2 achieves spine fusion when combined with an osteoconductive bulking agent in non-human primates. Spine, 30, (10) 1127-1133

Best, S.M., Porter, A.E., Thian, E.S., & Huang, J. 2008. Bioceramics: Past, present and for the future. Journal of the European Ceramic Society, 28, (7) 1319-1327

Beutner, E.H. 1961. Immunofluorescent Staining - Fluorescent Antibody Method. Bacteriological Reviews, 25, (1) 49-76

Bhumiratana, S., Bernhard, J., Alfi, D.M., Yeager, K., Eton, R., Bova, J., Shah, F., Gimble, J., Lopez, M., Eisig, S.B., & Vunjak-Novakovic, G. 2013. Engineered bone graft with autogenous stem cell improved bone reconstruction through enhancing graft integration and preventing entropic graft resorption. Journal of Oral and Maxillofacial Surgery, 71, (9 SUPPL.1) 34-36

Bianchi, G., Muraglia, A., Daga, A., Corte, G., Cancedda, R., & Quarto, R. 2001. Microenvironment and stem properties of bone marrow-derived mesenchymal cells. [Review]. Wound Repair & Regeneration, 9, (6) 460-466

Bianco, P., Riminucci, M., Gronthos, S., & Robey, P.G. 2001. Bone marrow stromal stem cells: Nature, biology, and potential applications. Stem Cells, 19, (3) 180-192

Bianco, P., Robey, P.G., Saggio, I., & Riminucci, M. 2010. "Mesenchymal" Stem Cells in Human Bone Marrow (Skeletal Stem Cells): A Critical Discussion of Their Nature, Identity, and Significance in Incurable Skeletal Disease. Human Gene Therapy, 21, (9) 1057-1066

Bicknell, R. & Harris, A.L. 2004. Novel angiogenic signaling pathways and vascular targets. Annual Review of Pharmacology and Toxicology, 44,(0) 219-238

Bjornson, C.R.R., Rietze, R.L., Reynolds, B.A., Magli, M.C., & Vescovi, A.L. 1999. Turning brain into blood: A hematopoietic fate adopted by adult neural stem cells in vivo. Science, 283, (5401) 534-537

Boden, S.D., Schimandle, J.H., & Hutton, W.C. 1995. An Experimental Lumbar Intertransverse Process Spinal-Fusion Model - Radiographic, Histologic, and Biomechanical Healing Characteristics. Spine, 20, (4) 412-420

Bostrom, M.P.G., Aspenberg, P., Jeppsson, C., & Salvati, E.A. 1998. Enhancement of bone formation in the setting of repeated tissue deformation. Clinical Orthopaedics and Related Research,0 ,(350) 221-228

Boudreau, J. & Jones, P.L. 1999. Extracellular matrix and integrin signalling: the shape of things to come. Biochemical Journal, 339, (3) 481-488

Bruder, S. & Caplan, A. 1989. Discrete stages within the osteogenic lineage are revealed by alterations in the cell surface architecture of embryonic bone cells. Connective Tissue Research, 20, 73-79

Bruick, R.K. & McKnight, S.L. 2001. Building better vasculature. Genes & Development, 15, (19) 2497-2502

Bryant, J. 2011. Deriving Hounsfield units from the grey scale of a CBCT? Dentomaxillofacial Radiology, 40, (1) 65

Burdick, J.A. & Vunjak-Novakovic, G. 2009. Engineered microenvironments for controlled stem cell differentiation. Tissue engineering.Part A, 15, (2) 205-219

Busuttil Naudi, K., Ayoub, A., McMahon, J., Di Silvio, L., Lappin, D., Hunter, K.D., & Barbenel, J. 2012. Mandibular reconstruction in the rabbit using beta-tricalcium phosphate (beta-TCP) scaffolding and recombinant bone morphogenetic protein 7 (rhBMP-7) - histological, radiographic and mechanical evaluations. Journal of cranio-maxillo-facial surgery, 40, (8) e461-e469

Castano-Izquierdo, H., Alvarez-Barreto, J., van den Dolder, J., Jansen, J.A., Mikos, A.G., & Sikavitsas, V.I. 2007. Pre-culture period of mesenchymal stem cells in osteogenic media

influences there in vivo bone forming potential. Journal of Biomedical Materials Research Part A, 82A, (1) 129-138

Chao, M., Donovan, T., Sotelo, C., & Carstens, M.H. 2006. In situ osteogenesis of hemimandible with rhBMP-2 in a 9-year-old boy: osteoinduction via stem cell concentration. Journal of Craniofacial Surgery, 17, (3) 405-412

Chen, F.L., Chen, S.J., Tao, K., Feng, X., Liu, Y.P., Lei, D.L., & Mao, T.Q. 2004. Marrow-derived osteoblasts seeded into porous natural coral to prefabricate a vascularised bone graft in the shape of a human mandibular ramus: experimental study in rabbits. British Journal of Oral & Maxillofacial Surgery, 42, (6) 532-537

Cheung, L.K., Samman, N., Chow, T.W., Clark, R.K.F., & Tideman, H. 1997. A bone graft condensing syringe system for maxillofacial reconstructive surgery. British Journal of Oral & Maxillofacial Surgery, 35, (4) 267-270

Clokie, C.M. & Sandor, G.K. 2008. Reconstruction of 10 major mandibular defects using bioimplants containing BMP-7. Journal (Canadian Dental Association), 74, (1) 67-72

Coetzee, A.S. 1980. Regeneration of Bone in the Presence of Calcium-Sulfate. Archives of Otolaryngology-Head & Neck Surgery, 106, (7) 405-409

Cook, S.D., Salkeld, S.L., & Patron, L.P. 2005. Bone defect healing with an osteogenic protein-1 device combined with carboxymethylcellulose. Journal of Biomedical Materials Research Part B-Applied Biomaterials, 75B, (1) 137-145

Cornelison, D.D.W. & Wold, B.J. 1997. Single-cell analysis of regulatory gene expression in quiescent and activated mouse skeletal muscle satellite cells. Developmental Biology, 191, (2) 270-283

Costantino, P.D., Friedman, C.D., Jones, K., Chow, L.C., & Sisson, G.A. 1992. Experimental Hydroxyapatite Cement Cranioplasty. Plastic and Reconstructive Surgery, 90, (2) 174-185

Daculsi, G., Passuti, N., Martin, S., Deudon, C., Legeros, R.Z., & Raher, S. 1990. Macroporous Calcium-Phosphate Ceramic for Long-Bone Surgery in Humans and Dogs - Clinical and Histological Study. Journal of Biomedical Materials Research, 24, (3) 379-396

Dalby. M.J., Yarwood. S.J., Riehle. M.O., Johnstone. H.J., Affrossman. S., Curtis. A.S.2002. Increasing fibroblast response to materials using nanotopography: morphological and genetic measurements of cell response to 13-nm-high polymer demixed islands. Experimental Cell Research, 276, (1)1-9

Dalby, M.J., Gadegaard, N., Curtis, A.S.G., & Oreffo, R.O.C. 2007. Nanotopographical control of human osteoprogenitor differentiation. Current stem cell research & therapy, 2, (2) 129-138

De Carvalho Crusoe Silva, I.M., de Freitas, D.Q., Bovi Ambrosano, G.M., Boscolo, F.N., & Almeida, S.M. 2012. Bone density: comparative evaluation of Hounsfield units in multislice and cone-beam computed tomography. Brazilian Oral Research, 26, (6) 550-556

De, G.J. 1998. Carriers that concentrate native bone morphogenetic protein in vivo. Tissue Engineering, 4, (4) 337-341

Denecke, B., Wöltje, M., Neuss, S., & Jahnen-Dechent, W. 2008, "Tissue Engineering - Combining Cells and Biomaterials into Functional Tissues," In Bioengineering in Cell and Tissue Research, 1st ed. G. A. Artmann & S. Chien, eds., Springer, pp. 139-214.

Detamore, M.S. & Athanasiou, K.A. 2005. Evaluation of three growth factors for TMJ disc tissue engineering. Annals of Biomedical Engineering, 33, (3) 383-390

Diaz-Flores, L., Gonzalez, T., & Gutierrez, R. 1991. Inducible perivascular cells contribute to the neochondrogenesis in grafted perichondrium. Anatomical Record., 229,1-8

Doherty, M. & Canfield, A. 1999. Gene expression during vascular pericyte differentiation. Critical Review Eukaryot Gene Expression, 9,1-17

Dolores, W., Christian, R., Harald, N., Hildegunde, P., & Georg, W. 2004. Cellular and molecular composition of fibrous capsules formed around silicone breast implants with special focus on local immune reactions.   Journal of Autoimmunity, 23, (1) 81-91

Dreesman, H. 1892. Ueber Knochenplombierung. Bietr Klin Chir, 9,804-810

Dumas, J.E., Brownbaer, P.B., Prieto, E.M., Guda, T., Hale, R.G., Wenke, J.C., & Guelcher, S.A. 2012. Injectable reactive biocomposites for bone healing in critical-size rabbit calvarial defects. Biomedical Materials, 7, (2) 024112

Eck, K.R., Lenke, L.G., Bridwell, K.H., Gilula, L.A., Lashgari, C.J., & Riew, K.D. 2000. Radiographic assessment of anterior titanium mesh cages. Journal of Spinal Disorders, 13, (6) 501-509

Egan, K.P., Brennan, T.A., & Pignolo, R.J. 2012. Bone histomorphometry using free and commonly available software. Histopathology, 61, (6) 1168-1173

Emery, S.E., Brazinski, M.S., Koka, A., Bensusan, J.S., & Stevenson, S. 1994. The Biological and Biomechanical Effects of Irradiation on Anterior Spinal Bone-Grafts in A Canine Model. Journal of Bone and Joint Surgery-American Volume, 76A, (4) 540-548

Evans, C., Liu, F., Glatt, V., Hoyland, J., Kirker-Head, C., Walsh, A., Betz, O., Wells, J., Betz, V., Porter, R., Saad, F., Gerstenfeld, L., Einhorn, T., Harris, M., & Vrahas, M. 2009. Use

of Genetically Modified Muscle and Fat Grafts to Repair Defects in Bone and Cartilage. European Cells & Materials, 18, 96-111

Feiertag, M.A., Boden, S.D., Schimandle, J.H., & Norman, J.T. 1996. A rabbit model for nonunion of lumbar intertransverse process spine arthrodesis. Spine, 21, (1) 27-30

Ferrari, G., Cusella-De Angelis, G., Coletta, M., Paolucci, E., Stornaiuolo, A., Cossu, G., & Mavilio, F. 1998. Muscle regeneration by bone marrow derived myogenic progenitors. Science, 279, (5356) 1528-1530

Ferretti, C. & Ripamonti, U. 2002. Human segmental mandibular defects treated with naturally derived bone morphogenetic proteins. Journal of Craniofacial Surgery, 13, (3) 434-444

Friedenstein, A.J., Piatetzky-Shapiro, I.I., & Petrakova, K.V. Osteogenesis in transplants of bone marrow cells.1966. Journal of embryology and experimental morphology, 16, (3) 381-390

Friedenstein, A.J., Chailakhjan, R.K., & Lalykina, K.S.1970. The development of fibrofolast colonies in monolayer cultures of guinea pig bone marrow and spleen cells. Cell and Tissue Kinetics, 3, (4) 393-403

Friedl, P. & Brocker, E.B. 2000. The biology of cell locomotion within three-dimensional extracellular matrix. Cellular and Molecular Life Sciences, 57, (1) 41-64

Friedman, C.D., Costantino, P.D., Jones, K., Chow, L.C., Pelzer, H.J., & Sisson, G.A. 1991. Hydroxyapatite Cement .2. Obliteration and Reconstruction of the Cat Frontal-Sinus. Archives of Otolaryngology-Head & Neck Surgery, 117, (4) 385-389

Frost H, Griffith D, Jee W, Kimmel D, Mc Candlis, Teielbaum S 1981. Histomorphometric changes in trabecular bone in renal failure patient treated with calcifediol.Metabolic disease and related research, (2) 285-295

Frost, H.M. 1999. On the trabecular "thickness" - Number problem. Journal of Bone and Mineral Research, 14, (11) 1816-1821

Fu, J., Miao, B., Jia, L., & Lu, K. 2009. Nano-hydroxyapatite for repair of rabbit jaw bone defect* Bone mineral density analysis. Journal of Clinical Rehabilitative Tissue Engineering Research, 13, (12) 2387-2390

Gan, Y., Dai, K., Zhang, P., Tang, T., Zhu, Z., & Lu, J. 2008. The clinical use of enriched bone marrow stem cells combined with porous beta-tricalcium phosphate in posterior spinal fusion. Biomaterials, 29, (29) 3973-3982

Gao, X., Usas, A., Lu, A., Proto, J., Tebbets, J., Li, H., Cummins, J., Huard, M., & Huard, J. 2011. Muscle Derived Stem Cells Transduced with BMP4 Interact Broadly with host cells

to Promote Bone Healing in Critical Sized Skull Defect. Molecular Therapy, 19,(1) s145-s146.

Gauthier, O., Khairoun, I., Bosco, J., Obadia, L., Bourges, X., Rau, C., Magne, D., Bouler, J.M., Aguado, E., Daculsi, G., & Weiss, P. 2003. Noninvasive bone replacement with a new injectable calcium phosphate biomaterial. Journal of Biomedical Materials Research Part A, 66A, (1) 47-54

Gauthier, O., Muller, R., von Stechow, D., Lamy, B., Weiss, P., Bouler, J.M., Aguado, E., & Daculsi, G. 2005. In vivo bone regeneration with injectable calcium phosphate biomaterial: A three-dimensional micro-computed tomographic, biomechanical and SEM study. Biomaterials, 26, (27) 5444-5453

Gerber, H.P., Vu, T.H., Ryan, A.M., Kowalski, J., Werb, Z., & Ferrara, N. 1999. VEGF couples hypertrophic cartilage remodeling, ossification and angiogenesis during endochondral bone formation. Nature Medicine, 5, (6) 623-628

Giavazzi, R., Sennino, B., Coltrini, D., Garofalo, A., Dossi, R., Ronca, R., Tosatti, M.P.M., & Presta, M. 2003. Distinct role of fibroblast growth factor-2 and vascular endothelial growth factor on tumor growth and angiogenesis. American Journal of Pathology, 162, (6) 1913-1926

Gimbel, M., Ashley, R.K., Sisodia, M., Gabbay, J.S., Wasson, K.L., Heller, J., Wilson, L., Kawamoto, H.K., & Bradley, J.P. 2007. Repair of alveolar cleft defects: Reduced morbidity with bone marrow stem cells in a resorbable matrix. Journal of Craniofacial Surgery, 18, (4) 895-901

Gindraux, F., Selmani, Z., Obert, L., Davani, S., Tiberghien, P., Herve, P., & Deschaseaux, F. 2007. Human and rodent bone marrow mesenchymal stem cells that express primitive stem cell markers can be directly enriched by using the CD49a molecule. Cell and Tissue Research, 327, (3) 471-483

Goh, B.T., Lee, S., Tideman, H., & Stoelinga, P.J. 2008. Mandibular reconstruction in adults: a review. International Journal of Oral and Maxillofacial Surgery, 37, (7) 597-605

Gonzalez-Garcia, R. & Monje, F. 2013. The reliability of cone-beam computed tomography to assess bone density at dental implant recipient sites: a histomorphometric analysis by micro-CT. Clinical Oral Implants Research, 24, (8) 871-879

Goshima, J., Goldberg, V.M., & Caplan, A.I. 1991. Osteogenic Potential of Culture-Expanded Rat Marrow-Cells as Assayed Invivo with Porous Calcium-Phosphate Ceramic. Biomaterials, 12, (2) 253-258

Groh, M.E., Maitra, B., Szekely, E., & Koc, O.N. 2005. Human mesenchymal stem cells require monocyte-mediated activation to suppress alloreactive T cells. Experimental Hematology, 33, (8) 928-934

Groger, A., Klaring, S., Merten, H.A., Holste, J., Kaps, C., & Sittinger, M. 2003. Tissue engineering of bone for mandibular augmentation in immunocompetent minipigs: Preliminary study. Scandinavian Journal of Plastic and Reconstructive Surgery and Hand Surgery, 37, (3) 129-133

Gronthos, S. & Simmons, P. 1995. The growth factor requirement of STRO-1 postive human bone marrow stromal precursors under serum-deprived condition in vitro. Blood, 85,(0) 929-940

Gronthos, S. & Simmons, P.J. 1996. The biology and application of human bone marrow stromal cell precursors. Journal of hematotherapy, 5, (1) 15-23

Guerinreverchon, I., Chardonnet, Y., Chignol, M.C., & Thivolet, J. 1989. A Comparison of Methods for the Detection of Human Papillomavirus Dna by Insitu Hybridization with

Guo, J., Meng, Z.S., Chen, G., Xie, D., Chen, Y.L., Wang, H., Tang, W., Liu, L., Jing, W., Long, J., Guo, W.H., & Tian, W.D. 2012. Restoration of Critical-Size Defects in the Rabbit Mandible Using Porous Nanohydroxyapatite-Polyamide Scaffolds. Tissue Engineering Part A, 18, (11) 1239-1252

Halvorsen, Y.C., Wilkison, W.O., & Gimble, J.M. 2000. Adipose-derived stromal cells - their utility and potential in bone formation. International Journal of Obesity, 24, S41-S44

Hamada, Y., Kondoh, T., Noguchi, K., Iino, M., Isono, H., Ishii, H., Mishima, A., Kobayashi, K., & Seto, I. 2005. Application of limited cone beam computed tomography to clinical assessment of alveolar bone grafting: A preliminary report. Cleft Palate-Craniofacial Journal, 42, (2) 128-137

Hartman, E.H.M., Spauwen, P.H.M., & Jansen, J.A. 2002. Donor-site complications in vascularized bone flap surgery. Journal of Investigative Surgery, 15, (4) 185-197

Hassel, S., Schmitt, S., Hartung, A., Roth, M., Nohe, A., Petersen, N., Ehrlich, M., Henis, Y.I., Sebald, W., & Knaus, P. 2003. Initiation of Smad-dependent and Smad-independent signaling via distinct BMP-receptor complexes. Journal of Bone and Joint Surgery-American Volume, 85A, (0) 44-51

Haynesworth, S.E., Barsr, M.A., & Caplan, A.I. 1992. Chracterization of Cells with osteogenic potential from human marrow .Bone, 13, 81-88

He, Y., Zhang, Z.y., Zhu, H.g., Qiu, W., Jiang, X., & Guo, W. 2007. Experimental study on reconstruction of segmental mandible defects using tissue engineered bone combined bone

marrow stromal cells with three-dimensional tricalcium phosphate. Journal of Craniofacial Surgery, 18, (4) 800-805

He, D., Genecov, D.G., Herbert, M., Barcelo, R., Elsalanty, M.E., Weprin, B.E., & Opperman, L.A. 2010. Effect of recombinant human bone morphogenetic protein-2 on bone regeneration in large defects of the growing canine skull after dura mater replacement with a dura mater substitute Laboratory investigation. Journal of Neurosurgery, 112, (2) 319-328

Heliotis, M., Lavery, K.M., Ripamonti, U., Tsiridis, E., & di Silvio, L. 2006. Transformation of a prefabricated hydroxyapatite/osteogenic protein-1 implant into a vascularised pedicled bone flap in the human chest. International Journal of Oral and Maxillofacial Surgery, 35, (3) 265-269

Henkel, K.-O., Gerber, T., Dorfling, P., Gundlach, K.K.H., & Bienengraber, V.2005. Repair of bone defects by applying biomatrices with and without autologous osteoblasts. Journal of Cranio-Maxillofacial Surgery.33 (1) 45-49

Herford, A.S., Boyne, P.J., Rawson, R., & Williams, R.P. 2007. Bone morphogenetic protein-induced repair of the premaxillary cleft. Journal of Oral and Maxillofacial Surgery, 65, (11) 2136-2141

Herford, A.S. & Cicciu, M. 2010. Recombinant Human Bone Morphogenetic Protein Type 2 Jaw Reconstruction in Patients Affected by Giant Cell Tumor. Journal of Craniofacial Surgery, 21, (6) 1970-1975

Herford, A.S., Stoffella, E., & Tandon, R. 2011. Reconstruction of mandibular defects using bone morphogenic protein: can growth factors replace the need for autologous bone grafts? A systematic review of the literature. Plastic surgery international 2011:7 pages.165824,

Hernandez-Alfaro, F., Ruiz-Magaz, V., Chatakun, P., & Guijarro-Martinez, R. 2012. Mandibular reconstruction with tissue engineering in multiple recurrent ameloblastoma. The International journal of periodontics & restorative dentistry, 32, (3) e82-e86

Hidalgo, D.A. & Pusic, A.L. 2002. Free-flap mandibular reconstruction: A 10-year follow-up study. Plastic and Reconstructive Surgery, 110, (2) 438-449

Hing, K.A., Best, S.M., Tanner, K.E., Bonfield, W., & Revell, P.A. 1999. Quantification of bone ingrowth within bone-derived porous hydroxyapatite implants of varying density. Journal of Materials Science-Materials in Medicine, 10, (10-11) 663-670

Hoeben, A., Landuyt, B., Highley, M.S., Wildiers, H., Van Oosterom, A.T., & De Bruijn, E.A. 2004. Vascular endothelial growth factor and angiogenesis. Pharmacological Reviews, 56, (4) 549-580

Hollinger, J.O. & Kleinschmidt, J.C. 1990. The critical size defect as an experimental model to test bone repair materials. The Journal of craniofacial surgery.1, (1) 60-68

Hollinger, J.O. & Leong, K. 1996. Poly (alpha-hydroxy acids): Carriers for bone morphogenetic proteins. Biomaterials, 17, (2) 187-194

Hollister, S.J. 2005. Porous scaffold design for tissue engineering. Nature Materials, 4, (7) 518-524

Honma, K., Kobayashi, T., Nakajima, T., & Hayasi, T. 1999. Computed tomographic evaluation of bone formation after secondary bone grafting of alveolar clefts. Journal of Oral and Maxillofacial Surgery, 57, (10) 1209-1213

Horwitz, E.M., Le, B.K., Dominici, M., Mueller, I., Slaper-Cortenbach, I., Marini, F.C., Deans, R.J., Krause, D.S., Keating, A., & International Society for Cellular Therapy 2005. Clarification of the nomenclature for MSC: The International Society for Cellular Therapy position statement. Cytotherapy, 7, (5) 393-395

Hou, Q., De Bank, P., & Shakesheff, K. 2004. Injectable scaffolds for tissue regeneration. Journal of Materials Chemistry, 14, (0) 1915-1923

Hu, G., Xiao, L., Fu, H., Bi, D., Ma, H., & Tong, P. 2010. Study on injectable and degradable cement of calcium sulphate and calcium phosphate for bone repair. Journal of Materials Science-Materials in Medicine, 21, (2) 627-634

Huan, Z. & Chang, J. 2007. Self-setting properties and in vitro bioactivity of calcium sulfate hemihydrate-tricalcium silicate composite bone cements. Acta Biomaterialia, 3, (6) 952-960

Huang, G., Gronthos, S., & Shi, S. 2009. Mesenchymal Stem Cells Derived from Dental Tissues vs. Those from OtherSources: Their Biology and Role in Regenerative Medicine. Journal of Dental Research, 88, (9) 792-806

Hubbell, J.A. 2003. Materials as morphogenetic guides in tissue engineering. Current Opinion in Biotechnology, 14, (5) 551-558

Hughes, G.C., Biswas, S.S., Yin, B.L., Coleman, R.E., DeGrado, T.R., Landolfo, C.K., Lowe, J.E., Annex, B.H., & Landolfo, K.P. 2004. Therapeutic angiogenesis in chronically ischemic porcine myocardium: Comparative effects of bFGF and VEGF. Annals of Thoracic Surgery, 77, (3) 812-818

Huibregtse, B.A., Johnstone, B., Goldberg, V.M., & Caplan, A.I. 2000. Effect of age and sampling site on the chondro-osteogenic potential of rabbit marrow-derived mesenchymal progenitor cells. Journal of Orthopaedic Research, 18, (1) 18-24

Ilan, D.I. & Ladd, A.L. 2002. Bone graft substitutes. Operative Techniques in Plastic and Reconstructive Surgery, 9, (4) 151-160

Jager, M. & Wilke, A. 2003. Comprehensive biocompatibility testing of a new PMMA-hA bone cement versus conventional PMMA cement in vitro. Journal of Biomaterials Science, Polymer Edition, 14, (11) 1283-1298

Jędrusik-Pawłowska. M., Kromka-Szydek. M., Katra. M., Niedzielska. I. 2013. Mandibular reconstruction – biomechanical strength analysis (FEM) based on a retrospective clinical analysis of selected patients. Acta of Bioengineering and Biomechanicsol, 15, (2) 24-31.

Jensen, M.E., Evans, A.J., Mathis, J.M., Kallmes, D.F., Cloft, H.J., & Dion, J.E. 1997. Percutaneous polymethylmethacrylate vertebroplasty in the treatment of osteoporotic vertebral body compression fractures: technical aspects. Ajnr: American Journal of Neuroradiology, 18, (10) 1897-1904

Jiang, X., Gittens, S., Chang, Q., Zhang, X., Chen, C., & Zhang, Z. 2006. The use of tissue-engineered bone with human bone morphogenetic protein-4-modified bone-marrow stromal cells in repairing mandibular defects in rabbits. International Journal of Oral and Maxillofacial Surgery, 35, (12) 1133-1139

Jovanovic, S.A., Hunt, D.R., Bernard, G.W., Spiekermann, H., Wozney, J.M., & Wikesjoe, U.M. 2007. Bone reconstruction following implantation of rhBMP-2 and guided bone regeneration in canine alveolar ridge defects. Clinical Oral Implants Research, 18, (2) 224-230

Joyner, C.J., Bennett, A., & Triffitt, J.T. 1997. Identification and enrichment of human osteoprogenitor cells by using differentiation stage-specific monoclonal antibodies. Bone, 21, (1) 1-6

Kaiser, S., Hackanson, B., Follo, M., Mehlhorn, A., Geiger, K., Ihorst, G., & Kapp, U. 2007. BM cells giving rise to MSC in culture have a heterogeneous CD34 and CD45 phenotype. Cytotherapy, 9, (5) 439-450

Kang, S.W., Yang, H.S., Seo, S.W., Han, D.K., & Kim, B.S. 2008. Apatite-coated poly (lactic-co-glycolic acid) microspheres as an injectable scaffold for bone tissue engineering. Journal of Biomedical Materials Research.Part A, 85, (3) 747-756

Kamegai, A., Shimamura, N., Naitou, K., Nagahara, K., Kanematsu, N., & Mori, M. 1994. Bone formation under the influence of bond morphogenetic protein/self-setting apatite cement composite as a delivery system. Bio-medical materials and engineering, 4, (4) 291-307

Karageorgiou, V. & Kaplan, D. 2005. Porosity of 3D biornaterial scaffolds and osteogenesis. Biomaterials, 26, (27) 5474-5491

Karr. J.C., Lauretta. J., Keriazes. G.2011. In Vitro Antimicrobial Activity of Calcium Sulfate and Hydroxyapatite (Cerament Bone Void Filler) Discs Using Heat-Sensitive and Non-Heat-sensitive Antibiotics Against Methicillin-Resistant Staphylococcus aureus and Pseudomonas aeruginosa. Journal of the American Podiatric Medical Association ,101, (2)146-52

Kelly, C.M. 2001. The use of a surgical grade calcium sulfate as a bone graft substitute: results of a multicenter trial. Clinical Orthopedics, 382, (0) 42-50

Kern, S., Eichler, H., Stoeve, J., Klueter, H., & Bieback, K. 2006. Comparative analysis of mesenchymal stem cells from bone marrow, umbilical cord blood, or adipose tissue. Stem Cells, 24, (5) 1294-1301

Kessler, P., Thorwarth, M., Bloch-Birkholz, A., Nkenke, E., & Neukam, F.W. 2005. Harvesting of bone from the iliac crest - comparison of the anterior and posterior sites. British Journal of Oral & Maxillofacial Surgery, 43, (1) 51-56

Khadka, A., Li, J., Li, Y., Gao, Y., Zuo, Y., & Ma, Y. 2011. Evaluation of hybrid porous biomimetic nano-hydroxyapatite/polyamide 6 and bone marrow-derived stem cell construct in repair of calvarial critical size defect. Journal of Craniofacial Surgery, 22, (5) 1852-1858

Kim, J.W., Choi, K.H., Yun, J.H., Jung, U.W., Kim, C.S., Choi, S.H., & Cho, K.S. 2011. Bone formation of block and particulated biphasic calcium phosphate lyophilized with Escherichia coli-derived recombinant human bone morphogenetic protein 2 in rat calvarial defects. Oral Surgery Oral Medicine Oral Pathology Oral Radiology and Endodontology, 112, (3) 298-306

Kim, B.C., Yoon, J.H., Choi, B., & Lee, J. 2013b. Mandibular reconstruction with autologous human bone marrow stem cells and autogenous bone graft in a patient with plexiform ameloblastoma. The Journal of craniofacial surgery, 24, (4) e409-e411

Kim, J., Yang, H.J., Cho, T.H., Lee, S.E., Park, Y.D., Kim, H.M., Kim, I.S., Seo, Y.k., Hwang, S.J., & Kim, S.J. 2013a. Enhanced regeneration of rabbit mandibular defects through a combined treatment of electrical stimulation and rhBMP-2 application. Medical & Biological Engineering & Computing, 51, (12) 1339-1348

Kinoshita, Y., Kobayashi, M., Hidaka, T., & Ikada, Y. 1997. Reconstruction of mandibular continuity defects in dogs using poly (L-lactide) mesh and autogenic particulate cancellous

bone and marrow: Preliminary report. Journal of Oral and Maxillofacial Surgery, 55, (7) 718-723

Kimsal .J. Baack. B., Candelaria. L., Khraishi. T., Lovald. S. 2011.   Biomechanical Analysis of Mandibular Angle Fractures. Craniomaxillofacil trauma; doi:10.1016/j.joms.2010.12.042

Kirkerhead, C.A., Gerhart, T.N., Schelling, S.H., Hennig, G.E., Wang, E., & Holtrop, M.E. 1995. Long-Term Healing of Bone Using Recombinant Human Bone Morphogenetic Protein-2. Clinical Orthopaedics and Related Research, 0, (318) 222-230

Kokemueller, H., Spalthoff, S., Nolff, M., Tavassol, F., Essig, H., Stuehmer, C., Bormann, K., Ruecker, M., & Gellrich, N. 2010. Prefabrication of vascularized bioartificial bone grafts in vivo for segmental mandibular reconstruction: experimental pilot study in sheep and first clinical application. International Journal of Oral and Maxillofacial Surgery, 39, (4) 379-387

Kolf, C.M., Cho, E., & Tuan, R.S. 2007. Mesenchymal stromal cells - Biology of adult mesenchymal stem cells: regulation of niche, self-renewal and differentiation. Arthritis Research & Therapy, 9, (1) 204

Kokubo, T., Miyaji, F., Kim, H.M., & Nakamura, T. 1996. Spontaneous formation of bonelike apatite layer on chemically treated titanium metals. Journal of the American Ceramic Society, 79, (4) 1127-1129

Kokubo, S., Fujimoto, R., Yokota, S., Fukushima, S., Nozaki, K., Takahashi, K., & Miyata, K. 2003. Bone regeneration by recombinant human bone morphogenetic protein-2 and a novel biodegradable carrier in a rabbit ulnar defect model. Biomaterials, 24, (9) 1643-1651

Kon, E., Muraglia, A., Corsi, A., Bianco, P., Marcacci, M., Martin, I., Boyde, A., Ruspantini, I., Chistolini, P., Rocca, M., Giardino, R., Cancedda, R., & Quarto, R. 2000. Autologous bone marrow stromal cells loaded onto porous hydroxyapatite ceramic accelerate bone repair in critical-size defects of sheep long bones. Journal of Biomedical Materials Research, 49, (3) 328-337

Krebsbach, P.H., Kuznetsov, S.A., Satomura, K., Emmons, R.V., Rowe, D.W., & Robey, P.G. 1997. Bone formation in vivo: comparison of osteogenesis by transplanted mouse and human marrow stromal fibroblasts. Transplantation, 63, (8) 1059-1069

Kuboki, Y., Saito, T., Murata, M., Takita, H., Mizuno, M., Inoue, M., Nagai, N., & Poole, A.R. 1995. Two distinctive BMP-carriers induce zonal chondrogenesis and membranous ossification, respectively; Geometrical factors of matrices for cell-differentiation. Connective Tissue Research, 32, (4) 219-226

Kulakov, A., Goldshtein, D., V, Grigoryan, A., Rzhaninova, A., Alekseeva, I., Arutyunyan, I., V, & Volkov, A., V 2008. Clinical Study of the Efficiency of Combined Cell Transplant on the Basis of Multipotent Mesenchymal Stromal Adipose Tissue Cells in Patients with Pronounced Deficit of the Maxillary and Mandibulary Bone Tissue. Bulletin of Experimental Biology and Medicine, 146, (4) 522-525

Kulterer, B., Friedl, G., Jandrositz, A., Sanchez-Cabo, F., Prokesch, A., Paar, C., Scheideler, M., Windhager, R., Preisegger, K.H., & Trajanoski, Z. 2007. Gene expression profiling of human mesenchymal stem cells derived from bone marrow during expansion and osteoblast differentiation. Bmc Genomics, 8, (0) 70-81

Laquerriere, P., Grandjean-Laquerriere, A., Jallot, E., Balossier, G., Frayssinet, P., & Guenounou, M. 2003. Importance of hydroxyapatite particles characteristics on cytokines production by human monocytes in vitro. Biomaterials, 24, (16) 2739-2747

Laschke, M.W., Elitzsch, A., Vollmar, B., Vajkoczy, P., & Menger, M.D. 2006. Combined inhibition of vascular endothelial growth factor (VEGF), fibroblast growth factor and platelet-derived growth factor, but not inhibition of VEGF alone, effectively suppresses angiogenesis and vessel maturation in endometriotic lesions. Human Reproduction, 21, (1) 262-268

Lazary, A., Balla, B., Kosa, J.P., Bacsi, K., Nagy, Z., Takacs, I., Varga, P.P., Speer, G., & Lakatos, P. 2007. Effect of gypsum on proliferation and differentiation of MC3T3-E1 mouse osteoblastic cells. Biomaterials, 28, (3) 393-399

Le Nihouannen.D., Daculsi, G., Saffarzadeh, A., Gauthier, O., Delplace, S., Pilet, P., & Layrolle, P. 2005. Ectopic bone formation by microporous calcium phosphate ceramic particles in sheep muscles. Bone, 36, (6) 1086-1093

Le Nihouannen, D., Saffarzadeh, A., Gauthier, O., Moreau, F., Pilet, P., Spaethe, R., Layrolle, P., & Daculsi, G. 2008. Bone tissue formation in sheep muscles induced by a biphasic calcium phosphate ceramic and fibrin glue composite. Journal of Materials Science-Materials in Medicine, 19, (2) 667-675

Lee, K.J.H., Roper, J.G., & Wang, J.C. 2005. Demineralized bone matrix and spinal arthrodesis. The Spine Journal, 5, (6) S217-S223

Lee, H.J., Choi, B.H., Min, B.H., & Park, S.R. 2007. Low-intensity ultrasound inhibits apoptosis and enhances viability of human mesenchymal stem cells in three-dimensional alginate culture during chondrogenic differentiation. Tissue Engineering, 13, (5) 1049-1057

Lee, J., Sung, H.M., Jang, J.D., Park, Y.W., Min, S.K., & Kim, E.C. 2010a. Successful Reconstruction of 15-cm Segmental Defects by Bone Marrow Stem Cells and Resected Autogenous Bone Graft in Central Hemangioma. Journal of Oral and Maxillofacial Surgery, 68, (1) 188-194

Lee, T.J., Kang, S.W., Bhang, S.H., Kang, J.M., & Kim, B.S. 2010b. Apatite-Coated Porous Poly (lactic-co-glycolic acid) Microspheres as an Injectable Bone Substitute. Journal of Biomaterials Science-Polymer Edition, 21, (5) 635-645

Lee, B.K., Choi, S.J., Mack, D., & Oh, S.H. 2011. Isolation of mesenchymal stem cells from the mandibular marrow aspirates. Oral Surgery Oral Medicine Oral Pathology Oral Radiology and Endodontology, 112, (6) E86-E93

Lendeckel, S., Jodicke, A., Christophis, P., Heidinger, K., Wolff, J., Fraser, J.K., Hedrick, M.H., Berthold, L., & Howaldt, H.P. 2004. Autologous stem cells (adipose) and fibrin glue used to treat widespread traumatic calvarial defects: case report. Journal of Cranio-Maxillofacial Surgery, 32, (6) 370-373

Lewis, G. 2011. Viscoelastic properties of injectable bone cements for orthopaedic applications: state-of-the-art review. Journal of Biomedical Materials Research.Part B, Applied Biomaterials , 98, (1) 171-191

Li, J., Li, Y., Ma, S., Gao, Y., Zuo, Y., & Hu, J. 2010. Enhancement of bone formation by BMP-7 transduced MSCs on biomimetic nano-hydroxyapatite/polyamide composite scaffolds in repair of mandibular defects. Journal of Biomedical Materials Research Part A, 95A, (4) 973-981

Lieberman, J.R., Daluiski, A., & Einhorn, T.A. 2002. The role of growth factors in the repair of bone - Biology and clinical applications. Journal of Bone and Joint Surgery-American Volume, 84A, (6) 1032-1044

Lindon, C., Montarras, D., & Pinset, C. 1998. Cell cycle-regulated expression of the muscle determination factor Myf5 in proliferating myoblasts. Journal of Cell Biology, 140, (1) 111-118

Lippens, E., Vertenten, G., Girones, J., Declercq, H., Saunders, J., Luyten, J., Duchateau, L., Schacht, E., Vlaminck, L., Gasthuys, F., & Cornelissen, M. 2010. Evaluation of Bone Regeneration with an Injectable, In Situ Polymerizable Pluronic (R) F127 Hydrogel Derivative Combined with Autologous Mesenchymal Stem Cells in a Goat Tibia Defect Model. Tissue Engineering Part A, 16, (2) 617-627

Liu, H.Y., Liu, X., Zhang, L.P., Ai, H.J., & Cui, F.Z. 2010. Improvement on the performance of bone regeneration of calcium sulfate hemihydrate by adding mineralized collagen. Tissue engineering.Part A., 16, (6) 2075-2084

Liu, F., Porter, R.M., Wells, J., Glatt, V., Pilapil, C., & Evans, C.H. 2012. Evaluation of BMP-2 gene-activated muscle grafts for cranial defect repair. Journal of Orthopaedic Research, 30, (7) 1095-1102

Liu, X., Wang, X.M., Chen, Z.G., Cui, F.Z., Liu, H.Y., Mao, K.Y., & Wang, Y. 2010. Injectable bone cement based on mineralized collagen. Journal of Biomedical Materials Research Part B-Applied Biomaterials, 94B, (1) 72-79

Louis, P., Holmes, J., & Fernandes, R. 2004. Resorbable mesh as a containment system in reconstruction of the atrophic mandible fracture. Journal of Oral and Maxillofacial Surgery, 62, (6) 719-723

Lu, J.X., Blary, M.C., Vavasseur, S., Descamps, M., Anselme, K., & Hardouin, P. 2004. Relationship between bioceramics sintering and micro-particles-induced cellular damages. Journal of Materials Science-Materials in Medicine, 15, (4) 361-365

Lynch, S., Marx, R.E., Nevins, M., & Wisner-Lynch, L. 2008. Introduction. Tissue Engineering Application in Oral & Maxillofacial Surgery and Periodontics, 2nd edn ed. Quintessence book

Ma, X., Wang, Y., Guo, H., & Wang, J. Nano-hydroxyapatite/chitosan sponge-like biocomposite for repairing of rat calvarial critical-sized bone defect.2011. Journal of Bioactive and Compatible Polymers, 26, (4) 335-346

Mah, P. & Mcdavid, W. D. 2012, Radiographic device for deriving correlation between measured grey levels in image, attenuation coefficients and computed tomography numbers of e.g. adipose tissues, has reference objects placed in or on body positioned in mouth of human, WO2013003533-A1, Univ Texas System, (patent)

Mankani, M.H., Kuznetsov, S.A., Wolfe, R.M., Marshall, G.W., & Robey, P.G. 2006. In vivo bone formation by human bone marrow stromal cells: Reconstruction of the mouse calvarium and mandible. Stem Cells, 24, (9) 2140-2149

Mankani, M.H., Kuznetsov, S.A., Marshall, G.W., & Robey, P.G. 2008. Creation of New Bone by the Percutaneous Injection of Human Bone Marrow Stromal Cell and HA/TCP Suspensions. Tissue Engineering Part A, 14, (12) 1949-1958

Mao, J., Giannobile, W., V, Helms, J., Hollister, S., Krebsbach, P., Longaker, M., & Shi, S. 2006. Craniofacial tissue engineering by stem cells. Journal of Dental Research, 85, (11) 966-979

Marcia, S., Boi, C., Dragani, M., Marini, S., Marras, M., Piras, E., Anselmetti, G.C., & Masala, S. 2012. Effectiveness of a bone substitute (CERAMENT®) as an alternative to PMMA in percutaneous vertebroplasty: 1-year follow-up on clinical outcome. European spine journal, 21, (Suppl 1) S112-S118

Mareschi, K., Biasin, E., Piacibello, W., Aglietta, M., Madon, E., & Fagioli, F. 2001. Isolation of human mesenchymal stem cells: bone marrow versus umbilical cord blood. Haematologica, 86, (10) 1099-1100

Martin, I., Muraglia, A., Campanile, G., Cancedda, R., & Quarto, R. 1997. Fibroblast growth factor-2 supports ex vivo expansion and maintenance of osteogenic precursors from human bone marrow. Endocrinology, 138, (10) 4456-4462

Marukawa, E., Asahina, I., Seto, I., Omura, K., & Enomoto, S. 2002. Tissue Engineering For Therapeutic Use 6 International congress series, Application of bone morphogenetic proteins (BMP) to oral rehabilitation. Elsevier Science Bv, Amsterdam, pp- 129-132

Marx, R.E., Armentano, L., Olavarria, A., & Samaniego, J. 2013. rhBMP-2/ACS Grafts Versus Autogenous Cancellous Marrow Grafts in Large Vertical Defects of the Maxilla: An Unsponsored Randomized Open-Label Clinical Trial. International Journal of Oral & Maxillofacial Implants, 28, (5) e243-e251

Masala, S., Nano, G., Marcia, S., Muto, M., Fucci, F.P.M., & Simonetti, G. 2012. Osteoporotic vertebral compression fractures augmentation by injectable partly resorbable ceramic bone substitute (CERAMENT (TM)|SPINE SUPPORT): a prospective nonrandomized study. Neuroradiology, 54, (6) 589-596

Matos, M.A., Gonçalves, R.R., Araújo, F.P. 2001. Experimental model for osteotomy in immature rabbit. Acta Ortopédica Brasileira, 9, 21-6

McBeath, R., Pirone, D.M., Nelson, C.M., Bhadriraju, K., & Chen, C.S. 2004. Cell shape, cytoskeletal tension, and RhoA regulate stem cell lineage commitment. Developmental Cell, 6, (4) 483-495

McMurray, R.J., Gadegaard, N., Tsimbouri, P., Burgess, K.V., McNamara, L.E., Tare, R., Murawski, K., Kingham, E., Oreffo, R.O., & Dalby, M.J. 2011. Nanoscale surfaces for the long-term maintenance of mesenchymal stem cell phenotype and multipotency. Nature Materials, 10, (8) 637-644

Merkx M.A., Fennis J.P., Verhagen C.M., Stoelinga P.J.2004. Reconstruction of the mandible using preshaped 2.3 mm titanium plates, autogenous particulate cortico-can- cellous bone grafts and platelet rich plasma: a report on eight patients, International Journal of Oral Maxillofacial. Surgery, 33, (8) 733– 739.

Mesimaki, K., Lindroos, B., Tornwall, J., Mauno, J., Lindqvist, C., Kontio, R., Miettinen, S., & Suuronen, R. 2009. Novel maxillary reconstruction with ectopic bone formation by GMP adipose stem cells. International Journal of Oral and Maxillofacial Surgery, 38, (3) 201-209

Mezey, E., Chandross, K.J., Harta, G., Maki, R.A., & McKercher, S.R. 2000. Turning blood into brain: cells bearing neuronal antigens generated in vivo from bone marrow. Science, 290, (5497) 1779-1782

Minamide, A., Yoshida, M., Kawakami, M., Yamasaki, S., Kojima, H., Hashizume, H., & Boden, S.D. 2005. The use of cultured bone marrow cells in type I collagen gel and porous hydroxyapatite for posterolateral lumbar spine fusion. Spine, 30, (10) 1134-1138

Moghadam, H.G., Urist, M.R., Sandor, G.K., & Clokie, C.M. 2001. Successful mandibular reconstruction using a BMP bioimplant. Journal of Craniofacial Surgery, 12, (2) 119-127

Moghadam, H.G., Sandor, G.K.B., Holmes, H.H.I., & Clokie, C.M.L. 2004. Histomorphometric evaluation of bone regeneration using allogeneic and alloplastic bone substitutes. Journal of Oral and Maxillofacial Surgery, 62, (2) 202-213

Mohan, S. & Baylink, D.J. 1991. Evidence That the Inhibition of Te85 Human Bone Cell-Proliferation by Agents Which Stimulate Camp Production May in Part be Mediated by Changes in the Igf-Ii Regulatory System. Growth Regulation, 1, (3) 110-118

Molteni, R. 2013. Prospects and challenges of rendering tissue density in Hounsfield units for cone beam computed tomography. Oral Surgery Oral Medicine Oral Pathology Oral Radiology, 116, (1) 105-119

Morejon-Alonso, L., Barsiro Ferreira, O.J., Garcia Carrodeguas, R., & Alberto dos Santos, L. 2012. Bioactive composite bone cement based on a-tricalcium phosphate/tricalcium silicate. Journal of Biomedical Materials Research Part B-Applied Biomaterials, 100B, (1) 94-102

Mulconrey, D.S., Bridwell, K.H., Flynn, J., Cronen, G.A., & Rose, P.S. 2008. Bone morphogenetic protein (RhBMP-2) as a substitute for iliac crest bone graft in multilevel adult spinal deformity surgery. Spine, 33, (20) 2153-2159

Muller, A. 1933. Die Kaumuskulatur des Hydrochoerus capybara und ihre Bedeutung fur die Formgestaltung des Schadels. Gegen- baurs Morphol. Jahrb,72, l-59.

Muller, R. and Ruegsegger, P., 1997. Micro-tomographic imaging for the nondestructive evaluation of trabecular bone architecture. Bone Research In Biomechanics Studies In Health Technology And Informatics., vol. 40:I O S press,Amsterdam, pp.61-79.

Muller, R., Van Campenhout, H., Van Damme, B., Van Der Perre, G., Dequeker, J., Hildebrand, T., & Ruegsegger, P. 1998. Morphometric analysis of human bone biopsies: A quantitative structural comparison of histological sections and micro-computed tomography. Bone, 23, (1) 59-66

Muschler, G.F. & Midura, R.J. 2002. Connective tissue progenitors: Practical concepts for clinical applications. Clinical Orthopaedics and Related Research, (395) 66-80

Nagasao T., Kobayashi M., Tsuchiya Y., Kaneko T., Nakajima T.2002. Finite element analysis of the stresses around endosseous implants in various reconstructed mandibular models, Journal of Craniomaxillofacial Surgery, 30, (3) 170–177

Naito, H., Dohi, Y., Zimmermann, W.H., Tojo, T., Takasawa, S., Eschenhagen, T., & Taniguchi, S. 2011. The Effect of Mesenchymal Stem Cell Osteoblastic Differentiation on the Mechanical Properties of Engineered Bone-Like Tissue. Tissue Engineering Part A, 17, (18) 2321-2329

Naito, H., Yoshimura, M., Mizuno, T., Takasawa, S., Tojo, T., & Taniguchi, S. 2013. The advantages of three-dimensional culture in a collagen hydrogel for stem cell differentiation. Journal of Biomedical Materials Research Part A, 101, (10) 2838-2845

Nakano, M., Hirano, N., Ishihara, H., Kawaguchi, Y., & Matsuura, K. 2005. Calcium phosphate cement leakage after percutaneous vertebroplasty for osteoporotic vertebral fractures: risk factor analysis for cement leakage. Journal of Neurosurgery Spine, 2, (1) 27-33

Niemeyer, P., Kornacker, M., Mehlhorn, A., Seckinger, A., Vohrer, J., Schmal, H., Kasten, P., Eckstein, V., Suedkamp, N.P., & Krause, U. 2007. Comparison of immunological properties of bone marrow stromal cells and adipose tissue-derived stem cells before and after osteogenic differentiation in vitro. Tissue Engineering, 13, (1) 111-

Nilsson, M. 2003. Injectable Calcium Sulphate and Calcium Ohosphate Bone Substitutes. PhD Lund University, Faculty of Medicine, Lund, Sweden.

Nilsson, M., Wielanek, L., Wang, J.-S., Tanner, K.E., & Lidgren, L. 2003. Factors influencing the compressive strength of an injectable calcium sulfate-hydroxyapatite cement. Journal of Materials Science: Materials in Medicine, 14, (5) 399-404

Nunamaker, D.M. 1998. Experimental models of fracture repair. Clinical Orthopic Related Research, 355s, 56-65.

Oberoi, S., Chigurupati, R., Gill, P., Hoffman, W.Y., & Vargervik, K. 2009. Volumetric Assessment of Secondary Alveolar Bone Grafting Using Cone Beam Computed Tomography. Cleft Palate-Craniofacial Journal, 46, (5) 503-511

Ohgushi, H. & Caplan, A.I. 1999. Stem cell technology and bioceramics: From cell to gene engineering. Journal of Biomedical Materials Research, 48, (6) 913-927

Ohishi, M. & Schipani, E. 2010. Bone Marrow Mesenchymal Stem Cells. Journal of Cellular Biochemistry, 109, (2) 277-282

Ohura, K., Irie, H., & Hamanishi, C. 2000. Healing of segmental ulnar defects in dog using bioresorbable calcium phosphate cement added with recombinant human bone morphogenetic protein-2.13th International Symposium on Ceramic in Medicine /Symposium on Ceramic Materials in Orthopaedic Surgery: Clinical Results in the Year 2000, Bologna, Italy.

Ormsby, R., McNally, T., O'Hare, P., Burke, G., Mitchell, C., & Dunne, N. 2012. Fatigue and biocompatibility properties of a poly(methyl methacrylate) bone cement with multi-walled carbon nanotubes. Acta Biomaterialia, 8, (3) 1201-1212

Orr, T.E., Villars, P.A., Mitchell, S.L., Hsu, H.P., & Spector, M. 2001. Compressive properties of cancellous bone defects in a rabbit model treated with particles of natural bone mineral and synthetic hydroxyapatite. Biomaterials, 22, (14) 1953-1959

Oswald, J., Boxberger, S., Jorgensen, B., Feldmann, S., Ehninger, G., Bornhauser, M., & Werner, C. 2004. Mesenchymal stem cells can be differentiated into endothelial cells in vitro. Stem Cells, 22, (3) 377-384

Owen, M. & Friedenstein, A.J. 1988. Stromal stem cells: marrow-derived osteogenic precursors. Ciba Foundation Symposium, 136, (0) 42-60

Palarie, V.P. 2008. Collagen/calcium phosphate and bone marrow aspirate in new bone formation at the mandible jaw. Bone, 42, S27-S28

Payton E, Nolze G 2013. The Backscatter Electron Signal as an Additional Tool for Phase Segmentation in Electron Backscatter Diffraction. Microscopy and Microanalysis;19(04) 929-941

Peltier, L.F. 1961. The use of plaster of Paris to fill defects in bone. Clinical orthopaedics, 21, 1-31

Pepiol, A., Teixidor, F., Saralidze, K., van der Marel, C., Willems, P., Voss, L., Knetsch, M.L., Vinas, C., & Koole, L.H. 2011. A highly radiopaque vertebroplasty cement using tetraiodinated o-carborane additive.   Biomaterials, 32, (27) 6389-6398

Perciaccante, V. & Jeffery, J. 2007, "Oral & maxillofacial Reconstruction," In Oral &Maxillofacil Secrets, 2 ed. O. AbuBake & K. Benson, eds., PA, Philiadephia, USA: Elsevier, pp. 389-403.

Petrie, A., Bulman, J.S., & Osborn, J.F. 2002. Further statistics in dentistry - Part 1: Research designs 1. British Dental Journal, 193, (7) 377-380

Pietrzak, W.S. & Ronk, R. 2000. Calcium sulfate Bone Void filler: A review and a look ahead. Journal of Craniofacial Surgery, 11, (4) 327-333

Pittenger, M.F., Mackay, A.M., Beck, S.C., Jaiswal, R.K., Douglas, R., Mosca, J.D., Moorman, M.A., Simonetti, D.W., Craig, S., & Marshak, D.R. 1999. Multilineage potential of adult human mesenchymal stem cells. Science, 284, (5411) 143-147

Porada, C., Zanjani, E., & Almeida-Porad, G. 2006. Adult mesenchymal stem cells: a pluripotent population with multiple applications. Current Stem Cell Research Therapy, 1, 365-369

Presta, M., Dell'Era, P., Mitola, S., Moroni, E., Ronca, R., & Rusnati, M. 2005. Fibroblast growth factor/fibroblast growth factor receptor system in angiogenesis. Cytokine & Growth Factor Reviews, 16, (2) 159-178

Qing, X., Rong-Fa, B., Hong-chen, L., & Tian-qiu, M. 2006. Reconstruction of caprine mandibular segmental defect by tissue engineered bone reinforeced by titanium reticulum. Chinese Journal of Traumatology, 9, (2) 67-71

Rappaport, I. 1971. The particulate graft in tumour surgery. Am J Surg, 122, (0) 748-755

Rauschmann, M.A., Wichelhaus, T.A., Stirnal, V., Dingeldein, E., Zichner, L., Schnettler, R., & Alt, V. 2005. Nanocrystalline hydroxyapatite and calcium sulphate as biodegradable composite carrier material for local delivery of antibiotics in bone infections. Biomaterials, 26, (15) 2677-2684

Rauschmann, M., Vogl, T., Verheyden, A., Pflugmacher, R., Werba, T., Schmidt, S., & Hierholzer, J. 2010. Bioceramic vertebral augmentation with a calcium sulphate/hydroxyapatite composite (Cerament [TM] SpineSupport) in vertebral compression fractures due to osteoporosis. European Spine Journal, 19, (6) 887-892

Rawlings, C.E., Wilkins, R.H., Hanker, J.S., Georgiade, N.G., & Harrelson, J.M. 1988. Evaluation in Cats of A New Material for Cranioplasty - A Composite of Plaster of Paris and Hydroxylapatite. Journal of Neurosurgery, 69, (2) 269-275

Reikeras, O., Reinholt, F.P., Zinoecker, S., Shegarfi, H., & Rolstad, B. 2011. Healing of Long-term Frozen Orthotopic Bone Allografts is not Affected by MHC Differences Between Donor and Recipient. Clinical Orthopaedics and Related Research, 469, (5) 1479:

Ren, T.B., Ren, J., Jia, X.Z., & Pan, K.F. 2005. The bone formation in vitro and mandibular defect repair using PLGA porous scaffolds. Journal of Biomedical Materials Research Part A, 74A, (4) 562-569

Resnick, D.K. 2002. Vitoss bone substitute. Neurosurgery, 50, (5) 1162-1164

Reyes, M., Dudek, A., Jahagirdar, B., Koodie, L., Marker, P.H., & Verfaillie, C.M. 2002. Origin of endothelial progenitors in human postnatal bone marrow. Journal of Clinical Investigation, 109, (3) 337-346

Reyes, M., Lund, T., Lenvik, T., Aguiar, D., Koodie, L., & Verfaillie, C.M. 2001. Purification and ex vivo expansion of postnatal human marrow mesodermal progenitor cells. Blood, 98, (9) 2615-2625

Riccio, M., Resca, E., Maraldi, T., Pisciotta, A., Ferrari, A., Bruzzesi, G., & De Pol, A. 2010. Human dental pulp stem cells produce mineralized matrix in 2D and 3D cultures. European Journal of Histochemistry, 54, (4) 213-221

Rodan, S.B., Wesolowski, G., Thomas, K.A., Yoon, K.G., & Rodan, G.A. 1989. Effects of Acidic and Basic Fibroblast Growth-Factors on Osteoblastic Cells. Connective Tissue Research, 20, (4) 283-288

Ruhe, P.Q., Hedberg, E.L., Padron, N.T., Spauwen, P.H.M., Jansen, J.A., & Mikos, A.G. 2003. rhBMP-2 release from injectable poly(DL-lactic-co-glycolic acid)/calcium-phosphate cement composites. Journal of Bone and Joint Surgery-American, 85A, (0) 75-81

Ryu, Y.M., Hah, Y.S., Park, B.W., Kim, D.R., Roh, G.S., Kim, J.R., Kim, U.K., Rho, G.J., Maeng, G.H., & Byun, J.H. 2011. Osteogenic differentiation of human periosteal-derived cells in a three-dimensional collagen scaffold. Molecular Biology Reports, 38, (5) 2887-2894

Samman, N., Luk, W.K., Chow, T.W., Cheung, L.K., Tideman, H., & Clark, R.K.F. 1999. Custom-made titanium mandibular reconstruction tray. Australian Dental Journal, 44, (3) 195-199

Santic .V. Zori., Cvek. Z.C., Branko.S., Bobinac. S.,Tudor. A., Miletic.D., Nemec. B.2009 Treatment of Tibial Bone Defect with Rotational Vascular Periosteal Graft in Rabbits. Collegium Antropologicum, 33, (1) 43–50

Satomura, K., Krebsbach, P., Bianco, P., & Robey, P.G. 2000. Osteogenic imprinting upstream of marrow stromal cell differentiation. Journal of Cellular Biochemistry, 78, (3) 391-403

Scaglione, P.H. & Buchman, M.T. 1997. Collagraft bone substitute in upper extremity fractures: A preliminary study. Surgical Forum, 48, 563-565

Schantz, J.T., Hutmacher, D.W., Lam, C.X., Brinkmann, M., Wong, K.M., Lim, T.C., Chou, N., Guldberg, R.E., & Teoh, S.H. 2003. Repair of calvarial defects with customised tissue-

engineered bone grafts II. Evaluation of cellular efficiency and efficacy in vivo. Tissue Engineering, 9, (Suppl) 127-139

Schliephake, H., Knebel, J.W., Aufderheide, M., & Tauscher, M. 2001. Use of cultivated osteoprogenitor cells to increase bone formation in segmental mandibular defects: an experimental pilot study in sheep. International Journal of Oral and Maxillofacial Surgery, 30, (6) 531-537

Schliephake, H., Zghoul, N., Jager, V., van, G.M., Zeichen, J., Gelinsky, M., & Szubtarsky, N. 2009. Bone formation in trabecular bone cell seeded scaffolds used for reconstruction of the rat mandible. International Journal of Oral and Maxillofacial Surgery.38, (2) 166-172

Schmitz, J.P. & Hollinger, J.O. 1986. The Critical Size Defect As An Experimental-Model for Craniomandibulofacial Nonunions. Clinical Orthopaedics and Related Research ,0 ,(205) 299-308

Schwartz, R.E., Reyes, M., Koodie, L., Jiang, Y., Blackstad, M., Lund, T., Lenvik, T., Johnson, S., Hu, W.S., & Verfaillie, C.M. 2002. Multipotent adult progenitor cells from bone marrow differentiate into functional hepatocyte-like cells. Journal of Clinical Investigation, 109, (10) 1291-1302

Seeherman, H.J., Bouxsein, M., Kim, H., Li, R., Li, X.J., Aiolova, M., & Wozney, J.M. 2004. Recombinant human bone morphogenetic protein-2 delivered in an injectable calcium phosphate paste accelerates osteotomy-site healing in a non-human primate model. Journal of Bone and Joint Surgery-American Volume, 86A, (9) 1961-1972

Sen, M. & Miclau, T. 2007. Autologous iliac crest bone graft: Should it still be the gold standard for treating nonunions? Injury-International Journal of the Care of the Injured, 38, (0) S75-S80

Shields, L.B.E., Raque, G.H., Glassman, S.D., Campbell, M., Vitaz, T., Harpring, J., & Shields, C.B. 2006. Adverse effects associated with high-dose recombinant human bone morphogenetic protein-2 use in anterior cervical spine fusion. Spine, 31, (5) 542-547

Shindo, M.L., Costantino, P.D., Friedman, C.D., & Chow, L.C. 1993. Facial Skeletal Augmentation Using Hydroxyapatite Cement. Archives of Otolaryngology-Head & Neck Surgery, 119, (2) 185-190

Shors, E.C. 1999. Coralline bone graft substitutes. Orthopedic Clinics of North America, 30, (4) 599-608

Shore, E.M. & Laplan, F.S. 2008. Insights from a rare genetic disorder of extra-skeletal bone formation, fibrodysplasia ossificans progressiva (FOP). Bone, 43, (3) 427-433

Sikavitsas, V.I., Van Den Dolder, J., Bancroft, G.N., Jansen, J.A., & Mikos, A.G. 2003. Influence of the in vitro culture period on the in vivo performance of cell/titanium bone tissue-engineered constructs using a rat cranial critical size defect model. Journal of Biomedical Materials Research - Part A.67, (3) 944-951

Simon, C.G.J., Guthrie, W.F., & Wang, F.W. 2004. Cell seeding into calcium phosphate cement. Journal of Biomedical Materials Research.Part A, 68, (4) 628-639

Smiler, D., Soltan, M., & Albitar, M. 2008. Toward the identification of mesenchymal stem cells in bone marrow and peripheral blood for bone regeneration. Implant Dentistry, 17, (3) 236-244

Smucker, J.D., Rhee, J.M., Singh, K., Yoon, S.T., & Heller, J.G. 2006. Increased swelling complications associated with off-label usage of rhBMP-2 in the anterior cervical spine. Spine, 31, (24) 2813-2819

Stephan, S.J., Tholpady, S.S., Gross, B., Petrie-Aronin, C.E., Botchway, E.A., Nair, L.S., Ogle, R.C., & Park, S.S. 2010. Injectable Tissue-Engineered Bone Repair of a Rat Calvarial Defect. Laryngoscope, 120, (5) 895-901

Stevenson, S., Emery, S.E., & Goldberg, V.M. 1996. Factors affecting bone graft incorporation. Clinical Orthopaedics and Related Research, 0, (324) 66-74

Stewart, N.T., Byrne, K.M., Hosick, H.L., Vierck, J.L., & Dodson, M.V. 1999. Traditional and emerging methods for analyzing cell activity in cell culture. Methods in Cell Science, 22, (1) 67-78

Stoltny, T., Koczy, B., Wawrzynek, W., & Miszczyk, L. 2007. Heterotopic ossification in patients after total hip replacement. Ortopedia, traumatologia, rehabilitacja, 9, (3) 264-272

Strocchi, R., Orsini, G., Iezzi, G., Scarano, A., Rubini, C., Pecora, G., & Piattelli, A. 2002. Bone regeneration with calcium sulfate: evidence for increased angiogenesis in rabbits. The Journal of oral implantology, 28, (6) 273-278

Su, J., Xu, H., Sun, J., Gong, X., & Zhao, H. 2013. Dual Delivery of BMP-2 and bFGF from a New Nano-Composite Scaffold, Loaded with Vascular Stents for Large-Size Mandibular Defect Regeneration. International Journal of Molecular Sciences, 14, (6) 12714-12728

Tanner, K.E. 2010. Bioactive composites for bone tissue engineering. Proceedings of the Institution of Mechanical Engineers Part H-Journal of Engineering in Medicine, 224, (H12) 1359-1372

Tay, B.K.B., Patel, V.V., & Bradford, D.S. 1999. Calcium sulfate- and calcium phosphate-based bone substitutes - Mimicry of the mineral phase of bone. Orthopedic Clinics of North America, 30, (4) 615-623

Taylor, G.I. & Ham, F.J. 1976. Free Vascularized Nerve Graft - Further Experimental and Clinical Application of Microvascular Techniques. Plastic and Reconstructive Surgery, 57, (4) 413-426

Thomas, M.V. & Puleo, D.A. 2009. Calcium Sulfate: Properties and Clinical Applications. Journal of Biomedical Materials Research Part B-Applied Biomaterials, 88B, (2) 597-610

Tideman H& Lee.S. 2006. The TL endoprosthesis for mandibular reconstruction – a metallic yet biological approach. Asian J Oral Maxillofac Surg, 16,(0) 5-8

Tideman, H., Samman, N., & Cheung, L.K. 1998. Functional reconstruction of the mandible: a modified titanium mesh system. International Journal of Oral and Maxillofacial Surgery, 27, (5) 339-345

Tiselius, A., Hjerten, S., & Levin, O. 1956. Protein Chromatography on Calcium Phosphate Columns. Archives of Biochemistry and Biophysics, 65, (1) 132-155

Torroni, A. 2009. Engineered Bone Grafts and Bone Flaps for Maxillofacial Defects: State of the Art. Journal of Oral and Maxillofacial Surgery, 67, (5) 1121-1127

Trojani, C., Boukhechba, F., Scimeca, J.C., Vandenbos, F., Michiels, J.F., Daculsi, G., Boileau, P., Weiss, P., Carle, G.F., & Rochel, N. 2006. Ectopic bone formation using an injectable biophasic calcium phosphate/Si-HPMC hydrogel compsite loaded with undifferentiated bone marrow stromal cells. Biomaterials, 27, (0) 3256-3264

Truedsson, A., Wang, J., Lindberg, P., Gordh, M., Sunzel, B., & Warfvinge, G. 2010. Bone substitute as an on-lay graft on rat tibia. Clinical Oral Implants Research, 21, (4) 424-429

Truumees, E. & Herkowitz, H. 1999. Alternative to autologous bone harvest in spine surgery. Univ of Pennsylvania Orthoped Journal, 19,77-88

Turner, C.H., Chandran, A., & Pidaparti, R.M.V. 1995. The Anisotropy of Osteonal Bone and Its Ultrastructural Implications. Bone, 17, (1) 85-89

Ulman, A. 1996. Formation and structure of self-assembled monolayers. Chemical Reviews, 96, (4) 1533-1554

Urist, M.R. 2002. Bone: formation by autoinduction. 1965. Clinical Orthopaedics and Related Research, (395) 4-10

Van der Stelt, P.F. 2008. Better imaging - The advantages of digital radiography. Journal of the American Dental Association, 139, 7S-13S

Van Den Dolder, J., Vehof, J.W.M., Spauwen, P.H.M., & Jansen, J.A. 2002. Bone formation by rat bone marrow cells cultured on titanium fibre mesh: Effect of in vitro culture time. Journal of Biomedical Materials Research, 62, (3) 350-358

Van Gaalen, S.M., Dhert, W.J., Kruyt, M.C., Yuan, H., Oner, F., van Blitterswijk, C.A., Verbout, A.J., & de Bruijn, J.D. 2010b. Goat Bone Tissue Engineering: Comparing an Intramuscular with a Posterolateral Lumbar Spine Location. Tissue Engineering Part A, 16, (2) 685-693

VanderVen, P.F.M. & Furst, D.O. 1997. Assembly of titin, myomesin and M-protein into the sarcomeric M band in differentiating human skeletal muscle cells in vitro. Cell Structure and Function, 22, (1) 163-171

Vannier, M.W. 2003. Craniofacial computed tomography scanning: technology, applications and future trends. Orthodontics & craniofacial research, 1, (6) 23-30

Viswanath, B., Raghavan, R., Gurao, N., Ramamurty, U., & Ravishankar, N. 2008. Mechanical properties of tricalcium phosphate single crystals grown by molten salt synthesis. Acta Biomaterialia, 4, (5) 1448-1454

Von Wilmowsky, C., Schwarz, S., Kerl, J.M., Srour, S., Lell, M., Felszeghy, E., & Schlegel, K.A. 2010. Reconstruction of a mandibular defect with autogenous, autoclaved bone grafts and tissue engineering: An in vivo pilot study. Journal of Biomedical Materials Research Part A, 93A, (4) 1510-1518

Wada, M.R., Inagawa-Ogashiwa, M., Shimizu, S., Yasumoto, S., & Hashimoto, N. 2002. Generation of different fates from multipotent muscle stem cells. Development, 129, (12) 2987-2995

Waitzman, A.A., Posnick, J.C., Armstrong, D.C., & Pron, G.E. 1992. Craniofacial Skeletal Measurements Based on Computed-Tomography .1. Accuracy and Reproducibility. Cleft Palate-Craniofacial Journal, 29, (2) 112-117

Wang, H., Springer, I.N., Schildberg, H., Acil, Y., Ludwig, K., Rueger, D.R., & Terheyden, H. 2004a. Carboxymethylcellulose-stabilized collagenous rhOP-1 device-a novel carrier biomaterial for the repair of mandibular continuity defects. Journal of Biomedical Materials Research.Part A, 68, (2) 219-226

Wang, H., Li, Y., Zuo, Y., Li, J., Ma, S., & Cheng, L. 2007. Biocompatibility and osteogenesis of biomimetic nano-hydroxyapatite/polyamide composite scaffolds for bone tissue engineering. Biomaterials, 28, (22) 3338-3348

Wang, S., Zhang, Z., Zhao, J., Zhang, X., Sun, X., Xia, L., Chang, Q., Yea, D., & Jiang, X. 2009. Vertical alveolar ridge augmentation with beta-tricalcium phosphate and autologous osteoblasts in canine mandible. Biomaterials, 30, (13) 2489-2498

Wang, J., Qiao, P., Dong, L., Li, F., Xu, T., & Xie, Q. 2014. Microencapsulated rBMMSCs/calcium phosphate cement for bone formation in vivo. Bio-medical materials and engineering, 24, (1) 835-843

Weir, M.D., Xu, H.H.K., & Simon, C.G. 2006. Strong calcium phosphate cement-chitosan-mesh construct containing cell-encapsulating hydrogel beads for bone tissue engineering. Journal of Biomedical Materials Research Part A, 77A, (3) 487-496

Weldon, E., Brockelbank, I., Narin, N., Naudi, K., & Ayoub, A. 2008, Cone beams CT for in vitro research: A practical approch for using the i-CAT radiography, Glasgow Dental School& Hospital.

Whang, K., Goldstick, T.K., & Healy, K.E. 2000. A biodegradable polymer scaffold for delivery of osteotropic factors. Biomaterials, 21, (24) 2545-2551

Wiedmann-Al-Ahmad, M., Gutwald-, R., Gellrich, N., Huebner, U., & Schmelzeisen, R. 2007. Growth of human osteoblast-like cells on beta-tricalciumphosphate (TCP) membranes with different structures. Journal of Materials Science-Materials in Medicine, 18, (4) 551-563

Wolff, J., Sandor, G.K., Miettinen, A., Tuovinen, V.J., Mannerstrom, B., Patrikoski, M., & Miettinen, S. 2013. GMP-level adipose stem cells combined with computer-aided manufacturing to reconstruct mandibular ameloblastoma resection defects: Experience with three cases. Annals of maxillofacial surgery, 3, (2) 114-125

Woodbury, D., Schwarz, E.J., Prockop, D.J., & Black, I.B. 2000. Adult rat and human bone marrow stromal cells differentiate into neurons. Journal of Neuroscience Research, 61, (4) 364-370

Wu, W., Chen, X., Mao, T., Chen, F., & Feng, X. 2006. Bone marrow-derived osteoblasts seeded into porous beta-tricalcium phosphate to repair segmental defect in canine's mandibula. Turkish journal of trauma & emergency surgery, 12, (4) 268-276

Xia, Y., Mei, F., Duan, Y., Gao, Y., Xiong, Z., Zhang, T., & Zhang, H. Bone tissue engineering using bone marrow stromal cells and an injectable sodium alginate/gelatin scaffold. 2012. Journal of Biomedical Materials Research - Part A.100 A, (4)1044-1050

Yamada, Y., Boo, S.J., Ozawa, R., Nagasaka, T., Okazaki, Y., Hata, K.I., & Ueda, M. 2003. Bone regeneration following injection of mesenchymal stem cells and fibrin glue with a biodegradable scaffold. Journal of Cranio- Maxillofacial surgery, 31,(0) 27-33

Yan, W.Q., Nakamura, T., Kawanabe, K., Nishigochi, S., Oka, M., & Kokubo, T. 1997. Apatite layer-coated titanium for use as bone bonding implants. Biomaterials, 18, (17) 1185-1190

Yin, L., Morishige, K.i., Takahashi, T., Hashimoto, K., Ogata, S., Tsutsumi, S., Takata, K., Ohta, T., Kawagoe, J., Takahashi, K., & Kurachi, H. 2007. Fasudil inhibits vascular endothelial growth factor - induced angiogenesis in vitro and in vivo. Molecular Cancer Therapeutics, 6, (5) 1517-1525

Yoshimi, R., Yamada, Y., Ito, K., Nakamura, S., Abe, A., Nagasaka, T., Okabe, K., Kohgo, T., Baba, S., & Ueda, M. 2009. Self-Assembling Peptide Nanofibre Scaffolds, Platelet-Rich Plasma, and Mesenchymal Stem Cells for Injectable Bone Regeneration with Tissue Engineering. Journal of Craniofacial Surgery, 20, (5) 1523-1530

Yuan, J., Cui, L., Zhang, W.J., Liu, W., & Cao, Y. 2007. Repair of canine mandibular bone defects with bone marrow stromal cells and porous β-tricalcium phosphate. Biomaterials, 28, (6) 1005-1013

Yudell, R.M. & Block, M.S. 2000. Bone gap healing in the dog using recombinant human bone morphogenetic protein-2. Journal of Oral and Maxillofacial Surgery, 58, (7) 761-766

Zamiri, B., Shahidi, S., Eslaminejad, M.B., Khoshzaban, A., Gholami, M., Bahramnejad, E., Moghadasali, R., Mardpour, S., & Aghdami, N. 2013. Reconstruction of human mandibular continuity defects with allogenic scaffold and autologous marrow mesenchymal stem cells. The Journal of craniofacial surgery, 24, (4) 1292-1297

Zey, A. 1939 Funktion des Kauapparates und Schadelgestaltung bei den Wiederkauern. Thesis. Univ. Frankfurt a Main.

Zhao, L., Weir, M.D., & Xu, H.H. 2010. An injectable calcium phosphate-alginate hydrogel-umbilical cord mesenchymal stem cell paste for bone tissue engineering. Biomaterials, 31, (25) 6502-6510

Zhou, H. & Xu, H.H. 2011. The fast release of stem cells from alginate-fibrin microbeads in injectable scaffolds for bone tissue engineering. Biomaterials, 32, (30) 7503-7513